Dissertation

Zur Erlangung eines Doktorgrades der Naturwissenschaften

MAPK related phenotypic decisions in yeast

vorgelegt von
Johann Jarzombek

bei der Fakultät Chemie der TU Dortmund

26.03.2015

1. Gutachter: Prof. Dr. Philippe I. H. Bastiaens

2. Gutachter: Prof. Dr. Andrea Musacchio

Eidestattliche Erklärung

Ich versichere hiermit an Eides Statt, dass ich die vorliegende Dissertationsarbeit selbständig verfasst und ohne unzulässige fremde Hilfe erarbeitet habe. Ich habe keine anderen als die hier angegebenen Quellen und Hilfsmittel benutzt, sowie wörtliche und sinngemäße Zitate durch Angabe der Quelle als Entlehnung kenntlich gemacht. Diese Arbeit ist bisher weder in Teilen noch als Ganzes für die Erlangung eines Promotionstitels eingereicht worden.

Ort, Datum Unterschrift

CONTENTS

List of Figures and Tables

Figures

Tables

Abbreviations

ACor	autocorrelation
bp	base pair
dNTP	deoxynucleotide-5'-triphosphate
CBD	catalytic binding domain
CC	complex concentration
CCor	cross-correlation
CDK	cyclin dependent kinase
DNA	desoxyribonucleic acid
EC	effective concentration
EGF	epidermal growth factor
EGFR	epidermal growth factor receptor
ES	enzyme-substrate complex
FCS	fluorescence correlation spectroscopy
FCCS	fluorescence cross-correlation spectroscopy
FLIM	fluorescence lifetime imaging microscopy
FRE	Filamentous response elements
FRET	Förster resonance energy transfer
FUS(1,3)	fusion-
g	acceleration of gravity
GAP	GTPase activating protein
GDP	guanodine di-phosphat
GEF	guanosine exchange factor
GFP	green fluorescent protein
GPCR	G-protein coupled receptor
GTP	guanodine tri-phosphat
HOG-1	high osmolarity/glycerol-1
HRG	heregulin
JNK	June N-terminal kinase
K_d	Dissociation constant
Kss1	kinase suppressor of Sst2
KSR	kinase suppressor of Ras
M	mol/L
µ	micro
MAP	mitogen-activated protein
MAPK	MAP kinase
MAPKK	MAP kinase kinase
MAPKKK	MAP kinase kinase kinase
MAT	mating type
min	minute
MRA	modular response analysis
NA	numerical aperture
NGF	neuronal growth factor
nM	nanomol/L

PAK	p21-activated protein kinase
PCR	Polymerase chain reaction
PH	plethrin homology
PIP_2	Phosphatidylinositol 4,5-bisphosphate
PM	plasma membrane
POI	protein of interest
PRE	pheromone response elements
RBD	Ras-binding-domain-like
RING	really interesting new gene
SAM	sterile alpha motif
Ser	serine
SH3	Scr-homology-3
Slt2	suppressor of LYT2
STE	sterile
ssDNA	single stranded DNA
TC	Total concentration
TCS	Tec1 binding site
Thr	threonine
Tyr	tyrosine
VWA	Willebrand type a
WT	wild type

Abstract

The demand of cells to quantitatively interpret their environment, to maintain robustness to uncertainties and at the same time sense and translate a potential signal into a specific biological response, triggered the evolution of signalling systems exhibiting a complex network architecture with several layers of feedback regulation. The evolutionarily conserved mitogen-activated protein kinase (MAPK) network is such a signalling module, which enables the coordination and processing of various extracellular stimuli. It thereby guarantees a specific biological response to a precise dose of a given stimuli. The haploid yeast *Saccharomyces cerevisiae* uses this network to select particular mating partners by quantitatively interpreting the pheromone concentration gradient generated by potential mates. Activation of the mating MAPK module occurs only above a certain pheromone concentration threshold and relies on the pheromone-induced recruitment of the scaffold Ste5 to the membrane[1], which then coordinates the hierarchical interactions between the MAPKs Ste11, Ste7 and Fus3[2,3], respectively. This module ensures a robust morphological response in form of a mating projection to a defined pheromone concentration and allows cells to gauge the distance to a potential mating partner[4,5,6]. Yet it remains unclear which of the module's features interpret the pheromone concentration to decide when and where to generate a mating projection.

To infer the network structure of the mating MAPK module, we developed a reverse engineering approach, which is based on the detection of pheromone response dependent changes in protein complex abundances. Interactions within the MAPK module were measured by fluorescence correlation spectroscopy (FCS), of which all possible protein-species in the MAPK module were resolved by applying a linear regression analysis (LRA). Using this approach, we were able to identify a cytosolic kinase-substrate interaction between Fus3 and the upstream Ste11, which constitutes a hitherto uncharacterized negative feedback. It affects the readout of the pheromone gradient and provides robustness to changes in the components involved in the loop. This negative feedback occurs by phosphorylation of S243 on Ste11 that hinders its binding to the scaffold Ste5 and thereby uncouples Ste11 from Fus3 activity. Controlling this mechanism provides ultrasensitivity at the first step of the MAPK cascade, as part of the hierarchical cascade arrangement, ensures a switch-like mating response and triggers shmoo formation at the right distance to a partner. This cytoplasmic feedback has a spatial component that confines the cytoplasmic Fus3 phosphorylation gradient. It thereby generates and maintains a localized source of active Fus3 at the mating tip, which in turn spatially restricts shmoo formation.

This work shows how a network motif in the MAPK module enables the interpretation of the pheromone concentration gradient to sense potential mates, and how this extracellular gradient is translated into an intracellular activity gradient by spatial control of signalling, ultimately deciding both when and where to respond.

Zusammenfassung

Zellen erfordern eine quantitative Interpretation ihrer Umwelt um Robustheit gegenüber Unsicherheitsfaktoren und gleichzeitig potenzielle Signale wahrzunehmen, und diese in eine spezifische biologische Antwort umzuwandeln. Diese Anforderungen haben die Entwicklung einer komplexen Netzwerk-Architektur mit verschiedenen Ebenen der „Feedback“ Kontrolle hervorgebracht. Das evolutionär konservierte Mitogen-aktivierte Protein-Kinase (MAPK) Netzwerk ist solch ein Signalmodul, welches die Koordination und die Verarbeitung von diversen extrazellulären Signalen ermöglicht. Es garantiert eine spezifische biologische Antwort auf eine präzise Stimulus-Dosis. Die haploide Hefe *Saccharomyces cerevisiae* benutzt dieses Netzwerk zur quantitativen Interpretation eines von potenziellen Paarungspartnern produzierten Pheromon-Gradienten. Die Aktivierung des MAPK-Moduls erfolgt ausschließlich wenn eine bestimmten Pheromon-Konzentration überschritten wird und ist abhängig von der Rekrutierung des Gerüstproteins Ste5 zur Zellmembran, welches die hierarchische Interaktion zwischen den MAPK Ste11, Ste7 und Fus3 koordiniert. Dieses Modul sichert eine robuste morphologische Antwort in Form einer Konjugationsspitze auf eine definierte Pheromon-Konzentration, und erlaubt es damit den Zellen die Distanz zu potenziellen Paarungspartnern abzuschätzen. Es bleibt jedoch unklar welche Netzwerk Motive dieses Modul zur Interpretation der Pheromon-Konzentration benötigt um zu entscheiden wann und wo eine Konjugationsspitze ausgebildet wird.

Um Rückschlüsse ziehen zu können über die Netzwerkstruktur des MAPK-Moduls des Paarungssignalwegs haben wir einen „Reverse Engineering“ Ansatz entwickelt, welcher auf der Detektion von Pheromon-abhängigen Änderung der Menge von Proteinkomplexen basiert. Interaktionen in diesem Modul wurden mit Hilfe von Fluoreszenz Korrelations Spektroskopie (FCS) Messungen ermittelt. Aus diesen Messungen wurden anschließend mit dem „Reverse Engineering“ Ansatz die Konzentrationen von allen möglichen Protein Spezies extrahiert. Weiterhin konnte ein Enzym-Substrat Komplex von Fus3 mit Ste11 ermittelt werden, welcher die Basis für einen bis dato unbekannten negativen „Feedback“ darstellt. In diesem „Feedback“ wird Ste11 an der Stelle S243 phosphoryliert was die Bindung an Ste5 behindert und dadurch die Aktivität von Ste11 von Fus3 entkoppelt. Die Kontrolle dieses Mechanismus generiert Ultrasensitivität auf dem Level von Ste11 als Teil der hierarchischen Organisation der MAPK Kaskade, erlaubt eine „switch-like“ Antwort und löst die Formation der Konjugationsspitzen im richtigen Abstand zum Paarungspartner aus. Dieser „Feedback“ hat eine räumliche Komponente, welche den zytoplasmischen Gradienten von phosphorylierten Fus3 einschränkt und definiert. Dadurch wird ein Pool an aktivierten Fus3 an der Konjugationsspitze aufrecht erhalten, welcher die Formation dieser restriktiert.

Diese Arbeit zeigt wie ein Netzwerk-Motiv im MAPK-Modul die Interpretation des Pheromon-Gradienten zu Erkennung potenzieller Partner ermöglicht, und wie dieser extrazelluläre Gradient in einen intrazellulären Gradient übersetzt wird um entscheiden zu können wann und wo auf ein Signal zu antworten.

1. Introduction

Living cells use protein-signalling networks to sense, process and convert extracellular information into distinct decisions that determine future cellular events. A classical example for complex cell fate decisions is the phenotypic outcome of rat pheochromocytoma PC-12 cells following stimulation by either epidermal or neuronal growth factor (EGF, NGF)[7]. Using the same set of signalling components EGF stimulation promotes cell proliferation while NGF stimulation on the other hand induces the formation of neuronal outgrowth. Similarly, in human breast adenocarcinoma MCF-7 cells an EGF stimulus induces proliferation while heregulin (HRG) leads to differentiation[8,9]. In the yeast *Saccharomyces cerevisiae* the response to mating pheromone and to environmental stresses (nutrient deprivation, hyperosmolarity) is processed by distinct signalling pathways with distinct phenotypic responses although signal transmission is partially conducted by the same proteins[3].

These examples demonstrate that signal transduction does not proceed in a linear manner, simply connecting an external signal to a genetic response but rather by a signalling network of specifically wired protein interactions and cascades. This mediates the decision whether to proliferate, differentiate, to survive or to undergo apoptosis[10]. Defective regulation of these signalling networks results in random cellular transformation and altered proliferation and consequently can be the origin for the development of many human diseases[11]. Therefore it is of particular interest to decode both the constitution of the network, its structure, and how the signalling proteins interact and are wired, its dynamics. These together constitute the architecture of a signalling network and enable the biological system to adapt to changing environments and to respond to a specific dose of stimuli by distinct changes in cytoskeletal organization, cell cycle control, spatial protein and cellular organization and genetic programs. It is the concerted regulation of these processes that maintains the specific biological response.

1.1 Signalling via mitogen-activated protein kinases

The transduction of extracellular signals, like growth factors, to the interior of the cell is initiated by membrane bound receptors and further propagated through the cytosol via the assembly of a three-tired MAPK cascade, which is conserved from yeast to humans (Fig. 1.1)[12,13,14]. This MAPK module is activated by a sequential phosphorylation event: upstream-activated MAPK kinase kinase (MAPKKK) phosphorylates the MAPK kinase, which in turn activates the MAPK. These components were first identified by an "upstream" approach, starting with a cellular response known to be affected by growth factors and proceeding upstream towards the receptor[13]. The first MAPKKK shown to phosphorylate and activate MAPKK was cRaf-1, a serine/threonine kinase, which was identified by Kyriakis *et al.*[15]. Raf is activated either via phosphorylation by a MAPKKK kinase or through interaction with a small GTP-binding protein of the Ras or Rho family. However, the exact mechanism of how Raf itself becomes activated remains unclear. Recent studies revealed that a dimerization dependent mechanism contributes to the activation of Raf[16,17].

The next kinase in the MAPK cascade is the MAPKK, which is also referred to as Mek. It phosphorylates both the threonine and the tyrosine residues of a Thr-X-Tyr motif in the activation loop of its target MAPK[13]. This dual-specific kinase is also capable of serine phosphorylation[18,19]. The final kinase in the cascade is the MAPK ERK1/ERK2, which is phosphorylated on Thr183 and on Tyr185[20,21]. This MAPK subsequently phosphorylates a variety of other proteins, like transcription factors, on a serine and threonine residue.

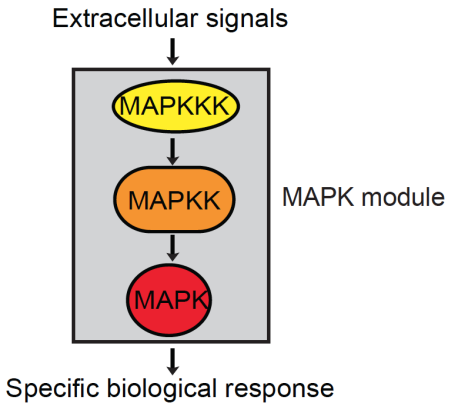

Fig. 1.1: Schematic representation of the MAPK module. Geometrical symbols represent the modules (grey) components: MAPKKK (yellow), MAPKK (orange) and MAPK (red). Arrows indicate activation.

Six different groups of MAPKs have been characterized thus far in mammals: (ERK)1/2, ERK3/4, ERK5, ERK7/8, Jun N-terminal kinase (JNK)1/2/3 and the p38 isoforms α/β/γ(ERK6)/δ. Whereas each of these MAPKs is regulated by a specific MAPKK, each MAPKK can be regulated by more than one MAPKKK which, in turn, can theoretically be activated by distinct stimuli[22]. This composition generates a complex MAPK network with diverse signalling

possibilities, which plays a central role in the regulation of proliferation, differentiation, cell metabolism, embryogenesis, cell survival and apoptosis[23,24].

1.2 MAPK signalling in the yeast *Saccharomyces cerevisiae*

The three-tiered MAPK module and its components are not only biologically versatile but also highly conserved through the metazoan evolution. Human ERK2 for example shows 51% sequence homology with the *Saccharomyces cerevisiae* mating MAPK Fus3 and 50% sequence homology with the filamentous growth MAPK Kss1[25]. Exploiting this homology in cloning approaches promoted the discovery of new mammalian MAPK components[26].

Pioneering studies of MAPK signalling in yeast demonstrated the existence of multiple parallel MAPK pathways in which specific MAPK isoforms can be differentially activated by distinct stimuli[13,27]. Genetic and biochemical studies in *S. cerevisiae* in the Thorner, Errede and Fink labs in the late 80s identified the first eukaryotic components of the MAPK module: the MAPKKK Ste11[28], the MAPKK Ste7[29] and the MAPKs Kss1[30] and Fus3[31]. Further studies demonstrated that the *S. cerevisiae* genome encodes at least four MAPKKKs, four MAPKKs and six distinct MAPKs, which constitute five well-characterized MAPK signalling pathways (Fig. 1.2). The MAPKs Fus3 and Kss1 are similar to mammalian ERK1/2, and regulate the mating response to mating pheromones. Kss1 initiates and adjusts filamentous growth of yeast in a nutrient poor environment. Hog1 is similar to mammalian p38 and is required for survival under hyperosmotic conditions. Mpk1, which is also known as Slt2, is involved in the maintenance of cell wall integrity. Two additional MAPK-related kinases, Smk1 and Ime2, regulate spore wall assembly during meiosis and sporulation[14,32].

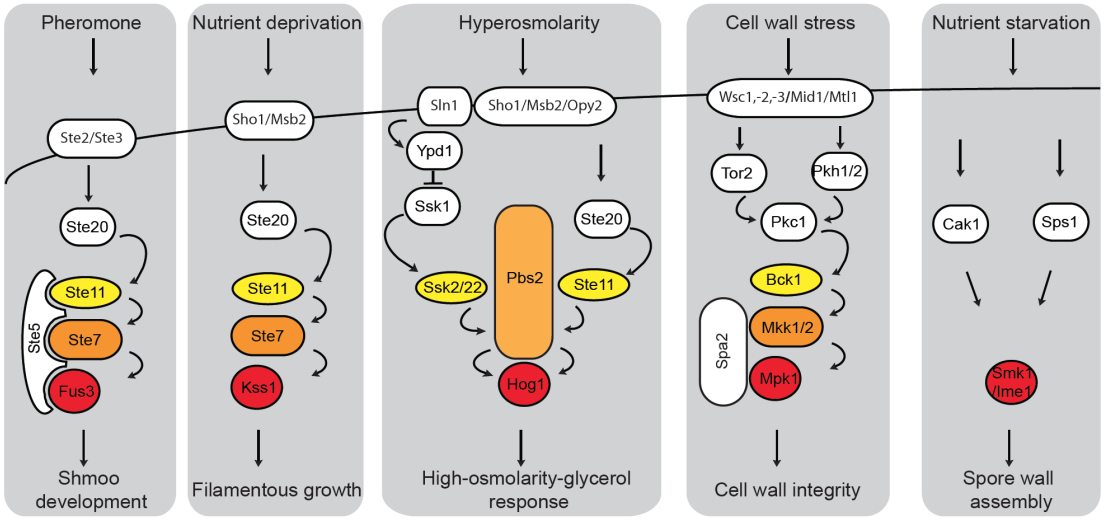

Fig. 1.2: Signalling via the MAPK pathways in the yeast *Saccharomyces cerevisiae*. Scheme mainly shows receptors, MAPKs and related components. G-proteins, phosphatases and other regulators are omitted for reasons of clarity. Symbols and colour code are the same as in Figure 1.1. T-bar indicates inhibition. This scheme is based on Chen *et al.*[3].

1.2.1 The yeast mating pheromone response pathway

The yeast *Saccharomyces cerevisiae* can exist either as a haploid or as a diploid organism. The haploid yeast cells can be distinguished by their mating types *MAT***a** or *MAT*$\boldsymbol{\alpha}$. Mating of the two cell types results in the formation of a *MAT***a**/*MAT*$\boldsymbol{\alpha}$ diploid cell. A complex series of cellular responses underlies this process, including a modulation in the expression of nearly 200 genes[25,33,34], changes in cytoskeletal structure and the arrest in the G1 phase of the cell cycle[35,36]. This ultimately leads to polarized cell growth towards the mating partner and the establishment of the site for cell fusion, the mating projection also called the shmoo[37]. After plasmogamy of the mating partners the nuclei are fused and zygote formation is completed[25,38].

Mating is initiated in response to the recognition of peptide pheromones secreted by the different haploid cells: the *MAT*$\boldsymbol{\alpha}$ cells secrete α-Factor[39], a tridecapeptide (WHWLQLKPGQPMY) and *MAT***a** cells secrete a-Factor[40], a C-terminally farnesylated dodecapeptide (YIIKGVFWDPAC)[41]. The presence of these extracellular pheromone peptides is sensed and transduced via the yeast mating pheromone response pathway.

1.2.1.1 G-protein signalling

First insights into this pathway were obtained approximately 40 years ago by isolation of sterile mutants, called STE mutants[42,43]. These mutants exhibited general mating defects including, in some cases, a complete lack of the morphological or cell cycle response to purified mating pheromone.

In healthy cells, however, mating is initiated by binding of the a-Factor to the G-protein coupled receptor (GPCR) Ste3[44] on the cell surface of *MAT*$\boldsymbol{\alpha}$ cells or by binding of α-Factor to the GPCR Ste2[45,46] in *MAT***a** cells. Both pheromone receptors are coupled to the same heterotrimeric G-protein, which consist of the subunits G_α(Gpa1), G_β(Ste4) and G_γ(Ste18)[44,47]. Receptor occupancy stimulates the G_α subunit to exchange GDP for GTP resulting in lower affinity to the dimer $G_{\beta\gamma}$ (Ste4-Ste18) and its subsequent release (Fig. 1.3)[48]. Although early models predicted that the role of the G_α subunit was to simply hold the $G_{\beta\gamma}$ dimer in check, later studies, however, revealed additional regulatory properties, including binding the mating MAPK Fus3[49] and regulation of Ste5 recruitment of the $G_{\beta\gamma}$ dimer[5].

While G_γ(Ste18) is responsible for anchoring the $G_{\beta\gamma}$(Ste4-Ste18) dimer to the plasma membrane (PM) via farnesyl and palmitoyl groups at the C-terminal – CAAX box, the G_β(Ste4) subunit mediates further signal transmission. This necessitates the binding of different effectors to the surface of G_β(Ste4) that was initially masked in the heterotrimeric G-protein. One of these effectors activated by Ste4 binding is Cdc24, a guanosine exchange factor (GEF) for the Rho-family GTPase Cdc42[50]. Activation of this GTPase is required for cell morphological processes like the generation of cell polarity, budding in dividing cells and the formation of the mating tip projection[38]. It was shown that binding of Cdc24 to Ste4 could only occur in the presence of Far1, a CDK inhibitor. The complex of

Far1-Cdc24 is largely sequestered in the nucleus and exclusively upon pheromone stimulation Far1 transports its cargo Cdc24 into the cytosol and further localizes it to the plasma membrane in a Cdc24-Far1-Ste4-Ste18 complex[51,52]. Here, a RING-H2 domain in the N-terminal region of Far1 binds to G_β(Ste4) while its C-terminus associates with Ccd24[51]. Far1 was also shown to control G1 cell cycle arrest by inhibition of the cyclin dependent kinase cdc28[53].

The second effector that binds G_β(Ste4) is Ste20, the first eukaryotic member of the p21-activated protein kinase (PAK) family[54]. This binding occurs via the C-terminal motif in Ste20. The p21 protein activating Ste20 is the formerly described Cdc42, which binds the CRIB domain in the N-terminus of Ste20 in its GTP bound state[55]. This binding releases an autoinhibitory conformation of Ste20 and thereby antagonizes the inhibition of its kinase domain[56]. Subsequent autophosphorylation of the now-exposed catalytic loop can fully activate the MAPKKKK[54]. Ste20 itself is localized to the PM via the adaptor protein Bem1. It interacts through its tandem N-terminal Src-homology-3 (SH3) domains to proline rich motifs in Ste20 and is tethered by an internal phosphoinositide-binding Phox-homology (PX) domain to the PM[57]. Cdc42, which binds to and activates Ste20, is also permanently tethered to the plasma membrane due to geranylgeranylation of its C-terminal -CAAX box[58].

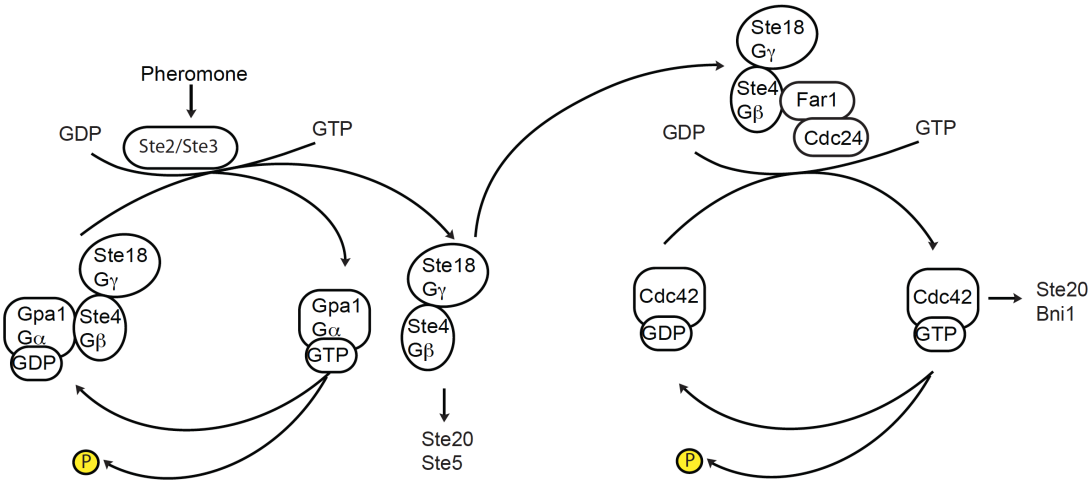

Fig. 1.3: G-protein circuits in the yeast mating pheromone response pathway. Signalling components are represented by geometrical symbols. Arrows indicate activation, and yellow P represents a phosphate group.

These binding mechanisms of the GPCR regulated effectors ensure a massive and dense localization of the active MAPKKK Ste20 at the spot with the highest number of pheromone bound receptors on the plasma membrane

Ste20 activates the downstream kinase in the yeast pheromone MAPK cascade, the MAPKKK Ste11[59]. Recruitment and subsequent activation of the cytosolic components of the MAPK module is ensured by two proteins, the adaptor protein Ste50 and the scaffold protein Ste5. First, an indirect interaction of Ste11 with Cdc42 is promoted through Ste50. This adaptor binds Cdc42 via its C-terminal Ras-association (RA) domain[60] and Ste11 via N-terminal sterile-alpha-motif (SAM) domain binding[59].

1.2.1.2 Signalling via the MAPK module

Ste11 is brought in close proximity to its activators by binding to the scaffold protein Ste5, as shown by two-hybrid interaction analysis[2]. Later studies examined this interaction in detail and revealed binding of a Ras-binding-domain-like (RBD) region in Ste11 to the pleckstrin homology (PH) domain in Ste5[61,62]. This domain was found to be responsible for membrane tethering by phosphoinositide binding and to be critical for initiation of downstream signalling. Ste5 is further tethered to the membrane by a short N-terminal phospholipid binding amphipathic α-helical domain, which is simply called the PM domain[57]. Additional binding of Ste5 to G_{β}(Ste4) through a RING-H2 domain in its N-terminal region, delivers Ste11 for activation by Ste20[63]. The stable PM recruitment of Ste5 and a full response to pheromone requires the cooperative effect of these three mechanisms (Fig. 1.4).

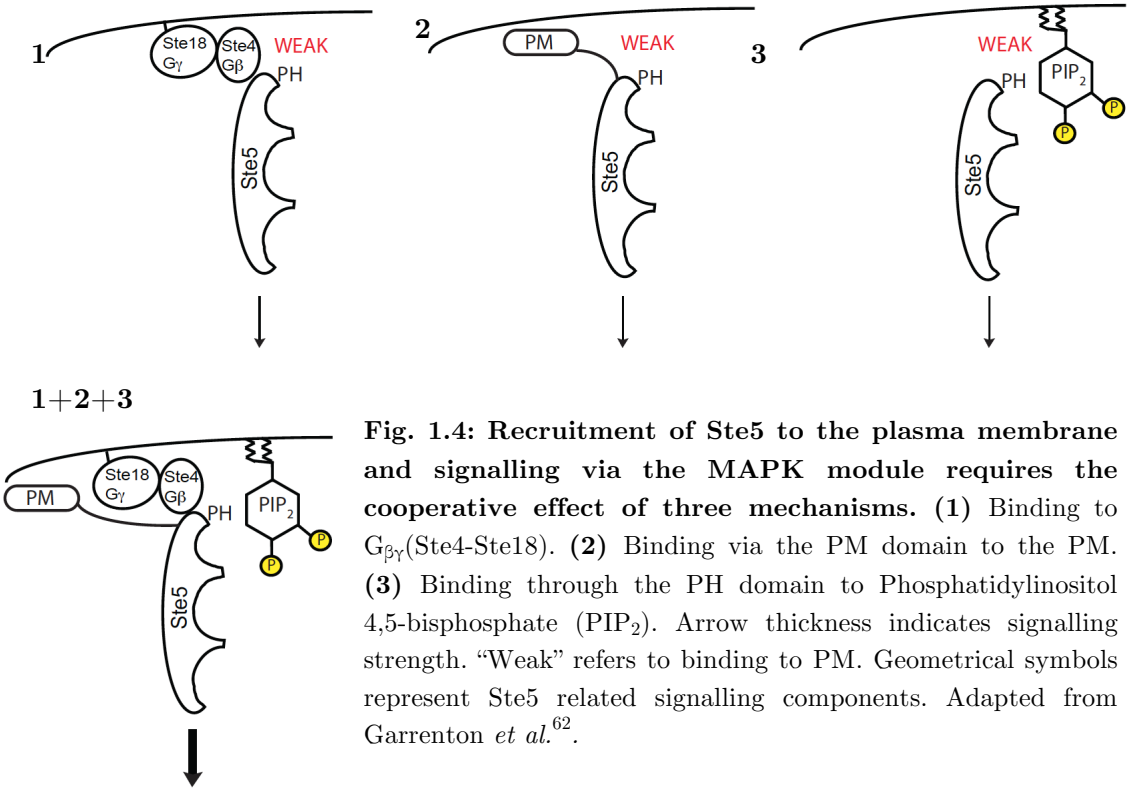

Fig. 1.4: Recruitment of Ste5 to the plasma membrane and signalling via the MAPK module requires the cooperative effect of three mechanisms. **(1)** Binding to $G_{\beta\gamma}$(Ste4-Ste18). **(2)** Binding via the PM domain to the PM. **(3)** Binding through the PH domain to Phosphatidylinositol 4,5-bisphosphate (PIP_2). Arrow thickness indicates signalling strength. "Weak" refers to binding to PM. Geometrical symbols represent Ste5 related signalling components. Adapted from Garrenton *et al.*[62].

However, localizing Ste5 to the Golgi instead of to the PM by replacement of the PM domain with a FAPP1 PH domain is also sufficient for cells to respond to pheromone[57]. Ste5 that is artificially targeted to the PM causes constitutive pheromone response even in the absence of G_{β}(Ste4) and pheromone stimulation[1]. In this regard it has been proposed that changes in the conformation of Ste5 (e.g. by its dimerization[64] or oligomerization[65,66]) might contribute to Ste5 mediated signalling. Indeed, recent studies by W. Lim and co-workers discovered a conformation-based mechanism initiated at the PM, which activates Ste5 mediated signalling[67]. Here, the intramolecular interaction of the PH domain with the von Willebrand type a (VWA) domain keeps the scaffold in an inactive conformation. Binding to the plasma membrane and interaction of the PH domain with PIP_2 disturbs the PH-VWA binding and the autoinhibition, thereby triggering Ste5 mediated signalling.

The function of Ste5 in the mating pathway is to assemble the protein kinases[68,69] of the pheromone-activated MAPK cascade at the PM to enhance signal transmission from MEKK to MAPK[70]. When Ste5 is bound to the PM, Ste11 is phosphorylated by Ste20 in the N-terminal regulatory region on Ser302 and/or Ser306 and Thr307 in the catalytic binding domain (CBD)[71]. Phosphorylation of these sites activates Ste11 by preventing the binding of CBD to the kinase domain, thereby releasing autoinhibition. In this respect, binding of the adaptor Ste50 to Ste11 via N-terminal SAM domains contributes to phosphorylation of Ste20 by weakening the interaction of the Ste20 termini[59]. Consistently, Ste50 deficient cells are still able to mate, but with a roughly 10-100 fold reduced efficiency[25]. The next step in the cascade is the activation of the MAPKK Ste7 through phosphorylation of Ser359 and Thr363 in its activation loop. This event is probably mediated via Ste5, because Ste11 has not been reported to directly bind Ste7 so far[2,68]. Activated Ste7 binds its targets Fus3 and Kss1 with high affinity and phosphorylates the sites T180 and Y182 in the Fus3 activation loop[72,73] and T183 and Y185 in Kss1[74]. *In vitro* studies revealed a K_{d} of approximately 5 nM for these Ste7 MAPK complexes. Determination of these interactions by fluorescence correlation spectroscopy (FCS) revealed a K_d of 174 nM[75] and 111 nM[76] for the Ste7-Fus3 complex and a K_{d} of 33 nM[76] for the Ste7-Kss1 complex. The high stability of these complexes can be explained by binding through specific binding motifs (D-sites)[77,78]. These motifs are short peptide sequences in substrates that tightly bind to a groove on the surface of the MAPK. The consensus sequence of these sites for MAPK in general is $(K/R)_{2\text{-}3}$-$X_{1\text{-}6}$L/I-X-L/I.

1.2.1.3 Transcriptional control of the mating response

Upon pheromone stimulation the active Fus3 is accumulated in the nucleus[79] where it targets its main substrates: the transcription factor Ste12[80,81] and the two repressors Dig1 and Dig2 (Fig. 1.5)[82,83]. Phosphorylation of Dig1 and Dig2 impedes their interaction with Ste12 thereby permitting binding to pheromone response elements (PRE)[84,85], which induces their transcription. This DNA motif with the consensus sequence (A/T)GAAACA[86,87] is localized in the promoters of about 200 mating related genes[34] that are involved in the process of mating like Fus1, Fus2[88] and Prm1[89], and components of the mating pheromone response pathway (Ste2, Fus3, Far1)[34]. Strains which lack the Ste12 repressors Dig1 and Dig2 exhibit constitutively upregulated levels of these pheromone induced genes[83,90,34].

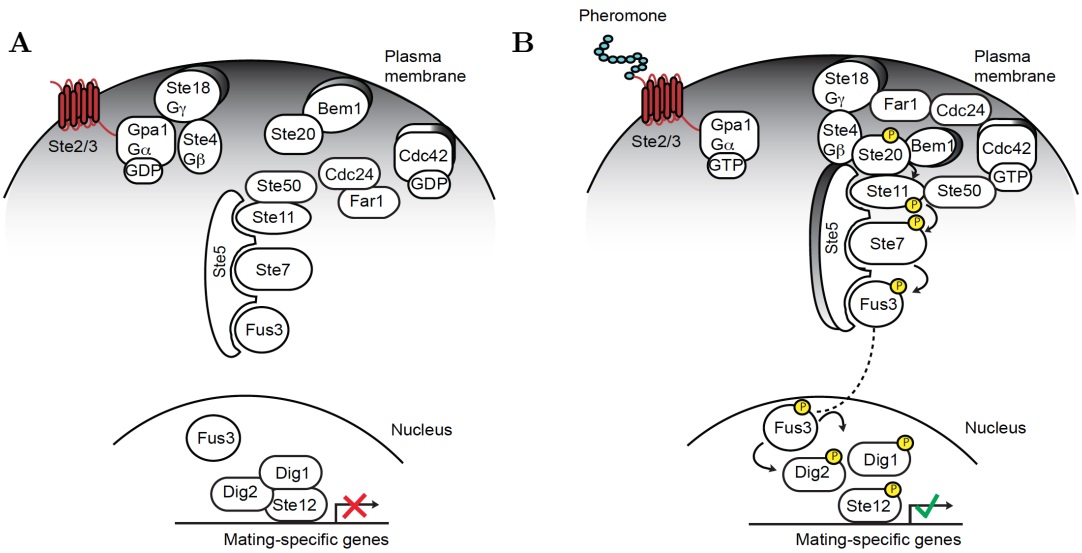

Fig. 1.5: Schematic representation of the yeast mating pheromone response pathway. (A) Localization of the components in unstimulated vegetatively growing cells. **(B)** Signalling is initiated by pheromone binding to the receptor and further continues via recruitment of the MAPK module to the PM via sequestering by Ste5. Activated Fus3 initiates transcription of mating-specific genes. Symbols: proteins with shadow are membrane-localized, red cross – no gene transcription, green hook - gene transcription. Arrows indicate activation through phosphorylation. Dotted line indicates translocation. All signalling components are represented by geometrical symbols.

1.2.2 Polarized growth of yeast

The mating signal initiates arrest in the G_1 phase and polarized cell growth leading first to the growth of a mating projection and subsequently to the fusion of two mating cells to a diploid zygote (Fig. 1.6). Cell polarity is established by four steps[91]. First, an origin of polarity is determined by intrinsic or extrinsic cues, like pheromone-receptor binding. During mating this site is marked by a "landmark protein", the complex of Far1-$G_{\beta\gamma}$(Ste4-Ste18)[52]. This is followed by the activation of small GTPase proteins, like Cdc42, which reorganizes the actin cytoskeleton[37]. This promotes the localization of cell fusion specific factors critical for cell wall remodelling like Fus1, an O-glycosylated 1-pass PM protein[92]. Finally, cell fusion of two mating cells occurs in two steps through the remodelling of the cell wall and the formation of fusion pores[93]. Diploid yeast cells can transform back to haploid cells by the developmental program of sporulation, a process of meiosis and spore morphogenesis that results in four haploid spores.

Cell polarity is the driving force of two further phases of the *Saccharomyces cerevisiae* "life cycle" (Fig. 1.6). Vegetatively growing yeast cells show an ovoid shape and divide by budding in environments containing ample nutrients. During mitotic budding chromosomes are delivered from the mother to the separated daughter cell[37]. At this site a chitin plug termed the bud scar is deposited to mark a budding event. The position of the site of further budding to the site of previous budding defines the polarity of cell division[94,95]. In axial budding of haploid cells

the mother and the daughter cell bud off adjacent to their cell pole that defined the previous mother-daughter junction[96]. In polar budding in diploid $MAT\mathbf{a}/MAT\boldsymbol{\alpha}$ cells buds are generated at the pole opposite of the pole that defined the junction to its mother[96].

A third phase in the yeast "life cycle" that exhibits polarized growth is filamentous growth. It is a distinct pattern of mitotic morphogenesis in cell division. In a nutrient deprived environment cells respond by a dimorphic transition, becoming more elongated and tube-like shaped. These cells proliferate in a unipolar pattern in which daughter cells are only generated at the cell pole opposite the birth-end of their mother[97,98]. The characteristics of this filamentous growth-form are increased cell-cell adhesion and an increased ability to penetrate the cells substratum, which allows to better forage the surroundings of a colony for additional nutrients[3].

Depending on the cell type, diploid cells exhibit pseudohyphal growth in response to limited nitrogen sources and haploid cells show filamentous growth in response to glucose deprivation[99]. However, it was shown the both haploid and diploid cells execute a similar filamentous growth program using that same pathways and components[100].

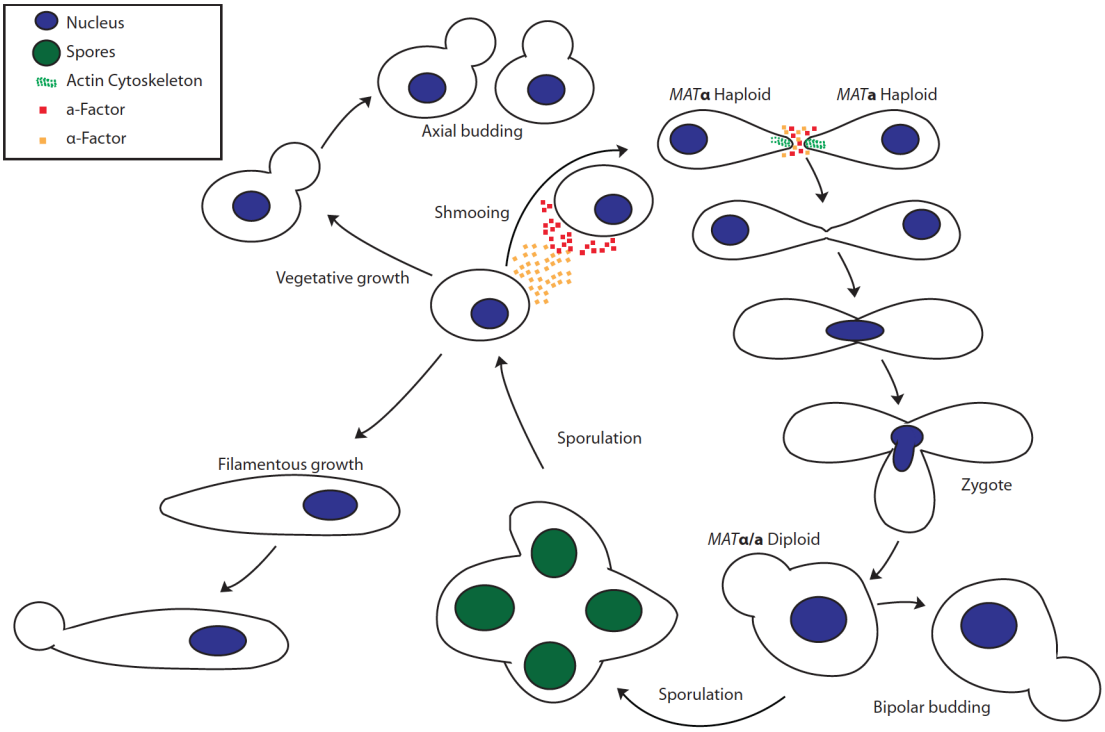

Fig. 1.6: The *Saccharomyces cerevisiae* "life cycle". The scheme shows different morphological developments depending on the ploidity of the organism and the environmental conditions. Vegetative growth occurs under ample nutrient condition. Haploid and diploid cells can convert by either mating or sporulation. Both can filament in nutrient deprived conditions. Symbols and colours are explained in the legend. Every arrow indicates a step in the morphological development.

1.2.3 The filamentous growth pathway: a distinct path of mitotic division

The switch from budding to filamentous growth is controlled by three distinct protein kinases acting in independent signalling pathways: the Snf1a 5'-AMP dependent protein kinase (AMPK); Tpk2, an isoform of 3',5'-cyclic-AMP dependent protein kinase (PKA) and the MAPK Kss1[3].

MAPK signalling in filamentous growth is initiated via several transmembrane proteins, including Mep2[101], Gpr1[102], Sho1[103] and Msb2[103]. The high-affinity ammonia permease Mep2 acts as a nitrogen sensor in pseudohyphal growth of diploid cells. The glucose-binding GPCR Gpr1 serves as a carbon sensor[104]. The signalling mucins Sho1 and Msb2 initiate filamentous growth via MAPK signalling (Fig. 1.7) and deletion of either Sho1 or Msb2 prevents activation of Kss1 and filamentous growth[103]. These two cell-surface proteins were shown to form hetero-oligomeric complexes. Deletion within the highly O-glycosylated extracellular domain of Msb2 causes constitutive activation of the filamentous growth response in haploid cells pointing at a possible glycosylation-dependent activation mechanism[103]. It was shown that activation of Msb2 is not regulated via glycosylation of the extracellular domain but rather via the processing and release of this domain by the aspartyl-protease Yps1[105], whose expression is induced during nutrient limitation. The processed Msb2 further associates with Sho1 and Cdc42 to initiate signalling via the filamentous growth MAPK module[103].

The activation of Cdc42 during filamentous growth was shown to be dependent on active Ras2[106], a homologue of the mammalian H-Ras. Cells with constitutively activated Ras2(V19) are sensitive to nitrogen[107], exhibit enhanced cAMP[108] levels and a strong filamentous growth phenotype[96].

Cdc42, which further activates Ste20, requires the association of the two 14-3-3 proteins Bhm1 and Bhm2[109]. It was speculated that these proteins route the signal from Ras2 to Ste11 without the scaffolding function of Ste5[110]. Indeed, activation of the filamentous growth was proven to be independent from the scaffold protein Ste5[111,112]. The recruitment of Ste11 to the plasma membrane is probably mediated by Opy2[113], which was interacts with Ste50, the adaptor protein of Ste11[114].

Upon nutrient deprivation the active Kss1 is localized to the nucleus where it binds and phosphorylates the transcriptional complex consisting of Dig1/Dig2/Ste12[82], which is also regulated by the mating MAPK Fus3. Dig1 (down-regulator of invasive growth) and Dig2 can associate with either Fus3 or Kss1 and function as negative regulators in both pathways. The specific transcription of filamentous growth genes is ensured by the co-regulation of Ste12 by another transcription factor, Tec1[115,116]. Dimeric Tec1 interacts with Ste12 in a complex either with Dig1 or Dig2, which binds to PREs adjacent to a Tec1-binding site (TCS), defined as filamentous response elements (FREs). Most of the filamentous growth genes do not contain FREs but TCS motifs[117]. Active Kss1 phosphorylates Ste12, Dig1 and Dig2 leading to dissociation of Dig1 or Dig2 from the transcriptional complex. Interestingly, inactive Kss1 represses Ste12 through direct binding[90]. It is therefore mainly localized in the nucleus in vegetative cells[74].

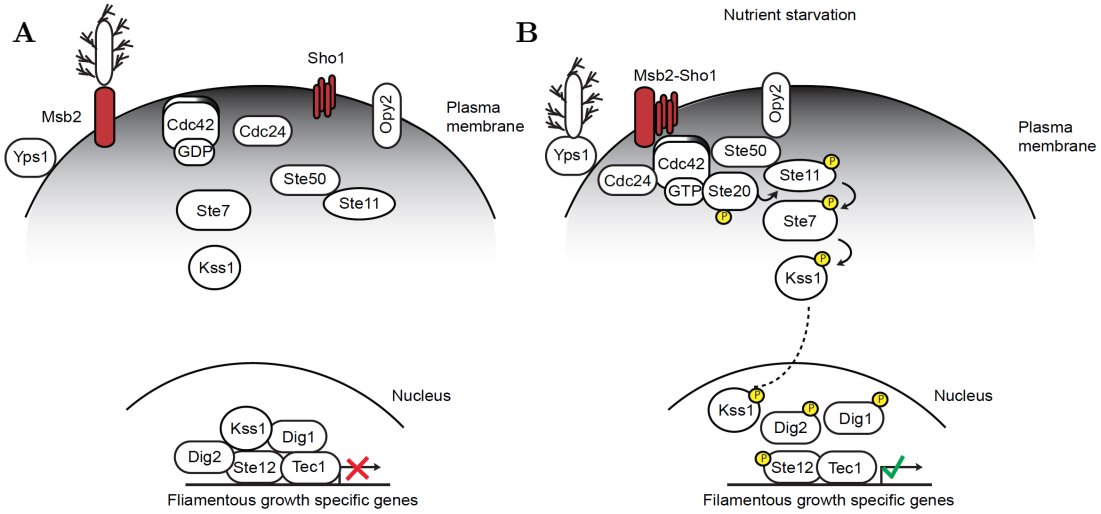

Fig. 1.7: Schematic representation of the filamentous growth pathway. (A) Localization of the components in unstimulated vegetative cells. **(B)** Signalling is initiated by nutrient starvation and further procession of the signalling mucin Msb2. Activated Kss1 initiates transcription of filamentous growth specific genes. Symbols: proteins with shadow are membrane-localized, red cross – no gene transcription, green hook - gene transcription. White symbol with ramification on top of Msb2 represents the heavily glycosylated extracellular domain. Arrows indicate activation through phosphorylation. Dotted line indicates translocation. All signalling components are represented by geometrical symbols.

1.2.4 MAPK signalling specificity in the differentiation of yeast

Signalling via the MAPK Kss1 in the filamentous growth pathway utilizes the same core components as signalling via Fus3 in the mating pathway: the MAP kinases Ste20, Ste11, Ste7 and the transcription factor Ste12[118]. Furthermore, Ste50 which is the adaptor protein of Ste11, and the upstream G-protein Cdc42 and its GEF Cdc24 are shared in both pathways[55,118,119]. Besides this overlap in signalling components, Fus3 and Kss1 also share about 55% sequence homology.

Therefore, the question arises of how distinct external stimuli can generate differential activation of Fus3 and Kss1 using the same MAPK components and achieve a precise and appropriate biological response.

It was thought that signalling specificity between these two responses is mainly ensured by the specialized functions of Fus3 and Kss1 in signalling. Indeed, deletion of Kss1 leads to hypoinvasive growth[120] and Fus3 deletion strongly impairs formation of a mating projection[121]. However, both kinases show functional redundancy in both pathways to a certain extent. Kss1 can partially overtake Fus3 function and sustain a mating efficiency up to 10% in its absence[120,121]. Fus3, in contrast, has an antagonistic function to Kss1 during invasive growth[100], which gets lost upon deletion resulting in hyperinvasive growth[100].

Since both MAPKs are exclusively activated by the same MAPKK Ste7, the question arises of how signalling specificity is achieved at this level. Both interactions Ste7-Fus3 and Ste7-Kss1 show a high stability, which can be attributed to binding through docking sites, as described above. Binding of Fus3 and Kss1 by Ste7 at these sites occurs with a similar affinity ($K_D \approx 100nM$)[122], excluding the regulation of specificity by differential binding. *In vitro* kinase assay studies by Good *et al.*, on the other hand, revealed that Kss1 is an excellent substrate of Ste7, whereas Fus3 is an intrinsically poor substrate of Ste7[123]. However, in presence of a minimal domain of the scaffold protein Ste5 (Ste5ms), the k_{cat} of the Fus3-phosphorylation by Ste7 is increased approx. 5000 fold, whereas the phosphorylation of Kss1 by Ste7 is not affected. This effect was shown to be mediated by catalytically unlocking Fus3 by this Ste5 domain thereby improving Fus3 as a substrate for Ste7[123]. It is therefore the scaffold Ste5 that ensures the selective activation of Fus3 in the mating pathway. This corroborates the proposed role of scaffolds as active signalling components and not simply as passive docking sites for other effector molecules[124].

It was also demonstrated that Ste5 insulates against intrusions of competing proteins and thereby prevents leakage of signal and cross-talk within the MAPK pathways[125,126]. In fact, when Ste5 is activated it even redirects some of the upstream signalling from competing MAPK modules into the mating pathway[111]. This Ste5 "activity" is conformationally controlled and regulated by its subcellular localization. In absence of pheromone, it exhibits a "closed" conformation that autoinhibits Fus3 and upon pheromone stimulated PM recruitment, Ste5 changes its conformation and thereby enables the release and activation of Fus3[67]. Signalling specificity in the mating pathway is thereby maintained by locally "activating" Ste5 at the PM[1] whereas Kss1 activation by nutrient deprivation does not require Ste5[111] nor its specific localization.

Activated Fus3 phosphorylates two targets amongst others, which promotes the specific mating response on both morphological and transcriptional levels. One of these targets is the CDK inhibitor Far1[127]. Phosphorylation of Far1 supports its association with the Cdc28p/Clnp complex to thereby stop the cell cycle at START in G_1 and initiate the mating process[53]. On a transcriptional level, cross-talk between the mating and the filamentous growth pathway is prevented by the phosphorylation and subsequent degradation of Tec1, a filamentation specific transcription factor[116,128].

Interestingly, although both MAPKs Fus3 and Kss1 are rapidly phosphorylated upon pheromone stimulation, only the formation of mating tips is initiated while filamentous growth is not engaged. This signalling specificity on the MAPK level is achieved through specific MAPK activation dynamics with Fus3 exhibiting a sustained activity over time while Kss1 exhibits a more transient activation profile[129]. Here, the duration and the strength of Kss1 phosphorylation is controlled by the opposing Fus3 activity, inactivating Ste7 for Kss1 phosphorylation through a negative feedback mechanism[130]. Accordingly, deletion or inactivation of Fus3 has been shown to convert the transient Kss1 response into a sustained profile. This

change in the activation dynamics results in a loss of signalling specificity and Kss1 induced filamentous growth.

Similar dynamics of MAPK regulation were found to control the fate of PC12 cells to different stimuli. Following EGF stimulation, the MAPK network exhibits negative feedback, leading to proliferation. On NGF stimulation, the same MAPK network exhibits positive feedback that triggers differentiation[131]. These examples further demonstrate the importance of stimulus context in determining the topology of the MAPK network.

This leads to the question of how this dynamic behaviour of the cell is generated, what are the underlying dynamics and how do they determine the response of signalling system.

1.3 Signalling dynamics in MAPK networks and response properties – Network topology

Cells have to decide when to respond and how to respond to certain stimuli strengths. This decision-making is determined by the dynamics of the signalling system, which emerge from simple molecular interactions. These impart causal connections in a signalling network to generate spatiotemporal patterns. The collective interplay of these causal connections, which can be negative or positive in their effect, determines the topology of the signalling network and ultimately the morphological response to a defined dose of stimuli.

1.3.1 Dose-response properties of signalling networks

In the sexual reproduction of the haploid *Saccharomyces cerevisiae*, for example, the essential first step is the decision whether to respond to a potential mating partner. Partner selection, in general, occurs by sensing and measuring the concentration of secreted pheromone in the environment[132]. This is promoted by polarized morphogenesis in a pheromone gradient[133] in the direction of highest pheromone concentration[132]. Sensing pheromone concentration and thus gauging the distance to a partner depends on receptor occupancies but is mainly mediated by downstream signalling network responses[5]. Early studies in the 80s had already shown that cells that lack Sst2 (Super-sensitivity 2), a GTPase activating protein that stimulates GTP hydrolysis[134], become supersensitive to pheromone[135] and lose the ability to discriminate between mating partners[133]. Twenty years later it was shown that Sst2 promotes Ste5 recruitment to the PM and that Fus3 regulates this response through a negative feedback to control the pheromone input-output sensitivity[5].

The above-mentioned examples of feedback regulation in yeast mating demonstrate the importance of precise regulation of signalling events in time and space in cellular development. A signal that is produced in the wrong time or place, or with the wrong amplitude or duration will not produce an appropriate

developmental response to a given stimulus[136].

Signalling in protein networks is transduced and regulated to a great extent by the phosphorylation and dephosphorylation of signalling proteins. It was first shown by Cori and Green[137] and others[138], that a protein can exist in a phosphorylated and a dephosphorylated state, and that these modifications control different biological responses[139]. On this basis, the simplest, controllable and universal motif in cellular signalling networks was defined as a cycle of two or more forms of a single signalling protein[140], that can be controlled by enzymes with opposing functions. Two important examples of this motif are the combination of a guanine nucleotide exchange factor (GEF) and a GTPase-activating protein (GAP) in controlling the activity of small G proteins, and the kinases and phosphatases that regulate the activity of phosphoproteins (Fig. 1.8). In MAPK signalling these cycles are serially connected in a cascade of three kinases, which transduces and amplifies an extracellular signal into a precise and robust response. However, other systems like the adenylate cyclase-cAMP (cyclic adenosine monophosphate) pathway or the JAK-STAT system require only a single protein kinase to transmit a signal[141]. So then why have cells evolved a MAPK cascade consisting of three kinases in series to propagate a signal instead of employing just a single kinase?

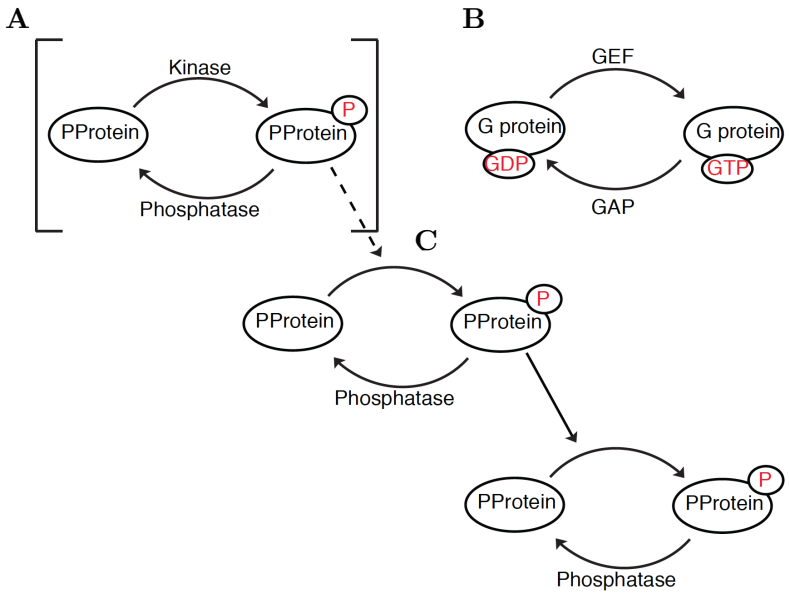

Fig. 1.8: Basic motifs in a signalling network. (A) Phosphorylation cycle of a protein phosphorylated by a kinase and dephosphorylated by the opposing phosphatase. **(B)** Cycle of G protein activation/deactivation. The GEF catalyses the transformation of inactive GDP-bound G-protein to an active GTP-bound G-protein. **(C)** Cascade of three phosphorylation cycles in series.

Sensing and processing of environmental signals like hormones or the sensing of photons, requires efficient signal amplification of very low doses of stimuli. At the same time it requires the ability to threshold background stimuli in order to adapt and not saturate the sensing system[142]. Three-kinase-cascades exhibiting signal amplification at each level could in principle provide this high-degree amplification.

In the visual system for example the bleaching of one rhodopsin molecule can hydrolyse 10^5 molecules of cyclic guanosine monophosphate (cGMP)[143]. However, if a similar degree of amplification would occur in a kinase cascade, an avalanche of signal would be produced. In fact, considering the volume of an average mammalian cell, amplification of a single signalling molecule by a cascade of three steps each amplifying 10^4 would result in an unphysiological effector protein concentration of 1 M[142]. Comparing the abundance of receptors, G-proteins and the downstream MAPKs shows that this high rate of amplification is not necessary[141]. The signal amplification from the receptor to the MAPK in the yeast pheromone response pathway, for instance, is approximately 20-fold and the Ras mediated activation of human Erk1/2 is about 100-500 fold higher than in yeast mating[141]. Therefor this amplification rate could be accomplished without a three-step cascade, indicating that the three-tiered MAPK cascade rather serves as a moderate amplifier.

1.3.2 Sensitivity amplification in signalling

The MAPK signalling network is an adaptive system that is employed by the cell to switch from one state to another. In the yeast mating response a vegetative cell differentiates into a shmooing cell. It is of particular importance to distinguish between different concentrations of stimuli and to filter insignificant background that could inappropriately trigger a signal. One way to increase the signal-to-background (noise) ratio is through sensitivity amplification. This process regulates the dose-response relationship and determines the percentage change in the output compared to the input[142]. This input-output relationship can be represented in a response profile to stimuli, which can either show a hyperbolic or a sigmoidal behaviour. Michaelis-Menten type responses produce a characteristic hyperbolic relationship, where at low input levels the output increases linearly but eventually reaches levels where with increasing input the output becomes progressively smaller (Fig. 1.9, black curve). In contrast, ultrasensitive responses produce a sigmoidal relationship, where the output increases rapidly to its maximum at a critical input level (Fig. 1.9, red curves)[142]. In general, both input-output relations can be described by the Hill function[144]:

$$Output = \frac{Input^n}{K^n + Input^n} \tag{1.1}$$

Here, the effective Hill exponent n (n_H) quantifies the sensitivity and the constant K represents the $EC50$ (concentration showing half maximal effect). If n equals 1, this equation is similar to a Michaelis-Menten equation based on enzyme kinetics described by the law of mass action and not on Michaelis-Menten kinetics[145]. Any response with $n > 1$ shows ultrasensitivity. In these cases, small percentage changes in the input can give much larger percentage changes in the output. The higher the n is the bigger these changes are and the greater the sensitivity of the system is. This is reflected in the steepness of the sigmoidal curve (Fig. 1.9).

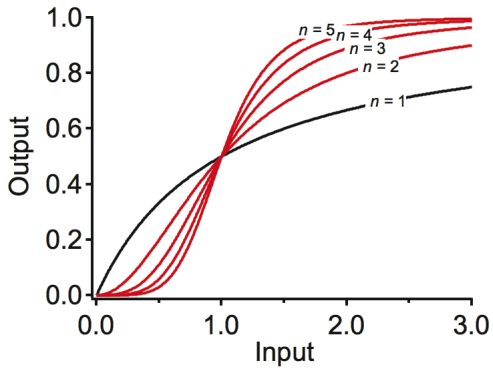

Fig. 1.9: Input-output relationships. Curve progression can be described by Hill functions with thecorresponding coefficients $n = 1,2,3,4,5$. For $n = 1$ (black) the curve shows Michaelian response. For $n > 1$ (red) the curves show an ultrasensitive response.

These stimuli-response relationships can be also described by the ratio of the 10 and 90 percentages of the maximum response ($EC90$:$EC10$). In a hyperbolic response the change from 10 to 90 % of maximum output requires a 81-fold increase in input, whereas an ultrasensitive response shows this change in a much more narrow range. In this context the ultrasensitive response was defined by Goldbeter and Koshland as any response with an $EC90$:$EC10$ ratio smaller than 81[142]. The $EC90$:$EC10$ ratio is related to the effective Hill coefficient as follows[145]:

$$n = \frac{Log[81]}{Log\left[\frac{EC90}{EC10}\right]} \tag{1.2}$$

A system that is ultrasensitive has the ability and the need to quickly "switch" cell fate from one existing steady state to another state by only a small change in stimuli. This behaviour is also called an all-or-none response or a switch-like response[146].

Sensitivity amplification and the resulting ultrasensitive input-output relationship can be generated by several mechanisms. The first experimentally revealed was the cooperative binding mechanism of oxygen to hemoglobin[147,144]. Cooperativity in general describes a multistep process, where a performed first step enhances the completion of further steps. In case of hemoglobin, the binding of oxygen to the first docking site promotes the binding of further oxygen molecules to other sites. This results in a sigmoidal binding curve of oxygen to hemoglobin with an apparent Hill coefficient of 2.7[145].

Further mechanisms that can produce ultrasensitivity are the suppression of the activating enzyme by a stoichiometric inhibitor[141], or zero-order ultrasensitivity[139]. In the latter, phosphorylation and dephosphorylation processes in a phosphorylation cycle are running close to saturation. The protein to be modified is present in excess compared to the converting enzyme, which operates in the "zero-order" region. This system can exhibit ultrasensitivity comparable to a cooperative protein with high Hill coefficients and can also be described by the Goldbeter-Koshland equation[142].

Returning to the MAPK cascade system in this context, it was revealed by Huang and Ferrell that the MAPK cascade arrangement in *Xenopus* oocytes maintains an ultrasensitive response[146]. With each step in the cascade the stimulus-response curves of the kinases become progressively steeper, reflected in an increase in the Hill coefficient from 1.7 for Mek-1 to 2.5 for Erk-1. Here, zero-order ultrasensitivity as well as multistep ultrasensitivity contributes to the overall response of the cascade. Multistep ultrasensitivity is generally described as a process where the same effector enters and impacts a signalling route at several steps[142]. In MAPK signalling this can emerge in form of the required dual phosphorylation for activation of both the MAPK and the MAPKK. If both phosphorylation steps each require a separate binding step, this means the single-phosphorylated kinase must first dissociate before the second phosphorylation can occur, the rate of MAPK activation will increase as the square of the input[141].

This example demonstrates that each level in the MAPK cascade can exhibit ultrasensitivity. The overall sensitivity of the linear cascade is the product of the sensitivities at each level. Therefore the MAPK cascade arrangement itself can cause high ultrasensitivity[148]. If for example an ultrasensitivity with a Hill coefficient of 2 is assumed at each level, the overall sensitivity of the MAPK cascade will be 8[148,149]. The MAPK cascade can thus convert graded inputs into switch-like outputs.

1.3.3 Feedback loops dictate response dynamics

The MAPK signalling system is a cascade of multi phosphorylation cycles, each with the potential to respond to a number of allosteric stimuli. It therefore can be subjected to a high degree of regulation and flexibility[150,150]. The most fundamental control mechanism in such signalling processes is the notion of feedbacks. In feedback regulation, the information about a process influences the process itself[151]. Feedbacks have been used in human-made systems[151], like float regulators for water clocks or feedback amplifiers in electrical circuits[152] and are widely used in metabolic pathways[153], gene regulatory networks, and signalling networks[136]. In signalling systems positive feedbacks amplify a signal whereas negative feedbacks attenuate the signal. The wiring of these feedbacks in the MAPK cascade can modulate the temporal response to a stimulus and therefore cause a transient adaptive response or a switch-like response from one morphological state to another.

Negative feedback loops produce adaptation and robustness to variations of the components involved in the feedback loop and are therefore thought to stabilize the MAPK cascade output, and to dampen noise[154]. Becsksei and Serrano demonstrated this the first time by quantifying a two-fold gain in stability in a negative feedback regulated gene circuit[155]. Negative feedback loops play an important role in regulating growth and cell differentiation and disturbing this regulation can lead to cancer. The tumor suppressor p53 for example, which is one of the most frequent targets mutated in cancer, is regulated by a negative feedback. In this loop p53 activity is inhibited by Mdm2, whose transcription is activated by

p53 itself[156].

Feedback loops dictate dynamics of network components, which in turn determine the genotypic and phenotypic responses of a cell. Responses like cell proliferation and differentiation are both initiated by growth factors and processed by ERK-signalling. It was shown that these different phenotypic response types are dependent on the temporal response of the ERK signal[7], which in turn is dictated by different feedback topologies. On EGF stimulation of PC-12 cells, the MAPK network exhibits negative feedback, resulting in a transient ERK response and proliferation, whereas on NGF stimulation it exhibits a positive feedback leading to a sustained ERK activity and differentiation[131,157]. The temporal response of a signalling cascade controlled by a strong negative feedback is characterized by a short burst in output, which is rapidly downregulated to basal signalling levels[140] (Fig. 1.10). A less strong negative feedback control will also downregulate the initial strong output, however, not completely, resulting in a plateau of continuous cascade-output. Above a certain threshold strength this feedback can also induce damped or sustained oscillations and thereby destabilize the system[158].

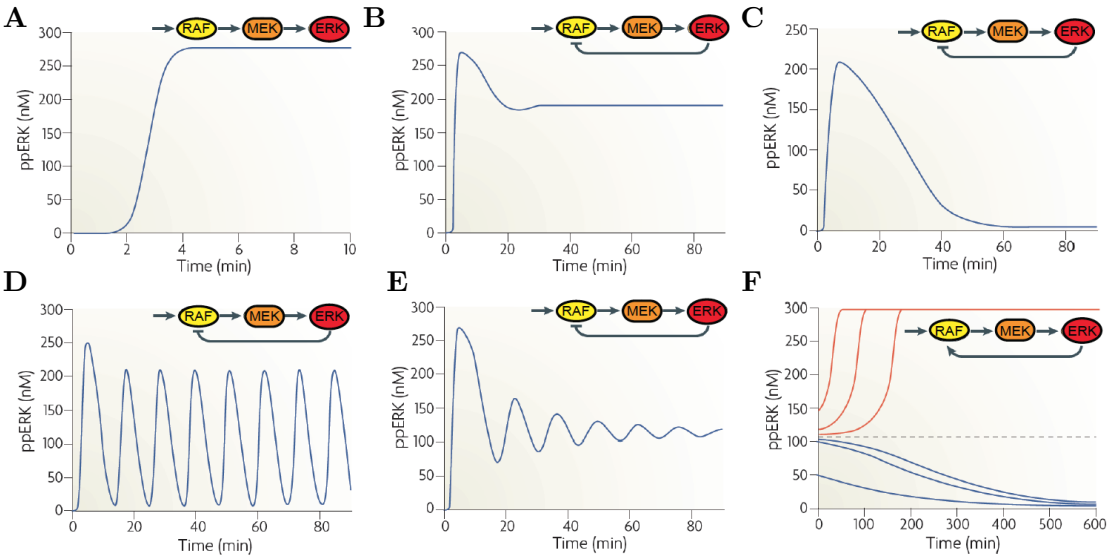

Fig. 1.10: How feedback mechanisms modulate MAPK dynamics. Temporal ppERK response in the three-tiered MAPK cascade Raf-Mek-ERK regulated by feedbacks from ERK to Raf. **(A)** No feedback regulation. **(B)** Negative feedback from ERK to Raf with modest strength causing sustained ERK activity. **(C)** Strong negative feedback from ERK to Raf causing transient ppERK response. **(D)**, **(E)** Negative feedback producing sustained or damped sustained oscillations. **(F)** Positive feedback leads either to a low activity (blue lines) or high activity state (red lines) depending on the pre-existing activity in the cascade. Geometrical symbols as in Fig. 1.1. Adapted from[10].

Oscillations in MAPK activity were predicted to result from negative feedback control by Kholodenko[158]. He calculated the period of oscillations to be about 20 min exhibiting a general range of 2-100 min. Experimental validation revealed oscillations in ERK activity[159] and in the shuttling from the cytoplasm to the nucleus[160], which were caused by a negative feedback from ERK to the cascade input and SOS. Oscillations maintained by negative feedbacks have been suggested

to function as molecular clocks, to cause mitotic oscillations and to set the circadian clock[158]. Oscillatory dynamics have also been shown to be generated by positive feedbacks, but typically they require combinations of positive and negative feedback loops with time delays[151,161]. These delays can be caused by processes like protein degradation, translocation and molecular diffusion in the cell.

Positive feedback loops alone cause instability. But how and on which level does the inherent instability of a positive feedback contribute to signalling? Both, signalling cascades and the network motifs discussed above have the same property of reversibility. Protein phosphorylation occurs in a timescale of seconds and minutes and proteins can rest for hours. The question how usage of these reversible cycles can regulate and generate an irreversible biological transition was already addressed more than 50 years ago by Monod and Jacob[162]. They proposed that irreversibility could be achieved by specific wiring of regulatory systems and the usage of feedbacks. Furthermore, it was proposed, that this theoretically could be achieved by the design of a "switch", based on an intermolecular auto-phosphorylating kinase, which once activated would maintain its own phosphorylation[163]. Indeed, this bistable property has subsequently been experimentally observed in the activation-deactivation cycle of EGFR[164].

These ideas of Monod and Jacob were confirmed at cellular levels by Ferrell and coworkers[165,166]. They demonstrated that the bistability that is required for an irreversible biological transition, the maturation of *Xenopus* oocytes, can be generated by positive feedback loops can generate the. Oocytes convert a graded, reversible stimulus of the hormone progesterone into an all-or-none, irreversible cell fate decision with a Hill coefficient of at least 35. This conversion is enabled by two properties in the MAPK cascade. First of all, the MAPK cascade itself generates ultrasensitivity, which to some extend arises from a two-step non-processive dual phosphorylation activation of the p42 MAPK[167,168]. This property establishes a threshold for the activation of the second property, a positive feedback where p42 MAPK stimulates the accumulation of its upstream activator Mos[169,170]. This ensures that the oocytes cannot rest in a state with intermediate MAPK phosphorylation but only can switch between two states.

Positive feedback loops in general do not inevitably generate irreversibility. Depending on their strength they can theoretically modulate the steepness of an input-output relationship. As the strength of the feedback increases, the Hill coefficient of the dose-response curve increases. At a certain input strength the curve splits into two and the system becomes bistable for certain stimulus values. (Fig. 1.11). However, this dose-response relationship still shows reversibility. This curve can rather be conceptualized as a loop, which is described as hysteresis. This means that depending on whether the system begins in the off (low) state or on (high) state the dose-response relationship shows different behaviour. The dose required to activate the system is different than the dose that is required to maintain the system in its on state[166,171]. Theoretically, bistable systems can toggle between two distinct steady states but cannot rest in intermediate states (Fig. 1.11). As the strength of the feedback further increases it can become strong enough to lock in the on state once activated. At this point the bistable system

becomes irreversible.

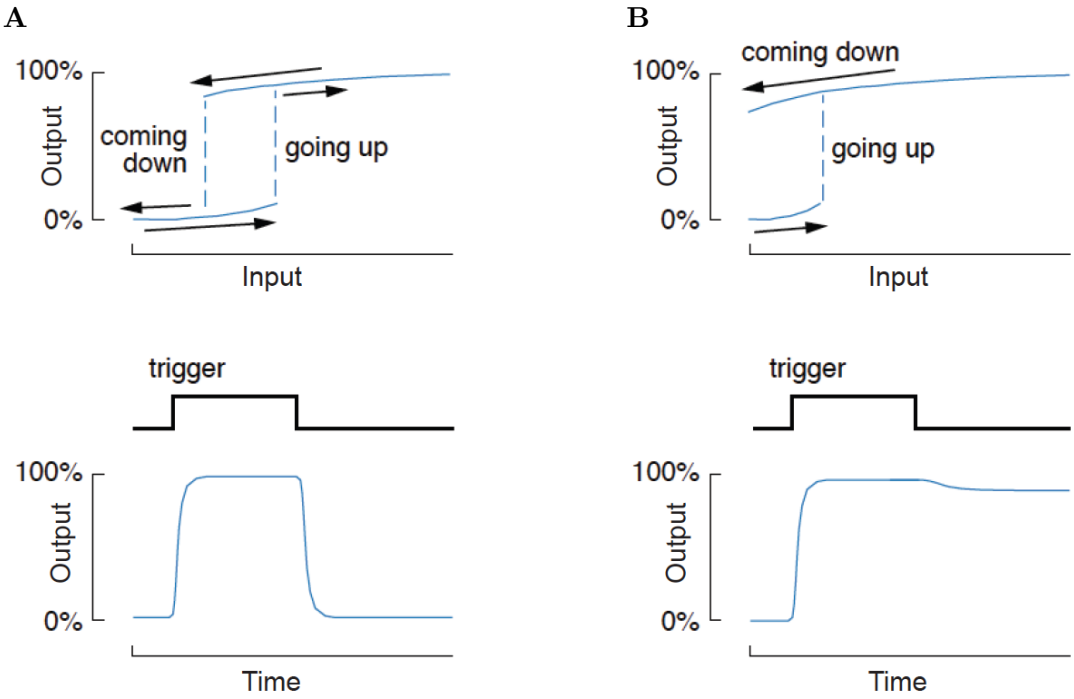

Fig. 1.11: Bistable signalling circuits. (A) Upper: Dose-response in a reversible bistable signalling circuit showing hysteresis. Lower: Temporal dynamics in the same. **(B)** Upper: Dose-response in an irreversible bistable signalling circuit. Lower: Temporal response of the same. Adapted from[166].

Bistable response properties can also arise from double negative feedback loops, as shown in an engineered artificial gene regulatory system in *E. coli*[172]. In this system two repressors are arranged to repress the transcription of each other, and one repressor additionally represses the expression of the reporter GFP. This system shows a switch-like expression of GFP once the concentration threshold of the trigger of this repressor is exceeded.

1.3.4 Spatial dimension of signalling

Dynamic behaviour in signalling is regulated in time by feedback mechanisms but can also be controlled in space, by the spatial organization of signalling components within the cell. Activation and signalling via cell surface receptors, like the receptor tyrosine kinases (RTK) is initiated and maintained via spatial control and different properties of spatial compartments. RTKs are activated at the PM via growth factor binding. This promotes their dimerization and oligomerization and enables their phosphorylation and activation via intrinsic RTK activity[173,174]. This oligomerization can even happen in the absence of ligand. In cells expressing a moderate number of receptors, like COS7 or BAF/3 cells, the degree of receptor oligomerization is low and can be controlled by counter acting phosphatase activity[164,175]. But once the receptor is activated the balance of phosphatase-kinase is shifted in favour of the kinase, and it remains in an on state. Its activity can only be controlled by spatial control, by removing active EGFR from the PM via

endocytosis and targeting it for degradation.

In cancer cells EGFR is highly expressed, which increases the degree of receptor oligomerization, thereby increasing the basal activity and the sensitivity of receptor signalling[176]. The basal activity of RTKs and its activation efficiency mainly depends on its localization at the PM. Here, the likelihood of RTK self-association is order of magnitude higher than in the cytoplasm and a change in concentration can therefore have a much bigger impact[177].

1.3.5 Localization of signalling molecules determines the response

The spatial relocalization of signalling molecules to the membrane is a key mechanism in switching on signalling pathways[178]. Their recruitment to the activated receptor reduces the diffusible space from the three dimensional cytosol to the two dimensional PM[179]. This dimensionality reduction of the signalling space, first described by Adam and Delbrück, dramatically increases the concentration of these signalling molecules and their collision frequency[180]. In EGFR signalling, Ras-mediated dimensionality reduction enhances the interaction of cytoplasmic BRaf with Ras and the following conformational change favours the asymmetric BRaf dimerization[181]. The function of membrane recruitment is therefor to enhance the number of signalling complexes and the extent of downstream signalling[178]. The localization of molecules in different subcellular regions can determine the signalling output by orienting broad unspecific enzymes to specific targets. For example in the case of the Raf-Mek-ERK cascade, the sensitivity to input and the duration of Mek and ERK activity differs with its localization[182]. At the PM the threshold for activation is low and Mek and ERK phosphorylation remains for about 2 h, whereas when targeted to the cytosol, the activation looses sensitivity and Mek and ERK show phosphorylation only up to 30 min post stimulation.

Furthermore, in the response to Ca^{2+} for example, Ras is positively regulated by its GEF RasGRP1 at the Golgi, whereas Ras at the PM is negatively regulated via the GAP CAPRI[183]. These examples clearly show that localization of signalling components in the cell can determine function and causality in the network

1.3.6 Gradients in signalling

The spatial segregation of two counteracting signalling components, like an activating protein kinase and a deactivating phosphatase, can generate an activity gradient. Gradients of signalling molecules maintain signalling around cellular structures thereby providing positional cues for physiological processes, directing morphogenesis and generating biological patterns. The polymerization of microtubules which organizes these processes, for instance, is regulated by the stathmin-oncoprotein 18 amongst other destabilizing factors.[184]. By using a Förster resonance energy transfer (FRET) biosensor to measure the interaction of Stathmin with tubulin, phosphorylation gradients of Stathmin could be observed the first time and were shown to be essential for correct spindle assembly[185]. Using the

same, a gradient of Ran-GTP was visualized in mitotic *Xenopus* egg extracts and revealed to be required for the assembly and the maintenance of spindle structures as well[186].

Most signal transmitters like protein kinases are activated at the cell membrane and then translocate through the cytoplasm to cytosolic structures or to the nucleus[187]. On their way they are dephosphorylated by freely diffusing cytosolic phosphatases, which generate a gradient of the phosphoform emanating from the membrane. The form of a possible phosphoprotein gradient was estimated by Kholodenko for the first time[188]. Based on a simple protein-modification cycle and provided that the dephosphorylation reaction is far from saturation, the phosphorylated fraction decays roughly exponentially with distance from the membrane[187]. This decay, and therefore the shape of the gradient, strongly depends on the kinase and phosphatase activity (k) and the diffusivity of the phosphoprotein (D). Changes in the gradient become noticeable only in the periphery of the membrane (Fig. 1.12A).

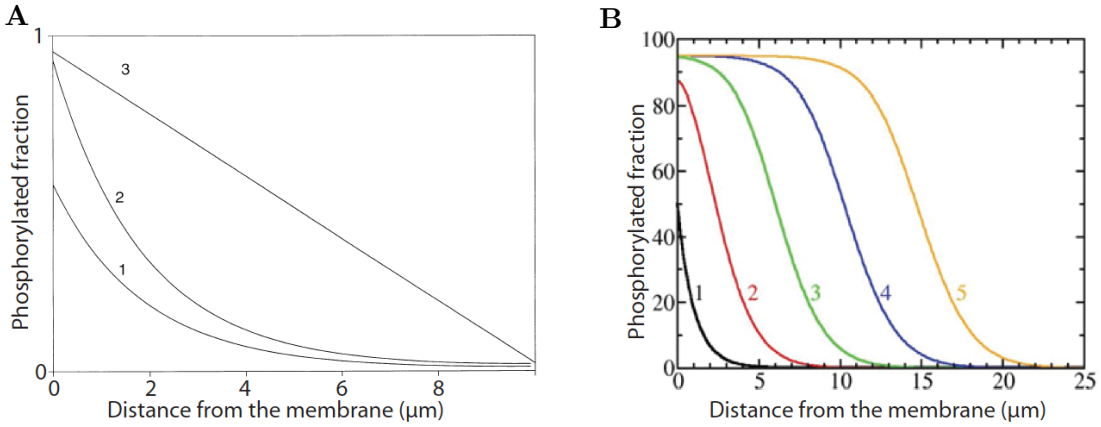

Fig. 1.12: Spatial distribution of phosphorylated proteins. (A) Curves show the decrease in phosphorylation with the distance from the plasma membrane into the cell with a radius of 10 µm. Phosphatase activity is $k_P = 2\ s^{-1}$ and the diffusion coefficient of the phosphoprotein is $D = 5*10^{-8}\ cm^2/s$. Kinase activity in curve 1 and 2 is $k_{kin} = 1$ and $10\ s^{-1}$. Curve 3 represents the situation where the kinase is located at the membrane and the phosphatase at an internal membrane. Adapted from[188]. **(B)** Phosphorylation gradient of consecutive active levels of a five-kinase cascade. Numbers represent the number of levels. Diffusion coefficient is $D = 1\ \mu m^2/s$ and the ratio of k_{kin} to k_P is 0.05. Adapted from[187].

However, this precipitous gradient organization has a limited range of signalling. Several mechanism for long-range signalling have been proposed, like the spatial distribution of signalling cascades[189]. Here, the activated kinase of the first level diffuses inside the cell and serves as an activator for the next level (Fig. 1.12B). The range of the gradient signalling can be modulated by the number of levels in the cascade[140].

The shape of the activity gradient of a signalling molecule in a cell is mainly dependent on the systems response dynamics, which in turn are regulated by the feedback architecture of the protein network. Neves *et al.* reported that gradients of active cAMP and PKA get more precipitous and locally confined by negative feedback loops[190]. In relation to this, it was proposed by Kholodenko, that it is the

ultrasensitive responses that may generate precipitous, short-length gradients, whereas a linear response would generate shallow gradients[140].

1.3.7 Scaffold proteins: hubs for spatial and temporal control

The basis for spatial activity gradients is the signal-dependent localization of signalling protein complexes to the PM, which can either be accomplished by anchoring subunits or by tethering them to scaffolds proteins. Aside from localization, the physical assembly on scaffolds can generate diverse properties by insulating signalling modules or the direction of feedback regulation. These scaffolding functions shape the signalling response in concert.

The simplest function of a scaffold is the tethering of signalling molecules. This can increase the "effective concentration", the probability of interaction of enzymes with their substrates, by decreasing the translational and rotational entropy (Fig. 1.13A)[191,192]. The amount of interacting scaffolded components can therefore theoretically be increased by upregulating the scaffold abundance. However, at high scaffold concentrations single interaction partners might be bound in separate complexes[193], an effect which is called "combinatorial inhibition" (Fig. 1.13B). Whenever a scaffold binds to two or more signalling proteins to form a complex, increasing the concentration of one binding partner will decrease the equilibrium level of the whole scaffolded complex. The mammalian scaffold KSR (kinase suppressor of Ras) shows this biphasic effect: at low levels of expression it strengthens Ras signalling, whereas at high levels it attenuates the signalling[194]. Thus, scaffold mediated signalling is a question of balance[195].

Multiple stages in signal transduction can have the general function of amplification. In theory, a single signalling molecule at a given stage can transmit the signal to several others of the next stage and so forth. Tethering a cascade to a scaffold reduces this amplification substantially (Fig. 1.13C). Scaffold-mediated signalling, however, can be enhanced by scaffold mediated allosteric mechanisms. The mammalian scaffold KSR, for example, triggers Raf activation by promoting its side-to-side dimerization[196].

In Raf-Mek-ERK signalling, two distinct scaffold proteins modulate the response of the cascade in time and space, β–arrestin and KSR[192]. KSR mediates a rapid and transient ERK activation and allows its nuclear translocation, whereas β–arrestin extends ERK activation and confines signalling to the cytosol[10,197]. In this case the scaffold serves as a kind of "signalling splitter" setting the course of signalling by defining its space.

Scaffold proteins can work as platforms for regulatory control; they can organize circuit relationships like feedbacks between tethered signalling molecules (Fig. 1.13D). The simplest way of wiring pathways is by setting a linear pathway among a set of signalling proteins and thereby insulating them. Scaffolds can also be directly targeted for modification to indirectly activate or inactivate the connected enzymes. For example, the activation of T-cells is mainly triggered by phosphorylation induced assembly of the scaffold proteins LAT and SLP-76 with

Src homology 2 (SH2) domain-containing proteins[198,199].

Do scaffolds impact the dose-response behaviour? Do they make a response more graded or switch-like? Ferrell and Sternberg proposed that scaffolds could prevent ultrasensitive kinase cascades from inducing switch-like responses[193,195]. The non-processive two-step phosphorylation of ERK by Mek[168], which confers ultrasensitivity to the cascade[167], might be converted into a processive mechanism, thus preventing the switch-like response. It was shown that scaffolds could indeed govern the signalling response dynamics by coordinating complex feedback loops (Fig. 1.13E). Feedback phosphorylation of KSR and Raf by active KSR-bound ERK leads to dissociation of Raf from the scaffold and thereby switches off further signalling. Mutation of these feedback sites to non-phosphorylatable alanine changed the transient Mek response to a sustained response[200].

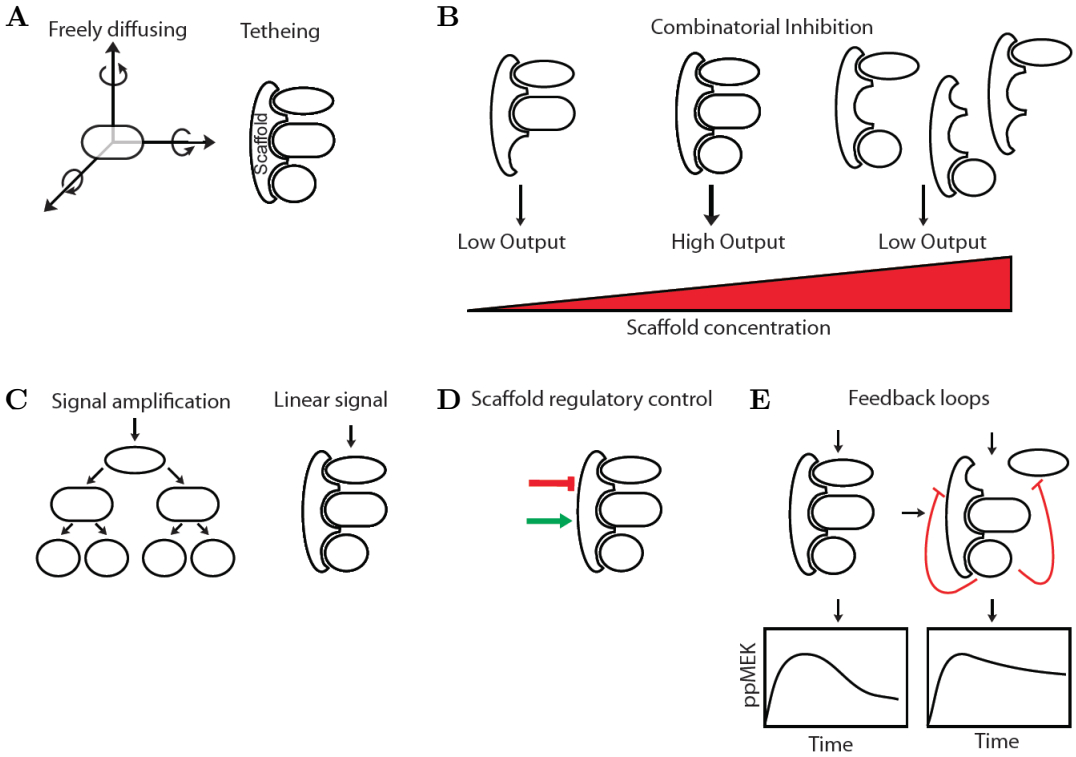

Fig. 1.13: Properties of scaffold mediated signalling. **(A)** Tethering of signalling components to a scaffold decreases translational and rotational entropy. Arrows indicate rotation along the axis. **(B)** Scaffold concentration modulates signalling output and shows an optimum. High concentrations of one component can decrease the output. Slope of the hypotenuse of the right triangle is synonymous with increasing scaffold concentration. **(C)** Scaffolding hinders signal amplification. **(D)** Regulatory mechanisms can directly target the scaffold. Green arrow means activation, red T-bar means inhibition. **(E)** Negative feedback regulates MAPK phosphorylation and signalling by changing binding affinities in the module. Adapted from[192].

1.4 Revealing network topology and how it dictates response dynamics

To understand how cells can quantitatively sense and interpret extracellular signals and convert these into a specific response, it is not sufficient to know about the genes or the proteins in the network, but rather essential to understand how they interact and behave in space and time. This information encodes the dynamic capabilities of a network and thereby its potential function[201]. Revealing the networks structure and its dynamics are the basic concept of systems biology, which is described as understanding biological processes as whole systems instead of as isolated parts[202].

In general a systems biology approach can be described as a loop of computational and experimental steps. First a model of a biological system is created based on experimental knowledge. The model is then tested by predicting a physiological response to a specific dose of genetic or environmental perturbation. This prediction is evaluated experimentally and the new insights obtained are further used to improve the initial model and the predictions.

Many structural characteristics of networks have been identified so far, but in many cases the connections leading to dynamic behaviour still need to be explored. This behaviour can range from simple steady states being robust to minor environmental changes, to switching and multistability or oscillation[203]. It is maintained by network motifs using feedback loops that mediate changes in the activity of the components of the loop. In signalling protein networks, these changes often involve the posttranslational modifications of signalling molecules, mainly phosphorylation. Therefore, the state of a network in terms of the composition of different protein forms can be simply analysed by biochemical approaches like Western blots, or by quantitative mass spectrometry[201]. These approaches can provide quantitative information about dose-dependent or time-dependent responses. Mass spectrometry for example was used to study the *in vivo* phosphoproteom as a function of growth factor stimulation, time and subcellular location[204]. Even though this provides a large proteomic data set, studying network states solely by these approaches cannot provide any information about the dynamics that maintain the a biological state and are required to regulate the transition between two states.

Information about network dynamics can be obtained by deducing the circuitry of a signalling module, like the MAPK cascade, by measuring its single components and by determining how changing the input is correlated with its output[205]. However, this particular reverse engineering problem is hard to solve. Interestingly, a similar complex situation exists in engineering, where the same design principles appear as in signalling network: recurring circuit elements, robustness and modularity[206]. John C. Doyle proposed, that if both systems are well designed in terms of robustness, then the "users are largely unaware of hidden complexities, except through systems failure"[207]. Therefore, a possible approach to experimentally probe the network response is by quantifying changes in protein activity states in response to perturbation of the signalling components. These perturbations might

target the abundance of proteins, their localization or their enzymatic activity. The inhibition of phosphatases in serum-starved cells, for example, leads to a rapid phosphorylation of their substrates without external stimuli, showing that basic reaction cycles generate steady states[208], and that these dynamics can be uncovered by reverse engineering. However, these approaches have several drawbacks. First, cells have to be lysed, which only gives a "snapshot" of the network state[201]. Second, whole cell populations are analysed and effects may be masked by cell-to-cell variability in the cell state and expression levels. Ferrell and co-workers could show, that the variation in the concentrations of progesterone required to "switch on" the MAPK response in oocytes indeed could affect the outcome of the measured dose-response relationship[165]: individual oocytes showed a switch-like response ($n_H \approx 35$) whereas for a group of oocytes a graded response ($n_H \approx 1$) was obtained. In the latter, an actual switch-like response appears to be graded by averaging a population of cells with different responses at different concentrations, exhibiting variable MAPK activity amplitudes.

The ideal conditions for probing network dynamics are provided by live cell imaging using fluorescent microscopy. This approach allows the monitoring of fluorescent protein fusion-variants of signalling proteins, changes of their activity, the formation of protein complexes and of bigger structures like microtubules, in high resolution, in time and space and in intact living cells. Due to the variety of live cell imaging approaches, I would like to focus here on two general concepts which where applied in this thesis and in the publication "A negative feedback in the yeast MAPK module determines where and how to become a shmoo"[209].

1.4.1 Fluorescent sensors – Measuring interactions and activities

Fluorescent sensors are widely used in live cell imaging to monitor changes in the concentration, the activity and the localization of signalling molecules[210]. The first fluorescent sensors were designed to recognize Ca^{2+} levels and applied in monitoring the response of lymphocytes to mitogenic doses of lectins[211,212]. Here, the binding of Ca^{2+} to a simple fluorescent probe like BAPTA, a calcium-chelating aminopolycarboxylic acid changes its emission and excitation spectra in dependence of the Ca^{2+} concentration.

Another class of sensors is based on detecting conformational changes by FRET. This process is a non-radiative transfer of energy by dipole-dipole coupling from a donor fluorophor to an acceptor fluorophor. The first FRET-based sensors were based on fluorescent dyes like fluorescein and rhodamine to monitor cAMP binding to PKA[213]. A further type of FRET sensors is based on genetically encoded fluorescent proteins fused to the proteins of interest (POI) and is frequently used to measure protein-protein interactions or enzyme activities (Fig. 1.14)[214]. These sensors can be also used as activity based sensors to detect conformational changes that result from substrate recognition. Small changes in protein interactions can be measured by sensors as FRET is distance dependent and occurs in a low nm scale (distances within $\approx$ 10nm) of typical protein size[215]. Here, maximal changes in FRET efficiency are achieved when the distance of donor to acceptor is close to the

Förster radius R_0 (distance with 50% FRET efficiency, is typically 4-6 nm for optimized fluorophor pairs)[216]. However, due to the nm-scale-dependency of the FRET efficiency the approach suffers from false negatives[217].

Quantitative imaging of FRET by fluorescence lifetime imaging microscopy (FLIM) can provide quantitative information on the fraction of interacting molecules[218]. This powerful approach was previously used to spatiotemporally quantify the EGFR phosphorylation state[208] and the enzymatic activity of PTP1B. Here, measuring its enzyme-substrate (ES) complex revealed a steady-state ES gradient in the cell.

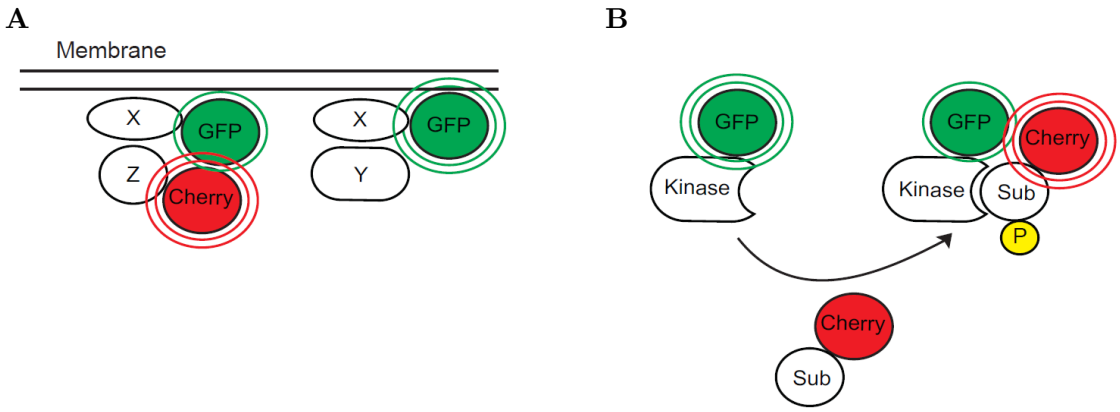

Fig. 1.14: FRET sensors. (A) FRET sensor to measure the interaction of protein X with protein Z. Interaction results in FRET from GFP to Cherry and in increase of Cherry excitation, which is schematically displayed by red rings. **(B)** Enzyme-substrate interaction measured by FRET. Binding of the Cherry-tagged substrate (Sub) enables FRET from GFP to Cherry. Schematic symbols as in A. Adapted from[215].

1.4.2 FCS/FCCS

An alternative approach to quantify protein-protein interactions is given by fluorescence correlation spectroscopy (FCS). In FCS the appearance of a protein of interest (POI) fused to a fluorescent molecule is monitored in a defined volume (Fig. 1.15). Each time this fusion-protein passes the volume it gets excited and emits a burst of photons, which is recorded as function of time resulting in intensity fluctuations. These fluctuations are analysed by temporal autocorrelation. FCS can be applied to locally monitor the concentration of single molecules, their mobility, or the size of a protein complex in a defined small volume of the cell[219]. In fluorescence cross-correlation spectroscopy (FCCS) the intensity fluctuations of two spectrally distinct fluorophors bound to two POIs are recorded simultaneously. If these proteins interact, they pass the excitation volume and emit photons at the same time. Cross-correlation of these two intensity fluctuations gives the degree to which the two fluorescent signals fluctuate at the same time thereby providing the degree of protein-protein interaction and the corresponding affinities of a complex. This method allows high temporal and spatial resolution of dynamic processes, additionally providing information about molecular mobility[220]. Further theoretical and technical details of FCS/FCCS are presented in the methods section 6.2.4.2 - 6.2.4.3.

The general concept of dual colour FCCS was experimentally verified by monitoring the efficiency of tobacco etch virus (TEV) in cleaving a construct consisting of a TEV recognition site flanked by GPF and dsRED domains[221]. Applying this technique enabled the detection of protein-protein interactions of the dimeric complex of Fos and Jun[222] or the measurement of the complex binding stoichiometry of calmodulin (CaM) with CaM-dependent protein kinase II (CaMKII)[223].

As FCS relies on intensity fluctuations of the monitored fluorophor, it is mainly suitable to measure mobile fractions and looses sensitivity when measuring slowly diffusing proteins. It thus limits the area of application mainly to the cytoplasm. However, as the structure of the cell membrane is very dynamic and dependent on its constitution and phase behaviour, FCS measurements at the PM can be feasible[224,225]. Furthermore, in-cell measurements exhibit a low signal-to-noise ratio due to the high cytosolic auto fluorescence that results in noise. This noise has a large influence and is particularly an issue for FCS, since the measurements require extremely diluted fluorescent molecules giving only a low signal. On the other hand low expression levels are advantageous in measuring interaction by FCCS, as higher expression levels come at the cost of affecting protein-protein interactions, which is an advantage over FRET measurements. Furthermore, the distance between the fluorophors to be detected does not play a role, which minimizes false negative results and simplifies the design and the construction of the fluorescent protein fusions. However, monitoring a protein interaction via FCCS can give false positive: two proteins can interact indirectly via a third protein or appear in the same complex, which still will give a signal in FCCS.

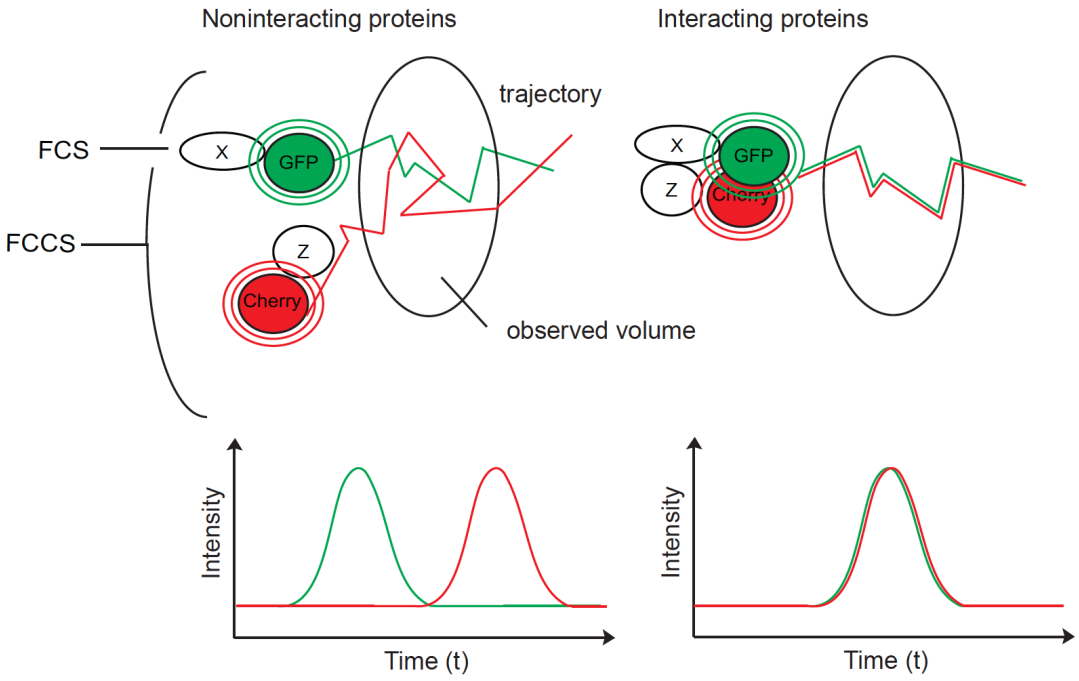

Fig. 1.15: Principles of FCS/FCCS. In FCS a POI fused to GFP is observed in a defined volume, whereas in FCCS two POI fused to GFP and Cherry are monitored. Non-interacting proteins exhibit different trajectories whereas interacting proteins will show the same trajectory. The non-interacting POI fluorescent-fusions emit photons at different time

points, which is represented by two time-shifted intensity peaks. The interacting proteins in contrast emit photons at the same time, represented by two overlapping peaks. This difference can by cross-correlating the traces. Green and red rings indicate emission of photons. Green and red lines represent the trajectories of the two fluorescent species.

1.4.3 Untangling the signalling wires - Network reconstruction

Biochemical approaches, mass spectrometry and live cell imaging can reveal the network structure and individual network motifs, but to understand the whole picture of the network architecture one needs to apply computational modelling based on mathematics and statistics. A mathematical model consists of a set of rules and the corresponding parameters[226]. This could be the phosphorylation status of a protein and the corresponding rate constants describing de/phosphorylation. Some mathematical modelling approaches define these rules by *a priori* biological understanding and use experimental data to determine the model parameters, which is referred to as regression analysis[226]. Other modelling approaches like the data-driven modelling extract these rules from experimental data, without making any assumptions[227]. In this regard, clustering algorithms have been applied to study genetic-regulatory networks in the yeast *S. cerevisiae.* Here, genes have been identified that are coexpressed with genes of known function, meaning that genes with a similar expression pattern were grouped[228,229]. These clustering/correlation-based approaches can reveal correlations in gene networks, but they are insufficient to determine the network topology.

In contrast, applying perturbations to signalling networks generate causal interference, which can be utilized to infer the directionality between the signalling nodes of a network. Perturbation approaches in network reconstruction are problematic because any perturbation to a protein may propagate throughout the network, therefore causing widespread changes[230]. De La Fuente and co-workers proposed an approach to circumvent this problem[231]. They introduced a weak perturbation to a single gene, instead of drastic perturbations like knockouts, and subsequently monitored the change in gene expression levels in a microarray experiment.

A more general approach, the modular response analysis (MRA) was developed by Kholodenko and applied by Bastiaens and colleagues[232,131]. This was used to resolve causal connections in the Raf-Mek-ERK signalling network depending on the stimulation context. This complex network was simplified to three functional modules, the MAPK/MAPKK/MAPKKK, which were targeted by successive small perturbations using small interfering RNAs (siRNA). The global response, the activity of each module, is measured at steady-state conditions monitoring time-dependent responses. By computing local response coefficients the sensitivity between the modules can be quantified and connections can be revealed. This approach uncovered topological differences in the network architecture depending on the stimulus, where EGF caused a negative feedback and NGF caused a positive feedback. However, chronic perturbations in reverse engineering approaches can

change the signalling network by adaptation, through changes in protein expression levels, for example. A solution for this problem is to use acute perturbations, like small molecule inhibitors that specifically target an enzyme[201].

1.5 Yeast: the ideal model organism for inferring network topology and resulting dynamics

One of the first studies correlating biological function to genetic analysis was the study of double mutants that cause a lethal phenotype only when combined, called "synthetic lethality"[233,234]. This approach was expanded to screens of thousands of genes in yeast, searching for those genes with the same function[235]. This was possible by exploiting the genetic amenability of yeast. It allows the deletion of whole genes and the combination of diverse genetically modified yeast strains by a series of mating and meiotic recombination that can generate haploid double mutants[236]. By revealing the complete sequence of the yeast genome in 1996[237] the repertoire of genetic modification was massively extended. This not only allowed a comprehensive understanding of the cell, but also the accomplishment of more comprehensive studies of network architecture and made yeast a frequently used model organism in systems biology and beyond.

Botstein and Fink highlighted the advantages of yeast by being a microorganism and a eukaryote at the same time[236]. On the one hand, they share the simplicity and rapidity of growth (roughly half as fast as *Escherichia coli*) and the genetic manipulability with bacteria. On the other hand, many fundamental cellular properties are conserved from yeast to higher eukaryotic organisms, like cytoskeletal organization or subcellular organelles. Furthermore, many human genes involved in the development of disease have functional homologues in yeast[238,239].

It is homologous recombination, the integration of heterologous DNA into the yeast genome, that provides yeast with its experimental genetic amenability[240]. Based on this feature, PCR-based methods were developed that enable deletion, replacement or integration of DNA at specific loci in the yeast chromosomes. This was used for selective tagging of genes at both the C and N-terminus[241,242]. By constructing fluorescent fusion-protein-variants of approx. 75% of the yeast proteome it was possible to provide localization information for most of these proteins[243]. Using the genetic amenability of yeast, Fields and Song developed the yeast-two-hybrid system[73] to detect protein-protein interactions, which has been a basis for several screenings of protein interaction networks[244]. These high-throughput methods benefit from a plethora of genetic collections and databases of mutants, deletion variants, and open reading frames tagged for diverse analysis[245].

From a practical point of view, yeast has the big advantage of controlled cultivation, allowing studies of high reproducibility. In addition, most of the laboratories working with yeast use the same reference strain S288c, which provides genetic continuity and comparability[246].

1.5.1 Dynamics and spatiotemporal control in the yeast mating MAPK signalling

Studying the spatial and temporal control of signalling networks in the yeast *Saccharomyces cerevisiae* greatly benefits from the possibility of genetically modifying proteins without changing their expression level. A change in the protein expression level would already perturb a signalling system. Using this genetic amenability, the pheromone-mating pathway in yeast has been extensively studied in the previous decades on a single cell level and population wise.

One of the main questions that has been addressed is how a pheromone gradient is sensed, interpreted and translated into an intracellular response leading to morphological changes.

It was shown by several groups that the kind of morphological response is correlated with the sensed pheromone concentration[247,248]. At low concentrations cells tend to elongate towards a gradient and divide similar to filamentous growth[249], whereas at high concentrations the cells form the typical cone-shaped mating projections[250]. Here, the MAPK Fus3 is responsible for growth arrest and shmoo formation at higher concentration, whereas the elongated cell morphology at lower concentrations is predominately sustained by Kss1 and to a lesser extent by Fus3[247].

The ability to respond differentially to distinct pheromone concentrations was shown to depend on regulatory mechanism such as feedback loops at different steps in signalling. Regulation by these network motifs is what modulates the information content about the pheromone concentration, as describe by Roger Brent[5]. Negative feedbacks are known to increase the signal-to-noise ratio in the output and to reduce the sensitivity of the output to variations. Analysing the cell-to-cell-variation in response to pheromone stimulation revealed that Fus3 suppresses variation upon high pheromone levels[251], indicating prominent negative feedback regulation by Fus3. Indeed, Fus3 was shown to mediate several negative feedbacks mechanisms and regulatory motifs via phosphorylation of different targets (Fig. 1.16)[5,6,130]. It activates the dual-specific phosphatase Msg5, which in turn dephosphorylates Fus3 itself[6,252]. Switching off this negative feedback circuit by deletion of Msg5 diminishes the adaptive response to pheromone[252]. Furthermore, Fus3 negatively regulates Ste5 recruitment to the membrane by upstream-phosphorylation of Sst2[5]. These features are reflected in the temporal Fus3 activation dynamics. The fast, peak-like activation of Fus3, which declines and remains active for longer times, switches to a sustained Fus3 phosphorylation when Fus3 is selectively inhibited[253]. This shows the loss of adaptation mediated by negative feedback regulation[5]. Furthermore, Fus3 negatively regulates the phosphorylation of Kss1 by feedback phosphorylation of Ste7 at several sites[112,130]. Consistently, its deletion leads to a significant increase in Kss1 phosphorylation when stimulated with pheromone[254]. This negative regulation occurs exclusively in the presence of Ste5[255]. This scaffold, which among others was often thought as a passive assembly platform, is the mediator of several regulatory processes and is

essential to precisely tune the input-output relationship. Lim and colleagues revealed that the binding of Ste5 to Fus3 triggers its autophosphorylation[4], which thereby leads to the phosphorylation of several sites on Ste5[6]. This phosphorylation provides stronger Ste5-Fus3 interaction, thereby decreasing the pathway output. Impairing the binding of Fus3 to Ste5, by a Fus3 non-docking mutant of Ste5 (Ste5ND) leads to an overall higher sensitivity to pheromone and to a loss of the switch-like pheromone response[6,247]. The same work shows that the switch-like response comes from a switch-like dissociation of Fus3 from Ste5, initiated by pheromone-induced dephosphorylation of the phosphosites on Ste5 by the phosphatase Ptc1. It is the architecture of the Fus3-Ste5-Ptc1 circuit that generates ultrasensitivity at this level.

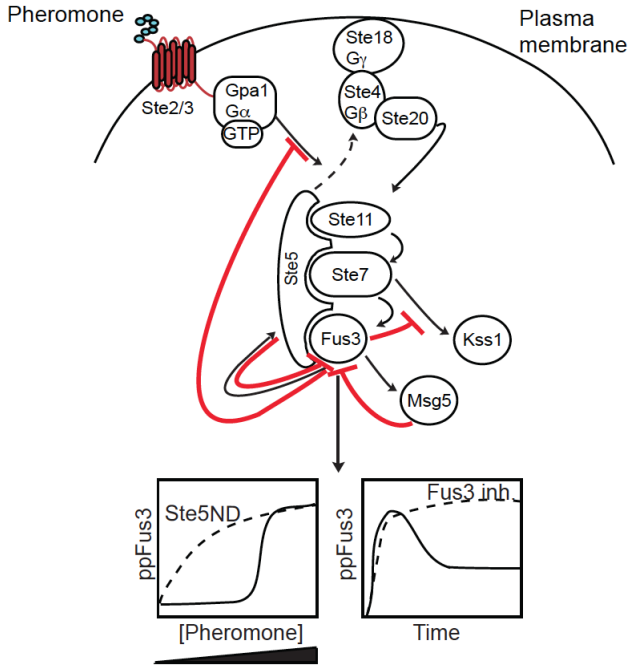

Fig. 1.16: Network topology of the yeast pheromone mating pathway. Fus3 mediates several negative feedbacks and regulatory processes and thereby ensures a switch-like and transient response to pheromone. Perturbing the system by Fus3 inhibition leads to a sustained Fus3 response. Impairing the Ste5-Fus3 binding by a Ste5ND mutant leads to a graded pheromone dose-response. Graphical symbols are the same as in Fig. 1.5. Red T-bar arrow indicates negative regulation. Inh means inhibition.

This switch-like dissociation releases the active Fus3 from the mating module at the PM into the cytoplasm, where it gets uniformly inactivated by the counteracting phosphatases Msg5 and Ptc2/3. Bastiaens and colleagues investigated the distribution of active Fus3 across the cytoplasm by applying FRET-FLIM and revealed a gradient emanating from the tip of the mating projection (Fig. 1.17)[75]. Signalling via the mating pathway is thereby spatially constrained keeping a pool of active Fus3 at the PM for localized activation of its targets.

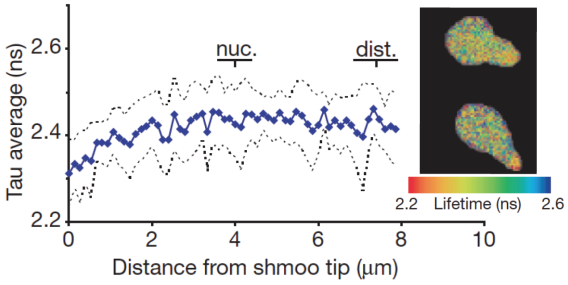

Fig. 1.17: Fus3 activity gradient in stimulated cells. Right: Fluorescence lifetime images with colour code. Adapted and modified from[75].

2 The Rationale and Purpose

The architecture of the yeast mating MAPK signalling network determines the time, the amplitude and the duration of the pheromone mediated signal and ensures a robust response to a defined pheromone concentration. This enables cells to interpret the amount of excreted pheromone by potential mates and thus gauge their distance. A complete mating response only takes place once a certain threshold of pheromone concentration is surpassed thereby protecting against inappropriate and random, energy-consuming attempts to mate. Recent studies revealed a network motif in the MAPK module, which is required for this ultrasensitive response[6]. It arises from the pheromone triggered switch-like dissociation of Fus3 from the scaffold Ste5, which is "negatively recruited" to the scaffold in absence of pheromone. This shows, that the specific assembly of the MAPK cascade Ste11, Ste7, Fus3 on the scaffold protein Ste5 and the dynamic interactions of these components, maintain the appropriate transmission and the processing of the pheromone mating signal, and govern the dynamic properties of the signalling system.

How the MAPK module components interact and how the constitution and the abundances of these complexes change upon pheromone stimulation still remains unsolved and could point at possible regulatory network motifs. These signalling dependent changes in the complex formation within the MAPK were analysed by Maeder *et al.* using dual-colour FCS[75]. Although significant complexes were observed in the cytosol, pheromone stimulation unexpectedly did not change the abundances of these complexes. One reason for this result might be that the formation of the mating signalling complex exclusively occurs at the PM and not in the cytosol as was measured. But most probably the detection of complex changes was not possible due to the restriction of the dual-colour FCS setup to pairwise measurements. These measured concentrations could have been affected by different higher order complexes, which were not detectable, and did therefor not represent exclusively the direct interactions of two proteins.

The main objective of this thesis was to reveal the underlying mating signalling-depended dynamic interactions of all possible MAPK module complexes, to uncover hitherto uncharacterized feedback loops. To enable this, FCS measurements adapted to temporal MAPK dynamics were required, and a theoretical approach to reverse engineering MAPK network architecture.

Using this approach the questions to solve were, which of these motifs are essential to interpret the pheromone concentration to decide when and where to mate? How are differentiation and the resulting morphology influenced by these motifs, and how do these motifs govern the dynamic properties of the signalling system?

3 Results

3.1 The influence of mating signalling on MAPK module abundances

The strength of interactions within the mating MAPK module was shown to have a direct impact on the MAPK signalling dynamics[6,247]. The temporal Fus3 response exhibits a transient adaptive response to pheromone with an initial rapid, high and transient activation declining to a sustained level of lower activity. Its shape, the amplitude and adaptivity[140], is manly dictated by feedback mechanisms arising in the MAPK module, like the negative feedback from Fus3 on Sst2[5], or the "negative recruitment" of Fus3 to Ste5 by auto-activated Fus3[6]. Therefore, measuring changes in the MAPK module concentrations at the different states of the temporal response, at steady state in absence of pheromone, at highest activity and after adaptation, could extract information about how this response is maintained by the MAPK network architecture.

3.1.1 MAPK module complex abundances as measured by FCS show little changes upon pheromone stimulation but high variance

Protein-protein interactions within the mating MAPK module were measured by FCCS, which will be referred as FCS in the following since FCCS is only a dual-colour extension of FCS. For these measurements yeast strains were utilized, each expressing a pair of the MAPK module components as triple fusions of meGFP or mCherry at endogenous levels. Since these kinds of measurements require movement of the proteins, they were obtained in the cytosol of the cell. Confocal microscopy imaging demonstrated in previous work that the MAPK module proteins were predominantly cytosolic in cells with vegetative growth and that after 60 min of pheromone stimulation all components except for Ste11 were enriched at the mating tip[75]. We additionally monitored the localization of 3mCherry fusion variants of all MAPK module components at different times of pheromone stimulation by confocal microscopy. Red fluorescence provides better spectral separation from the cellular autofluorescence, than green fluorescence[214], especially in yeast[256], and a higher signal-to-noise ratio when measuring low abundance cytosolic proteins. All MAPK module proteins were cytosolic in vegetatively growing cells, except for Fus3, which showed a high nuclear fraction (Fig. 3.1). This fraction is threefold higher than in the cytosol[75]. Pheromone stimulation did not change the localization of the MAPKs, whereas the scaffold Ste5 did immediately localize in punctate structures at the PM, which was already observed rudimentarily by others[5,257]. These structures remained randomly distributed at early times of stimulation and then concentrated in a "cap"-like structure at 30 - 60 minutes, marking the origin of shmoo formation. Only then translocation of the MAPKs to PM was detectable.

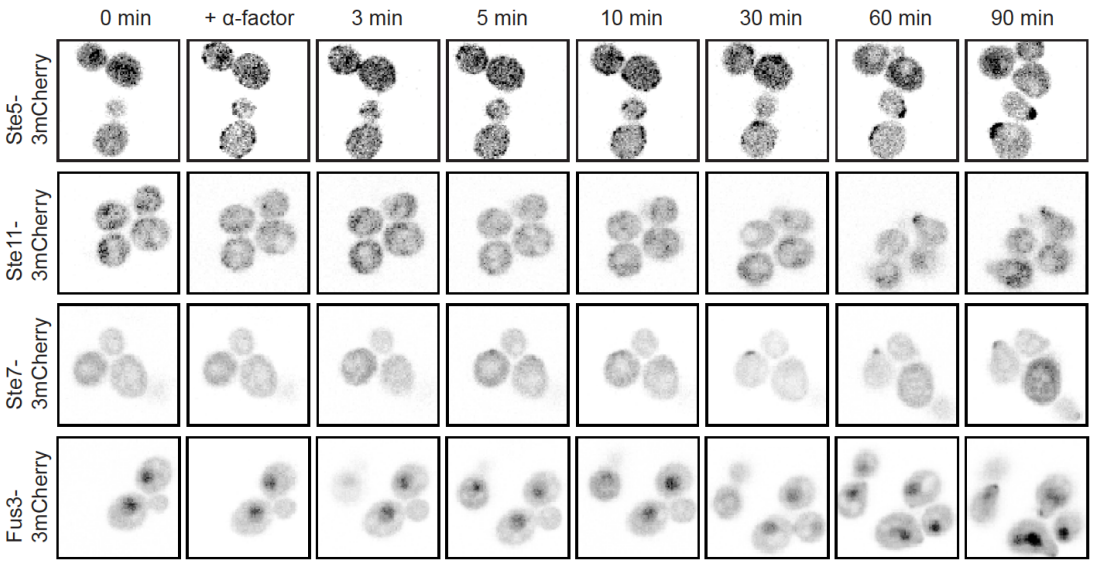

Fig. 3.1: Localization of 3mCherry fusion variants of the MAPK module components in vegetative and pheromone-stimulated cells. Cells were stimulated with 100 nM α-Factor and fluorescent confocal images were acquired at the indicated time points. Cells were immobilized by ConcanavlainA prior to imaging.

FCS measurements were firstly performed in unstimulated vegetative cells, the steady state of which is already determined by a specific feedback topology. Cells were then stimulated with pheromone to a final concentration of 100 nM and measurements were performed at two time points, in contrast to the study of Maeder *et al.*, where stimulated cells were measured after 0 – 60 min of pheromone exposure. First, measurement were performed between 2 – 7 minutes, when phosphorylation of Fus3 is at highest peak, and second at 40 - 60 minutes when the response adapts to a plateau level of lower Fus3 activity. Prior to each measurement, the autofluorescence of cells was measured, and a positive control consisting of a C- and N-terminal double fluorescent fusion variant of Don1 (meGFP-Don1-ymCherry), and a negative control, consisting of a fluorescently tagged non-interacting protein pair were measured (Fig. 8.1). All measurements yielded the total concentrations of the two observed proteins and their complex concentration, which provides a total of four total concentrations (TC) and six complex concentrations (CC) at the indicated time frames (Fig. 3.2). These values are composed of several measurements that are listed in Table 3.1.

Tab. 3.1: Overview of the performed pairwise FCS measurements at different times of stimulation. Measurements were performed in unstimulated, shortly pheromone stimulated (2 – 7 min) and long pheromone stimulated (40 – 60 min) cells at different days and each measurement was performed in a different cell to avoid bleaching effects. The measurements were done in cooperation with Sören Alsleben and Jörn Weisner (both Bachelor students with Dr. Christina-Maria Hecker (2011), Dept. 2).

Pairwise Measurements	Unstimulated cells	Shortly stimulated cells (2 - 7 min)	Long stimulated cells (40 - 60 min)
Ste7 Fus3	99	45	40
Ste11 Fus3	45	47	48
Ste11 Ste7	30	37	35
Ste11 Ste5	99	41	33
Fus3 Ste5	49	46	45
Ste5 Ste7	50	39	35
# Experiments	372	254	236
# Measured values	1216	762	708

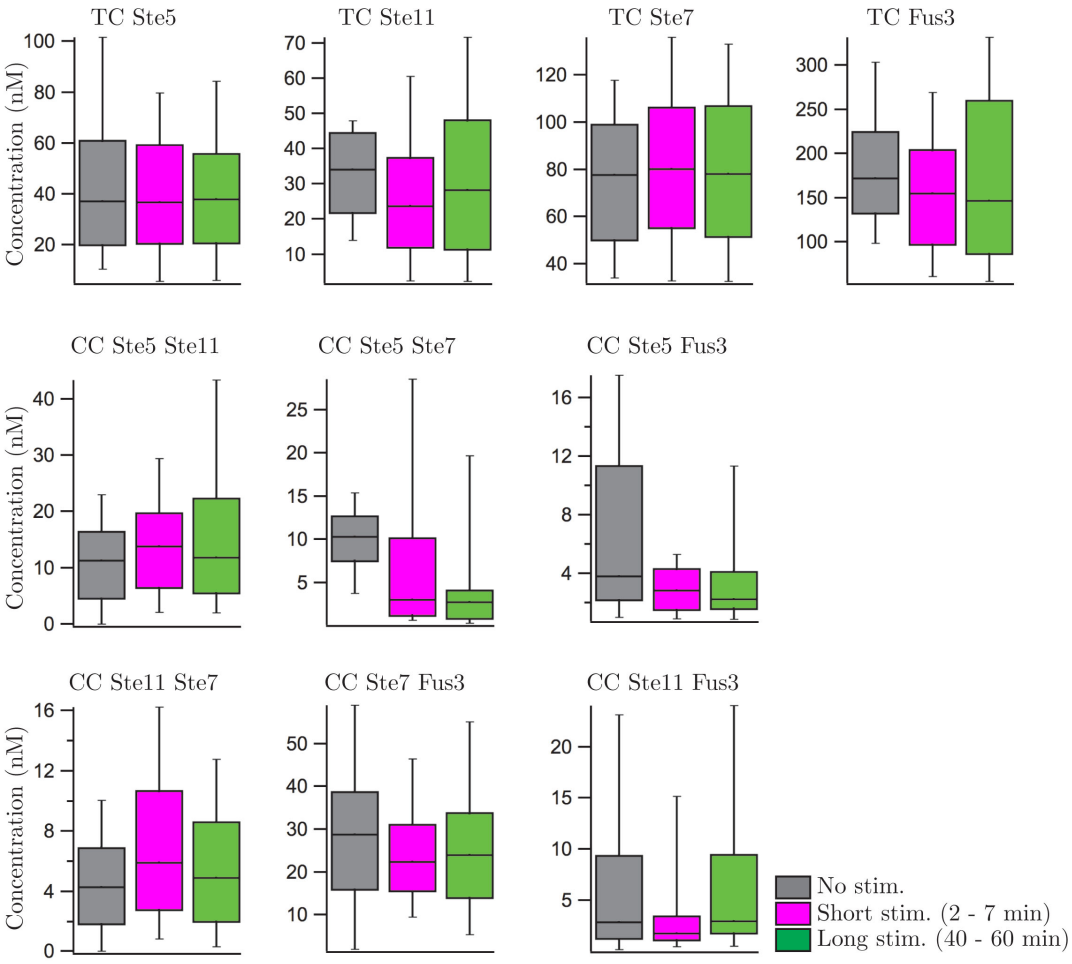

Fig. 3.2: Total (TC) and complex concentrations (CC) of MAPK module components determined by FCS. Fluorescence correlation measurements were performed in the cytosol of unstimulated cells, after short (2 – 7 min) and long stimulation

(4 – 60 min) with 100 nM α-Factor. Box plots depict the mean and the variance of the total (TC) and the six complex (CC) concentrations Ste5, Ste11, Ste7 and Fus3. Error bars indicate the 90/10 percentile. A measured complex is indicated by the nomenclature "Protein Protein", e.g. Ste11 Ste5.

No significant differences were detected in the total concentrations at the different conditions, as was confirmed by a two-tailed Student's *t*-test (Tab. 8.1). However, all measurements showed high cell-to-cell variance, which could have masked effective changes. TCs of the scaffold Ste5 remained stable upon pheromone stimulation at levels around 40 nM. This value is close to Ste5 concentrations of approx. 50 nM measured by Maeder *et al*[75]. The total concentration of Ste11 varied around 30 nM in unstimulated cells and during pheromone stimulation (30 – 40 nM in Maeder *et al.*), although a trend suggested a decrease in concentration at short stimulation times and an increase at longer times of stimulation (*p*-value (SS_Ste11 – LS_Ste11) = 0.01419). Ste7 total concentration ranged at 80 nM (60 – 70 nM in Maeder *et al.*) and was not affected by pheromone stimulation. In case of total Fus3, a similar behaviour to Ste11 was observed. First, at short times of stimulation with highest Fus3 activity levels the concentration appeared to decrease (*p*-value = 0.036), a possible consequence of trafficking of the protein to the nucleus. Moving from short to long times of stimulation the Fus3 concentrations raised again, which could be explained by its redistribution from the nucleus to the cytoplasm and by higher expression of Fus3, which is as a part of the transcriptional mating response. However, these trends could not be confirmed statistically.

The Ste5 Ste11 complex was not significantly influenced by pheromone signalling at all, anyway, the measured concentrations (≈ 10 nM) were consistent with concentrations measured in Maeder *et al.* (≈ 8 nM). In contrast, the complex of Ste5 with Ste7 was reduced significantly with ongoing stimulation. (*p*-value (SS_Ste5Ste7 – LS_Ste5Ste7) = 0.02701). Pheromone mediated dissociation of Ste7 from Ste5 would downregulate the pheromone response, thereby pointing at a possible regulatory mechanism initiated by pheromone stimulation. The complex of Ste5 with Fus3 showed a similar reduction in concentration upon mating pathway activation (*p*-value = 0.001974) and remained at this level with extended stimulation periods. This is in good agreement with the study from Malleshaiah *et al.* showing a rapid switch-like dissociation of Fus3 from Ste5 induced through pheromone signalling[6]. For the complex of Ste11 with Ste7 low concentrations around ≈ 5 nM were measured, which remained unchanged. The same low abundances were observed in Maeder *et al.*. The complex of Ste7 with Fus3 showed the highest abundances (≈ 25 – 30 nM), which also remained unchanged after stimulation. Finally, the Ste11 Fus3 complex concentration decreased upon pheromone stimulation and recovered to initial values at later times. (*p*-value (SS_Ste11Fus3 – LS_Ste11Fus3) = 0.06247).

3.1.2 Extracting information from cell-to-cell variance

All measured concentrations exhibited a high variance that could have arisen from technical issues, like bleaching or movement of the cells, but most probably can be attributed to noise resulting in a high cell-to-cell variance. It was shown that this variation in gene expression could for example emerge from pre-existing variations in the cell-cycle position from single cells at the time of signal induction. Beside this stochastic origins, it can be determined by the capacity of individual cells to transmit signal through the pathway[251] and is therefore not random, but rather deterministic and regulated[258].

Each cell in the measured population has a different gene expression, which produces the high cell-to-cell variance. This also strongly affects the interactions measured by FCS, which are depending on the gene expression of the pairwise measured proteins. Correlation that can be found in these measurements is thereby not because of the measurement itself but carries information about the interaction of the proteins. It therefore can be extracted by investigating the variance in these measurements. To initially test connectivity of the measured concentrations, a correlation analysis identifying interdependence of all measured concentrations was conducted (Fig. 3.3, 8.2).

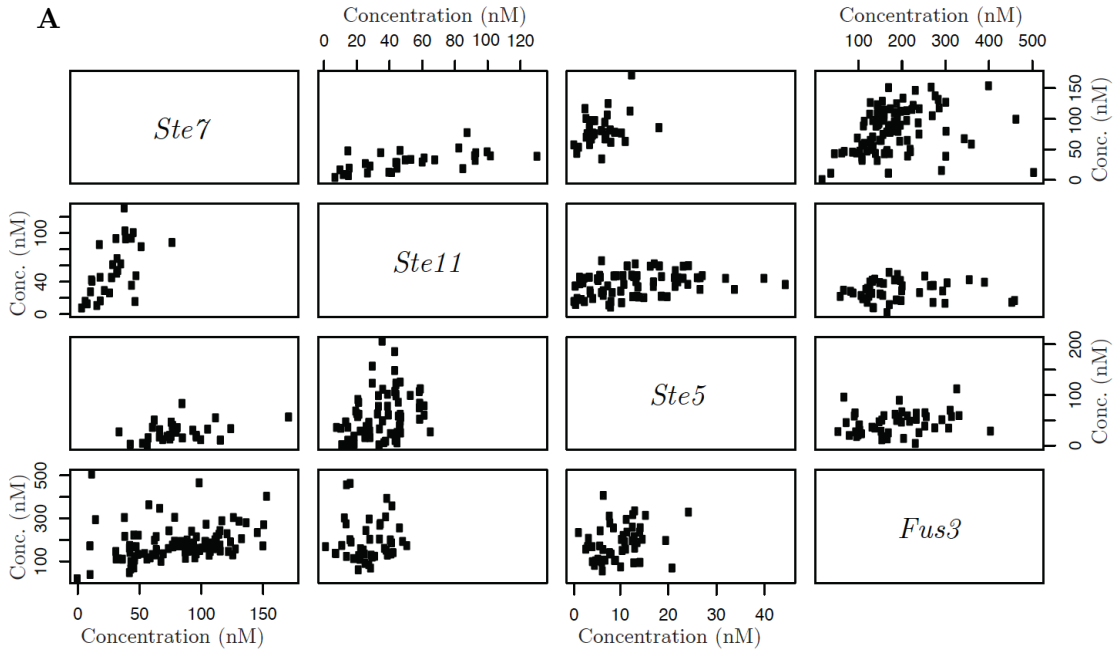

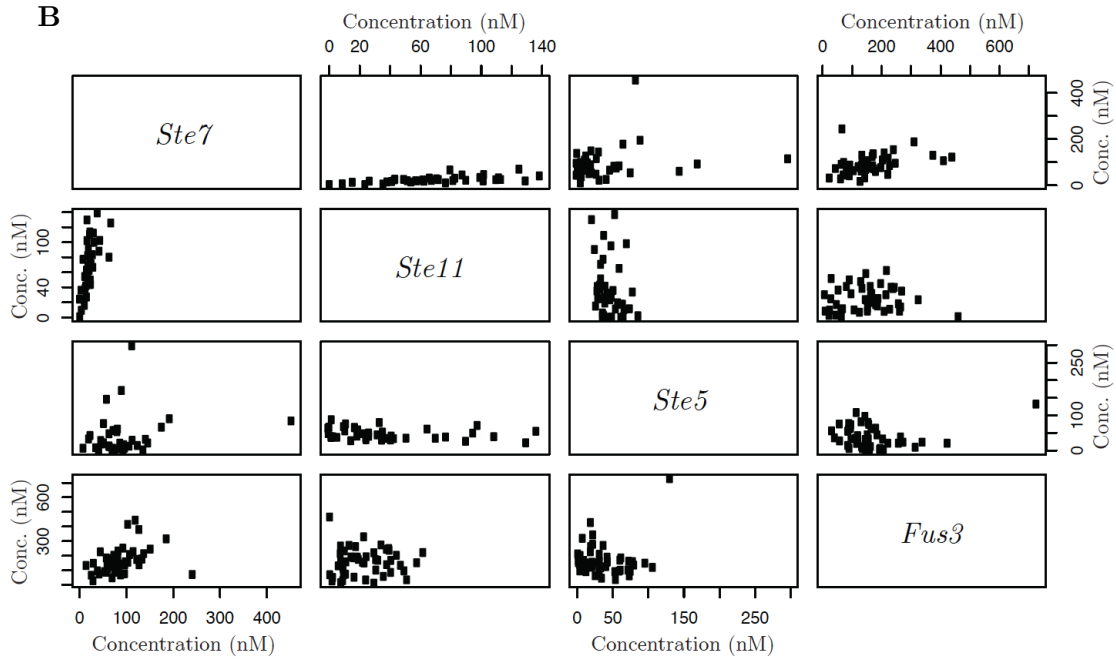

Fig. 3.3: Correlation analysis of the total concentrations of the MAPK module components Ste5, Ste11, Ste7 and Fus3. (A) TC values from measurements in unstimulated vegetative cells. **(B)** TC values from shortly stimulated cells.

Indeed, most of the data sets analysed showed positive or negative association. Ste7 for instance exhibited positive correlation with all components. Interestingly, only some of the concentration relationships were affected by pheromone stimulation. For example, the concentrations of Ste5 and Ste11 in unstimulated cells showed a low positive correlation, which was lost upon mating pathway activation.

3.1.3 Linear regression analysis (LRA) uncovers concentrations of MAPK module protein-species that contribute to mating signalling

3.1.3.1 Principle of LRA

A correlation analysis can only indicate possible relationships and connectivity between components, but is not capable of detecting causal connections and directionality between the elements of a network. Furthermore, due to technical limitations of dual-colour FCS measurements of pairwise interactions it is not possible to resolve direct protein interactions in a complex with more than two components with reasonable certainty. In theory, the four MAPK module components can exist as 15 different protein-species consisting of four unbound monomeric proteins, six dimeric complexes, four trimeric complexes and a tetrameric species of all components. Therefore, measurements of the total concentrations (four in total) coming from the autocorrelation (ACor) values and the complex concentrations (six in total) coming from the cross-correlation (CCor) values always include the influence of different protein-species (Fig. 3.4).

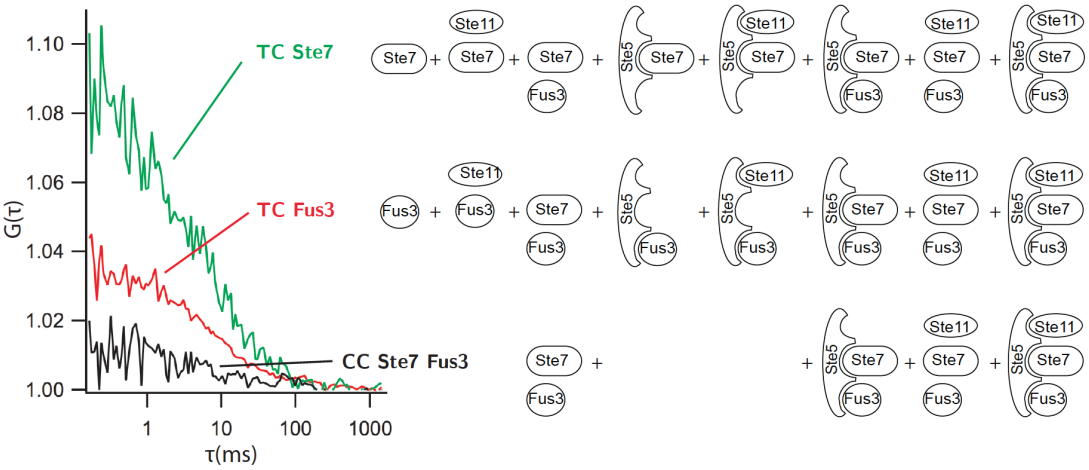

Fig. 3.4: Contributions of MAPK module protein-species to total and complex concentrations of Ste7 and Fus3 obtained by FCS. Autocorrelation (ACor) curve in green belongs to Ste7-3meGFP and in red to Fus3-3mCherry. Black curve shows cross-correlation curve (CCor) of Ste7-3meGFP interacting with Fus3-3mCherry. Geometrical symbols represent the MAPK module components that contribute to the measured TC and CC values.

To resolve the abundances of all possible protein-species from the measured binary interactions, a linear regression analysis (LRA) was approached, where the biological variance determined from multiple FCS experiments was exploited. This analysis was developed in cooperation with Prof. Katja Ickstadt from the faculty of statistics from the TU Dortmund. The linear regression model is based on the assumption of a linear relationship between the observed concentration values and the unknown concentrations of the possible protein-species, providing a set of linear equations (see also 5.2.6.2). The principle can be explained by a matrix X containing the vectors a and b (Fig. 3.5).

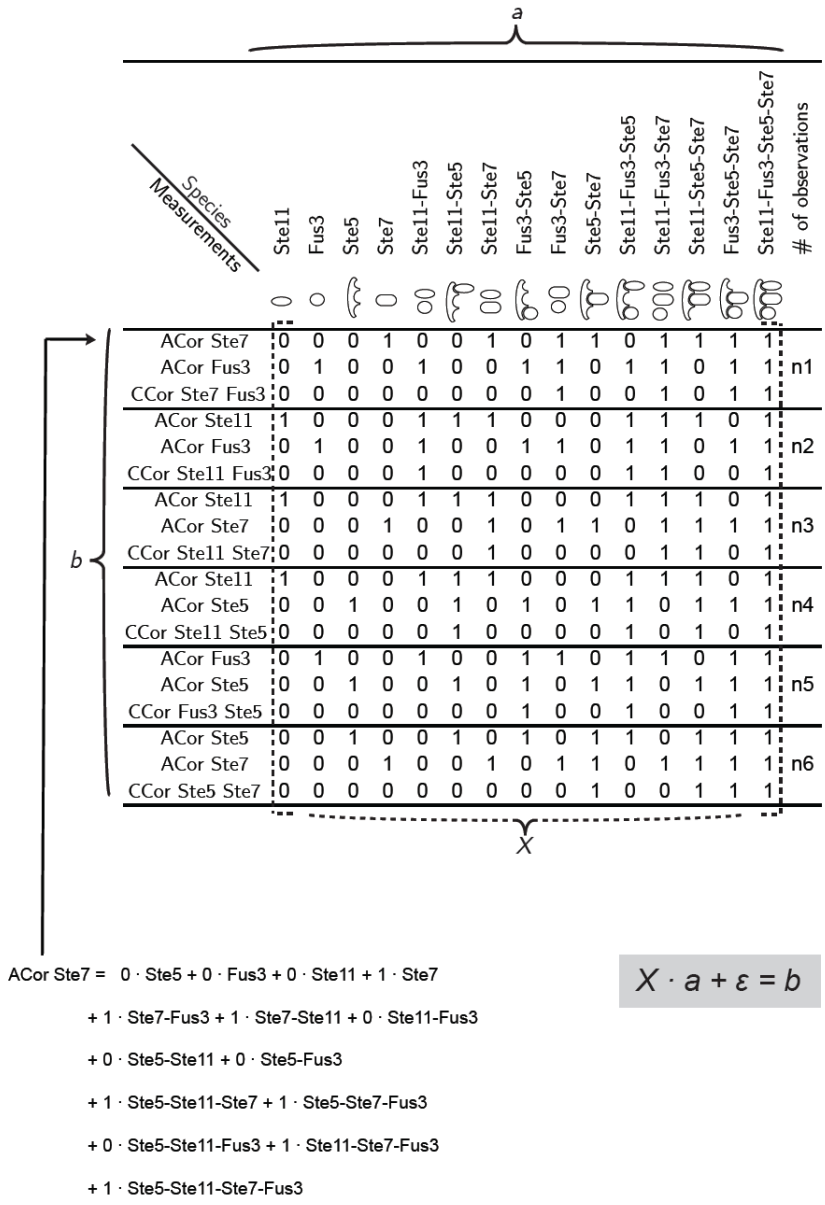

Fig. 3.5: The components of the LRA showing its main principle. *a* represents the vector of the unknown concentrations of the 15 possible protein-species. *b* represents the vector of the observed concentration values. *X* is the design matrix. ε represents measurement uncertainty. Geometrical symbols represent the MAPK module components. For each auto- (ACor) and cross-correlation (CCor) values different species contribute (1 = contribution, 0 = no contribution). Exemplary equation in the lower left shows the species composition of ACor Ste7. The linear equation system is based on the mathematical equation (Matrix equation) in the lower right corner.

By applying this particular linear equation system based on the mathematical equation displayed in Figure 3.5, all different protein-species can be calculated in theory. However, this system constitutes of 15 unknown concentrations (unknowns) but only 10 observed concentration values (equations) thereby posing the problem of an underdetermined system. This ill-posed problem can also be illustrated as a majority of freedom degrees or dimensions (of the domain of a vector) over a minority of constraints, which determine the subspace of a vector. In this case a unique mathematical solution does not exist. However, by approaching the

biological variance in the concentrations of the protein complexes determined from multiple FCS measurements (Tab. 3.1), the best values for a to fit the data were estimated.

3.1.3.2 LRA uncovers concentrations of MAPK module protein-species

This LRA yielded the probability distributions of all 15 protein-species at the different conditions. Both, monomers and dimers showed significant concentrations at all conditions (Fig. 3.6). However, oligomeric complexes were almost not-existent. The majority of the abundances of the monomeric MAPK module components remained stable upon pheromone stimulation with few exceptions (Tab. 8.2). Monomeric Ste11 shows the most significant change in abundances from the unstimulated to the longer stimulated conditions. The two probability distributions showed an overlap of 39 %, meaning that the probability that Ste11 has a higher concentration is 61 %. Monomeric Fus3 concentrations decreased upon pheromone stimulation as was already crudely determined from the raw FCS data (Fig. 3.2). This decrease is probably due to translocation of active Fus3 to the nucleus. Ste5 showed a slight decrease in concentrations at long times of stimulation compared to vegetative cells. Dimeric complexes exhibited the most significant and biggest changes in abundances. Surprisingly, significant concentrations were obtained for the dimer Ste11-Ste7 although its interaction could not be detected in yeast-two-hybrid screens, but which showed that both Ste11 and Ste7 interact with Ste5[2]. Furthermore, Ste11 did show a direct interaction with Fus3 that was not expected, although it was detected by the same study.

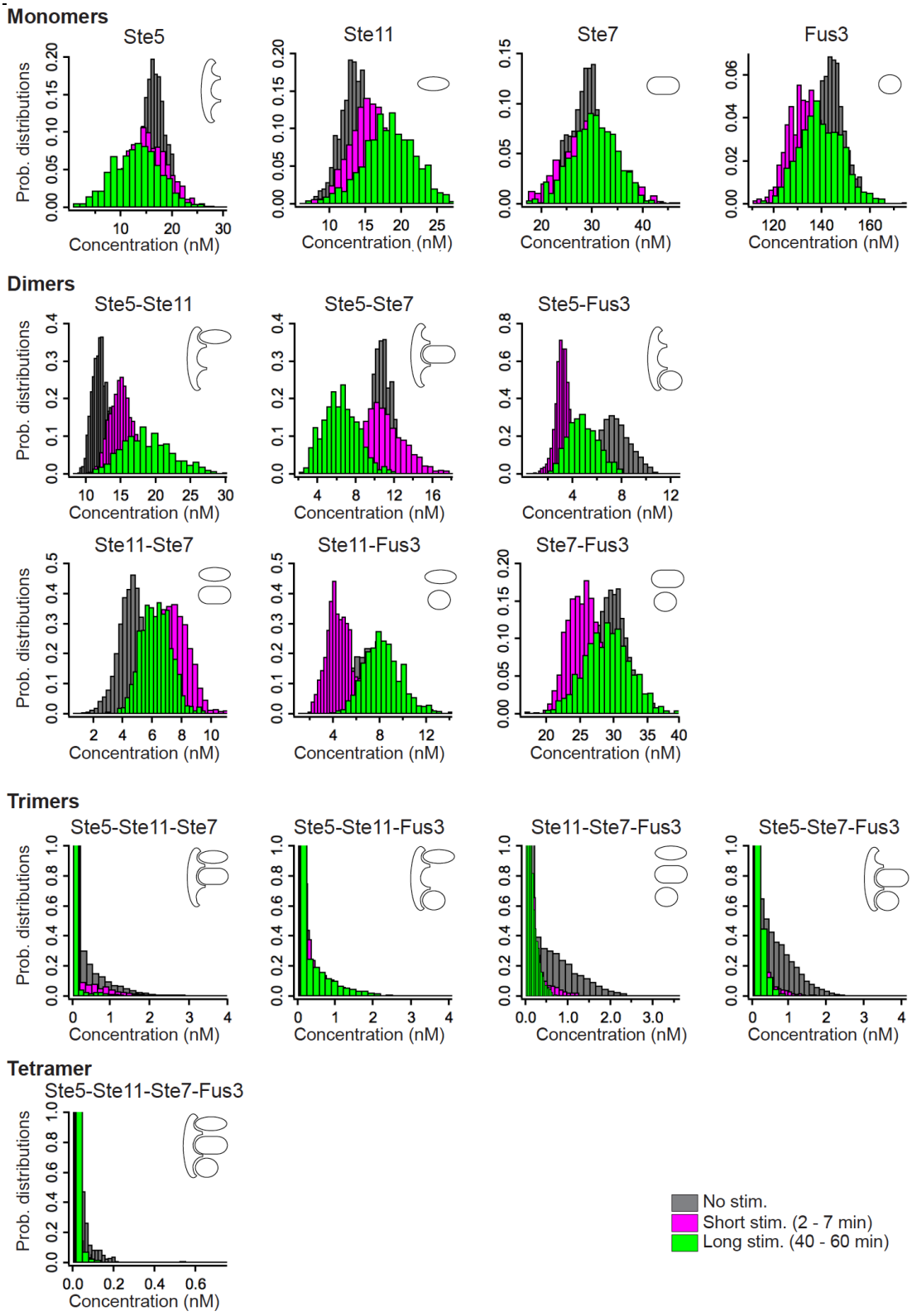

Fig. 3.6: LRA of FCS data yields concentrations of the protein-species in the mating MAPK module. LRA was performed with the FCS data presented in Fig. 3.2. Estimated probability distributions of the concentrations of the 15 different MAPK module protein-species divided in monomers, dimer, trimers and a tetramer at different conditions (indicated by colour code). Geometrical symbols are the same as in Fig. 3.5. This analysis was performed by Jakob Wieczorek from the Faculty of Statistics at the TU Dortmund University.

3.1.3.3 Ste11 interacts with Ste7 via Ste5 - Ste11 directly interacts with Fus3

To identify which of the MAPK complexes are direct interactions and thereby do not depend on the scaffold Ste5, the MAPK complex concentrations were measured by FCS in the corresponding unstimulated Ste5 deletion strains (ΔSte5).

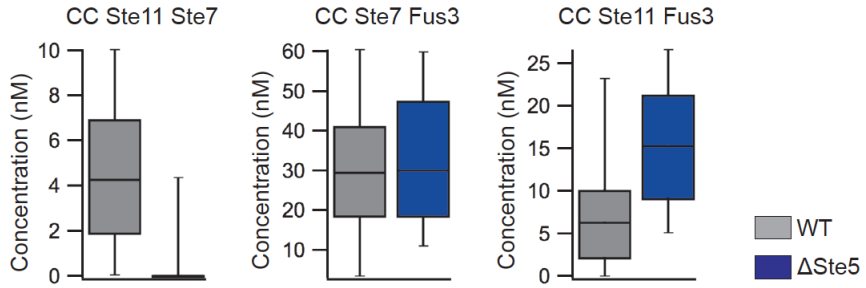

Fig. 3.7: Interactions among the mating MAPK Ste11, Ste7 and Fus3 in ΔSte5 strains. Interactions were measured in WT and ΔSte5 strains by FCS. Box plots depict the mean and the variance of the complex concentrations Ste11 Ste7, Ste7 Fus3 and Ste11 Fus3, error bars indicated the 90/10 percentile. Measurements were performed in unstimulated Ste5 deletions strains (blue) and corresponding WT cells.

The interaction of Ste11 with Ste7 was completely abolished in absence of Ste5, which obviously mediates this interaction (Fig. 3.7). In contrast, Ste5 deletion did not affect the complex of Ste7 with Fus3, which are known to interact via strong docking interactions[78]. Interestingly, the complex of Ste11 with Fus3 was preserved after Ste5 deletion and even exhibited a higher abundance. Linear regression analysis of this FCS data confirmed the absence of the Ste11-Ste7 dimer (Fig. 3.8). It also revealed a higher abundance of the monomeric Ste11, probably due to missing Ste5 tethering. Interestingly, concentrations of the monomeric Fus3 were strongly decreased. This may result from the shutdown of basic signalling levels that regulate Fus3 expression levels[34]. The dimers Ste11-Fus3 and Ste7-Fus3 exhibited an increase in abundance. These interactions compete for Ste5 binding, which contains docking motifs for both Ste7 and Fus[78,260]. In addition to the absence of the Ste11-Ste7 dimer, the LR analysis uncovered the absence of the trimer Ste11-Ste7-Fus3 (Fig. 3.8), which is most probably mediated by Ste5.

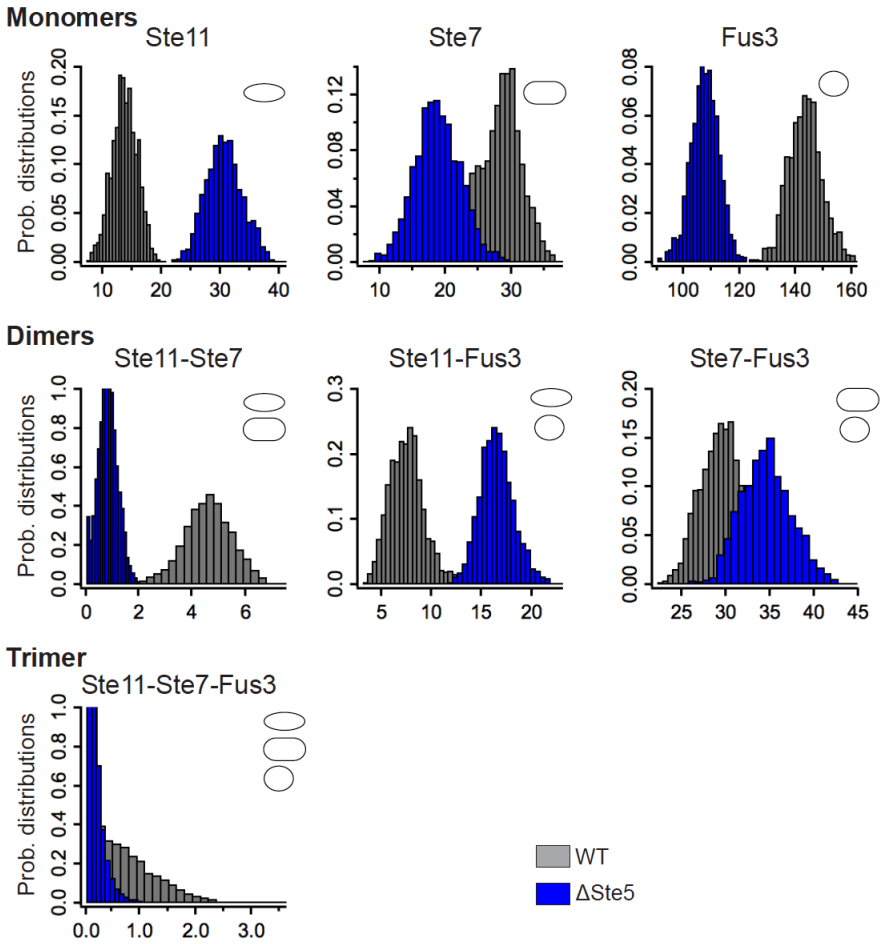

Fig. 3.8: LRA of FCS measurements in ΔSte5 strains. LRA was performed with the FCS data presented in Fig. 3.7. Probability distributions of the concentrations of seven MAPK species independent of Ste5 (blue) at unstimulated conditions, showing monomers, dimers and a single trimer compared to the probability distributions in WT cells (grey). MAPKs are represented by geometrical symbols. The analysis was performed by Jakob Wieczorek from the Faculty of Statistics at the TU Dortmund University.

3.1.3.4 Constrained LRA - Enzyme-substrate complex of Fus3-Ste11

The absence of these two protein-species imposed constraints on the linear regression analysis by excluding the dimer Ste11-Ste7 and the trimer Ste11-Ste7-Fus3 as possible solutions, thereby improving the estimation. The number of possible species was reduced to 13 and therefore the degrees of freedoms from five to three.

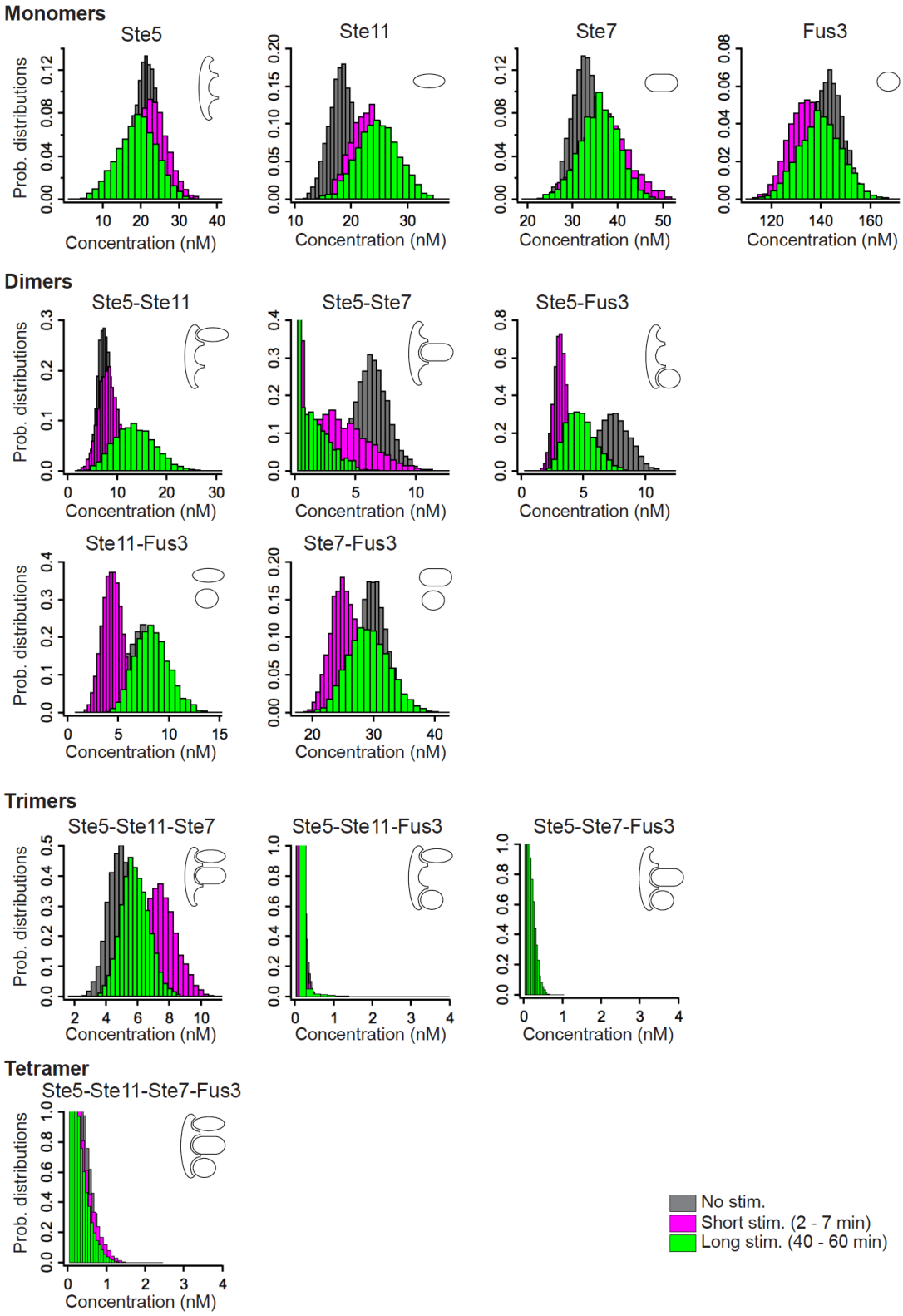

Fig. 3.9: Constrained linear regression analysis of FCS data. FCS data from Fig. 3.2. Constraints are the absence of the dimer Ste11-Ste7 and the trimer Ste11-Ste7-Fus3. Estimated probability distributions of the concentrations of 13 different MAPK module protein-species separated in monomers, dimer, trimers and a tetramer at different conditions (indicated by colour code). Geometrical symbols are the same as in Fig. 3.5. This analysis was performed by Jakob Wieczorek from the Faculty of Statistics at the TU Dortmund University.

The constrained linear regression analysis revealed that the MAPK module components predominantly occurred as unbound monomers or dimeric complexes in the cytoplasm (Fig. 3.9). In comparison to the unconstrained analysis, where higher order complexes were not present, the trimeric species Ste5-Ste11-Ste7 exhibited significant abundances at all conditions. Pheromone stimulation at short times triggered a clear increase in concentration (20 % overlap of prob. distributions, Tab. 8.3), which partially decreased at long-term conditions. This trimer was previously described as a latent platform for allosteric activation of Fus3 at the plasma membrane[67]. Its cytosolic presence in unstimulated cells hints at a preformed activation complex. Its increase in abundance corroborates the proposed pheromone-triggered formation of Ste5-MAPK complexes.

The monomeric Ste11 showed a shift towards higher concentrations upon pheromone stimulation (30 % overlap in prob. distributions), pointing at more freely diffusing Ste11 in the cytosol. The other monomer abundances remained unaffected. The concentrations of the dimers Ste5-Ste11 and St5-Ste7 had overall lower abundances than in the unconstrained analysis. The presence of the Ste5-Ste11 dimer is reduced at long times of stimulation. The complex of Ste5 with Ste7 showed ongoing degradation with duration of mating signalling. This could point at a regulatory mechanism influencing the activation of Fus3 especially at longer times where the system adapts. The dimeric complex Ste5-Fus3 was strongly reduced after stimulation (0.02 % overlap of prob. distributions), in accordance with the switch-like dissociation of Fus3 from Ste5[6]. At longer pheromone stimulation as the system adapts, the complex recovered partially to higher abundances.

Interestingly, the complexes of Fus3 with either Ste11 or Ste7 exhibited a similar temporal probability distribution profile. Both dimeric interactions were initially reduced (20/24 % overlap in prob. distributions) at short times, which then increased at longer times of pheromone signalling. Fus3 was previously shown to control Ste7 mediated cross-activation of the filamentous growth MAPK Kss1 through a feedback mechanism involving the phosphorylation of Ste7 at multiple sites[112,130]. Although Fus3 is not known to phosphorylate Ste11, this similar temporal profile and their direct interaction (Fig. 3.7) led to the assumption of a possible feedback loop from Fus3 on Ste11.

In order to reveal if this complex is enzyme-substrate mediated, the interaction of Ste11 with a catalytically inactive mutant Fus3(T180A/Y182F)[72] was measured. Here, the two phosphorylation sites in the activation loop of the kinase domain were mutated to the non-phosphorylatable alanine and phenylalanine, thus impairing the opening of the activation loop. Upon expression of this mutant the Ste11-Fus3 complex was completely abrogated, which proved the presence of an enzyme-substrate complex (Fig. 3.10). If phosphorylation of Ste11 by Fus3 would change the signalling activity of Ste11, this complex could generate a hitherto uncharacterized feedback from Fus3 to Ste11.

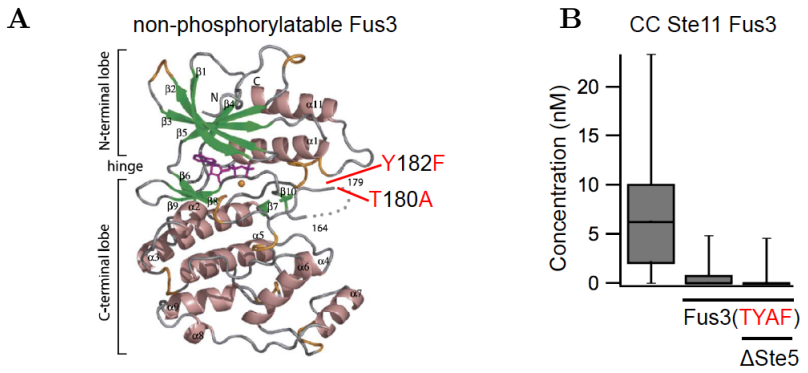

Fig. 3.10: FCS measurements of Ste11 Fus3 interaction. (A) Overall structure of Fus3. Flexible activation loop is represented by dashed-line. Position of the phosphorylation sites is marked with red line. Structure is from[260] **(B)** FCS measurements of the interaction of Ste11 with Fus3 and Fus3(TYAF) in Ste5WT and ΔSte5 strains. The non-phosphorylatable mutations are coloured in red. Box plots represent the mean and the variance of the CC values, Error bars represent the 90/10 percentile.

3.2 Negative feedback from Fus3 on Ste11 determines the signalling response to pheromone

3.2.1 Ste11 signalling activity is regulated via its phosphorylation on S243 by Fus3 and phosphorylation of T596

To investigate if phosphorylation on Ste11 could change its signalling activity, potential phosphorylation sites on Ste11 were analysed based on available literature. Ste11 is phosphorylated at the two serines S302 and S306 and on single threonine T307, but these are controlled by the PAK kinase Ste20[71]. Nevertheless, a recent quantitative phosphoproteomic study compared wild type cells to yeast mutants bearing either a Fus3 or a Ste7 deletion, and revealed several Fus3 dependent potential phosphorylation sites on Ste11 (Tab. 3.2)[261].

Tab. 3.2: Potential phosphorylation sites identified by mass spectrometry in ΔSte7 and ΔFus3 strains. Analysis was performed in unstimulated cells. Data from[261].

Position in Ste11	Phosphorylated in ΔFus3 strain	Phosphorylated in ΔSte7 strain
S243	No	Yes
S485	Yes	No
S616	No	Yes

The sites S243 and S616 did not exhibit a phosphorylation signal in the ΔFus3 strain but did in the ΔSte7 strain. Thus, these sites may already be phosphorylated in vegetative cells by Fus3. In order to identify if the afore listed potential phosphorylation sites on Ste11, S243, S485, S616 affect Ste11 signalling activity, they were replaced by either non-phosphorylatable alanine or phospho-mimicking glutamates and pheromone pathway output was assessed by a Fus1 reporter gene assay[251,262,263]. The expression of Fus1 is regulated by the mating pheromone[88] and it is localized to the shmoo tip (Fig. 3.11) prior to mating to coordinate polarization events required for fusion[264].

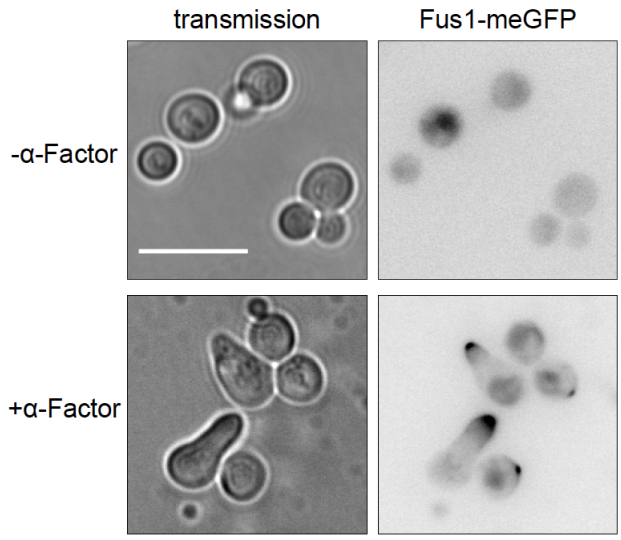

Fig. 3.11: Localization of Fus1 in reporter gene assay. Upper row shows unstimulated cells versus stimulated cells (100 nM α-Factor, 90 min) represented in the lower row. Intensity in GFP channel in unstimulated cells arises from background fluorescence of the cells. Fus1-meGFP is localized to the shmoo tips, or to the place of originating shmoo tips. Scale bar indicates 10 µm and are representative for all images.

The expression of a C-terminally fused meGFP variant of Fus1 was quantified by flow cytometry (See 6.2.5) in WT cells and the Ste11 mutants after stimulation with 1 µM α-Factor as function of time (for 90 min). The output was controlled by a Ste11-4 mutant (Ste11(T596I) which exhibits upregulated pheromone pathway output[262]. This constitutive variant of Ste11, which was identified by exploring suppressors of the deletion of the STE4 gene, was also proven to release autoinhibition of Ste11[71]. Since this site might be targeted by downstream kinases its phospho-mimicking variant was also investigated by quantifying Fus1 expression. All the measured strains had the same background bearing a deletion of the filamentous growth MAPK Kss1, which is supposed to be cross-activated by Ste7 and partially takes over the function of Fus3. This genetic background ensured exclusive activation of mating pheromone signalling.

Wild type cells exhibited very low basal Fus1 expression levels that continuously increased upon pheromone stimulation (Fig. 3.12). Mutations of the S485 site in Ste11 did not influence the Fus1 expression at all, while mutation of S616 resulted in a reduced expression of Fus1 irrespective of the nature of the replaced amino acid. This can be explained by the locality of the amino acid, specifically. This site is within the kinase domain of Ste11, and so may be critical for full Ste11 activity. The Ste11(T596I) mutant showed elevated Fus1 expression levels as expected. However, its phospho-mimic Ste11(T596E) completely abolished the signal, which indicated a possible regulatory mechanism through phosphorylation of this site. The Ste11(S243) mutants revealed the same regulatory behaviour, an increased Fus1 expression of the non-phosphorylatable mutant and inhibition of signalling through the phospho-mimicking mutant.

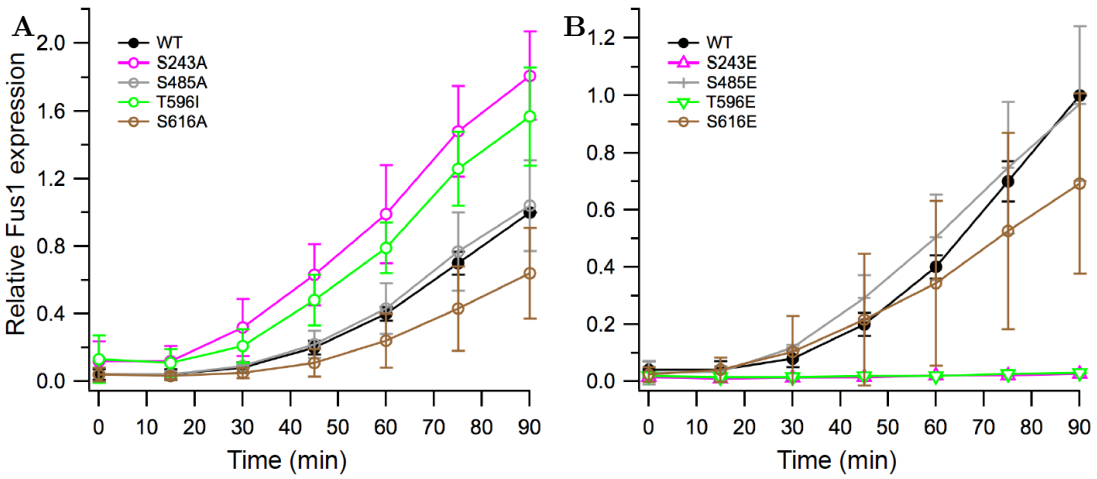

Fig. 3.12: Fus1 reporter gene expression of Ste11 mutant strains compared to WT cells. Potential Fus3 phosphorylation sites S243, S485, T596, S616 on Ste11 where replaced by either non-phosphorylatable alanine **(A)** or phospho-mimicking glutamate **(B)**. Fus1-meGFP expression was measured by flow cytometry as function of time. Cells were stimulated with 1 µM α-Factor. Data was normalized to maximum Fus1 expression levels in WT cells at 90 min. Values indicated the mean±s.d. of three independent experiments.

This data is in accordance with the aforementioned phosphoproteomic data[261], confirming the enzyme-substrate complex of Ste11 with Fus3 and the proposed role of this interaction as a negative feedback loop regulating the output of the pheromone signalling pathway.

To further examine phosphorylation of S243 on Ste11 by Fus3 and to evaluate the dependence of T596 phosphorylation on Fus3, affinity chromatography experiments were established separating phosphorylated from unphosphorylated proteins. Specifically, yeast lysates were added to a phosphoprotein-retaining column (PhosphoProtein Purification column, Qiagen) separating phosphorylated from unphosphorylated proteins to draw conclusion about the phosphorylation state of Ste11 (Fig. 3.13). Unfortunately, only the unphosphorylated flow-through could be quantified, which therefore only indirectly describes Ste11 phosphorylation.

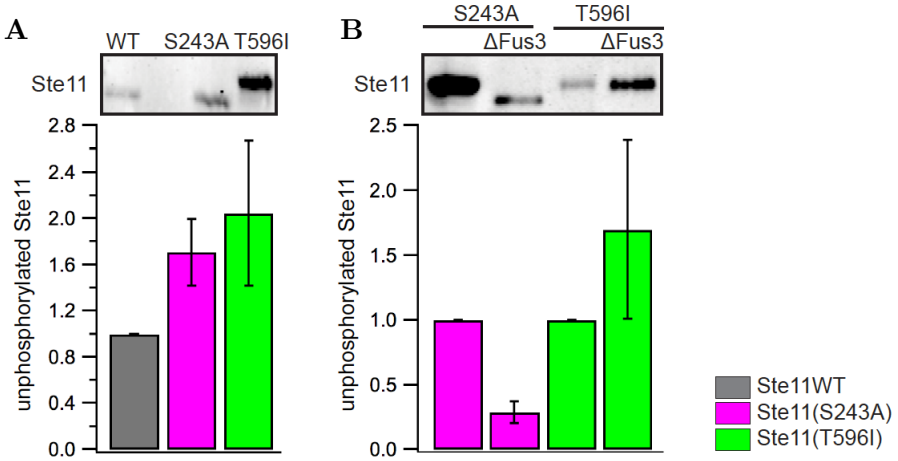

Fig. 3.13: Phosphorylation status of S243 and T596 in Ste11. (A) Unphosphorylated fractions of Ste11 mutants obtained by affinity chromatography.

Representative western blot of unphosphorylated Ste11WT, Ste11(S243A) and Ste11(T596I). Bar graphs show the mean±s.e. of four independent Western blots. **(B)** Unphosphorylated fractions of Ste11 mutants obtained by affinity chromatography. Representative Western blot of unphosphorylated Ste11(S243A) or Ste11(T596I) in ΔFus3 strains. Bar graphs show the mean±s.e. of three independent Western blots. Lisa-Marie Krieger performed affinity chromatography experiments and Western blots.

Affinity chromatography of unstimulated Ste11(S243A) and Ste11(T596I) cells yielded higher fractions of unphosphorylated Ste11 in comparison to the corresponding wild type strain, indicating that both sites were phosphorylated in the vegetatively growing cells (Fig. 3.13A). Fus3 was deleted in these strains to determine its impact on phosphorylation of S243 and T596. Indeed, the Ste11(S243A) mutant showed a strong reduction of the unphosphorylated fraction of Ste11 (Fig. 3.13B). This indicated that the opposing T596, which can still be phosphorylated, might be even more phosphorylated in the absence of Fus3. For this reason T596 is probably phosphorylated by another kinase other than Fus3, although phosphorylation at this site is still influenced by Fus3. In contrast, the Ste11(T596I) mutant exhibited an increase in unphosphorylated Ste11. This result implied that the opposing phosphorylatable S243 is less phosphorylated in absence of Fus3. S243 is thereby probably phosphorylated directly by Fus3, which is in good agreement with the mass spectrometry findings in Wu *et al.*[261]. However, to strengthen these results the phosphorylated fraction of Ste11 should be measured. This could be achieved by using Phos-Tag in Western blots, or by measuring phosphorylation of purified Ste11 by Fus3 in a kinase-assay.

These results, in combination with the Fus1 reporter gene assay results, revealed that Ste11 signalling activity is controlled via a negative feedback by Fus3 phosphorylation on S243, and possibly by a negative regulation on T596 in Ste11 via a different, as yet unidentified kinase.

In order to identify if the two regulatory sites are interdependent or are related in function, a series of Ste11 double mutants was established. Both combinations Ste11(S243A/T596E) and Ste11(S243E/T596I) each bearing one of the phospho-mimicking mutants completely prevented Ste11 mediated signalling (Fig. 3.14). However, combining the two non-phosphorylatable mutants in Ste11(S243A/T596I) resulted in high basal Fus1 expression levels, already exceeding the levels of stimulated wild type cells.

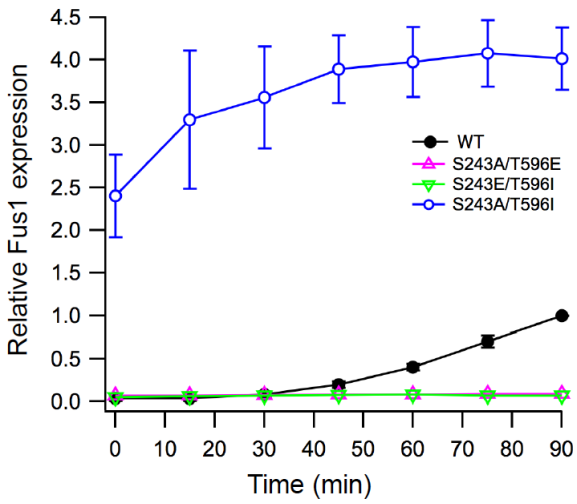

Fig. 3.14: Fus1 reporter gene expression of Ste11 double mutant strains. Fus1-meGFP expression was measured by FACS in strains with different combinations of non-phosphorylatable and phospho-mimicking mutants of S243 and T596 as function of time. Cells were stimulated with 1 µM α-Factor. Data was normalized to maximum Fus1 expression levels in WT cells at 90 min. Values depicted represent mean±s.d. of three independent experiments.

The Ste11(S243A/T596I) double mutant cells displayed strong phenotypic effects (Fig. 3.15). The vegetatively growing cells were highly enlarged in cell size and their cell shape was highly asymmetrical in comparison to WT cells. The cells grew in a mixture of various differentiated morphologies. Cells with the typical round, ellipsoid morphology coexisted aside thin elongated cells, cells with shmoo-like structures, filamenting morphologies and cells with undefined morphological structures. Interestingly, some of the cells already localized Fus1-meGFP at differently shaped membrane structures of which some showed similarity to mating tip projections. These cells most likely possessed high basal mating signalling activity.

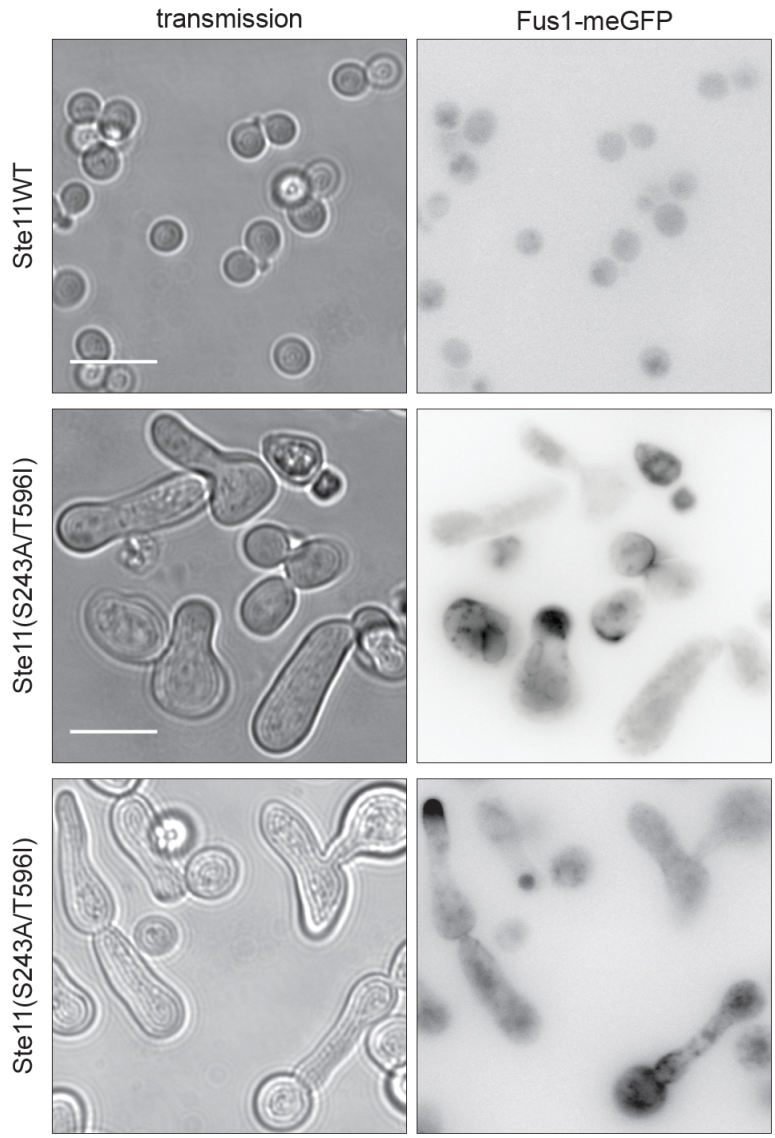

Fig. 3.15: Vegetative growth of Ste11(S243A/T596I) cells. Left column displays transmission images and right column shows Fus1-meGFP fluorescence in widefield microscopy. First row shows Ste11WT cells and the other two rows show the Ste11(S243A/T596I) cells with elongated and shmoo like morphologies. Cells remained unstimulated. Scale bar in the upper left image indicates 10 µm and is representative for all images.

3.2.2 The negative feedback on Ste11 maintains the adaptive ppFus3 response to pheromone

Both regulatory mechanisms, the negative feedback from Fus3 on Ste11 and the negative regulation of Ste11 activity by phosphorylation of T596, had a clear impact on the mating pathway output. To address how these mechanisms affect the pheromone mediated signal transduction, the levels of phosphorylated Fus3 (ppFus3) in response to pheromone stimulation were studied in the non-phosphorylatable Ste11 mutants as a function of time. The same strains as those used in the Fus1 reporter gene assay were stimulated with 100 nM α-Factor and

ppFus3 was quantified as function of time by Western blots, where each time-series comprised of nine time-points and was monitored on separate blots. Since comparison of values on different blots does not provide a measure of absolute quantity, the blots were corrected by a separate quantification of the last time-point on one blot (Fig. 8.3B). The Ste11WT cells exhibited a transient ppFus3 profile with an early peak activity at 2.5 min (Fig. 3.16). This peak activity declined rapidly to lower levels of about 60 % and remained on this plateau up to 150 min post-stimulation. Both the Ste11(S243A) and the Ste11(T596I) strain exhibited an overall higher, yet still transient ppFus3 profile, with increasing levels at later times of stimulation. Interestingly, the unstimulated double mutant Ste11(S243A/T596I) showed higher basal ppFus3 levels of about 50% of the maximum Fus3 phosphorylation in wild type cells. This corresponds to the previously detected high basal Fus1 expression levels (Fig. 3.14). Furthermore, the autonomous activation of Fus3 in these cells is probably responsible for the observed shmoo-like morphologies of these cells (Fig. 3.15). The ppFus3 peak level in the double mutant cells was as strongly elevated as in the other non-phosphorylatable mutants, however, it did not decrease to lower levels and remained sustained.

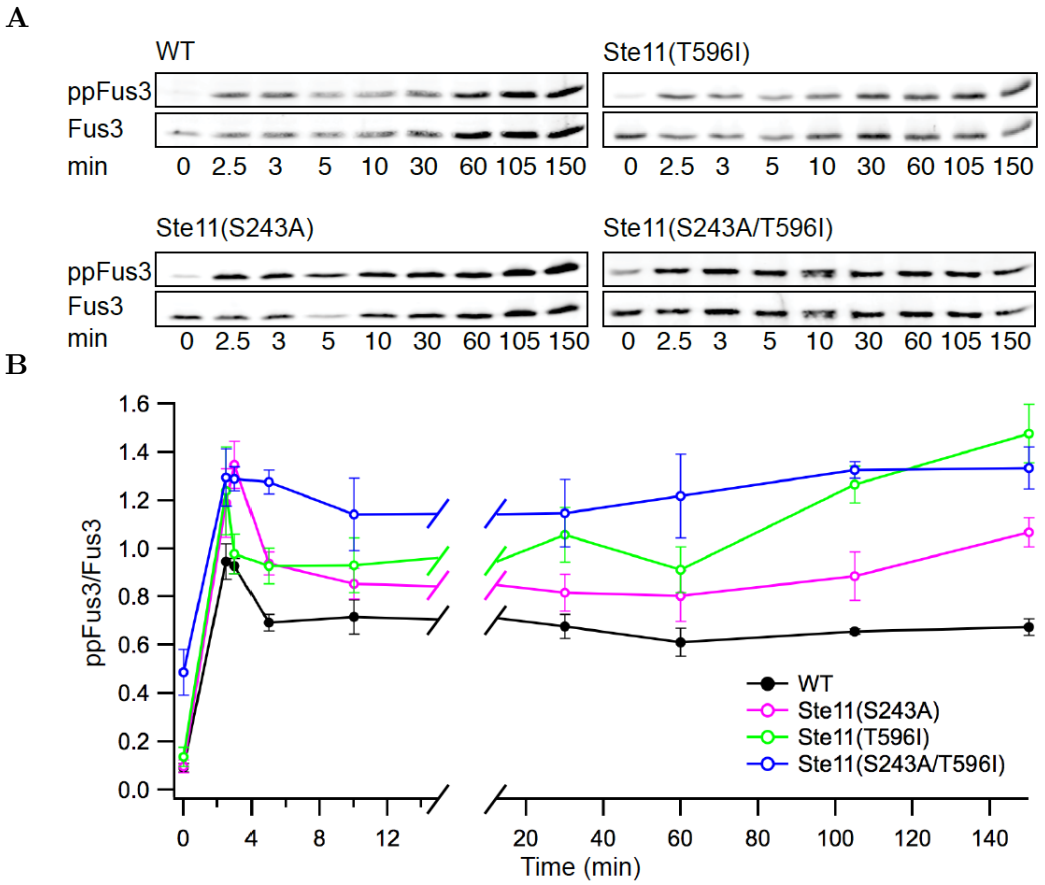

Fig. 3.16: ppFus3 response of the non-phosphorylatable Ste11 mutants to pheromone as function of time. (A) Representative Western blots showing ppFus3 and total Fus3 in WT, Ste11(S243A), Ste11(T596I) and Ste11(S243A/T596I) cells stimulated with 100 nM α-Factor. Samples were taken after 0, 5, 10, 30, 60, 90, 105 and 150 min post-stimulation. **(B)** Quantification of three independent Western blot experiments (Fig. 8.3A),

showing ppFus3/Fus3 as function of time. Data was normalized to maximum Fus3 phosphorylation in WT cells. The mean±s.e. from three independent Western blots is shown for every time point.

In contrast, the phospho-mimicking variants of Ste11(S243) and Ste11(T596) both suppressed a ppFus3 response upon stimulation with 100 nM α-Factor (Fig. 3.17). This mirrored the loss of Fus1 expression monitored in the FACS experiments (Fig. 3.12).

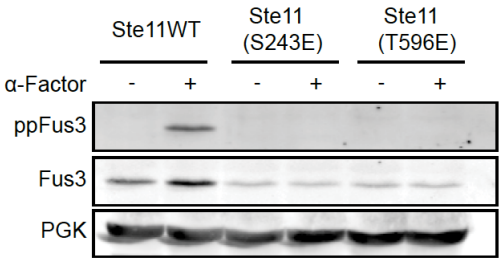

Fig. 3.17: ppFus3 pheromone response in cells bearing phospho-mimicking Ste11 mutants. Western blot showing ppFus3 and total Fus3 in WT, Ste11(S243E) and Ste11(T596I) cells in unstimulated cells and upon stimulation with 100 nM α-Factor for 30 min. Yeast Phosphoglycerate Kinase was used as loading control.

Thus, negative regulation of either of the phosphorylation sites S243 or T596 on Ste11 determines the amplitude of ppFus3 and keeps the Fus3 activity in check. Removing both Ste11 phosphorylation sites at once affects the regulation of Fus3 activity levels in absence of stimulus, and disrupts the transient ppFus3 response leading to more sustained Fus3 activity. These experiments show that changing the topology of the mating signalling network by removing regulatory mechanisms in the MAPK module reshapes the temporal Fus3 response thereby directly affecting the morphology of the cell.

3.2.3 The negative feedback on Ste11 preserves an ultrasensitive ppFus3 dose-response to pheromone

The yeast mating decision is an all-or-none response, where cells only undergo the cellular processes required for mating if a sufficiently high pheromone concentration above a certain threshold is sensed. On a protein level this is maintained *inter alia* by a switch-like dissociation of Fus3 from Ste5[6] which facilitates the ultrasensitive response of Fus3[247].

To address if and how the negative feedback from Fus3 on Ste11 contributes to the ultrasensitive Fus3 response, ppFus3 was quantified in the non-phosphorylatable strains Ste11(S243A), Ste11(T596I) and Ste11(S243A/T596I) in comparison to the corresponding wild type cells as function of pheromone dose (Fig. 3.18 & 8.4). Remarkably, the Ste11(S243A) and the Ste11 double mutant where less effective in the generation of a ultrasensitive response, apparent from the lower Hill coefficients (n_H) of 1.68 (Ste11(S243A) and 1.44 (Ste11(S243A/T596I) as compared to the WT cells (n_H = 6.44). This was also reflected in a significantly better representation of the WT data by a sigmoidal function (p-value: $1.48\times*10^{-8}$ for WT). In contrast to the sigmoidal response of the WT cells that exhibited an activation threshold at 30 nM α-Factor, the Ste11(S243A) mutant showed a hyperbolic response curve with higher sensitivity at lower concentrations, partially detected at 10 nM α-Factor and with higher significance at concentrations between 20 - 50 nM. The double mutant strain exhibited a clear hyperbolic response curve, with significantly raised sensitivity to lower pheromone doses. In contrast, the Ste11(T596I) strain retained the switch-like pheromone dose-response, which was less steep than the WT response curve (n_H = 2.81) and showed a slightly increased sensitivity by responding at lower pheromone concentrations of 20 nM (p-value (sigmoidal):0.003). Both non-phosphorylatable mutants Ste11(S243A) and Ste11(T596I) seemed to exhibit slightly higher ppFus3 levels at high pheromone concentrations, but which did not reach statistical significance. However, the double mutant exhibited a significantly increased ppFus3 activity at high pheromone levels, reflecting the results obtained by the temporal ppFus3 response analysis (Fig. 3.16).

Taken together, abolishing the negative feedback from Fus3 to Ste11 led to a more graded relationship between pheromone input and MAPK output, whereas disturbance of the negative regulation on T596 of Ste11 did not change the ultrasensitive response, but affected slightly the sensitivity to pheromone.

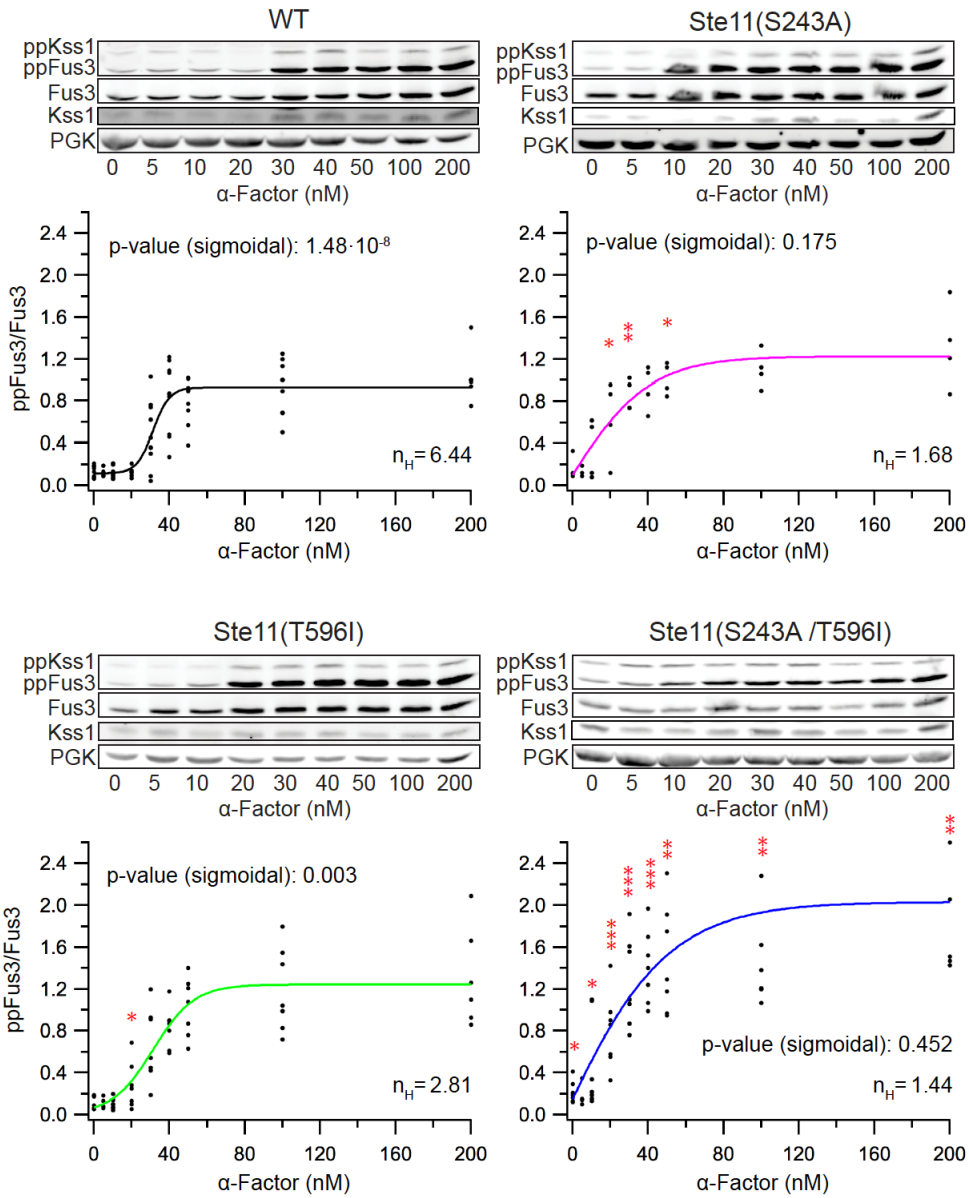

Fig. 3.18: ppFus3 pheromone dose-response of non-phosphorylatable Ste11 mutants. Representative Western blots of ppKss1 and ppFus3 dose-response measurements in WT, Ste11(S243A), Ste11(T596I) and Ste11(S243A/T596I) cells at 270 min post-stimulation and corresponding quantification of ppFus3. All quantified values were normalized to maximum Fus3 phosphorylation in WT. Yeast Phosphoglycerate Kinase was used as a loading control. Data of 4-10 independent Western blot experiments was fitted to a sigmoidal function (coloured lines) and displayed with the corresponding Hill coefficients n_H. Black dots represent single measurements. The red asterisks indicate the probability of significant differences between the WT cells and the mutants Ste11(S243A), Ste11(T596I) and Ste11(S243A/T596I) obtained by a two-tailed Student's *t*-test. One asterisk: marginal significance, 0.1>p>0.05. Two asterisks: significant changes, 0.05>p>0.01. Three asterisks: high significance 0.01>p. Hill coefficient analysis and the test if a sigmoidal or a hyperbolic function represents the data best was performed by Angel Stanoev (MPI-Dortmund, Dept. 2).

3.2.4 The response dynamics are reflected in Fus3 expression

Interestingly, the total Fus3 levels cells showed a similar response to pheromone as ppFus3 in the non-phosphorylatable Ste11 mutant. In the temporal response of wild type cells to pheromone, the Fus3 expression levels remained unchanged the first 10 – 30 min of mating signalling, whereas ongoing stimulation led to a strong increase in total levels at later times (Fig. 3.19), which was also observed for the strains bearing the non-phosphorylatable Ste11 mutants. These results indicated that active Fus3 stimulates its own expression[34]. The Ste11(S243A/T596I) mutant, however, exhibited constant Fus3 levels irrespective of the duration of pheromone stimulation.

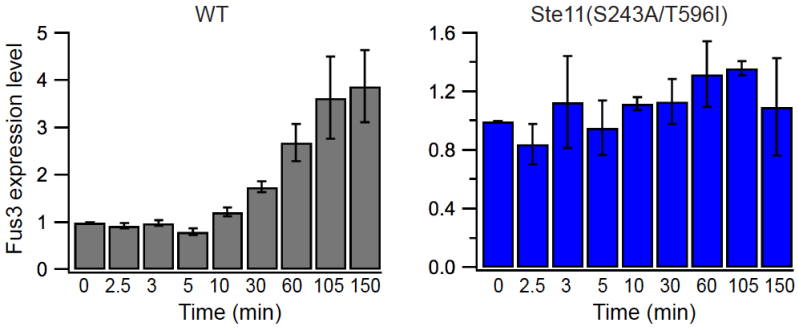

Fig. 3.19: Pheromone response of Fus3 expression in WT and Ste11(S243A/T596I) mutants as function of time. Quantification of relative Fus3 expression levels from ppFus3 response Western blots (Fig. 3.14). Values are each normalized to basal Fus3 expression levels. Values for WT and for Ste11(S243A/T596I) cells are not comparable with each other. The mean±s.e. from three independent Western blots is shown.

As Fus3 showed high basal activity in the Ste11 double mutant, and its activity seemed to be correlated with expression levels, elevated Fus3 abundances were expected in these cells. Indeed, expression of Fus3 was approximately three times higher than in wild type cells (Fig. 3.20), comparable to elevated Fus3 expression levels in cells stimulated for long times (Fig. 3.16, 105 – 150 min α-Factor).

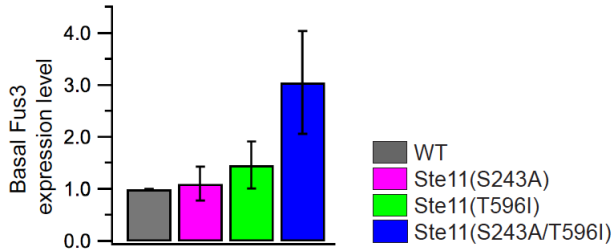

Fig. 3.20: Basal Fus3 abundance in WT and non-phosphorylatable Ste11 mutant strains. Expression levels are quantified from dose-response Western blot analysis of WT, Ste11(S243A), Ste11(T596I) and Ste11(S243A/T596I) cells (Fig. 3.18). Total Fus3 levels were first normalized to the loading control PGK and afterwards normalized to wild type total Fus3. The mean±s.e. from three independent Western blots is shown.

Remarkably, Fus3 expression levels also exhibited similar pheromone dose-response dynamics to the ppFus3 dose-response. In wild type cells, Fus3 expression remained unchanged up to 20 nM pheromone stimulation, while exceeding this concentration threshold induced a maximum of four times higher total Fus3 abundances (Fig. 3.21). A similar Fus3 expression profile was observed for the Ste11(T596I) mutant, showing a "switch" at 30 nM pheromone concentrations, whereas gradually increasing expression levels were observed for the feedback deficient strain Ste11(S243A). Here, a two-fold increase in Fus3 expression was achieved with as little as 5 nM α-Factor stimulation. The Ste11(S243A/T596I) mutant only showed a minor increase in Fus3 levels to pheromone-dose, in contrast to the steep hyperbolic ppFus3 response.

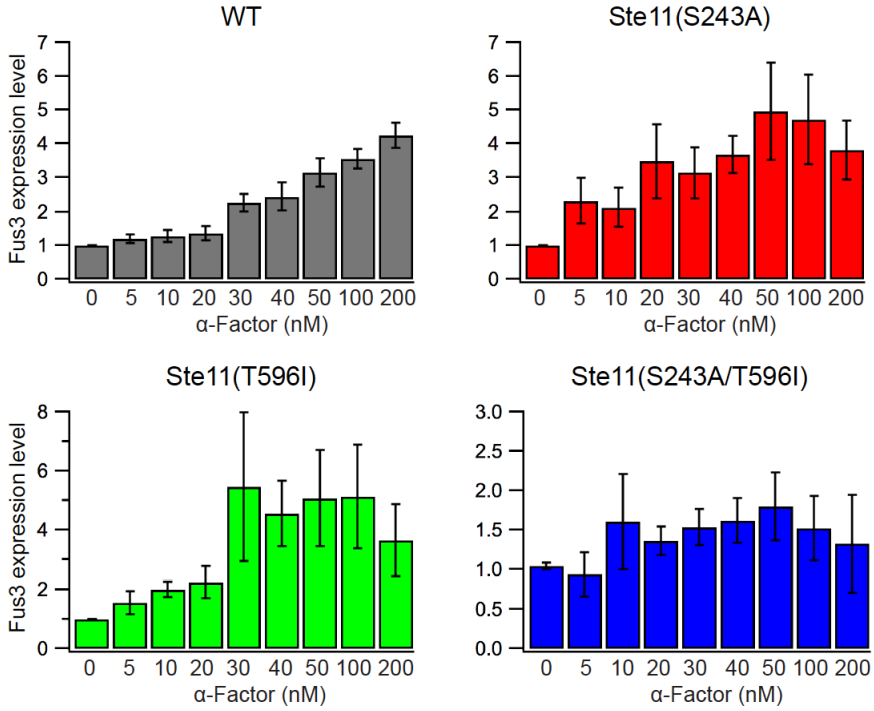

Fig. 3.21: Pheromone dose-response of total Fus3 in non-phosphorylatable Ste11 mutant cells. Expression levels are quantified from dose-response Western blot analysis of WT, Ste11(S243A), Ste11(T596I) and Ste11(S243A/T596I) cells (Fig. 3.18). Total Fus3 levels were first normalized to the loading control PGK and afterwards normalized to basal total Fus3 of the particular strain. The mean±s.e. from 4-10 independent Western blots is shown.

The phospho-mimicking Ste11 mutants both indicated a reduction in total Fus3 levels, which was in good agreement with the suppressed ppFus3 response (Fig. 3.17). This implies that autoactivated Fus3, which is partially active in vegetatively growing cells[4], maintains a certain level of basal signalling and therefore a distinct abundance of total Fus3.

These experiments demonstrate that Fus3 activity positively regulates its own expression. Thus, preventing the control of Fus3 activity by disrupting the negative feedback from Fus3 on Ste11 and the negative regulation via phosphorylation on T596 leads to a loss of control of Fus3 expression.

3.2.5 Dose-response of Kss1 activity to mating pheromone

Stimulation with mating pheromone triggers the phosphorylation of Fus3, but also the phosphorylation of filamentous growth MAPK Kss1. Kss1, however, was shown to exhibit different activation dynamics compared to Fus3: a transient adaptive ppKss1 response with rapid adaptation to basal levels[129] and a graded response to dose of pheromone[247]. In order to address if the negative feedback on Ste11 is mating specific or if the negative regulation via T596I in Ste11 also impacts Kss1 phosphorylation, its pheromone dose-response behaviour was investigated. In general, ppKss1 showed less consistent phosphorylation patterns with a higher variance than ppFus3.

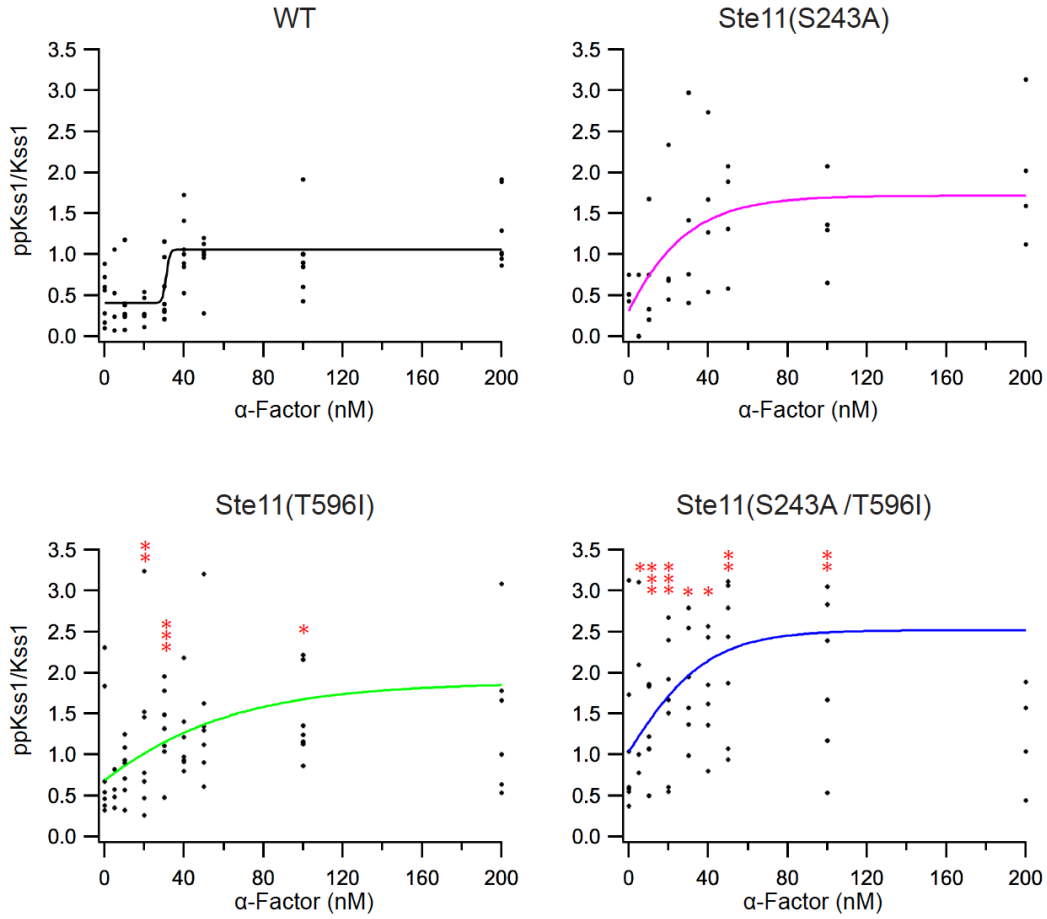

Fig. 3.22: ppKss1 pheromone dose-response of non-phosphorylatable Ste11 mutants. ppKss1 data extracted from Western blots from Figure 3.18 (dose-response measurements in WT, Ste11(S243A), Ste11(T596I) and Ste11(S243A/T596I) cells at 270 min post-stimulation). All quantified values were normalized to maximum ppKss1 phosphorylation in WT. Data of 4-10 independent Western blot experiments was fitted to a sigmoidal function (coloured lines). Black dots represent single measurements. Red asterisks indicate the significance between between the WT cells and the mutants Ste11(S243A); Ste11(T596I) and Ste11(S243A/T596I) obtained by a two-tailed Student's *t*-test. One asterisk: marginal significance, $0.1>p>0.05$. Two asterisks: significant changes, $0.05>p>0.01$. Three asterisks: high significance $p<0.01$.

Wild type cells exhibited a similar ultrasensitive response to pheromone of ppKss1 as ppFus3 with the same response threshold of approximately 30 – 40 nM (Fig. 3.22). In contrast, the response curve started at higher basal levels around 50 % of Kss1 activity. Fitting the data to a sigmoidal function yielded a more graded ppKss1 response curve for both mutants, Ste11(S243A) and Ste11(T596I). However, while the Ste11(T596I) mutant exhibited a significantly higher sensitivity to lower pheromone doses (20 – 30 nM) and elevated levels at higher pheromone concentrations, the Ste11(S243A) mutant did not show significant differences to the WT, as determined by a Student's *t*-test. The double mutant exhibited a hyperbolic ppKss1 dose-response curve with overall higher levels. Here, basal levels were partially increased and sensitivity was significantly increased to lower (10, 20, 50 nM) and higher doses (100 nM) of pheromone.

Unexpectedly, ppKss1 exhibited a similar pheromone dose-response in WT cells as ppFus3, which could be ascribed to leakage in mating signalling from the MAPK module to Kss1. This leakage could also have been responsible for the slightly affected response in the Ste11(S243A) cells, exhibiting a higher signalling activity of Ste11. The Ste11(T596I) mutant, however, clearly changed the ppKss1 dose-response, especially at lower concentrations, but retained the switch-like response of ppFus3. Thus, the feedback from Fus3 on Ste11 regulates ppFus3 mediated signalling rather than Kss1 activity, while the control of T596 phosphorylation on Ste11 rather affects pKss1 mediated signalling.

3.3 Phosphorylation of S243 and T596 on Ste11 regulates signalling through different mechanisms

Both regulation sites S243 and T596 exhibited a negative effect on signalling when phosphorylated and a positive effect when unphosphorylated, although both differentially effect the pheromone response. The negative regulation of the T596 site leads to slightly increased sensitivity to pheromone at lower concentrations and stronger mating pathway output, whereas the negative feedback via the S243A site dictates specific response dynamics.

In order to understand how regulation of these sites via phosphorylation generates the differential responses, their underlying mechanisms were investigated.

3.3.1 Phosphorylation of T596 on Ste11 regulates its activity – Kss1 activity during mating is controlled by a Fus3 mediated feedback

The isoleucine substituted variant of Ste11(T596) was first generated by Stevenson *et al.*[262] and was shown to hyperphosphorylate Ste7 and to activate the yeast pheromone signalling in the absence of pheromone. This mutant was extensively employed by others as a constitutive active variant of Ste11[62,71,111,255,265].

T596 resides in the kinase subdomain VII in front of the aa-triplet Asp597-Phe598-Gly599 (DFG). This aa-triplet, called the DFG motif, is usually flanked on either side by two hydrophobic or near neutral residues and represents the most

highly conserved short stretch in the catalytic domain[266]. The Asp in this motif chelates the Mg^{2+} ions that bridge the β- and the γ-phosphates of the ATP to orient the γ-phosphate for transfer to the target residue (Fig. 3.23A)[267]. Its position and orientation is therefore essential for kinase activity. Introducing negative charges in front of the Asp in the DFG motif of Ste11 by phosphorylation of the T596 might therefore influence the binding of ATP in the catalytic domain or the transfer of the γ-phosphate. The downregulation of Ste11 signalling in the T596E mutant could be caused theoretically either by a non-specific unregulated perturbation in the ATP-binding pocket, or be attributed to an intended regulatory mechanism. To test the latter, the sequences of other kinase subdomains VII were examined for the presence of phosphorylatable residues at the same position. Interestingly, several human kinases such as PKC and the yeast PAK Ste20, which functions upstream of Ste11, posses a threonine in front of the DFG motif (Fig. 3.23B)[267]. However, substitution of the T756 in Ste20 to a phospho-mimicking glutamate or a non-phosphorylatable alanine did not affect the response to pheromone at all. This indicates that introducing a negative charge at the DFG motif does not perturb the kinase activity *per se*. It also shows that this site is probably not a general target for phosphorylation control.

A

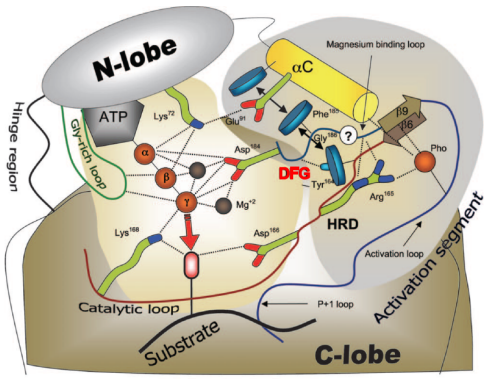

B

Kinase	subdomain VII
Ste11	-QCVKLTDFGISKKKLSPLMKKQN-
Ste20	-GDIKLTDFGFCAQINEKLNL----
EGFR	-GHVKITDFGLAKLLGAKKKEY---
PKA-Cα	--GYIVTDFGFAKRVKG--------
S6K	-GHVKLTDFGLCKKSIHDGT-----

Fig. 3.23: Localization and function of the DFG motif. (A) Scheme displaying interactions in the kinase catalytic core. Red arrow indicates transfer of γ-phosphate to the substrate residue. Catalytically important structures are highlighted in yellow. Dashed black lines represent polar contacts like the contact of the Asp in the DFG motif to ATP. Amino acid numbering in PKA is used. Adapted from[268]. **(B)** Sequence alignment of DFG and surrounding (subdomain VII)[267]. Phosphorylatable threonine is highlighted in green and the DFG motif in red.

In order to further characterize the regulation via T596 in Ste11, phosphorylation of its direct target Ste7 was monitored using Western blots. Ste7 is hyperphosphorylated at multiple serines and threonines in the C- and N-terminal domains in vegetatively growing cells in a feedback via Fus3[112,269]. Due to this strong phosphorylation it shows a mobility shift in gel-electrophoresis and can be separated from the unphosphorylated Ste7.

Western blots confirmed the hyperphosphorylation of Ste7 under basal conditions (Fig. 3.24), which was strengthened upon pheromone stimulation. This was displayed by an increase in the intensity of the band of the slower migrating

Ste7 and the corresponding pThr-band detecting the phosphorylated threonines in Ste7. The non-phosphorylatable Ste11(T596I) exhibited even stronger Ste7 phosphorylation in unstimulated cells, whereas substitution by a phospho-mimic completely abolished the hyperphosphorylation. Comparing the WT Ste11 and the T596I substituent in Fus3 deletion strains did not show any changes at all, which indicates that hyperphosphorylation of Ste7 is mediated via Fus3 and not directly through Ste11. Consequently, the Ste11(T596I) mutant must trigger higher Fus3 activity leading to stronger feedback phosphorylation of Ste7.

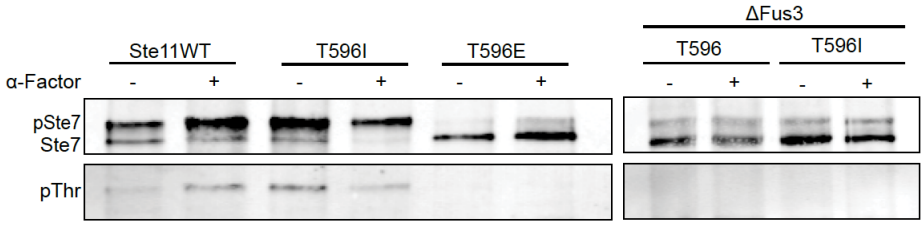

Fig. 3.24: Influence of Ste11(T596I) on Ste7 phosphorylation. Western blots show two total Ste7 bands (upper lane), which are separated by a mobility shift of the hyperphosphorylated Ste7 (upper band), and phosphorylated threonines in Ste7 (lower lane) in Ste11WT, Ste11(T596I) and Ste11(T596E) cells. Right panel displays same quantities in the corresponding ΔFus3 strains.

Basal ppFus3 levels, however, seemed not to be affected by Ste11(T596I), whereas ppKss1 levels were elevated (Figure 3.25A). Deletions of Fus3 in wild type cells enhanced basal ppKss1 levels to a similar extent. Pheromone stimulation of these cells led to the formation of filamentous growth-like elongations (Fig. 3.25B). Ste11(T596I) cells with a Fus3 deletion background exhibited even stronger activated Kss1 already at basal levels, resulting in cell differentiation into filaments.

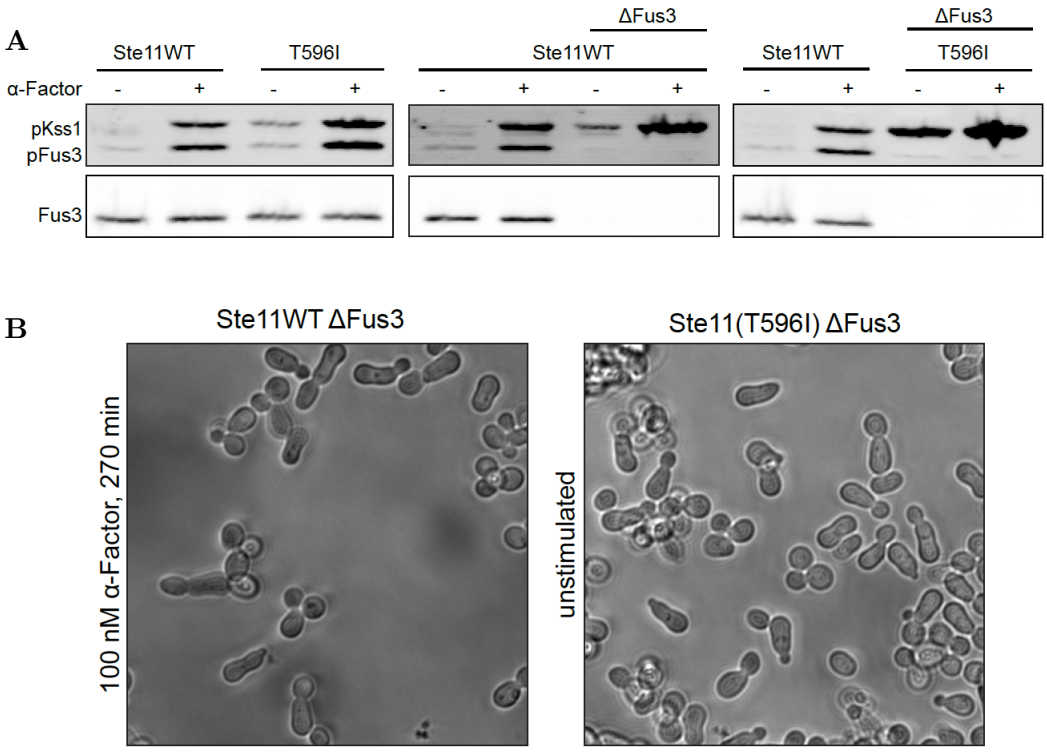

Fig. 3.25: Influence of Ste11(T596I) on ppFus3 and ppKss1. (A) Western blots show ppFus3 and ppKss1 bands (upper lane) and the total Fus3 (lower lane) in either Fus3 expressing or Fus3 deleted Ste11WT and Ste11(T596I) cells. Cells were stimulated with 100 nM α-Factor for 15 min. **(B)** Transmission images of Ste11WT and Ste11(T596I) cells with deleted Fus3. Cells in the left panel were stimulated with 100 nM a-Factor whereas the cells in the right panel remained unstimulated.

These results show that Fus3 keeps Kss1 activity in check by hyperphosphorylation of Ste7. The non-phosphorylatable T596I tunes the activity of Ste11 and thereby increases Ste7 hyperphosphorylation by Fus3. However, elevated ppFus3 levels could not be detected, whereas basal ppKss1 levels were increased. Removing the feedback control by Fus3 releases strong activation of Kss1 by Ste11(T596I) thereby changing the cell fate. Thus, phosphorylation of T596 in Ste11 most likely regulates kinase activity independently of pathway input.

3.3.2 Phosphorylation of S243 on Ste11 regulates Ste5-Ste11 binding and thereby switching from mating to filamentous growth

Substitution of S243 in Ste11 to glutamate was shown to completely abolish the signal in the Fus1 reporter gene assay (Fig. 3.12) and the ppFus3 response (Fig. 3.17). Consequently, stimulation of these cells did not initiate the formation of mating projections (Fig. 3.26). However, Ste5, which is localized in vegetatively growing cells in the cytosol and the nucleus, was detected as a 3mCherry fusion in punctate structures randomly distributed at the cell membrane. This demonstrated that mating signalling was initiated but that further signalling via the MAPK module, and finally the activation of Fus3, was impeded. The signal could

theoretically leak into the activation of the filamentous growth MAPK Kss1, but this was deleted in this strain (Fig. 3.26).

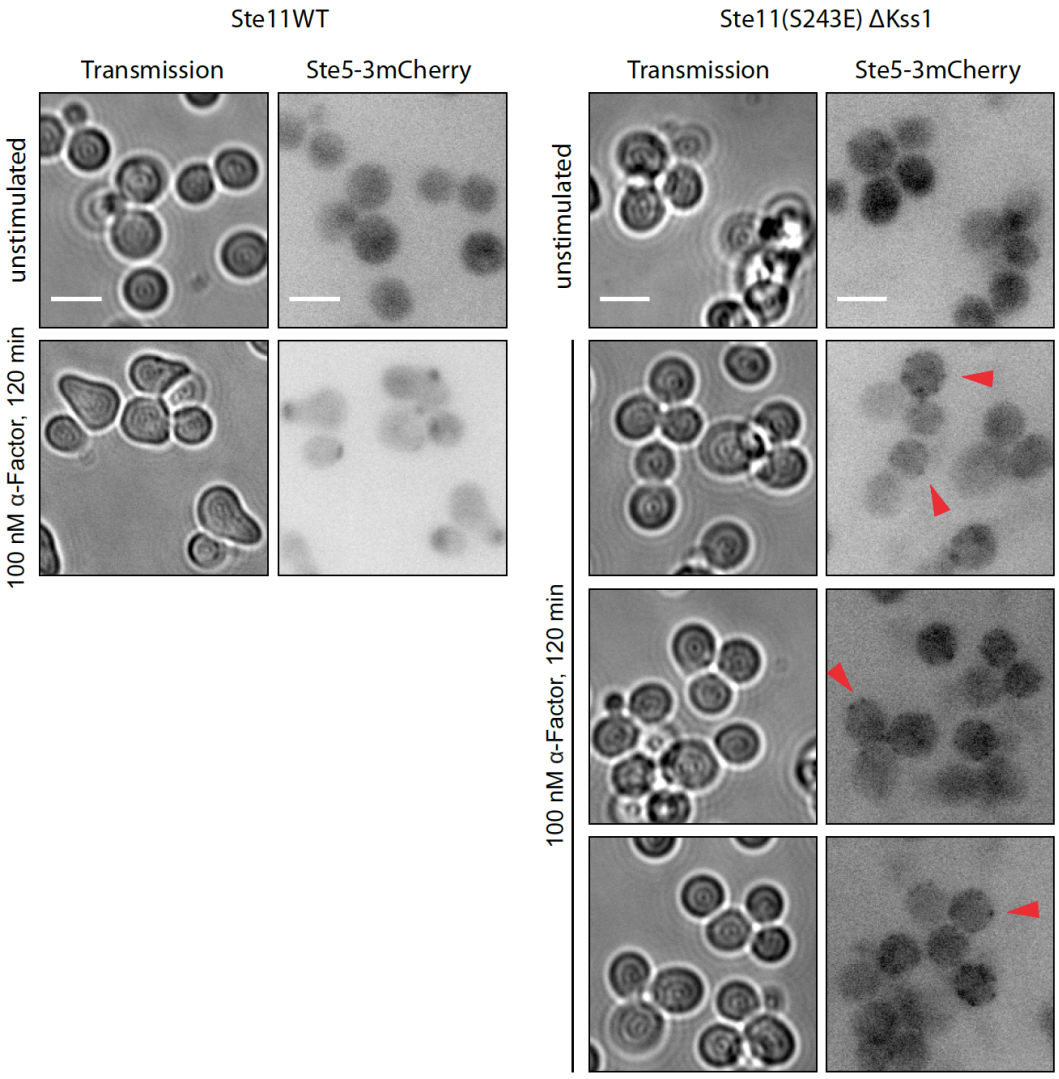

Fig. 3.26: The Ste11(S243E) mutant does not trigger shmoo formation. Left panel shows Ste11WT cells and right panel represents Ste11(S243E) cells with a ΔKss1 background. In both panels the left column displays transmission and the right column the Ste5-3mCherry fluorescence images. Cells in the first row are unstimulated and cells in the second row and further are stimulated with 100 nM α-Factor for 120 min. Red arrows point at punctate structures of Ste5-3mCherry. Scale bars indicate 5 µm and are representative for all images.

The Ste11(S243E) cells with Kss1 expression developed filamentous-like morphologies upon pheromone stimulation, as assumed (Fig. 3.27A). As filamentous growth is independent of Ste5, its localization was examined by a triple-meGFP variant in these cells and compared to WT cells. Ste11(S243E) did not show Ste5 localization at the tip of the growing projections and the PM at all, demonstrating its independence.

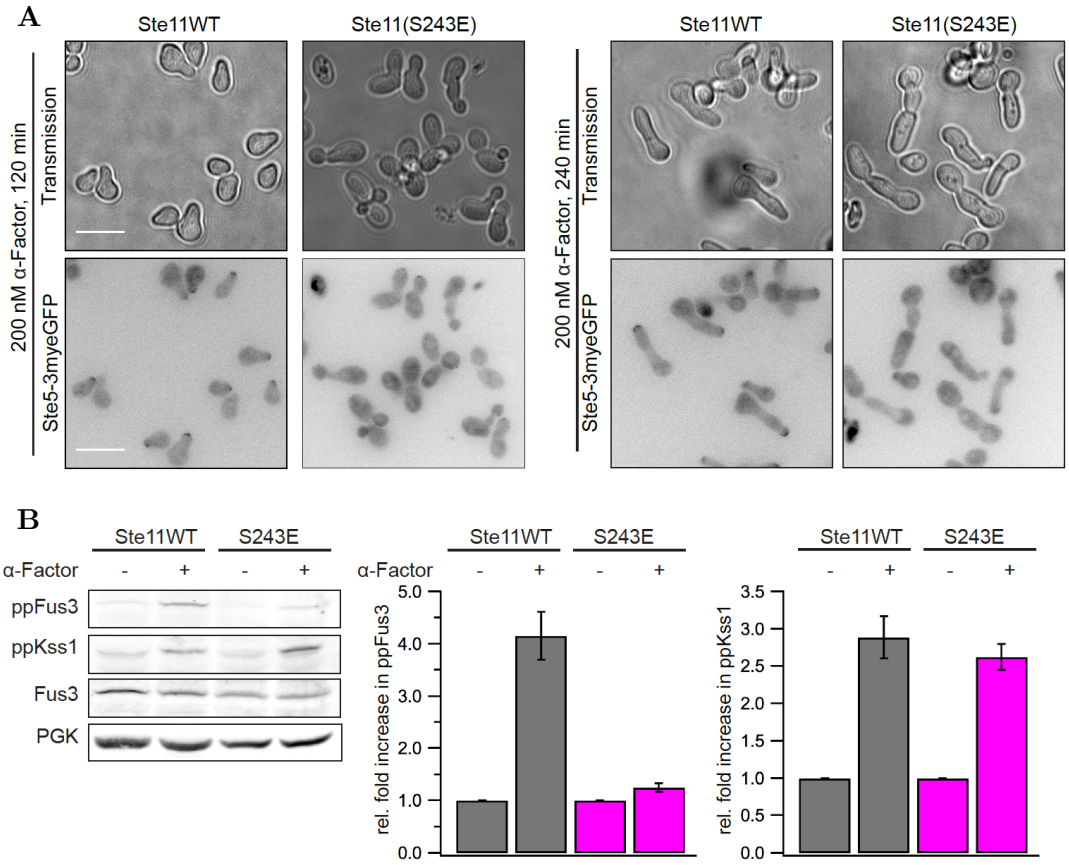

Fig. 3.27: Morphological and MAPK response of the Ste11(S243E) mutant cells. **(A)** Cell morphology and Ste5 localization in Ste11(S243E) cells (right column) compared to Ste11WT cells (left column) stimulated with 200 nM α-Factor for 120 (left panel) and 240 min (right panel).Upper row shows transmission images and lower row shows Ste5-3meGFP fluorescence images. Scale bars indicate 10 µm and are representative for all images. **(B)** Western blots of Ste11(S243E) compared to Ste11WT in response to 100 nM α-Factor for 15 min and quantification of relative fold increase of ppFus3 and ppKss1 from the same. Values are each normalized to basal phosphorylation levels. The mean±s.e. from three independent Western blots is shown.

The Ste11(S243E) mutant cells did not exhibit a ppFus3 response upon pheromone stimulation but a clear ppKss1 response (Figure 3.27B), explaining the filamentous growth-like morphology. As activation of Fus3 is Ste5-dependent and activation of Kss1 is not[112], mutation of S243 probably influences the Ste5 mediated activation of Fus3. S243 is located in the N-terminal regulatory domain of Ste5, close to a Ras-binding-domain-like region (RBL), which binds the PH-domain of Ste5 (Fig.3.28A)[61]. Therefore, the mutation of S243 could presumably alter the binding of Ste11 to Ste5, thereby regulating the Ste11 signalling activity in the pheromone MAPK module. In order to test this hypothesis, the interaction of Ste11(S243A) and Ste11(S243E) as 3-meGFP-fusion variants with 3mCherry-tagged Ste5 was measured by FCS and compared to the Ste5-Ste11 interaction in the corresponding Ste11WT cells (Fig. 3.28B). As S243A in Ste11 increases its signalling activity in mating, and the S243E impedes signalling activity, an increase in the Ste5-Ste11 complex concentration was expected in case of the Ste11(S243A) mutant and a decrease for the Ste11(S243E) mutant. A strain bearing a non-

activatable Fus3(TYAF), which should keep S243 in Ste11 unphosphorylated, was established as a positive control. As expected, this strain exhibited a slightly elevated complex concentration (CC) of Ste11-Ste5 (Fig. 3.28B). A similar increase was detected for the Ste11(S243A) mutant. The Ste11(S243E) mutant, however, did not affect the complex concentration. Furthermore, yeast with a Ste11(T596) mutation, which only impacts its kinase activity, did not alter the Ste11-Ste5 interaction either. To reduce the high variance in the measured complex concentrations and the skewed tails to higher values, the logarithm of these quantities was taken, resulting in symmetrical Gaussian profiles of the log/ln values[270]. Both the Fus3(TYAF) bearing strain and the Ste(S243A) mutant showed a Gaussian curve shifted to higher values, whereas the CC values of the Ste11(S243E) mutant showed a similar distribution as the Ste11WT complex concentrations. However, dissociation constants quantified from the raw CC values and the back converted logarithmic values did not expose any differences in Ste5-Ste11 interactions at all (Fig. 3.28C).

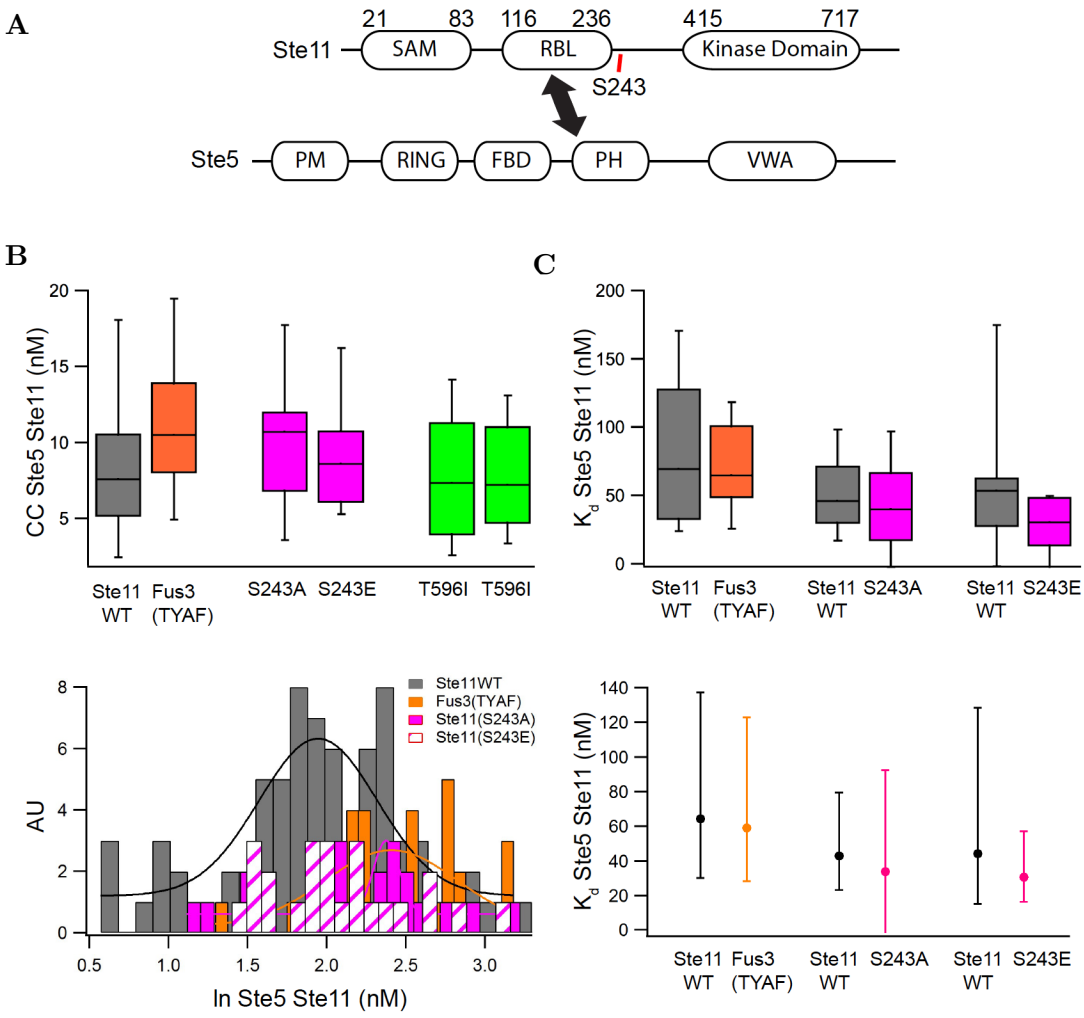

Fig. 3.28: Interaction of Ste5 with Ste11(S243A) and Ste11(S243E) determined by FCS. (A) Schematic representation of the domains in Ste11 and Ste5. Black double arrow indicates binding of the Ste11 RBL domain with the Ste5 PH domain. S243 on Ste11, which is feedback phosphorylated by Fus3, is adjacent to this binding interface. **(B)**

Quantification of the complex concentrations (CC) of Ste5 with Fus3(TYAF), Ste11(S243A), Ste11(S243E), Ste11(T596I) and Ste11(T596E) from 20-33 single FCS measurement (one measurement per cell). Upper panel shows raw data represented as box plots with top/bottom whiskers representing the 90/10 percentile. Lower panel displays Gaussian distributions of logarithmized CC Ste5 Ste11 values and corresponding Gaussian fits (Ste11(S243E) could not be fitted). AU indicates number of CC values in specific bin. **(C)** Dissociation constants (K_d) of the measured Ste5 Ste11 interaction in Ste11WT, Fus3(TYAF) and Ste11(S243A)/Ste11(S243E) cells. Upper graph shows K_d calculated from raw data. Error bars in box plots indicated the 90/10 percentile. Lower panel shows K_ds of reverse logarithmized CC values of the mutant cells with corresponding WT values. The mean±s.e from 20-33 measurements is shown.

However, these measurements involved only a small group of cells and the Ste11(S243) mutant strains did not always possess a homogeneous genetic background, which was obvious from sequencing data. Therefore, the interactions of the Ste11 mutants with Ste5 were analysed on a cell population level by co-immunoprecipitation of GFP-fused Ste5 with Ste11. The Ste11(T596I) mutant did not exhibit significant changes of the Ste5-Ste11 interaction (Fig. 3.29). The Ste11(S243A) mutant showed about 50 % more interaction with Ste5, whereas the phospho-mimicking Ste11(S243E) mutant was strongly impaired in binding Ste5.

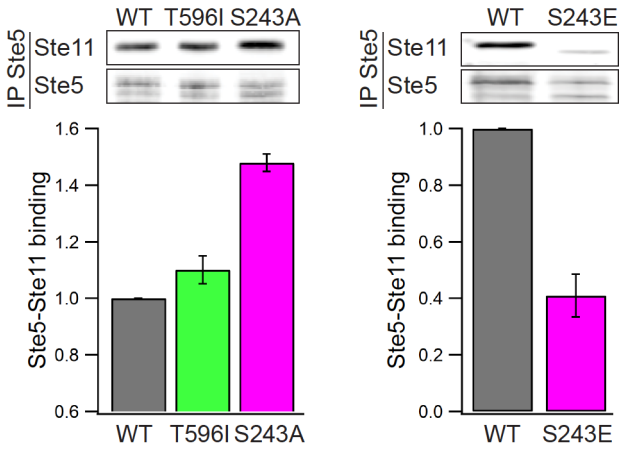

Fig. 3.29: Interaction of Ste5 with Ste11(S243A) and Ste11(S243E) determined by co-immunoprecipitation. Relative binding of Ste11WT and Ste11(S243A), Ste11(T596I), Ste11(S243E) mutants to Ste5 determined by co-immunoprecipitation of a Ste5-3meGFP variant with Ste11 in unstimulated cells. Ste5-Ste11 binding in WT is set to 1. The binding fraction of the Ste11 mutants is normalized to WT. The mean±s.e. from three independent Western blots is shown.

Taken together, these experiments show that feedback phosphorylation of Ste11 on S243 impairs its binding to the scaffold Ste5 and thereby completely abolishes the Ste5-mediated pheromone signalling. This further leads to activation of ppKss1 and to filamentous-like growth of the cells, pointing at a switch in the pathways at the level of Ste11.

3.4 Fus3-mediated control of Ste5-Ste11 binding is sufficient to generate ultrasensitivity

All findings about the regulation of Ste11 activity on either S243 or T596 were summarized and implemented into a model to describe Ste11 mediated signalling (Fig. 3.30A). Here, Ste11 can exist in different forms in terms of phosphorylation and localization. In the negative Fus3-Ste11 feedback Fus3 can phosphorylate only the freely diffusing Ste11. This phosphorylation impedes its binding to the scaffold Ste5. This Ste11 phosphoform, and the unbound unphosphorylated Ste11 can be phosphorylated additionally on T596, thereby switching-off the kinase activity to impede unspecific signal leakage into the filamentous growth pathway. To theoretically assess if the feedback from Ste11 on Fus3 can produce a switch-like response, a minimal model of ordinary differential equations (ODE) for phosphorylation dependent modulation of the Ste5-Ste11 interaction was constructed (by Aneta Koseska (MPI Dortmund, Dept. 2) (Fig. 3.30B, Chapter 6.2.6.4). In this model each of the Ste11 phosphoforms can be bound on Ste5 with a defined binding rate following first-order kinetics. Only the scaffolded phosphorylated Ste11 form activates the scaffolded Ste7 form. When the interaction of Ste11 with Ste5 is not affected, a clear graded ppFus3 was observed, whereas ultrasensitivity was generated when the phosphorylation induces ~15-fold increase in its binding affinity. A similar loss in binding of the phosphorylated Ste11 (from ~2×10^{1} nM to ~2×10^{2} nM) was calculated from the estimated concentrations provided by the LRA (Fig. 3.9) and the quantifications of the copurification of Ste5 with the Ste11(S243A) mutants (6.2.6.4) Thus, the regulation of Ste11 binding to Ste5 via the Fus3 mediated feedback enables activation of the mating MAPK module at a precise dose of pheromone.

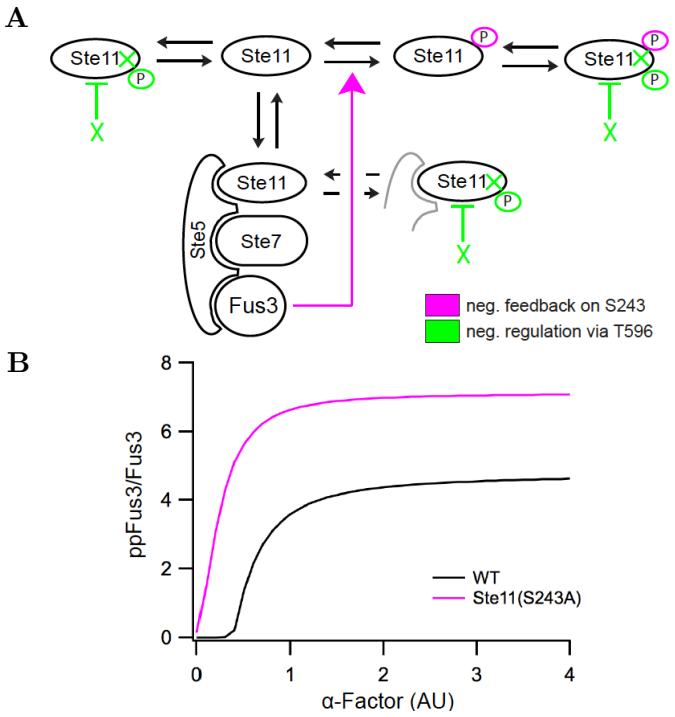

Fig. 3.30: Regulation of Ste11 mediated signalling. (A) Graphical representation of minimal ODE model (only including the negative feedback from Fus3 on Ste11) and the

negative regulation via phosphorylation of Ste11 on T596. Arrow in magenta shows negative feedback. P represents phosphorylation. Green T-bar arrow indicates negative regulation of Ste11 on T596 by an unidentified kinase X. Double arrows indicate interconversion of two Ste11 forms. Geometrical symbols represent MAPK module components. **(B)** Minimal ODE model shows ppFus3 pheromone dose-response of WT cell (black line) vs. Ste11(S243A) cells (magenta line). The model was developed by Aneta Koseska (MPI Dortmund, Dept. 2) (6.2.6.4).

3.5 The negative feedback from Fus3 on Ste11 confines the cytosolic ppFus3 gradient and the morphological response to pheromone

3.5.1 Spatial ppFus3 gradient is constrained by the Fus3-Ste11 negative feedback loop

It was previously shown by Maeder *et al.* that a gradient of cytosolic ppFus3, whose extent was postulated to affect the morphology of the shmoo, emanates from the tip of the mating projection[75]. The shape of the spatial gradient is supposed to depend on three different parameters, specifically (1) the activity of the kinase, (2) of the phosphatase and (3) their diffusion coefficients[188]. As the negative feedback from Fus3 on Ste11 determines the amplitude of ppFus3, it was investigated whether it also shapes the ppFus3 gradient.

In order to visualize the ppFus3 gradient, a novel fluorescence lifetime imaging microscopy (FLIM)-based fluorescence resonance energy transfer (FRET)[217] based method was developed by Lisa Sophia Karajannis, measuring the interaction of ppFus3-yemCitrine with the generic phosphobinder Phos-Tag[271] coupled to Cy3.5. In contrast to antibody-based immunostainings, this phosphobinder binds all phosphorylated residues like Ser, Thr and Tyr. It therefore can also detect both the mono- and the double-phosphorylated forms of Fus3. Fluorescence images of unstimulated and pheromone stimulated WT, Ste11(S243A) and Ste11(S243A/T596I) cells (100 nM α-Factor, 3 h) collected by Lisa Sophia Karajannis (MPI Dortmund, Dept. 2), showed both Fus3-yemCitrine and Phos-Tag-Cy3.5 localized at the tip of the mating projection and the nucleus (Fig. 3.31A). The α-images of unstimulated double mutant cells, which display the phosphorylated fraction of Fus3 (ppFus3/Fus3), already showed higher values in the cytoplasm compared to WT cells, consistent with the higher phosphorylation of Fus3. α-images of all stimulated cells showed higher values at the very tip of the mating projection. The double mutant, however, displayed high values at the shmoo tip, which were extended to the nucleus and beyond.

Quantifying the phosphorylation from the α-values revealed similar ppFus3 amplitudes (ppFus3 levels at the very shmoo tip) in WT and Ste11(S243A) cells. In contrast, a significantly shallower ppFus3 gradient between the shmoo tip and the nucleus was measured in the Ste11(S243A) cells as obvious from exponential fits of the cytosolic α-values (excluding nuclear Fus3 activity) (Fig. 3.31B). These

differences in steepness where confirmed by linear fits of the gradient between the shmoo tip and nucleus (Fig. 8.5). The Ste11(S243A/T596I) cells showed an overall higher phosphorylation of Fus3 throughout the cell, with significantly higher amplitude at the shmoo tip that extended the ppFus3 signal in the cell. This offset in Fus3 activity is consistent with the observed sustained temporal Fus3 activity and the overall strong response to pheromone of this strain (Fig. 3.16).

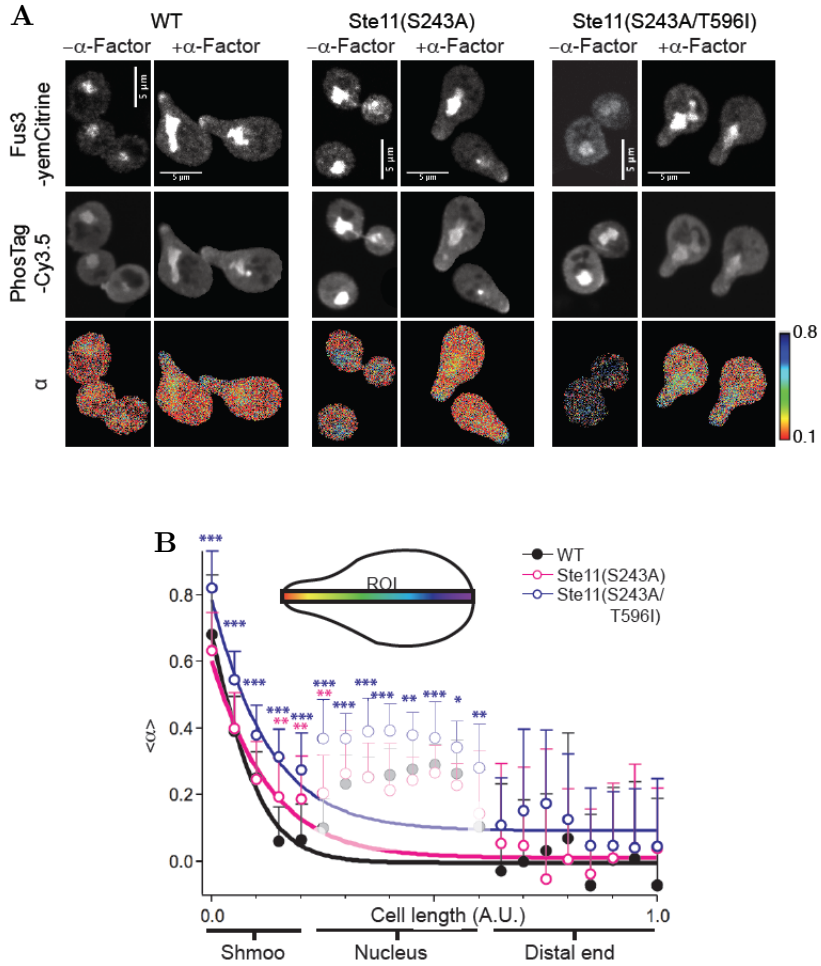

Fig. 3.31: ppFus3 gradient is constrained by the Fus3-Ste11 negative feedback. **(A)** Localization of Fus3 and ppFus3 in unstimulated and stimulated (100 nM α-Factor for 3 h) WT, Ste11(S243A) and Ste11(S243A/T596I) cells. Upper row: fluorescence intensity distribution of Fus3-yemCitrine. Second row: fluorescence intensity distribution of Phos-Tag-Cy3.5. Third row: molar fraction α of interacting Fus3-yemCitrine with Phos-Tag-Cy3.5.. Colour coding on the right. Scale bars in all micrographs indicate 5 µm. **(B)** Quantification of the ppFus3 gradient along the major cell axis calculated from FLIM data by global analysis. <α>±s.d. as function of the distance to the shmoo in WT, Ste11(S243A) and Ste11(S243A/T596I) cells. For each cell the intensity in a rectangular region of interest along the longer axis of the cell from the shmoo tip to the distal end was quantified. Cell length is normalized to 1 (N = 13-18). Data is fitted to an exponential function excluding the nuclear region (shadowed points). Data was recorded and analysed by Lisa Sophia Karajannis (MPI Dortmund, Dept. 2). Asterisks indicate the significance between the WT cells and the mutants Ste11(S243A) (red) and Ste1(S243A/T596I) (blue) obtained by a two-tailed Student's t-test. One asterisk: marginal significance, 0.1>p>0.05. Two asterisks: significant changes, 0.05>p>0.01. Three asterisks: high significance p<0.01.

Interestingly, observation of the morphological response to pheromone of these cells, in terms of shmoo formation, revealed that the Ste11(S243A) cells were more prone to form successive projections at high pheromone concentrations (fig. 3.32). This was probably resulting from their higher sensitivity to pheromone and the less confined ppFus3 gradient (Fig. 3.18, 3.31B).

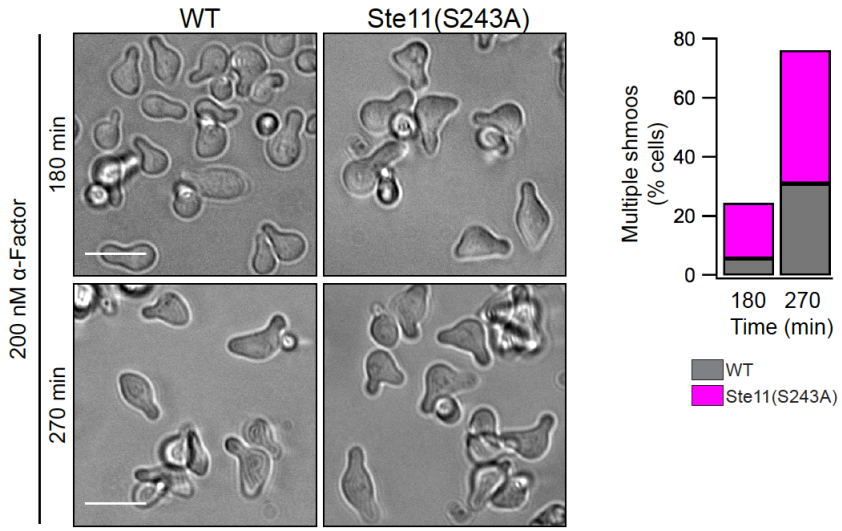

Fig. 3.32: Multiple shmoo formations in Fus3-Ste11 feedback deficient strain. Left panel shows transmission images of shmooing Ste11WT vs. Ste11(S243A) cells stimulated for 180, 270 min with 200 nM α-Factor. Bar graph on right site displays fraction of WT and Ste11(S243A) cells showing multiple shmoo tips (N>200) after 180/270 min of 200 nM pheromone stimulation. Scale bar indicates 5 µm and is representative for all images.

These results demonstrate, that the shape of the cytoplasmic ppFus3 gradient is directly related with the morphogenesis in mating. The negative feedback from Fus3 on Ste11 restricts the ppFus3 gradient and therefore spatially restricts shmoo formation to maintain a unique mating projection.

3.5.2 The phenotypic response to dose of pheromone is determined by the Fus3-Ste11 feedback loop

Since the previous experiment showed an altered morphological response of the feedback deficient strain to high doses of pheromone, and the same strained was impeded in its switch-like ppFus3 response (Fig. 3.18), the phenotypic pheromone dose-response of the Ste11 mutant strains was assessed. In this regard, changes in cell morphogenesis were investigated on a cell population level in the Ste11 non-phosphorylatable mutants (used in the Fus1 reporter gene assay, Fig. 3.1.2), by following Fus1 localization at the PM in conjunction with the mating tip formation. To reduce possible variance through heterogeneous cell cycle states, cells were imaged after 4.5 h (3 cell cycles) of stimulation with the specific α-Factor dose. As expected, the Ste11(S243A) strain was substantially more responsive to lower pheromone concentrations than the corresponding wild type cells, reflected in

both morphological parameters (Fig. 3.33). Unexpectedly, the Ste11(S243A) cells exhibited a similar graded dose-response of the Fus1 localization as the wild type cells, contrary to the observed switch from ultrasensitive to graded ppFus3 response. In the case of shmoo formation, the Ste11(S243A) cells exhibited a more graded response to pheromone than the corresponding wild type cells. Except for unexplainable low numbers of shmoo tips at high concentrations, the Ste11(T596I) strain maintained a similar responsiveness to pheromone as WT cells, consistent with the finding that phosphorylation of T596 only affects the overall amplitude of Fus3 activity.

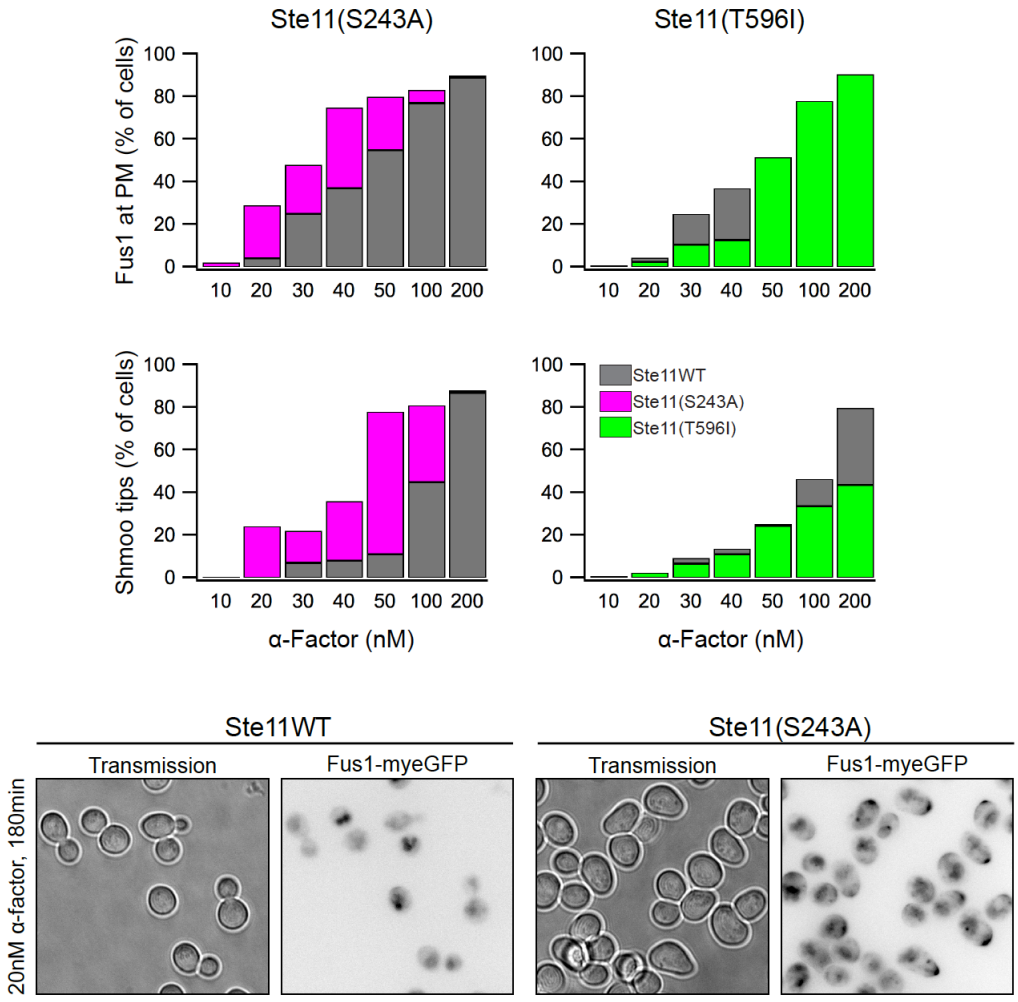

Fig. 3.33: Shmoo formation of Ste11(S243A) cells is more responsive to low pheromone concentration. Pheromone dose-response analysis of PM-localized Fus1 and shmoo tip formation in WT, Ste11(S243A) and Ste11(T596I) cells at 270 min post-stimulation. Results shown as overlaid bar charts ($N > 200$). Colour code in lower right bar graph. Images below are corresponding transmission and Fus1-meGFP fluorescence images of Ste11WT and Ste11(S243A) cells stimulated with 20 nM α-Factor for 270 min.

Detailed investigation of the morphology of the pheromone stimulated feedback deficient Ste11(S243A) cells, by quantifying their shape in terms of major axis length, compactness and eccentricity on a population level, revealed slightly altered

formations of mating projections and an increased cell length (Fig. 3.34). The mating projections of these cells were less pointed, which was obvious from transmission images and confirmed by increasing eccentricity values. An increase in this value represents a change from a circle shape to a line segment. These cells also exhibited an increased major axis length and were less compact in comparison to the stimulated wild type cells.

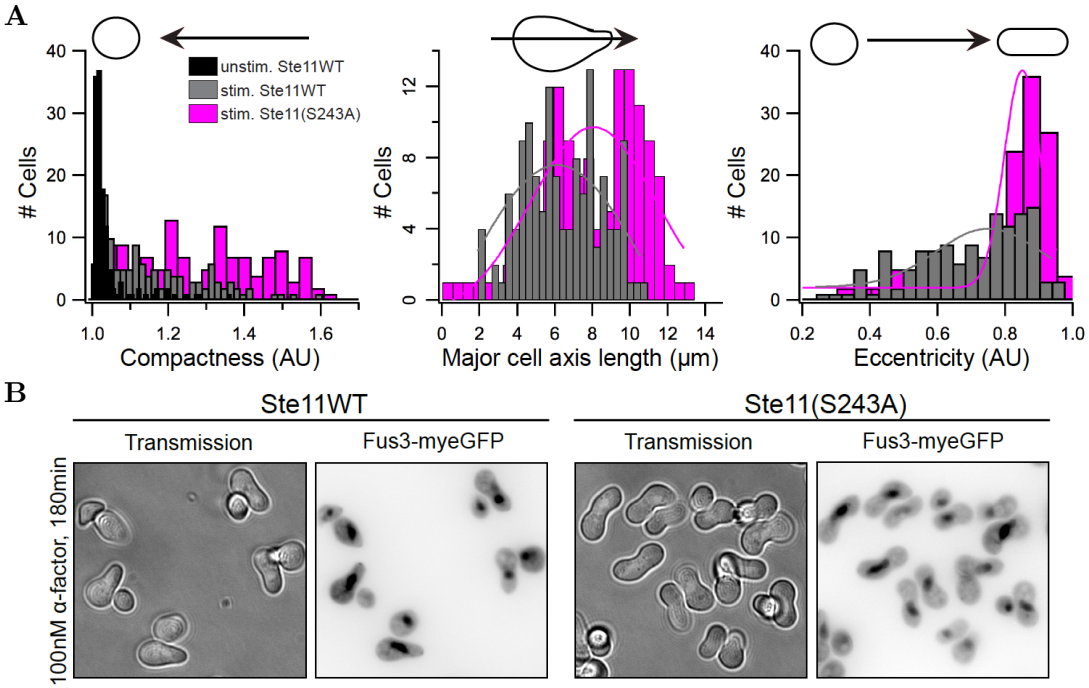

Fig. 3.34: Quantitative and qualitative analysis of shmoo formation of Ste11(S243A) cells. (A) Analysis of morphological features during shmoo formation of Ste11WT cells vs. Ste11(S243A) cells using CellProfiler. Data was binned using IgorPro. Left panel: compactness of cells. Cell with high compactness are small and exhibit round morphology. Middle panel: length of the major cell axis (in µm). Right panel: cell eccentricity (eccentricity of the ellipse, 0 = circle, 1 = line segment). The data was fitted by a Gaussian equation (Ste11(S243A)= solid line in magenta, Ste11(WT)= solid line on grey) ($N \approx 130$ cells). Legend in the left graph. **(B)** Example of transmission and Fus-3ymGFP fluorescence images of stimulated Ste11(S243A) cells with elongated and broadened shmoo tips, as compared to pointed shmoo tips of WT cells.

The Ste11(S243A/T596I) strain that exhibited the strongest phenotypic effect, reflected in an asymmetrical elongated cell shape (Fig. 3.15), showed elevated Fus1 expression at the PM, already apparent under unstimulated conditions (Fig. 3.35). These results were consistent with the findings from the Fus1 reporter gene assay (Fig. 3.14). With increasing pheromone concentrations the initial high Fus1 levels increased gradually but in a less steep manner than in Ste11WT cells. In the morphological response, the majority of the cells (approximately 70 %) retained the elongated morphology upon pheromone stimulation. The remaining cells showed vegetative growth. Cells did form the typical cone-shaped pointed mating only upon high pheromone concentration above 100 nM. A similar morphological threshold was observed for the other Ste11 mutant strains. Thus, these cells exhibit a lower sensitivity and responsiveness to pheromone, probably due to the

autonomously activated Fus3 and its high abundance. This high activity also misregulated the cell cycle, as demonstrated in a strongly reduced growth.

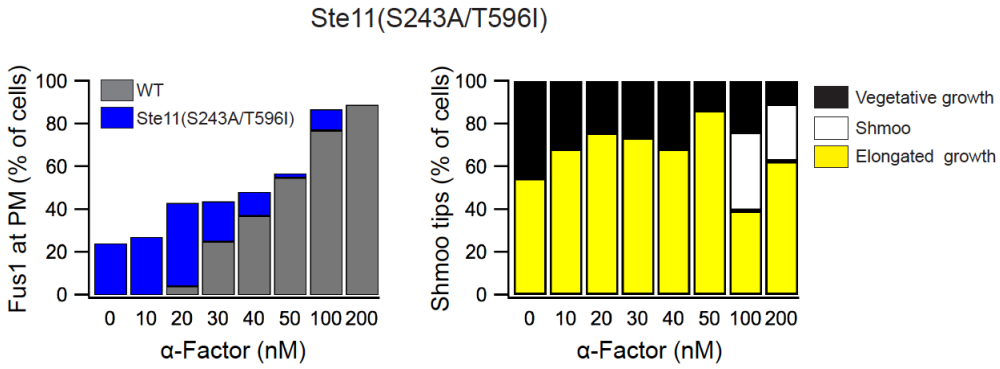

Fig. 3.35: Pheromone dose-response is disturbed in the Ste11(S243A/T596I) cells. Pheromone dose-response analysis of PM-localized Fus1 and morphological outcome in WT vs. Ste11(S243A/T596I) cells (left) and of Ste11(S243A/T596I). Observed morphologies: vegetative growth, elongated growth and the formation of shmoo tips (right). All cells were stimulated for 270 min with specific α-Factor concentrations ($N > 200$). In the left graph the results are represented as overlaid bar charts and in the right graph as stacked bar charts. Colour codes in upper left and upper right corner.

Taken together, these experiments show that the feedback from Fus3 on Ste11 is required to maintain robustness to low pheromone signals. Loosing this robustness by disturbing the feedback probably allows sensing of mating partners at longer distances. However, cells that additionally express the highly active Ste11(T596I), are strongly disturbed in sensing and responding to a pheromone gradient.

Remarkably, the Ste11(S234A/T596I) cells did exhibit different morphologies that were dependent on the presence of the filamentous growth MAPK Kss1. The Ste11(S243A/T596I) strain employed in the afore described experiments, bearing a deletion of Kss1, showed strong phenotypic effects (Fig. 3.36C). Unstimulated cells were generally elongated and showed mating-projection-like extrusions, filamentous-growth-like structures and an asymmetrical cell shape. However, double mutants that expressed Kss1 rather only exhibited mating-projection-like morphologies (Fig. 3.36A). In some of these cells, Fus3, whose localization is an indicator of mating signalling, was localized at mating-projection-like structures, indicating mating pathway activity (Fig 3 26B). Furthermore, the nuclei of these cells, visible by the localization of Fus3, were in close proximity to the projection-like structures. This nuclear positioning was probably regulated by the high basal Fus3 activity[272].

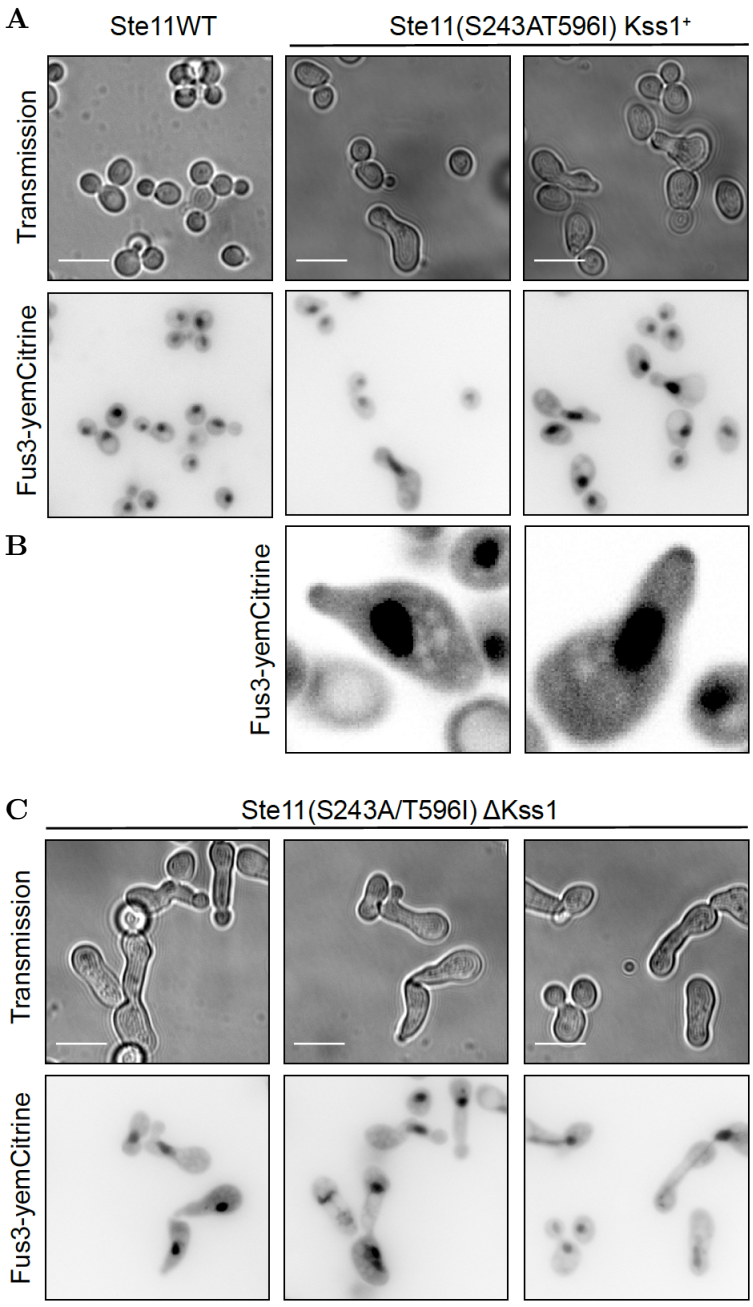

Fig. 3.36: Morphology of Ste11(S243A/T596I) cells depends on Kss1. Transmission and Fus3-yemCitrine widefield fluorescence images from **(A)** unstimulated, vegetatively growing Ste11WT and Ste11(S243A/T596I) Kss1$^+$ cells and **(C)** Ste11(S243A/T596I) ΔKss1 cells. Scale bars indicate 10 µm and are representative for all images. Cells in **(B)** are magnified confocal images of Fus3-yemCitrine showing its cellular localization in detail.

3.5.3 Gauging the distance of shmoo formation to potential mates is regulated by the Fus3-Ste11 negative feedback

To further investigate whether the negative Fus3-Ste11 feedback also controls at which distance to a mating partner a shmoo is formed, the mating response of the Ste11 mutant *MAT***a** cells to WT *MAT*$\boldsymbol{\alpha}$ cells was observed in liquid mating assays (LMA). In this experiment cell populations with a low density were mixed and their interaction was monitored continuously over a period of 7 h. The cell-to-cell response of the opposite mating types was analysed by quantifying specific phenotypic parameters: cell length, average shmooing distance, time required until shmoo formation, the amount of multiple shmoos and occurrence of cell death.

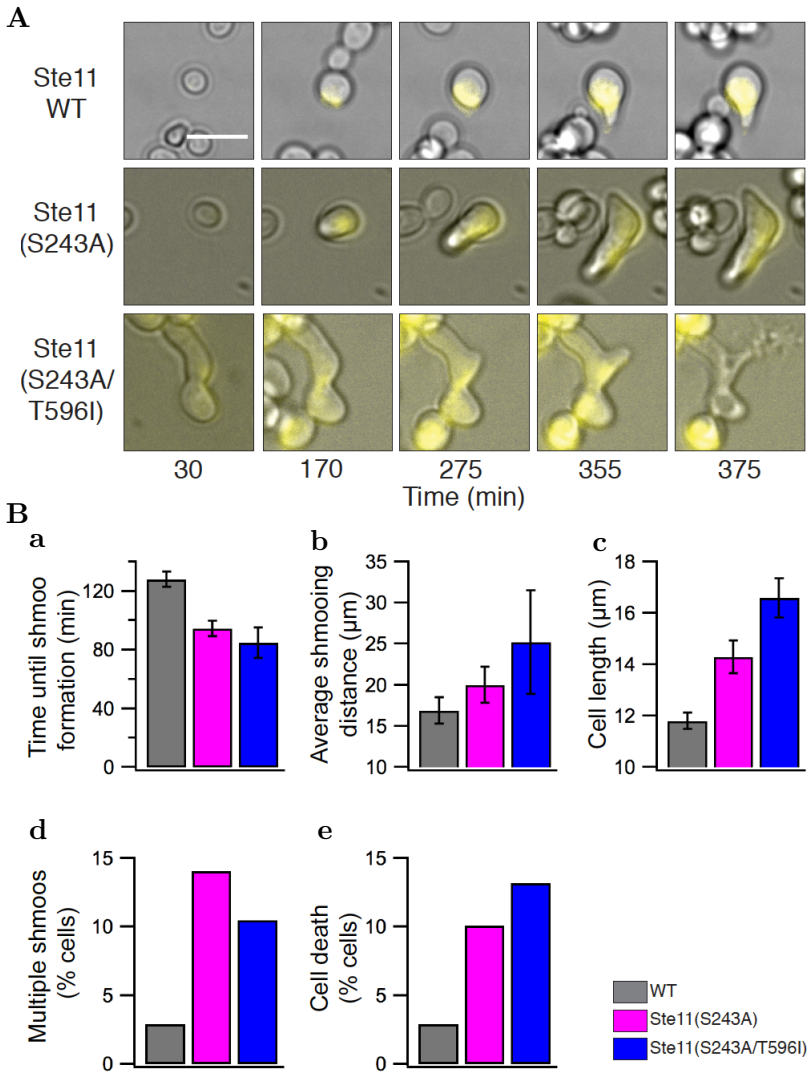

Fig. 3.37: Negative feedback from Fus3 on Ste11 controls the response to a physiological pheromone gradient. (A) Transmission images of mixed cell population of exemplary WT **α**-cells and Ste11(S243A), Ste11(S243A/T596I) mutant **a**-cells exhibiting Fus3-yemCitrine fluorescence at indicated time points after merging populations. Scale bar indicates 10 µm and is representative for all images. **(B)** Quantification of LMA: a. time until shmoo formation after mixing cell populations, b. average shmooing distance, c. cell length, d. fraction of cells with multiple shmoos, e. fraction of dying cells. Parameters in **b.**

– **e.** are determined 450 min after mixing cell populations. Legend on the right. The mean±s.d of N =20-40 cells is plotted.

The assays revealed, that both non-phosphorylatable mutant strains Ste11(S243A) and Ste11(S243A/T696I) were more prone to generate a second mating projection and to form mating projections at longer distances from potential mates (Fig. 3.37). The length of these projections exceeded that of wild type cells, when growing into the direction of a potential mate. In comparison to WT cells, a high fraction of the elongated Ste11 mutant cells burst and died, most often in the Ste11(S243A/T596I) cells that already exhibited a vegetative elongated and asymmetrical cell growth.

Yeast cells treated with high pheromone concentrations form successive mating projections and these formations occurs sequentially with regular periodicity and independently from each other, tip by tip[273,274]. However, feedback deficient Ste11(S243A) cells that were stimulated from a number of directions by $MAT\alpha$ cells, showed simultaneous mating projection formations towards the different pheromone sources (Fig. 3.38). Interestingly, the nuclear Fus3 and therefore the nucleus, which is usually positioned close to the mating projection, appeared to be moving continuously from one projection to the direction of the other and back.

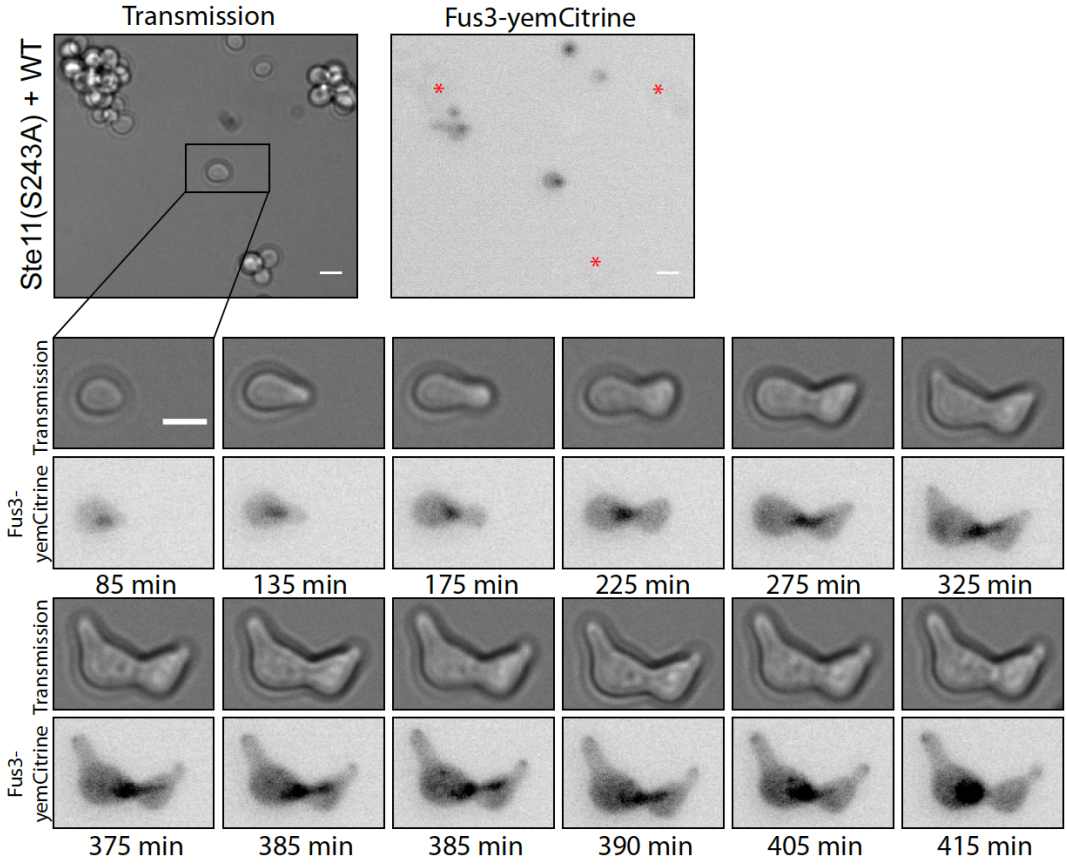

Fig. 3.38: Simultaneous formation of multiple mating projections in the Ste11(S243A) cells. Transmission images of a mixed cell population of exemplary WT α-cells and Ste11(S243A) mutant **a**-cells exhibiting Fus3-yemCitrine fluorescence at indicated time points after merging populations. Scale bar indicates 10 µm and are representative for

all images. Cell subpopulations that do not show signal in the Fus3-yemCitrine image, have the opposite mating type to the Ste11(S243A) cells and are indicated by a red asterisk.

These results on one hand demonstrate that the negative feedback from Fus3 on Ste11 determines the distance to potential partners at which the mating projection is formed and on the other hand determines its morphology. Consistent with the results obtained from former experiments, the negative feedback reduces the sensitivity to pheromone and increases the signal-to-noise ratio during mating in a cell population, thereby maintaining the formation of a single mating projection towards the source of highest pheromone concentration.

3.6 Concerted regulation of polarization events during mating by Fus3 and Kss1

Both in the liquid mating assays and in the dose-response experiments two different polarization events were observed: at low pheromone concentrations cells tended to elongate towards the gradient, similar to filamentous growth, and divided when concentrations were not increased, whereas above a defined pheromone concentration cell division was arrested and the cells formed the typical cone-shaped shmoo tips (Fig. 3.39A). Here, the expression of Fus1 was detected at the PM already at low concentrations, and its response curve followed the sum of quantified elongated and shmooing cells.

The observation of pheromone concentration-dependent differential morphogenesis is consistent with recent[248] and older[133] studies. In this regard we hypothesized that elongation of cells is mainly regulated by activation of the filamentous growth MAPK Kss1 while Fus3 controls mating tip formation. Furthermore, both polarization events might work in concert via differential activation and regulation of these MAPKs. It was shown that Fus3 exhibits a transient adaptive temporal activity and an ultrasensitive response to pheromone dose, while Kss1 exhibits a short abrupt transient temporal response and a graded pheromone dose-response[129,247]. Unexpectedly, response curves of ppFus3 and ppKss1 from the dose-response experiments in Figure 3.18 and 3.22 did not exhibit significant differences at all, neither at low nor at high pheromone concentrations. The relative phosphorylation levels, however, indicated a possible higher basal Kss1 activity (Fig. 3.39B), which could explain the cell elongation at low pheromone concentrations. To assess if Kss1 activity affects the growth of cells as a result of pheromone stimulation, the morphological response to α-Factor-dose of the Ste11(T596I) mutant was investigated, as it was shown to mainly affect Kss1 activity (Fig. 3.18, 3.22, 3.25). Interestingly, these cells tended to elongate in the absence of pheromone (Fig. 3.39C). At low pheromone concentration, cells exhibited strongly elongated cell growth in contrast to WT cells, while retaining the pointed cone-shaped shmoo formation at high concentrations. These preliminary results indicate a possible function of Kss1 in polarization events at low pheromone concentrations, probably to search for potential mating partners. Once an appropriate mating partner is found, by sensing higher pheromone

concentration, the cells start to arrest in G1 and form the mating projection, which is controlled by Fus3 activation.

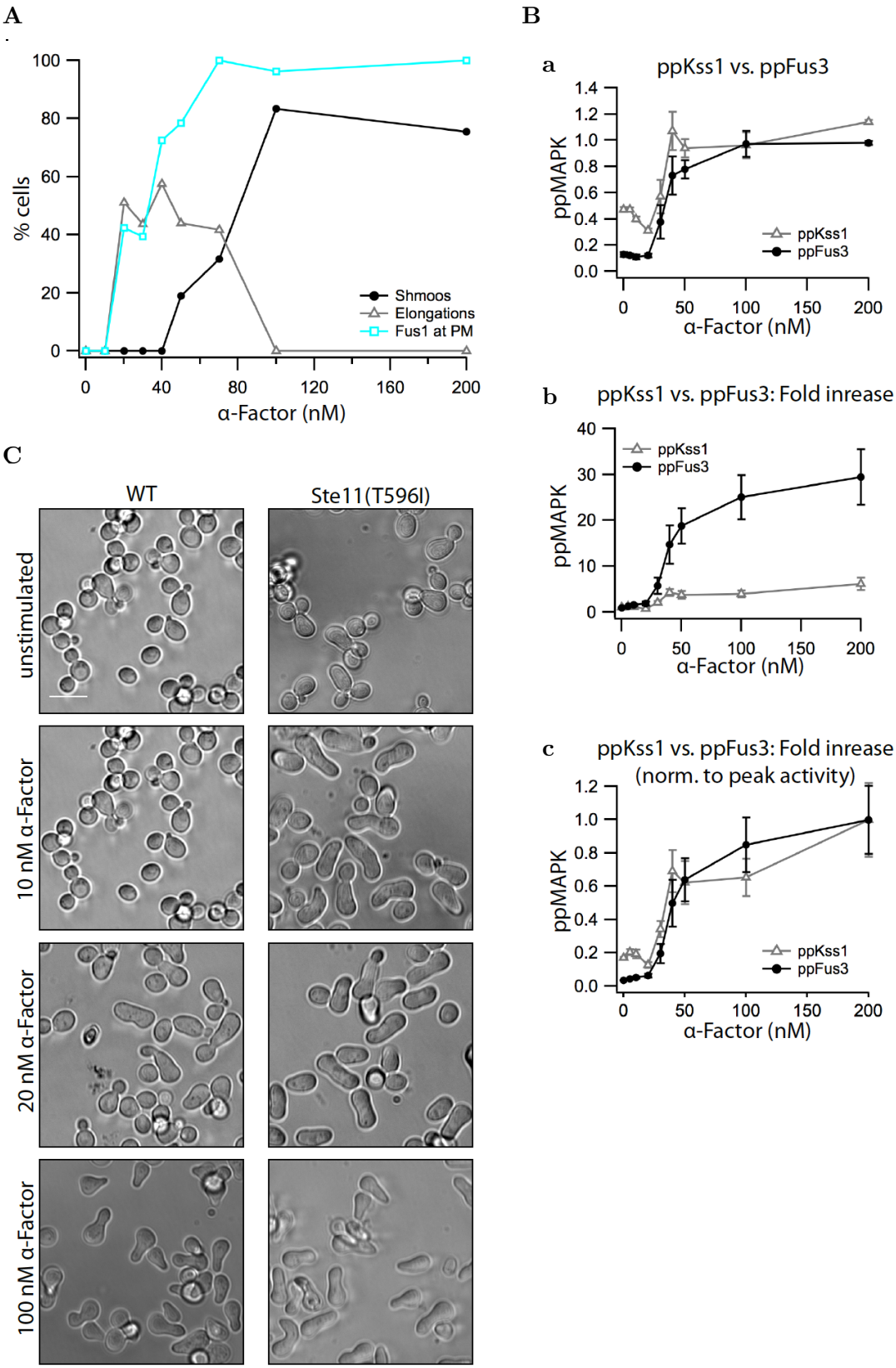

Fig. 3.39: Cells elongate at low and shmoo at high pheromone concentrations. (A) Morphological response to pheromone-dose in wild type cells. The

percentage of cells showing Fus1-ymeGFP localization at the PM (cyan square), cell with elongated growth (grey triangle) and cells with shmoo formation (black dots) were quantified (N = 70 -150 cells). **(B)** ppFus3 vs. ppKss1 response to dose of pheromone (data from fig. 3.18). The mean±s.e. from 8-9 independent western blots is shown**. a.** Values were normalized to maximal phosphorylation. **b.** Fold increase of the same values, setting basal levels to 1. **c.** Same fold increase quantification but normalized to maximum fold increase. **(C)** Transmission images of WT and Ste11(T596I) cells stimulated with different α-Factor concentrations for 270 min. Scale bar indicates 10 µm and is representative for all images.

4 Discussion

The MAPK network architecture constitutes positive and negative feedback loops, which dictate its spatiotemporal dynamics and its sensitivity to stimuli, thereby maintaining a specific response to a distinct dose of stimuli. Inferring the connections in this network and revealing feedback designs in MAPK cascades still constitutes experimental problems, since determining interactions between individual nodes comes at the cost of introducing perturbations that propagate through the network and thereby impact the global response. To circumvent this fundamental problem, we used the genetic amenability of the yeast *Saccharomyces cerevisiae* to measure the endogenous interactions within the mating MAPK module in a time-dependent response to pheromone stimulation. By applying a reverse engineering approach, that combines FCS measurement of the MAPK module protein complexes and a linear regression analysis of this data, we were able to uncover a hitherto uncharacterized feedback loop. This feedback loop is mediated via the phosphorylation of S243 on Ste11, which impedes its binding to the scaffold Ste5, and thereby regulates the signalling activity of Ste11. In this thesis it was further demonstrated how this network motif dictates the dynamic response properties of the mating signalling system, and how it translates the signal into a morphological response by spatial control of Fus3 activity.

4.1 A reverse engineering approach to infer the mating MAPK module network architecture

Signalling through the mating MAPK module produces a transient adaptive MAPK response, where a low basal Fus3 activity rapidly rises to highest peak levels[5] that subsequently relaxes to lower activity by adaptation. These time-points determine the dynamic mating response to pheromone that is dictated by the underlying feedback mechanisms and therefor were chosen for the cytosolic FCS measurements. However, signalling through the MAPK module and the activation of Fus3 is accomplished at the PM. Therefore, changes measured in complex abundances could be caused simply by translocation of MAPK module components to the PM upon pheromone stimulation. Furthermore, the impact of signalling on the interactions within the MAPK module might not be captured by cytosolic measurements. Are cytosolic measurements useful at all?

Interestingly, pheromone stimulation did not change the total concentrations of the MAPK module (Fig. 3.2), indicating that probably either only a small fraction is localized to the PM or that MAPK module complexes only transiently assemble at the PM. In contrast, we could detect an immediate translocation of Ste5 to the PM and a following translocation of the MAPKs at later times of stimulation (Fig. 3.1). Probably, an immediate localization of the MAPKs might not have been visible, because a large extent was and remained monomeric (20 – 40 nM) and therefore cytoplasmic, and only a small fraction was bound to the scaffold Ste5 upon pheromone stimulation (approximately 5 – 10 nM for all MAPKs) (Fig. 3.9).

But why could the translocation of Ste5 not be detected in the FCS measurements, in particular, since 80% of the total cellular Ste5 was demonstrated to be recruited to the PM[257]? On the one hand the measured complex concentrations showed a high variance, which could mask changes. On the other hand, the continuous nucleocytoplasmic shuttling of Ste5, which strengthens and sustains signalling by a pheromone triggered nuclear release of Ste5[275], could maintain constant cytoplasmic Ste5 levels even when Ste5 gets recruited to the PM to a large extent. However, since the total concentrations of the MAPK module as measured by FCS remained stable over time (Fig. 3.2)[75], changes in complex abundances would most probably be mating dependent and not simply result from protein translocation. Furthermore, feedback mechanisms that maintain the steady state in vegetatively growing cells depend on cytosolic interactions, like the feedback from Fus3 to Ste5, and therefore could be captured by measuring interactions in the cytosol.

In contrast to the study by Maeder *et al.*[75], some of the measured MAPK module complexes indicated mating signalling dependent changes. The Ste5-Fus3 complex for example showed a potential dissociation at short times of stimulation (Fig. 3.2), which was shown to be important for the switch-like mating response before[6]. This could be further investigated by measuring the mating independent formation of Ste5-Fus3 in a corresponding strain by deletion of the phosphatase Ptc1. However, all measured abundances were dominated by a high cell-to-cell variation. Variance in gene-expression can result from both the stochastic fluctuation in the expression of a protein called "intrinsic noise or fluctuations", and the differences in other cellular components that determine its expression called "extrinsic noise"[276]. This extrinsic noise dominates the total noise as experimentally proven[277]. How to benefit from the cell-to-cell variability can be explained by the following analogy. A signalling network with an unrevealed causal topology can be compared to a machine with unknown functions and settings. This machine can fabricate products of a certain size in a certain time and both quantities are unknown. If the machine produces only one product with clearly defined quantities (low variance) the spectrum of possible adjustments of the machine will remain unidentified. But if the machine fabricates products with a wide range of quantities (high variance) the whole range of possible functions and settings will become uncovered. Another analogy can be drawn by investigating the relation of human skin properties or colour to the response to UV-irradiation. If a group of people with the same skin colour is exposed to UV-irradiation of certain duration they will show similar responses, for example sunburn. But if a group of people with a variety of skin colours is exposed to the same UV-irradiation, depending on the colour of the skin it will take shorter or longer to get sunburn and thereby it will be possible to relate these two properties.

The interactions of the MAPK module investigated by FCS are on the one hand itself determined by feedback mechanisms and on the other hand determine the capacity to transmit a pheromone triggered signal and thereby the output of the mating pathway. It was shown, that cell-to-cell variation is dominated by differences in this capacity of individual cells to transmit the mating signal[5]. Thus,

cell-to-cell variance in the complex abundances encodes information about how signalling is regulated and therefore could be used to infer network architecture.

4.1.1 Higher order MAPK module complexes might only transiently assemble

Linear regression analysis of the FCS data showed clear changes especially in the abundances of the MAPK module dimeric interactions. To improve this estimation constrains were imposed that were revealed by systematic perturbations through the deletion of the scaffold Ste5. These showed that interaction of Ste11 with Ste7 was scaffolded and not direct (Fig. 3.7). However, Ste7 activation by Ste11 in filamentous growth does not require Ste5[111]. Although it was shown *in vitro* that Ste11 itself can activate Ste7[123], its activation in the filamentous growth response is most probably mediated via another scaffold or adaptor protein, like Bem4[278], as previously supposed[110]. Constraining the LRA using this perturbation data did not lead to significant changes in the overall concentration profiles, except for the rise of the so far undetected trimeric complex Ste5-Ste11-Ste7 (Fig. 3.9). Its appearance is most probably the logical consequence of removing the possibility of a direct Ste11-Ste7 interaction. Interestingly, this complex is already assembled in the cytoplasm prior to pheromone stimulation, and could therefore function as a passive activation platform, which is recruited to the PM for activation[67], as apparent from its increasing abundances. Its preassembly would allow a faster response to pheromone, and possibly a direct control of the activity, and potential interactions of Ste11 and Ste7 in other signalling pathways. The presence of the trimer Ste5-Ste7-Fus3 was not observed, although it is required to catalytically unlocking Fus3 for phosphorylation by Ste7[123]. This complex might only appear transiently, as supposed before[4] and therefore be difficult to detect. Also the tetrameric complex could not be observed in the cytosol, although its association was demonstrated by two hybrid-data and co-purification experiments[2]. This complex could be assembled by a Ste7-Fus3 dimer binding the Ste5-Ste11 complex[2]. But most probably, these higher order complexes only appear transiently at the PM upon pheromone stimulation, since Ste7 and Ste5 both compete for the same docking site on Fus3[260]. However, it remains unclear why the trimer of Ste5-Ste11-Fus3 was not present in the analysis, although both, the dimers Ste5-Ste11 and Ste5-Fus3 were clearly present. These complexes might be mutually exclusive. Ste11 binds the PH domain of Ste5, which also binds at the PM and thereby triggers a conformational change "activating" the scaffold[61,67], which releases Fus3 from the complex. Binding of Ste11 to Ste5 therefore might also trigger this allosteric Fus3 release.

Remarkably, the four monomeric MAPK module components remained cytosolic to a large extent (more than 50% of the total). Especially Fus3 was predominantly cytosolic (approximately 80%), consistent with its role as a signal transducer from the cytoplasm to the nucleus. Furthermore, the freely diffusing state of Fus3 could be preferred in mating signalling induction, since this form can

be activated with less effort, as shown with Ste5 non-docking mutants impaired in binding Fus3[4,6,247].

4.1.2 Different roles of Fus3 phosphoforms in maintaining signalling specificity

The biggest changes in protein-species abundances were detected in the dimeric complexes, indicating that these complexes mainly organize mating signalling and its regulation by feedback mechanisms. Interestingly, the temporal concentration profiles of the dimeric species Ste5-Fus3 and Ste5-Ste7 corroborated the trends that were already emerging from the pairwise FCS measurements. The complex of Ste5 with Fus3 was strongly disrupted upon pheromone stimulation, thereby releasing the "negative recruitment" of Fus3. The Ste5-Ste7 interaction showed a stepwise reduction with on-going pheromone stimulation, while the fraction of monomeric Ste7 increased, consistently. Interestingly, the changes in complex abundances of these two dimeric interactions exhibited interdependence. As Fus3 was released from Ste5, Ste7 was also released from Ste5. The interaction of Ste5 with Ste7 might therefore be controlled by the Ste5 auto-phosphorylated Fus3, which is known to hyper-phosphorylate Ste7[112] and control Kss1 activity[130]. Non-phosphorylatable and phospho-mimicking mutants of these multiple phosphorylation sites did not show a difference in Ste5 binding, as shown by Maleri *et al.*[112]. However, synchronic phosphorylation of these sites and the sites in the activation loop strongly diminished Ste5 binding. Therefore, regulation of this interaction might regulate MAPK module signalling and determine the pathway specificity of Ste7 mediated MAPK phosphorylation.

Remarkably, all Fus3-based dimeric complexes exhibited the same temporal concentration profiles reflected by a decrease in complex abundances upon pheromone stimulation and an increase at later times of stimulation. Remarkably, Fus3 is known to phosphorylate its interaction partner Ste5[4,6] and Ste7[112], and also Ste11 as shown in particular in this thesis by the detection of the Fus3-Ste11 enzyme-substrate complex (Fig. 3.10). As this cytosolic complex already evolves in unstimulated cells, it might be initiated by the autoactivated mono-phosphorylated form of Fus3 (pTyr-Fus3), such as the negative feedback of pFus3 on Ste5 and the regulatory phosphorylation of Ste7 by pFus3. The auto-phosphorylation of Tyr182 in Fus3 in cis leads to a disordered activation loop, which increases the accessibility for substrates and consequently its activity[4]. This auto-phosphorylation event occurs in all dual-specificity tyrosine phosphorylation-regulated kinases and is biochemically different to phosphorylation by an upstream kinase, regarding its substrate, the accessibility of the ATP-binding pocket, and the mechanism of phosphorylation[279]. We therefore propose that the cis mono-phosphorylated Fus3 might have a different role in mating signalling than in trans double-phosphorylated ppFus3. The pTyr-Fus3 mediated feedbacks on Ste5 and Ste11 maintain the state of vegetative cell growth by keeping Ste11 signalling activity and Fus3 activity in check. Disrupting the Fus3-Ste11 negative feedback in the double mutant cells Ste11(S243A/T596I) lead to a highly basal active Fus3 and

high Fus3 expression (Fig. 3.16, 3.20), whereas mimicking a 100% feedback controlled Ste11 in the Ste11(S243E) phospho-mimicking cells, showed a decreased expression level of Fus3 in unstimulated cells (Fig. 3.17). It was also shown, that when binding of Fus3 to Ste5 is disrupted its function as a molecular chaperone for the auto-phosphorylation of Fus3 in *cis* is abrogated. Cells then produce an enhanced transcriptional output[4] and show a higher sensitivity to pheromone in terms of shmoo formation[6]. Abolishing the negative feedback from Fus3 on Ste11 showed the same effects on transcriptional output and on response dynamics (Fig. 3.12, 3.14, 3.18). However, when mating signalling is induced, Fus3 gets double-phosphorylated in trans, thereby changing its role from a negative to a positive regulator of mating signalling. This is reflected in a reduction of all Fus3 dimeric complexes upon pheromone stimulation, which probably also reduces the strength of feedback mediated control. At later times of stimulation feedback control of the mating MAPK module is required to adapt to lower MAPK activation levels, which is reflected by increasing abundances of the Fus3 mediated dimeric complexes. Consistently, the Fus3-Ste11 feedback defective cells showed a reduced level of adaptation (Fig. 3.16).

To further analyse the possible dual regulation of the different Fus3 phosphoforms, experiments with the Ste5ND mutant, which prevents the generation of pTyr-Fus3, have to be acquired. Here, a loss of the adaptive response or an increase of basal Fus3 activity and higher basal Fus3 expression levels would be expected. Furthermore, partially non-phosphorylatable Fus3 mutants could be applied to investigate its role in response dynamics and its impact in the complex abundances of the Fus3 mediated dimers, in particular the enzyme-substrate complex formation of Fus3-Ste11. However, to monitor the temporal response of pTyr-Fus3 would require specific antibodies or other detection methods, like Phos-tag SDS-PAGE[75,271].

4.2 Dynamic properties of the mating response are dictated by a negative feedback

Negative feedback loops can buffer noise; they produce adaptation and robustness to variations of the components involved in the feedback loop and therefore are thought to stabilize the MAPK cascade output and determine its temporal response (Chapter 1.3.3) (Fig. 1.10).

When abolishing the negative feedback from Fus3 on Ste11, the transient adaptive temporal ppFus3 response changed, showing a higher burst of Fus3 activity and higher amplitude of Fus3 activity after adaptation (Fig. 3.16). Thus, loosing this feedback control, the signalling system is less effective to adapt to incoming stimuli. Since the decrease in adaptation is relatively small, it is likely that its impact, the strength of the feedback, is relatively mild, and that further feedback mechanisms maintain the adaptive properties. Abolishing this feedback and simultaneously increasing Ste11 activity by introducing the T596I mutation (Ste11(S243A/T596I) disrupted the adaptive ppFus3 response and led to a more

sustained Fus3 activity. Interestingly, these cells also exhibited high basal ppFus3 levels, strongly exceeding that of the WT cells. This confirms the maintenance of the steady state of the signalling system in vegetatively growing cells by this feedback, as already indicated by the concentration profiles of the Fus3 dimers (chapter 4.1). In contrast, upregulated Ste11 activity on its own in the Ste11(T596I) cells only changed the overall Fus3 activity but not adaptivity. Thus, the negative feedback form Fus3 on Ste11 on the one hand stabilizes and adapts signalling via the MAPK module, and on the other hand provides robustness to variations of the components involved in the feedback loop.

Robustness provided by negative feedbacks is a property of signalling systems that need to generate a precise and reliable output and therefore are in need of buffering variations generated by molecular noise or by environmental fluctuations[280]. In the MAPK mating response, cells have to switch from the state of vegetative growth to the state of mating differentiation, and this switch occurs at a certain pheromone concentration. Therefore, the cells need the ability, to sense and distinguish, to interpret concentration gradients produced by potential mates and thereby their distance. This property is maintained by cellular robustness on two levels. On the one hand cells must be robust to low pheromone concentrations to prevent inappropriate and random, energy-consuming attempts to mate below a critical value. On the other hand they require robustness to alterations in the components of the signalling system. The latter was observed as a property of the negative feedback from Fus3 on Ste11. Consistently, the cells which were feedback deficient also exhibited a diminished robustness and higher sensitivity to low pheromone concentrations, and were less effective in creating a switch-like response (Fig. 3.18). Both, the Ste11(S243A) and the Ste11(S243A/T596I) cells exhibited a more graded pheromone dose-response relationship apparent from low Hill coefficients of 1.68 (S243A) and 1.44 (S243A/T596I). In contrast, the dose-response of the highly active mutant Ste11(T596I) remained ultrasensitive and only showed a small shift of the activation threshold towards lower concentrations. Phosphorylation control of this site on Ste11 determines its activity, most probably by either regulating autoinhibition through conformational change[71], or by switching between the "in and out" orientation of the DFG motif[281]. Thus, only changing the strength of signal transmission within the MAPK module does not automatically change the activation kinetics. This shows, first, that the system is robust to perturbations of its components, and second, demonstrating that the arrangement of MAPK cascades does not serve to just amplifying a signal[141].

In an adaptive system that is continuously exposed to significant background stimuli, like in the yeast mating decision, it is more important to amplify and regulate the sensitivity to a certain dose of signal[142]. The negative feedback loop from Fus3 on Ste11 is doing so by modulating the binding of Ste11 to Ste5, as proven experimentally (Fig. 3.29) and elucidated by a mathematical model (Fig. 3.30). When the feedback is on, Ste11 is phosphorylated at S243 and binding to Ste5 is decreased, thereby keeping signal transmission via the mating MAPK module in check. It thereby works in concert with other regulatory mechanisms to

ensure the filtering of weak pheromone signals. However, above a critical pheromone concentration when signalling by the MAPK module is initiated, the Fus3-Ste11 feedback is either switched off or might be dominated by other regulatory mechanisms and Ste5-Ste11 binding should increase. Therefore, the interaction of Ste5 with Ste11 might also show a switch-like behaviour to pheromone stimulation. Interestingly, the LRA revealed an increase in Ste5-Ste11 abundances, but only at later times of stimulation, whereas the fraction of monomeric Ste11 increased immediately to stimulation and remained on this level (Fig. 3.9). The latter indicates less Ste11 in complex upon pheromone stimulation, which implicates a possible reduction of Ste11-Ste5 complexes and therefore does not support the proposed occurrence of a basal Fus3-Ste11 feedback. To reveal how the Ste5-Ste11 binding contributes to signalling, the pheromone dose-response relationship of the Ste5-Ste11 interaction has to be investigated.

Since Ste11 binds to Ste5 via its PH domain[62], which also mediates the binding to the PM and, as a result, gets released of its autoinhibition by an allosteric mechanism[67], the interaction of Ste11 to Ste5 through this domain could potentially regulate the "activation" of Ste5. Therefore, it would be interesting to monitor and compare the localization of Ste5 to the membrane in response to pheromone dose, in wild type cells and in cells lacking the Fus3-Ste11 feedback.

Interestingly, ultrasensitivity is generated by the negative feedback from Fus3 on Ste11, but also via the negative feedback from Fus3 on Ste5, and disrupting either of both transforms a switch-like pheromone response to a graded response. Thus, ultrasensitivity seems to be maintained by different network motifs in the mating MAPK module architecture. It remains unclear on which levels this response is developed, and how is this organized. This behaviour could emerge from a combined response of successive levels, each exhibiting ultrasensitive properties[141,282]. First, ultrasensitivity is generated at the level of Ste11 by modulating the Ste11-Ste5 interaction through feedback phosphorylation by Fus3. This feature passes downstream in the MAPK module to the next levels of ultrasensitivity, where the autoactivated $Fus3^4$ dissociates in a switch-like manner from $Ste5^6$, to be activated by $Ste7^{123}$. Because of the successive signal transmission in the hierarchical cascade arrangement[141], "switching-off" the ultrasensitivity at any level leads to a loss of the switch-like property of the MAPK-module output. Assuming that every level in the mating MAPK cascade exhibits ultrasensitivity ascribed by a Hill coefficient of 4, the successive signal transmission in the cascade will produce a final input-output relationship with a Hill coefficient of 81[282]. But, if one step in the cascade exhibits a Michaelian response to its upstream regulator, the fold-change in output and thereby the sensitivity to input would decrease in this step and in the cascade. A kinase in this cascade that would exhibit hyperbolic sensitivity would require a 81-fold increase in input to increase activation from 10% to 90% of its maximum[142]. This 9-fold decrease in sensitivity would pass down in the MAPK cascade and opposes the increase in sensitivity gained by ultrasensitive features. Thus, the cascade, combining its different levels of ultrasensitivity, behaves like a highly cooperative enzyme.

However, apart from the hierarchical cascade arrangement, the two feedbacks are probably depending on each other, provided that, both feedbacks are mediated by the autoactivated pTyr-Fus3. The binding of Fus3 to Ste5 generates this partially active form, which mediates the feedback on Ste5. This autoactivated pFus3 also phosphorylates Ste11 leading to a significantly decreased binding to Ste5. This in turn prohibits the full activation of Fus3 thereby maintaining the pool of partially active pTyr-Fus3. Disrupting either of the two feedbacks, by introducing the Ste11(S243A) mutant, or by mutation of the Ste5-Fus3 docking site, would deplete the source of autoactivated Fus3 that mediates these feedbacks, and therefore change the pheromone dose-response properties. However, if the Fus3-Ste11 negative feedback would be mediated by the fully active ppFus3, its disruption would lead to an increase in Ste5-Ste11 binding and thereby to activation of the MAPK module even at low concentrations. On the other hand, a disruption of the Ste5-Fus3 complex by Ste5ND, might also lead to a diminished phosphorylation of Ste11 by Fus3, which might require the initial allosteric release by Ste5.

The double mutant Ste11(S243A/T596I) exhibited the biggest changes in the pheromone response properties, showing high basal ppFus3 levels, a loss of the adaptive response, and a clear graded ppFus3 dose-response. This could be explained by the stronger interaction of a constitutive active Ste11 to the scaffold Ste5 on the one hand, or through a cooperative effect in multisite phosphorylation on the other hand[283]. Its underlying mechanism is a priming phosphorylation of one specific site, which does not show a big effect, but can for example produce a positive allosteric interaction that leads to cooperative phosphorylation of the second site. It is therefore able to generate a highly ultrasensitive response, as was observed in the regulation of CDK activity in yeast[284]. In the case of Ste11, the phosphorylation of one site might result in a conformational change, as proposed for the T596 residue[71], that than allows the phosphorylation of the other site on Ste11 which than shows a strong effect.

4.3 The mating MAPK module architecture regulates time and direction of shmoo morphogenesis

The double mutant cells exhibited significantly increased Fus3 expression (approximately 3-fold), which is regulated by an autoregulatory feedback loop (Fig. 3.20). As Fus3 not only regulates mating signalling, but also cell polarization[272,285] and the cell cycle[25,81], this feedback probably does not determine exclusively the signalling steady state of the cell, but also its morphology. Consistently, its deregulation accompanied by a constitutive active Ste11 in Ste11(S243A/T596I) cells led to reduced growth rates and significant morphological alterations, expressed in elongated and unsymmetrical growth, pointing at uncontrolled, highly active basal signalling. Interestingly, the extent of morphological changes was dependent on the presence of the filamentous growth MAPK Kss1 (Fig. 3.36). In its presence cells showed unsymmetrical growth and shmoo-like morphologies, with

localized Fus3 in some of the tip-like structures, whereas in a background with deleted Kss1, cells exhibited a higher heterogeneity in morphologies, additionally showing highly elongated structures, some of them being similar to filamentous growth-like morphologies. Furthermore, it seemed that the nucleus in the double mutant cells expressing Kss1 was positioned in close proximity to the tip-like structures, whereas the corresponding cells missing Kss1 did not show a specific nuclear positioning. This nuclear positioning by actin-based migration towards the mating projection is a clear indication for activated mating signalling[286,287]. Probably, the deletion of Kss1 led to an active filamentous growth response in these cells and thereby to the elongated cell growth, since inactive Kss1 represses the function of Ste12 by binding[90]. Therefore, its deletion in the double mutant strain would most likely activate Ste12 driven filamentous gene transcription leading to the observed elongations.

A mating MAPK signalling system senses information about the external pheromone gradient and transmits and interprets that information to decide to mate or not to mate. The Ste11(S243A/T596I) cells, however, remained their altered morphology at low and intermediate pheromone concentrations, and only weakly responded at high concentrations by the formation of shmoo tips. These cells were strongly disturbed in translating the information content of a pheromone gradient into a proper response (Fig. 3.35) and have probably lost their ability to read and interpret the pheromone gradient and thereby to gauge the distance to a potential partner. This was strongly reflected by a significantly faster response and shmoo morphogenesis to potential mates in longer distance (Fig. 3.37).

In case of the Fus3-Ste11 feedback deficient cells, the formation of mating projections was initiated already at low pheromone concentrations, at which wild type cells were not responsive at all (Fig. 3.33), reflecting the measured graded ppFus3 dose-response (Fig. 3.18). This indicated a response to potential mates at longer distances, which was confirmed in the mating assay. It was noticeable, that a high fraction of these cells was more prone to form successive projections both in response to a pheromone gradient (Fig. 3.37) and in response to homogenously distributed pheromone concentrations (Fig. 3.32). This “multiple shmooing” was demonstrated in former studies to occur periodically, approximately every 90 min. Therefor, high isotropic pheromone concentrations were required, present when cells are in immediate proximity to potential mates[273,274]. This was verified by showing that cells exposed to a gradient of low pheromone concentrations orient by polarized growth towards the gradient whereas at higher concentrations these cells orient by formation of a second shmoo[248]. Interestingly, we could observe a similar behaviour in the mating assays where WT cells attempted to reorient mating tip growth, whereas the Ste11(S243A) cells rather generated a second shmoo tip and occasionally two mating projections simultaneously (Fig. 3.38). These cells probably undergo “default mating”, where they probe in different direction for a partner and mate randomly with either pheromone excreting or non-excreting cells[274]. These attempts to mate are time-consuming and less efficient than the orientation along a pheromone gradient through chemotropic growth. This shows,

that the Fus3-Ste11 negative feedback takes part in the interpretation of the pheromone gradient, and thereby in sensing the distance to potential mates. When this feedback and thereby an ultrasensitivity response is disrupted, cells interpret lower pheromone concentrations as high pheromone concentrations.

But how can the MAPK network architecture, and especially a simple and commonly used motif like a negative feedback, specifically control polarized growth and the shape of the cell? On the one hand cell fate and thereby cell morphology is governed by response dynamics, which are dictated by the negative feedback from Fus3 on Ste11. Another important aspect is the spatial control of key signalling components and their interactions, like the localization of the MAPK Fus3 and its interaction with the MAPK module components. Fus3 is one of the key regulators of pheromone-induced polarized growth. It activates and localizes Bni1[272], a formin homologue, which is part of the "polarisome" (Bni1, Spa2, Pea2)[288,289] that regulates actin cable polymerization and cell polarization. Therefore, the activity of Fus3 and its localization will determine the localization of Bni1 and thereby the site of shmoo formation and the direction of growth. This basically explains why the double mutant cells, which exhibit a highly expressed active Fus3 at basal conditions, could already polarize in the absence of pheromone. But how can these cells develop well-defined mating tip-like structures? Either the pre-activated Fus3 could serve as a positional cue for morphogenesis or the pre-stimulated conditions could activate the "default mating pathway", where the presumptive bud site becomes a positional cue for the site of mating tip formation[290].

In shmooing cells the active Fus3 is mainly located in the nucleus and at the tip of the mating projection (Fig. 3.1). ppFus3 was previously shown to be distributed in a gradient across the cytoplasm, that emanates from the mating tip projection and its extent was supposed to affect the morphology of the shmoo[75]. We could detect a similar gradient that happens to exhibit a steep exponential decrease towards the nucleus. The question is how this sharp gradient is generated. The decay length of the ppFus3 gradient is confined by the diffusivity (D) of Fus3 and the kinetics of its dephosphorylation by the phosphatases Msg5 and Ptp3 (k_{dephos}). The distance d (µm) to which the gradient decays to 1/e is therefore dependent on the root of the ratio of $\mathrm{D}(\mu\mathrm{m}^2\mathrm{s}^{-1})/k_{\mathrm{dephos}}$. A higher diffusivity of Fus3 would therefore extent the gradient, whereas a faster dephosphorylation of ppFus3 shortens the gradient[188]. The phosphatases of Fus3, Msg5 and Ptpt3 work far from saturation[75,291], which occurs when the substrate concentrations are comparable to the *Michaelis* constant (K_{m}). Furthermore, dephosphorylation of Fus3 in the cytoplasm by these phosphatases is faster than the diffusion of Fus3[75]. The sharpness of the gradient is thereby mainly dependent on the dephosphorylation of ppFus3 in the cytoplasm.

However, we revealed that the shape and extent of the ppFus3 gradient is additionally maintained by the network architecture of the mating MAPK module, in particular by the negative feedback from Fus3 on Ste11 (Fig. 3.31). Disruption of this feedback led to a significantly shallower gradient between the shmoo tip and

the nucleus. Increasing Ste11 activity in these cells by the T596I mutation additionally increased the amplitude of ppFus3 that extended the ppFus3 signal in the cell. Here, the extent of the gradient could have been affected by the 3-fold higher Fus3 expression in the Ste11 double mutant cells (Fig. 3.20). Furthermore, both mutants showed increased cell size, which could probably change the concentration of the phosphatases and thereby might impact the dephosphorylation of Fus3 in the cytoplasm. Interestingly, the Ste11(S243A) cells exhibited a broader mating projection, which is consistent with the shallower gradient monitored in the tip of these cells (Fig. 3.34). But how can a negative feedback from Fus3 on Ste11, which is based on a cytosolic interaction, modulate the spatial ppFus3 gradient? Phosphorylation of Ste11 in this feedback impairs its binding to Ste5, thus restricting MAPK signalling to the PM where a local pool of active Ste5 is present. This in turn restricts ppFus3 activation and generates a localized source of active Fus3. The spatial separation of the opposing enzymes is what maintains a steep decrease of the ppFus3 activity towards the nucleus. If the Fus3-Ste11 negative feedback is disrupted, Ste11 will bind stronger to Ste5. This thereby increases the activation of the MAPK module at the tip of the mating projection leading to an increase of active Fus3 in this region. This can lead to a change in the steepness of the gradient and probably can also extend the gradient. The change in the distribution of active Fus3 might trigger polarization events apart from the source of highest pheromone concentration. The feedback on Ste11 by Fus3 is probably mediated through the double phosphorylated ppFus3 and therefore it would act strongest where active ppFus3 is localized, which is the very tip of the mating projection and along the gradient of ppFus3. Once the spatial organization of active Fus3 is initiated, the gradient would maintain itself in a recurrent manner.

Similar extension of a phosphorylation gradient was theoretically calculated for ppErk in the spatial Raf-MEK-ERK signalling, where Erk does not get phosphorylated on the membrane, but in the cell interior[187]. It was calculated that a negative feedback from Erk to upstream components would increase the steepness and decrease the length of the gradient, and a positive feedback would decrease the steepness and increase its length[292,293]. Our results provide proof for this theoretical work and show experimentally for the first time that the network structure of the MAPK module not only influences the gradient of active Fus3, but also translates the information from the extracellular gradient when to mate into an intracellular gradient where to shmoo.

4.4 Pheromone stimulated polarization events are determined by the interplay of Fus3 and Kss1

The switch-like properties of the mating response allow cells to switch only above a certain pheromone concentration from the state of vegetative growth to the state of differentiation into a mating tip projection. However, cells that are exposed to low pheromone levels undergo elongation of their cell shape showing a filamentous growth pattern, and bud in a bipolar fashion. But what is regulating this polarized

growth if Fus3 is not activated at these pheromone concentration levels? It was suggested that this response is controlled by both Fus3 and Kss1 and may enhance the ability of cells to search for potential mating partners through the modification of cell shape and morphological differentiation[249]. Interestingly, dose-dependent investigations of cell differentiation showed that deletion of Fus3 led to a concentration independent overall increase in elongated cells[247]. Furthermore, cell elongation was effected by Kss1 deletion at low but not at high pheromone concentrations[247]. In accordance with this, increasing the Kss1 activity by a constitutive active mutant of Ste11 (Fig. 3.22, 3.25A) enhanced generation of elongated patterns, but only at low pheromone concentrations (Fig. 3.39). These results point at differentiated roles of Kss1 and Fus3 in sensing and responding to different pheromone concentrations in a gradient. This could be explained by a model that accounts for the proposed regulatory role of the different Fus3 phosphoforms (Chapter 4.3), the role of Kss1 in determining cell elongation discussed in chapter 3.6, and for the transcriptional control of Ste12 by both MAPKs (Chapter 4.2) (Fig. 4.1)[116,128]. At basal conditions, the autophosphorylated pTyr-Fus3 takes control of the mating output by negative feedbacks on Ste11 and Ste5. However, this phosphoform of Fus3 does not target Tec1, which controls the filamentous growth output. This is kept in check by the repression of Ste12 by unphosphorylated Kss1. When cells are stimulated with low pheromone concentrations, Kss1 is phosphorylated and thereby activates transcription of filamentous growth specific genes by Ste12. Fus3, however, is not fully phosphorylated (Fig. 3.18) and Tec1 remains active. Cells respond by Kss1 mediated elongated growth. Hence, at high pheromone concentrations, Kss1 still gets phosphorylated, but at the same time, the fully activated Fus3 degrades Tec1, which down regulates the Kss1 mediated gene expression. Cells form mating projections. Therefore, sensing and responding to cells within different distances is maintained by distinct forms of differentiation, regulated by a concerted interplay of Fus3 and Kss1 activity. Yeast cells that sense low pheromone concentrations of potential mates that are located further away, first have to orient and to grow towards those cells, due to their immobility. The same mechanism is used in filamentous growth, which allows to better forage the surroundings of a colony for additional nutrients. Mating will only occur, if these cells get into certain proximity to potential mates, and thereby into an environment of high pheromone concentrations.

Interestingly, it was shown that both Fus3 and Kss1 have a concentration dependent impact on the variance in the quantitative output of the mating pathway. At low pheromone concentrations, only the deletion of Kss1 showed a change in variance, while at high concentrations only the deletion of Fus3 increased the noise[251]. This indicates a dose specific feedback regulation by these components: Kss1 rather determines regulatory processes at low pheromone concentration, while Fus3 predominantly at higher concentrations.

Using an overlapping set of signalling proteins is mostly thought to be critical because it can lead to signal leakage. It is therefore questioned how an undesired cross-talk can be prevented. But why are these conditions present in most of the MAPK signalling systems? Why did not independent signalling systems evolved to generate different responses? In the yeast mating it seems, as if crosstalk between the mating pathway and the filamentous growth pathways is not undesired but rather important. Using the same set of signalling molecules, the cell has low investments while still being able to respond to a wide range of stimuli.

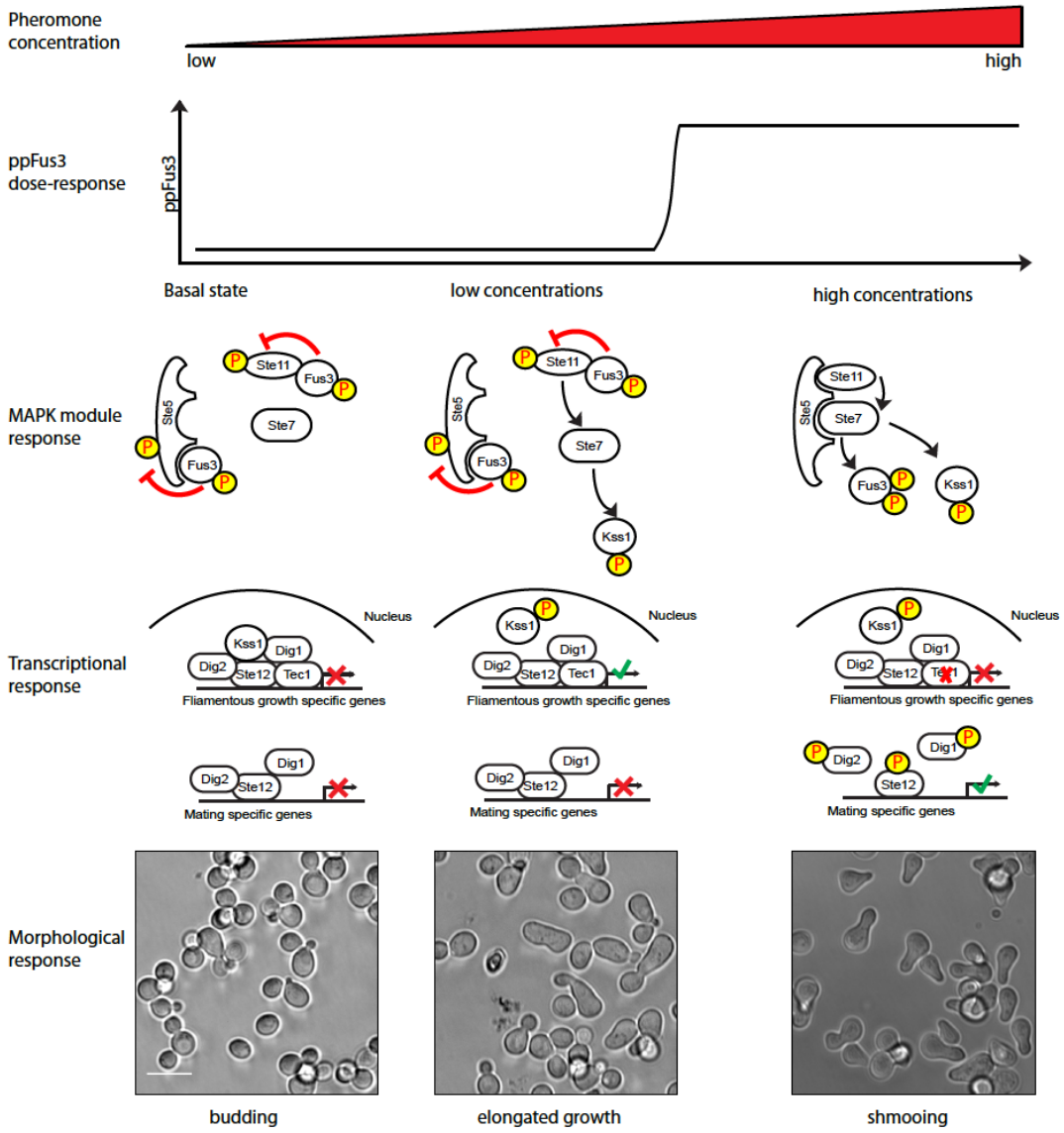

Fig. 4.1: Pheromone dose-dependent regulation of differentiation. Due to negative feedback mechanisms determined by autophosphorylated Fus3 and inhibitory function of Dig1, Dig2 and Tec1 the transcription of both filamentous growth and mating specific genes is prohibited. At pheromone concentrations underneath the activation threshold Kss1 can be phosphorylated leading to filamentous growth like patterns. At high pheromone concentrations Fus3 is fully activated and thereby inhibits the transcription of filamentous growth specific genes and trigger the formation of mating projections. Red T-bar indicates negative feedback, red cross indicated inactive and green hook active transcription.

5 Future directions

Reverse engineering of the MAPK modules network architecture uncovered a negative feedback from Fus3 on Ste11 and indicated different regulatory functions of the Fus3 phosphoforms in regulation of signalling. This approach, which combines FCS measurements of protein interaction and a linear regression analysis that estimates the concentrations of possible protein-species, still lacks accuracy due to the present underdetermined system. This problem could be solved by further protein deletion experiments to resolve which interactions are direct, which are mediated by other proteins and how these proteins mediate these interactions. The next step would be to expand the set of observed proteins to important upstream activators, like the MAPKKKK Ste20, or the MAPKs from the other pathways that use the same overlapping set of signalling components. Ste20 for instance, is known to activate all three main MAPK pathways, the pheromone response, the filamentous growth response and the osmostress adaptation, by phosphorylation of Ste11. How can signalling specificity be maintained and crosstalk be regulated using the same set of signalling components? On the one hand, Ste20 is bound and regulated by different pathway specific effectors and adaptor proteins, like Ste50[59], but on the other hand its specificity might also be regulated by pathway specific regulatory feedback mechanisms. Interestingly, the same mass spectrometry studies that detected Fus3 and Ste7 dependent phosphorylation sites on Ste11, also detected approximately 50 phosphorylation sites on Ste20[261]. These sites should be further analysed and might be the key to understand how Ste20 operates as a switch between these pathways. In the last chapter of the discussion it was suggested that the output of the mating response to a pheromone gradient might not only depend on regulation via Fus3, but most probably by a concerted regulation that additionally requires Kss1. As investigation of mating pathway output dependent cell-to-cell variance and morphological dose-response experiments indicated, Kss1 might rather operate as a regulator at low pheromone concentrations, while Fus3 maintains signalling at higher concentrations. To address this issue, the interactions of Fus3 and Kss1 with the other components of the MAPK module should be investigated in a pheromone dose-dependent manner. Since activation of Fus3 is Ste5 dependent and Kss1 activation in filamentous growth is Ste5-independent, the switch between Kss1 and Fus3 regulation might also be Ste5-dependent. A way to measure the "activation" of Ste5, its autoinhibitory release[67], is by monitoring its localization in response to pheromone-dose. This input-output relationship should exhibit a switch-like behaviour that could be influenced by targeting Fus3 mediated control like the feedback through phosphorylation of Ste11 by Fus3, but probably not by affecting Kss1 mediated feedbacks.

It was demonstrated in this thesis that the spatial control of signalling maintains dynamic response properties and cell morphogenesis. The feedback from Fus3 on Ste11 that occurs in the cytoplasm restricts the activation of Fus3 to the PM, thereby generating a steep ppFus3 gradient that spatially restricts shmoo

formation. Using the Phos-Tag approach developed in this lab this gradient could be further investigated with respect to its maintenance by the counteracting phosphatases Msg5 and Ptp3, but also how it is influenced and determined by the network architecture of the mating MAPK module. It could be addressed how the Ste5 non-docking mutant that lacks the Fus3-Ste5 negative feedback is still capable of generating proper mating tips. Furthermore it would be interesting to monitor what the ppFus3 gradient looks like in the unstimulated elongated Ste11(S243A/T596I) cells. How does the ppFus3 gradient in general affect the cell shape and morphogenesis? It seems that elongated cell shape at low pheromone concentrations is rather controlled and generated by ppKss1 than by ppFus3. If this is the case, this should also be reflected in the spatial organization of ppKss1.

Reverse engineering of a signalling systems network architecture relies on the quantification of changes in the network state in response to perturbations. The success of this approach depends on the readout and the perturbation. Instead of using protein mutations or deletion leading to a chronic perturbation that alters the global response by itself, acute perturbations like small molecule kinase inhibitors would be preferable. The general problem of inhibitor selectivity could be solved by using the "gatekeeper" strategy developed by Shokat and colleagues[253], by which a highly selective kinase-inhibitor interaction surface is generated. This method becomes particularly potent in yeast because of their genetic amenability. Using this perturbation strategy, changes in protein-protein interaction could be detectable by FCS, or detection of phosphorylation dependent changes by using the Phos-Tag approach could be possible. Furthermore, this could be performed on a single cell level, thereby excluding noise that might mask the effect of the perturbations. However, use of this cell-to-cell variance could be made as was done in this thesis. As already discussed above, Fus3 and Kss1 regulate noise in the mating pathways output at different pheromone concentrations, probably by feedback mechanisms. The driving force in the evolution of these different layers of feedback mechanisms is the demand for robustness to uncertain environments[207]. Therefore, measuring the cell-to-cell variation in the mating pathway output could be used to infer the network architecture.

6 Material and Methods

6.1 Material

6.1.1 Chemicals and Solutions

Chemicals	*Supplier*
Rotiphorese® NF-acrylamide/bis-solution 40 % (29:1)	Carl Roth GmbH
Ammonium persulfate (APS)	SERVA Electrophoresis GmbH
Bromphenolblue	Sigma-Aldrich®
cOmplete, Mini, EDTA-free Protease Inhibitor	Roche
Ethanol	J.T. Baker
Ethylenediaminetetracetic acid (EDTA)	Fluka® Analytical
Glycerol	GERBU Biotechnik GmbH
Glycine	Carl Roth GmbH
Isopropanol	J.T. Baker
Lithium acetate (LiAc)	Sigma-Aldrich®
Methanol	AppliChem GmbH
2-Mercapto-Ethanol	SERVA Electrophoresis GmbH
Polyethylenglycol 4000 (PEG)	Fluka® Analytical
Phosphatase Inhibitor Cocktail II	Sigma-Aldrich®
Phosphatase Inhibitor Cocktail III	Sigma-Aldrich®
RedSafe, DNA Stain	Chembio Ltd., Hertfords, UK
Sodium chloride (NaCl)	Fluka® Analytical
Sodium dodecyl Sulfate (SDS)	SERVA Electrophoresis GmbH
D-Sorbitol	Sigma-Aldrich®
N,N,N',N'-Tetramethylene-diamine (TEMED)	Sigma-Aldrich®
Tris-base	Carl Roth GmbH
Tris-HCl	Carl Roth GmbH
Triton X-100	SERVA Electrophoresis GmbH
Tween 20	SERVA Electrophoresis GmbH
UltraPure TM Agarose	Invitrogen Life™Technologies
Glass beads, acid washed	Sigma-Aldrich®
Roti®-Phenol/Chloroform/Isoamyl alcohol (25:24:1)	Carl Roth®

Solutions	*Supplier*
Big Dye® Terminator 5x Sequencing Buffer	Applied Biosciences
Odyssey Blocking Buffer	LI-COR Biosciences GmbH
Precision Plus Protein™ standards	Bio-Rad Laboratories, Inc.

2-log DNA ladder	New England Biolabs Inc.

6.1.2 Enzymes/Proteins

Enzymes	*Supplier*
Platinum AccuPrime Polymerase	Invitrogen Life™Technologies
Platinum Pfx Polymerase	Invitrogen Life™Technologies
Platinum Taq Polymerase	Invitrogen Life™Technologies

Proteins	*Supplier*
ConcanavalinA	Sigma-Aldrich®
Bovine Serum Albumins (BSA)	Sigma-Aldrich®

6.1.3 Antibodies/Protein beads

Antibodies	*Supplier*
Ste11 (yN-19) sc-6768	Santa Cruz Biotechnology
Ste7 (yN-18) sc-6770	Santa Cruz Biotechnology
Fus3 (yC-19) sc-6773	Santa Cruz Biotechnology
Fus3 (yN-19) sc-6772	Santa Cruz Biotechnology
Kss1 (y50) sc-28547	Santa Cruz Biotechnology
Living colors GFP antibody (632592)	Clontech
Living colors dsRed antibody (632496)	Clontech
Living colors mCherry antibody (632543)	Clontech
HA-antibody (MMS-101P)	Covanance
Phospho-Threonine (42H4)	Cell Signalling
Phosphoglycerate Kinase M. Antibody	Invitrogen Life™Technologies
Anti-Phospho-ERK1/ERK2 Antibody	R&D Systems®

All secondary antibodies used for detection and visualization of primary antibodies were obtained from LI-COR Biosciences GmbH.

Protein beads	*Supplier*
Protein A Sepharose™	GE Healthcare Life Sciences
Protein G Sepharose™	GE Healthcare Life Sciences

6.1.4 Oligonucleotides

All primers were purchased from MWG-Biotech AG.

6.1.5 Kits

Kits	*Supplier*
NucleoSEQ	MACHEREY-NAGEL

DlAquick® Gel Extraction Kit	Qiagen GmbH
DNeasy® Blood & Tissue Kit	Qiagen GmbH

6.1.6 Media and Buffers

Media	*Ingredients/Supplier*
YPD	1 % Yeast Extract, 2 % Bacto-Peptone, 2 % Glucose
SD complete	0.67 % Yeast nitrogen base without AA+590 mg AA mix
SD -HIS/LEU/TRP/URA	SD complete - AA used as selection marker

Buffer	*Ingredients/Supplier*
Yeast DNA extraction buffer	2% Triton X-100, 1% SDS, 100 mM NaCl, 10 mM Tris-Cl (pH8), 1 mM EDTA
SORB Buffer	100 mM LiAc (pH 7.8), 10 mM EDTA (pH 8), 1mM Sorbitol, adjust to pH 8
PEG Buffer 1mM	100 mM LiAc, 10 mM Tris, EDTA (pH 8), 1 M PEG 4000
Single-stranded (SS) carrier DNA	10 mg/mL Salmon sperm DNA
Yeast protein extraction buffer	100 nM TRIS (pH7.9), 200 mM NaCl, 20 % (v/v) Glycerol, 5 mM EDTA, 14mM 2-Mercaptoethanol add 100 µL cOmplete protease inhibitor + each 100 µL phosphatase inhibitor cocktail I & II to 9.4 mL Buffer
5x SDS sample buffer	60 mM Tris-HCl (pH 6.8), 25 (v/v) Glycerol, 2% SDS, 14.4 mM 2-Mercaptoethanol, 0.1 % bromphenolblue
Seperating gel buffer	1.5 M Tris-HCl (pH 8.8)
Stacking gel buffer	0.5 M Tris-HCl (pH 6.8)
Running buffer	25 mM Tris-Base, 192 mM Glycine, 0.1% (m/v) SDS
Transfer buffer	25 mM Tris-Base, 192 mM Glycine, 20 % (v/v) Methanol
TBS	10 mM Tris-Base, 150 mM NaCl, adjust to pH 7.6
TBST	TBS + 0.01 % Tween 20

All Buffers were prepared with double distilled water from the Millipore Q-Pod system that is referred as H_2O in the following.

6.2 Methods

6.2.1 Molecular biology techniques

6.2.1.1 Cloning in *Saccharomyces cerevisiae*

The modification of genes in yeast, which comprises the integration of mutations, the deletion of genes and the C-terminal and N-terminal tagging, was achieved by homologues recombination through chromosomal integration of PCR amplified cassettes. Therefore the target DNA is flanked by homologues sequences provided by PCR-primers and amplified by using Accu Prime Polymerase using the manufacturers protocol.

Tab. 6.1: Protocol of PCR based amplification of yeast cloning cassettes. Upper: components. Lower: PCR protocol

Components	Volume
H2O	40.7 µL
10x AccuPrime Pfx Reaction mix	5 µL
Forward Primer (10µM)	1.5 µL
Reverse Primer (10µM)	1.5µL
Template (≈1 - 200 ng)	1 µL
Accu Prime Pfx Polymerase	0.3 µL

Cycle	Temperature	Time	#Cycles
Initiale denaturation	97 °C	5 min	1
Denaturation	97 °C	15 sec	
Annealing	Tm - 3 °C bis 5 °C	30 sec	33
Elongation	68 °C	1 min/kb	
Finale	68 °C	7 min	1
elongation	4 °C	Hold	

This strategy is based on four different primers, that contain a sequence within the 5' end with about 50-55 bp homologues to the target gene and an artificial sequence at their 3' end that is homologues to a recognition sequence at the beginning of the cassette (yellow).

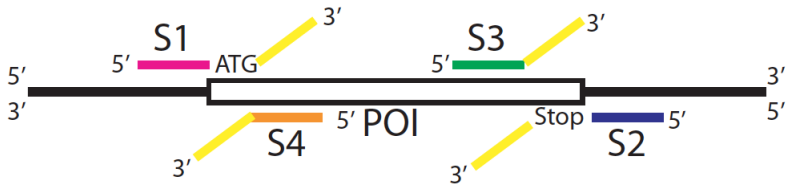

Fig. 6.1: Primer design for PCR-based tagging of yeast genes. Using primer S1-S4 genes can be tagged C- and N-terminally, promotors can be switched and genes can be deleted. S1 primer consist of 50-55 bp homologue sequence to the sequence upstream of the 5' end and a sequence at its 3'end which is homologues to a sequence prior to a selection marker on the cassette (yellow part). The other primers have the same design principle. Adapted from[242]

Using this method all genes can be tagged at the C- (S3 forward, S2 reverse primer) and N-terminus (S1 forward, S4 reverse primer). By using the N-terminal tagging approach it is also possible to replace the promotor of a gene. Amplifying selection markers by S1 forward and S2 reverse primers generate a template suitable for gene deletion.
For the construction of mutant genes two fragments were produced. The first fragment was amplified from the target gene DNA template by a forward primer contain the desired mutation and an S3 reverse primer. The second fragment was amplified using S3 forward and S2 reverse primer with a plasmid cassette.

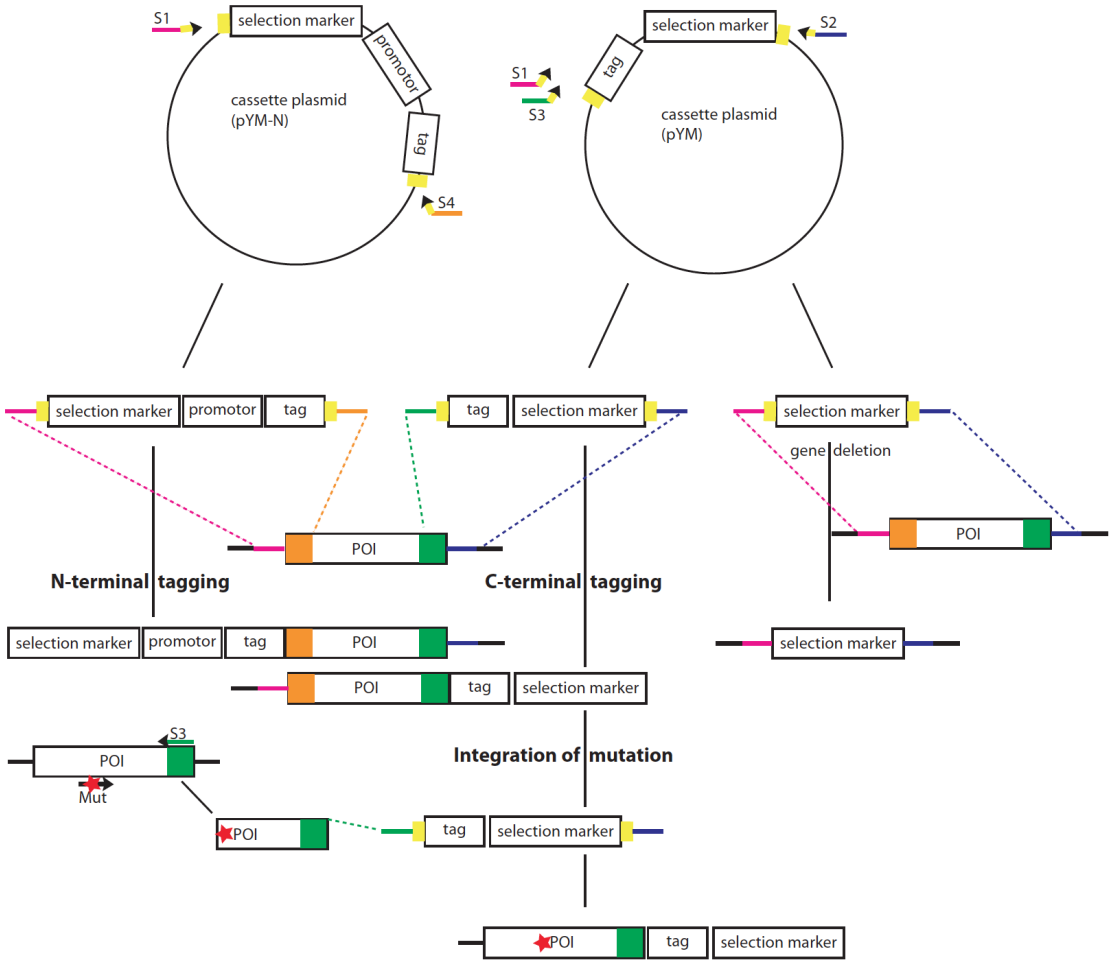

Fig. 6.2: The principle of PCR-based tagging of yeast genes. The first step is the amplification of the cassette from the appropriate cassette plasmid by the above-described primers S1, S2, S3, S4. In the second step the cassette that is flanked by homologues sequences is integrated into the genome at the specific position of the target gene by homologues recombination. Colours indicate homologues regions and are adopted from Figure 15. POI represents the gene of interest in the chromosomal DNA. Red star indicates mutation. Dotted lines indicated homologues recombination Adapted from[242].

All strains used in this thesis were generated using the above described PCR-based tagging of yeast genes and are listed in Table 8.4.

6.2.1.2 Isolation of genomic DNA

Initially a small culture (inoculated with the strain of interest) of 1 - 3 mL YPD was grown overnight at 30 °C. The culture was pelleted by centrifugation at 700 g for 3 min and the cells were resuspended and transferred to a 1.5 mL Eppendorf tube. The cells were then harvested by short centrifugation at top speed and the supernatant was discarded. 200 µL of Lysis buffer, 200 µL of Roti®-phenol/chloroform/isoamyl alcohol and a small spoon of acid-washed glass beads was added to the cell pellet and mixed for 10 minutes in an Eppendorf Shaker (Thermomixer confort) at 1400 rpm. The aqueous layer contains the genomic DNA and is transferred to a fresh tube. For additional purification the solution is then

mixed with 200 µL chloroform and centrifuged again for 5 min at maximum speed. 50 µL of the aqueous solution containing the genomic DNA are subjected for further analysis.

6.2.1.3 Gel electrophoretical DNA analysis and gel-extraction of DNA

DNA fragments obtained by PCR were separated by their size by gel electrophoresis, which relies on the movement in an electrostatic field. The matrix that was used to separate the target DNA fragments was an agarose gel with concentrations in the range of 0.8 – 1.2 % defining the size of the pores. Separation of the particles was regulated applying current (60 – 100 V). The agarose gel is treated either with Safe-Red to stain the DNA for visualization with UV-light.
To extract a DNA fragment of interest from an agarose gel the band was visualized with the SafeImager™ and was cut out of the gel. It was than purified using the "Gel Extraction Kit" from Qiagen following the manufacture's protocol.

6.2.2 Microbiological methods

6.2.2.1 Transformation of yeast

The transformation of yeast was conducted by two different protocols utilizing either freshly prepared cells or already prepared competent cells stored at -80 °C.

6.2.2.2 High efficiency transformation of yeast with freshly prepared cells

For transformation 50 mL of YPD medium are inoculated with the yeast strain to be modified. The culture was incubated at 30° overnight while shaking. Next day the culture was diluted to an OD_{600} of 0.5 with a volume of 50 mL and incubated at 30°C while shaking until an OD_{600}=1 was reached. Afterwards the yeast cells were harvested in a sterile 50 mL Falcon tube at 3000g for 5 min. After discarding the supernatant the cells were washed in 25 mL sterile H_2O and centrifuged again at 3000 g for 5 min. The H_2O is poured off and the cells were resuspended in 1 mL of 100 mM LiAc. This suspension was transferred to a sterile 1.5 mL Eppendorf tube. The cells were then pelleted at top speed for 5 seconds, the supernatant was removed and again resuspended in 400 µL of 100 mM LiAc. After vortexing, the suspension was aliquotted in 50 µL samples. The samples were pelleted again and the LiAc was discarded. The following components of the transformation mixture were added to the cells in the order listed below:

240 µL PEG (50%(w/v)

36 µL of 1 M LiAc

30 µL of SS carrier DNA

X µLDNA fragment

sterile H_2O (50 µL - volume of DNA fragment)

Afterwards the mixture was vortexed until a complete dissolution of the cell pellet. After 30 min incubation at 30°C the mixture was incubated in a water bath at 42°C for 20 min. The solution was then centrifuged at 8000 g for 15 seconds and the supernatant was removed.

In case of selection by the depletion of AA the pellet was resuspended in a SD medium missing the AA and was afterwards plated on AA deficient SD plates. In case of selection by antibiotics the pellet was resuspended in 700 µL YPD medium and was transferred to a 5 mL Falcon tube containing 3 mL YPD medium. After 3 to 5 h incubation at 30°C while shaking the samples were pelleted again. Finally the aliquots are plated on YPD plates containing the selective antibiotic.

6.2.2.3 Preparation of competent yeast cells

A 50 mL culture of a yeast strain with an OD_{600} of approx. 1.5 is prepared the same way described above. The culture was harvested in a sterile 50 mL Falcon tube at 700 g for 5 min and subsequently washed with 25 mL H_2O. After a second centrifugation step the cells were washed with 10 mL SORB medium. The cells were pelleted again and resuspended in 360 µL SORB medium and 70 µL SS carrier DNA was added. The cell solution was aliquoted in 100 µL portions and stored at -80 °C.

6.2.2.4 High efficiency transformation with competent yeast cells

Frozen cell aliquots were thawed at room temperature, 20-50 µL of the PCR product was added and subsequently mixed. 6 volumes PEG medium were added and the suspension was mixed thoroughly and incubated at RT for 30 min. Afterwards DMSO was added to a final concentration of 10 % and the suspension was incubated at 42 °C in a water bath. After pelleting the cells at 700 g for 3 min the cells were resuspended in the selective medium and plated on selective plates.

6.2.3 Biochemical Methods

6.2.3.1 Cell Lysis/Yeast protein extraction

2-20 ml YPD is inoculated with the yeast cells and grown until OD_{600nm} =1 - 1.5. The following procedure was done continuously at 4°C. Cells were initially collected by centrifuging at 700 g for 5 min and washed with 500 – 1000 µL yeast protein extraction buffer. Cells were collected again and resuspended in 40 – 100 µL yeast extraction buffer, and a spoon (approx. a volume of 100 -200 µL) of acid washed glass beads was added. The suspension was mixed virgously for 1 min using a vortex genie-2 and cooled on ice for the same time afterwards-. This procedure was repeated for 10-15 times prior to a 20 min centrifuging step at top speed (16000 g) to separate the beads, solid cell components and the protein solution. The supernatant was collected and the protein concentration was measured by Bradford assay, using a BSA calibration line (0.1, 0.5, 1, 2.5, 5, 10 µg/mL).

6.2.3.2 SDS-PAGE and Western blots

Protein analysis was performed utilizing a BioRad Precast gel system. A sample of 50 – 100 µg of the protein lysate was prepared with 5x SDS sample Buffer and boiled at 95°C for 5 min. This sample was centrifuged at top speed for 3 min and afterwards transferred to a 6 – 12 % polyacrylamide gel. The gel was run initially at 120 V until the samples reached the border of stacking and running gel and the voltage was than raised to 150 V for approx. 1 – 1.5 hours. Proteins were transferred to a PVDF membrane using tank blotting in the same BioRad system (100 V, 1 h). The membrane was subsequently incubated with 5- 10 mL Odyssey blocking Buffer for at least 1 h at RT or overnight while shaking at 4 °C. In a further step the membranes was incubated with specific primary antibodies overnight at 4°C while shaking. After three washing steps with TBST the membrane was incubated for 1 h at RT with 5 mL Odyssey blocking buffer solution containing specific secondary antibodies labelled with IRDye600RD or IRDye800CW in a specific ratio (mostly 1:1000). The membrane was then washed three times with 10 - 20 mL TBST for 10 min each. Detection of antibody labelled protein bands was performed with the Odyssey Infrared Imaging System (Li-COR Bio systems, Germany). Membranes were scanned at 700 nm and 800 nm at 169 µm resolution, medium quality; focus offset of 3.0 mm was used and the intensity setting was set to four.

However, these analyses are always semi-quantitative due to variations in loading, transfer and detection, and therefore comparison of different western blots can't provide an absolute measure of quantity. To compare ppFus3 levels in the Ste11 mutants to ppFus3 levels in WT cells more quantitatively, samples of both strains were run on the same blot or data was corrected by independent measurements of the last value (150 min) in the time-series. Unfortunately, it turned out later that at this time point Fus3 expression exhibited the highest variances (Fig. 3.19). Time points at which Fus3 expression exhibits lower variance would be favourable.

6.2.3.3 Co-immunoprecipitation

Immunoprecipitation was used to precipitate and concentrate a specific protein out of a cell lysate containing a multitude of different proteins. Immunoprecipitation in this work was mainly used to pull down Ste7 or as Co-immunoprecipitation to detect binding of the proteins Ste5 and Ste11. For detection of Ste5-Ste11, Ste5 fused to 3-meGFP (strain sJJ138-141) was immunopurified by using a GFP antibody (see Antibodies) and for detection of Ste7 either a Ste7 antibody was used, or a GFP antibody recognizing Ste7-3-meGFP. Yeast cells were initially lysed as described above and 400-700 µg of cell lysate was incubated with either 1 µg GFP or 1 µg Ste7 antibody overnight at 4°C while spinning. 30 µL of Protein G beads were washed three times with yeast protein extraction buffer and incubated with the cell lysate–antibody mixture for 3-4 h at 4°C while spinning. Afterwards the beads were washed three times with yeast protein extraction buffer. For SDS-PAGE analysis residual buffer was removed with an injection needle (27Gx3/4"), 30 µL 1x SDS-sample buffer was added and incubated for 5 min at 95°C. Co-immunopurified Ste5 and Ste11 was detected and quantified via Western blots

using GFP and HA antibodies. Immunopurified Ste7 was detected using Ste7 or GFP antibodies.

6.2.4 Microscopy

6.2.4.1 Fluorescence spectroscopy/microscopy/methods

Fluorescence is the emission of photons through the relaxation of an electron from the excited singlet S_1 state back to the ground state S_0 showing an emission rate (k_F) of 10^{-8} s^{-1}. These electronical states and the transitions between them can be described by the *Jablonksi* diagram (Fig. 6.3). The initial step, the transition of an electron to the excited state S_1 can occur to different vibrational energy levels (v), which is triggered by the emission of a photon whose energy has to be equivalent with the gap between these states. This process requires parallel orientation and polarisation of the dipol moments and a large transition dipole moment. The excited electron quickly relaxes to the lowest vibrational state of S_1. This process called vibrational relaxation occurs within 10^{-12}s.

Beside fluorescence the relaxation of the excited electron in S_1 to S_0 can also occur by internal conversion (IC) (k_{IC}), triggered by heat or collision, or by intersystem crossing (ISC) which is the transition into the first triplet state T1. Relaxation from this state to the singlet ground state is spin forbidden because of the different spin multiplicity of the triplet state. Thereby the rate constant for triplet emission (k_{ST}), which is called phosphorescence is lowered several orders of magnitude (10^3 to 10^0 s^{-1}).

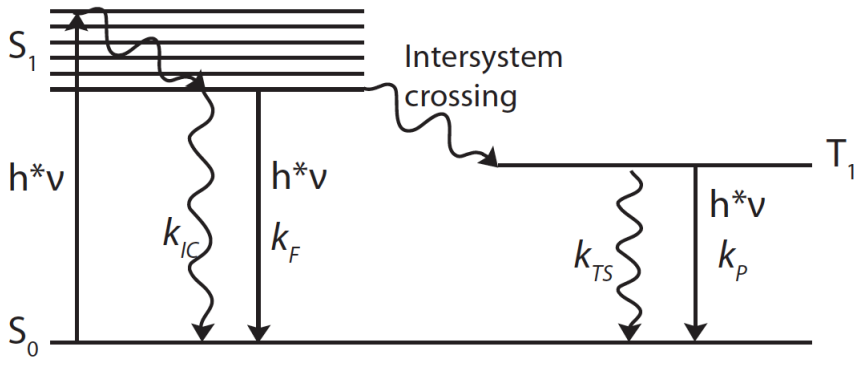

Fig. 6.3: *Jablonski* diagram. Shown is the transition on an electron by emission of an photon from the ground state (S_0) to the first excited state (S_1) and its transition to the lowest vibrational state. The relaxation takes place by different radiative (Fluorescence, F) and non-radiative (Internal conversion, IC) processes. The conversion of S_1 to T_1 is called intersystem crossing. The relaxation to the ground state from T_1 to S_0 occurs by internal conversion (TS) or by the emission of photons called phosphorescence (P). k represents the rates. Straight lined arrows represent non-radiative processes and waved lined arrows represent radiative processes.

The average time a fluorescent molecule remains in the excited state before it emits a photon is determined as the fluorescence lifetime. This quantity depends on the rate of all radiative and non-radiative processes as described by the following formula:

$$\tau = \frac{1}{k_F + k_{IC} + k_{TS}} \tag{6.1}$$

Fluorescence, the depletion of the excited state follows first order kinetics:

$$[S_1] = [S_1]_0 e^{-\frac{t}{\tau}} \tag{6.2}$$

A further important characteristic of fluorescent molecules is the quantum yield. It expresses the relation between the rates of fluorescence and non-radiative processes or the number of photons emitted in relation to the number of photons absorbed.

$$\phi = \frac{k_F}{k_F + k_{IC} + k_{TS}} = k_F * \tau \tag{6.3}$$

Each photon absorbed by the fluorescence molecule that triggers the excitation of an electron theoretically gives a single line in the absorption spectrum. Furthermore, the radiative relaxation of these electrons triggers the emission of a photon and theoretically gives a single line in the emission spectrum. However, the absorption and emission spectra of fluorescence molecules are shifted, which is caused by the relaxation of an excited electron to the lowest vibrational level of S_1. This rapid relaxation changes the energy levels of the subsequently emitted photon, therefore emission spectra are usually independent of the excitation wavelength (Kashas' rule). The excitation and emission spectra show symmetry, the emission is the mirror image of S_0 to S_1, which is a result of same transitions in the different vibrational states from S_0 to S_1 and S_1 to S_0 (Fig. 6.4). This is possible because of the same spacing of the vibrational energy level in S_0 and S_1. In addition, all electronic transitions are vertical, because they occur without a change in the position of the nuclei (Franck-Condon-Principle). Therefore if a transition probability is large in absorption, the reciprocal transition is very likely in emission.

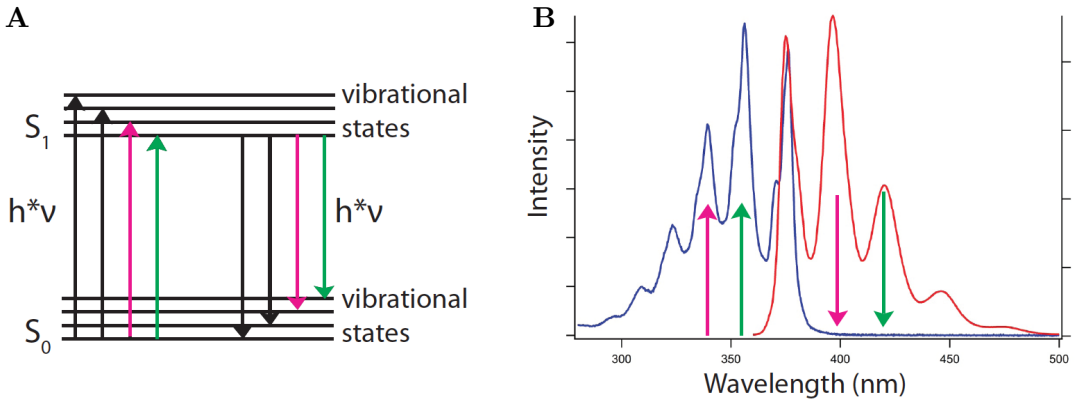

Fig. 6.4: Mirror-image rule in fluorescence spectra. (A) Transitions from S_0 to distinct vibrational states of S_1 triggered by photons with distinct energies and relaxation of the same electrons to distinct vibrational ground states (S_0). Transitions with the same

color are corresponding. **(B)** Absorption (blue) and emission (red) spectra of anthracene. Arrows represent corresponding transitions (as in A).

Fluorescence is used in a variety of spectroscopic and microscopic approaches in living cell, like fluorescence correlation spectroscopy (FCS) or FRET measurement or just simple time-lapse/localization approaches, to relate the function of a protein in space and time to the behaviour of the cell. In the following procedures and theoretical background of the fluorescence microscopy methods applied in this thesis will be described.

6.2.4.2 Fluorescence correlation spectroscopy (FCS) in theory

FCS was utilized in this thesis to measure protein concentrations and protein interactions. This fluorescence technique is capable of detecting diffusing single molecules within a defined observation volume. Each time a fluorescent molecule crosses this volume it gets highly excited by a laser beam and emits photons reflected in a single intensity peak. Continuous translational diffusion of the same and further molecules results in the fluctuation of the emission intensity over time. In order to detect fluctuations on this level a confocal microscopy setup with a pinhole providing a detection volume of approx. 1 fL (10^{-15} L) is used. The concentration of the fluorescent molecule has to be in the range where only a few molecules can occupy the volume that is in the low nM range for a femtolitre volume. The relation of the molecule number to the volume can be described by the Poisson distribution. It expresses the probability (P) of events (n fluorescent molecules) occurring with a known average rate (average number N) in a fixed range of time or space (observation volume).

$$P(n,N) = \frac{N^n}{n!}e^{-n} \tag{6.4}$$

If the fluorescent molecules diffuse slowly through the volume the burst of emitted photons is long lived, whereas at high diffusion speed the burst of photons is short lived. This is reflected directly in the time-dependent intensity fluctuations, where the width of a single peak directly reflects the dwell time of a fluorophor in the observation volume (Fig. 5.5). The size of the fluorescent molecules only modestly influences the diffusion. The change from a monomer to a dimer for instance decreases D only by the factor 1.26 ($2^{1/3}$) which can be calculated by the Stokes-Einstein equation for a sphere.

$$D = \frac{k \cdot T}{6 \cdot \pi \cdot \eta \cdot r} \tag{6.5}$$

Here, k is the Boltzmann constant, T is the temperature, η is the viscosity and r is the radius of the spherical particle. In case of a protein it is proportional to $V^{1/3}$ and $M^{1/3}$, which weighting the molecular weight only by $\sqrt[3]{\frac{1}{M}}$. A decrease in D by the factor 2 would therefore require a 6-fold ($6^{1/3}$) increase in M.

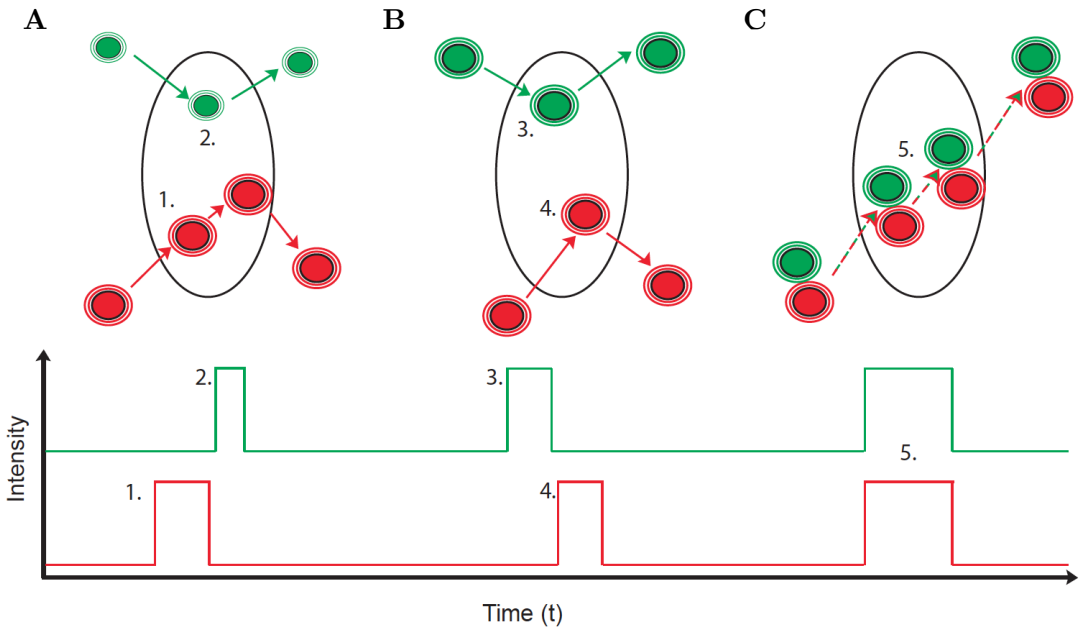

Fig. 6.5: Intensity fluctuations in FCS. Upper part shows the movement (indicated by arrows) of three different fluorescent molecule constellations through the observation volume getting excited. **(A)** Here, a small green and a larger red fluorescent molecule explain the influence of size. **(B)** Non-interacting green and red fluorescent molecules with similar size. **(C)** The same molecules, but interacting. Lower part of the graph shows the corresponding intensity fluctuations produced by the different fluorescent entities. Adapted from[294]

The strength of the intensity fluctuations is directly correlated with the fluorescence intensity and the number of particles. At high concentrations intensity fluctuations are decreasing whereas at low concentrations the fluctuations are increasing.

Statistical analysis of these intensity fluctuations is done by correlating the intensity given at a time F(t) with the same intensity shifted in time F(t+τ). Comparison of two molecules with different diffusion with the same F(t+τ), a low diffusion speed will show high correlation whereas a fast diffusion will show less correlation. These correlations are calculated by the autocorrelation function, where the value for the autocorrelation (Numerator) is averaged by the average intensity <F> squared.

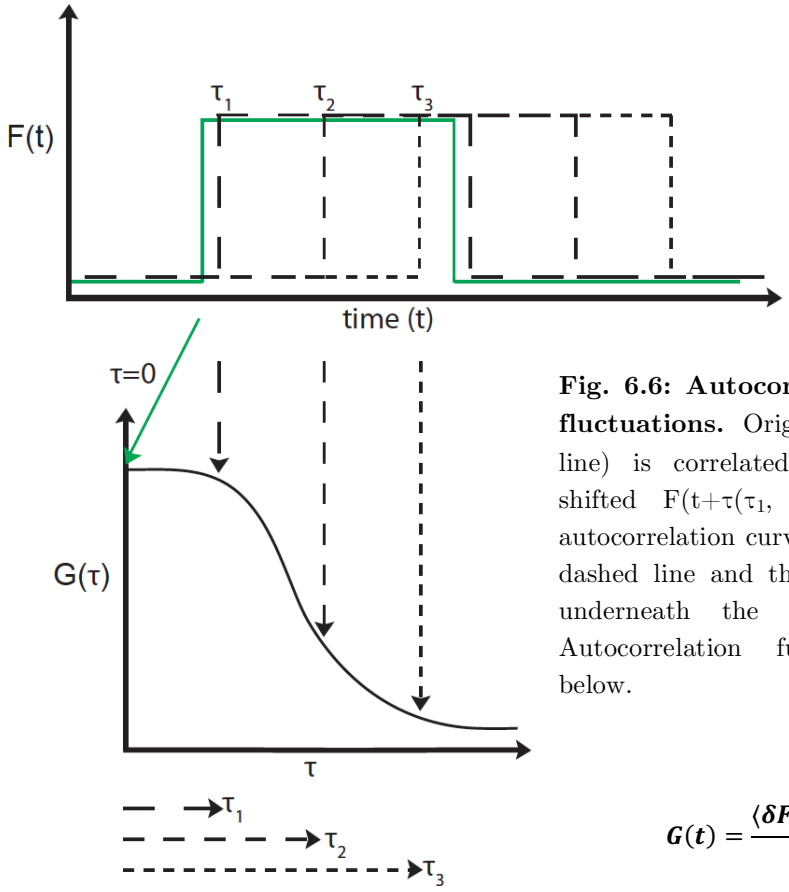

Fig. 6.6: Autocorrelation of intensity fluctuations. Original trace F(t) (green line) is correlated with different time-shifted F(t+τ(τ_1, τ_2, τ_3)) yielding an autocorrelation curve. $\tau_{1\text{-}3}$ are displayed by dashed line and their length is displayed underneath the autocorrelation curve. Autocorrelation function is displayed below.

$$\boldsymbol{G(t) = \frac{\langle \delta F(t) \cdot \delta F(t+\tau) \rangle}{\langle F \rangle^2}} \tag{6.6}$$

Here, intensity fluctuations around the average at a time t are described by:

$$\delta F(t) = \langle F \rangle - F(t) \tag{6.7}$$

Given that intensity fluctuations are correlated with the number of particles, the average number of particles in the observation volume can be obtained by reading the amplitude of the autocorrelation function (τ=0). Here, the intensity fluctuation is proportional with the intensity oft the fluorophor which is defined as the brightness per particle.

$$G(0) = \frac{\langle \delta F(t) \cdot \delta F(t) \rangle}{\langle F \rangle^2} = \frac{brigthness^2 \cdot \langle N(t) - N \rangle^2}{brightness^2 \cdot \langle N \rangle^2} = \frac{variance(N)}{\langle N \rangle^2} = \frac{\langle N \rangle}{\langle N \rangle^2} = \frac{1}{N} \tag{6.8}$$

Furthermore, the number of particles is Poisson distributed, where the variance equals the mean. Inserting $\sigma^2 = \langle \delta N^2 \rangle = N$ in equation... yields:

$$G(0) = \frac{variance \langle N \rangle}{\langle N \rangle^2} = \frac{\langle N \rangle}{\langle N \rangle^2} = \frac{1}{N} \tag{6.9}$$

The amplitude oft the autocorrelation function is therefore inversely

proportional to the number of molecules. It can be used as a direct readout for the molecules concentration if the size of the observation volume is known. This size is determined by the horizontal radius (w_{xy}) and the vertical radius (w_z) of the confocal volume. Knowing these values, and the dwell time of the fluorescent molecule in the volume which is given by the inflection point of the autocorrelation function (τ_D) and assuming an 3 dimensional diffusion of the observed particle, the diffusion coefficient D can be calculated.

$$D = \frac{w_{xy}^2}{4\tau_D} \tag{6.10}$$

The autocorrelation function can therefore be readout for the concentration and the diffusion coefficient of a fluorescent molecule. These values strongly modulate the shape of the curve thereby allowing first predictions. A shift to higher lag times (τ) indicates an increase in the diffusion time, whereas a shift towards lower amplitude indicates an increase in the concentration.

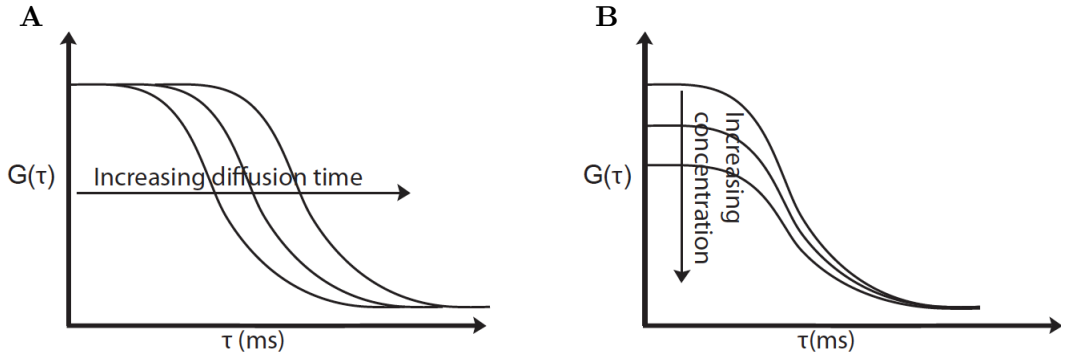

Fig. 6.7: Molecule concentration and diffusion time shape the autocorrelation curve. **(A)** Increasing diffusion time shifts the curve to higher lag times τ. **(B)** Increasing concentration shifts the amplitude of the curve lower amplitudes.

6.2.4.3 FCCS in theory

Due to the weak dependence of molecular weight to the diffusion time FCS is not usable for detection of protein-protein interactions. However, expansion of the setup by a second colour can overcome these limits. This required two spectrally well separated fluorophors (a and b), a second excitation source and two detectors. This dual-colour setup is capable of measuring intensity fluctuation of the two fluorophors at the same time. If two fluorescent-labelled proteins fully interact, the same intensity fluctuations will be observed in both detection channels. The degree of interaction can be calculated by cross correlating both time traces in the cross-correlation function

$$G_{AB}(\tau) = \frac{\langle \delta F_A(t) \cdot \delta F_B(t+\tau) \rangle}{\langle F_A(t) \rangle \cdot \langle F_B(t) \rangle} \tag{6.11}$$

where $G_{AB}(\tau)$ represents the statistical measure of the degree to which the fluctuations occur simultaneously. In contrast to the autocorrelation function, the amplitude of the cross-correlation is directly proportional to the number of moving particles a and b in complex.

$$G_{AB}(\tau) = \frac{N_{AB}}{(N_A + N_{AB})(N_B + N_{AB})} \tag{6.12}$$

6.2.4.4 FCS/FCCS data acquisition

All experiments were performed using an LSM-510 ConfoCor 3 (Carl Zeiss AG), and an Apochromat 40x water-immersion objective (1.2 numerical aperture (NA); Carl Zeiss AG). meGFP was excited with the 488 nm line of an argon laser and mCherry was excited using a 561 nm diode laser. The laser power was set not higher than 1.5 kW/cm^2 (488 nm) and 2.05 kW/cm^2 (561 nm), respectively, in order to minimize photobleaching effects of the fluorescent proteins. The emission light passed an adjustable pinhole that was set to 1 Airy unit. Fluorescence emission was split by a dichroic mirror (NFT565) and detected using a 505–540 nm band-pass and a 615-680 nm band pass filter for the green and red detection channel, respectively. The fluorescence was detected by avalanche photodiodes (APDs, Perkin-ElmerOptoelectronics, Canada) that were coupled to a photon-counting card (ISS, USA).

6.2.4.5 FCCS measurements in *Saccharomyces cerevisiae*

All Fluorescence correlation spectroscopy (FCS) measurements were carried out with triple fusions monomeric yeast enhanced GFP (3meGFP) and monomeric mCherry (3mCherry)[75]. In general the measurements were performed similar to Maeder *et al.*[75]. FPs were chosen due to fast maturation and well separated emission spectra. Initial to all FCS experiments the confocal volume was calibrated using Alexa488 and Alexa546 dyes. The intensity fluctuations of these dyes and Rhodamine green were measured to posterior obtain the size of the green the red and the cross-correlation observation volume. Then wild type cells without the FPs, positive and a negative control cells were measured. Wild type cells were measured in both channels to account for background auto-fluorescence. The obtained values were implemented in the analysis. The positive control cells (*YCM449-1*) expressed a construct of a neutral spacer protein Don1 flanked by the two fluorophors. The cross-correlation amplitude did not show 100% cross-correlation and rather corresponded to about 50-70% interaction. This value was corrected for each data set measured. The negative control (*YCM452-1*) consisted of two non-interacting constructs Ste11-3mCherry and meGFP-Don1. These cells showed extreme low cross-correlation which could be neglected. Measurements in single cells were not repeated to avoid for bleaching and statistical reason. In

general time traces of 1 min were recorded and only traces with stable fluctuations over time were saved. Measurements in vegetative cells were done only in non-budding cells. For pheromone stimulation, alpha factor (100 nM final concentration) was added for either 2-7 min or 40 min and only non-budding cells were measured with FCS. Cells exhibiting high auto-fluorescence were excluded.

6.2.4.6 FCS/FCCS data analysis

The raw intensity data was auto- and cross-correlated and analysed using the FCS Data processor 1.5 software (SSTC, Minsk, Belarussia). Unstable time traces of intensity fluctuations showing significant photobleaching, intensity drift or intracellular movement were discarded. Auto- (i and j) and cross-correlation curves (G_{ij}) were only generated from stable intensity fluctuations. Traces exhibiting both stable and unstable parts were cut and the stable intensity fluctuations were extracted for correlation. The minimal size of section of intensity fluctuations (τ datapoints) was set to 140 and the first τ value to be used in the calculation was set to $2*10^{-6}$ sec.

$$G_{ij}(\tau) = \frac{\langle \delta I_i(t) \cdot \delta I_j(t+\tau) \rangle}{\langle I_i \cdot I_j \rangle} \tag{6.13}$$

The auto- and cross-correlation curves were fitted between 100 µs and 100 ms according to a diffusion model that included terms for photophysical conversions of the fluorescent protein and an offset G_∞ to compensate for small intensity drifts. All fits were inspected in terms of amplitude and shape and overlap with the auto- and cross-correlation.

$$G_{ij} = 1 + \left(1 - \frac{I_{i,backgorund}}{I_{i,total}}\right)\left(1 - \frac{I_{j,background}}{I_{j,total}}\right) \cdot \left(\frac{1}{\langle N \rangle} \cdot \frac{1 - T + Te^{\left(\frac{-\tau}{\tau_t}\right)}}{(1-T)} \cdot \frac{1}{\left(1 + \frac{\tau}{\tau_{dif}}\right)\sqrt{1 + \frac{\tau}{sp^2 \cdot \tau_{dif}}}}\right) + G_\infty \tag{6.14}$$

T represents the fraction of molecules in the dark state and τ_t the relaxation rate of this state. τ_{dif} represents the diffusion time and depends on the shape of the observation volume (sp), which is defined by the ratio of the axial (ω_z) over the radial axis (ω_{xy}). These values were determined from the initial measurements of the Alexa dyes with known diffusion coefficients D[75].

$$\tau_{dif} = \frac{\omega_{xy}^2}{4D} \tag{6.15}$$

The first two terms of equation 6.14 account for correction of the background fluorescence measured in the two channels in wild type cells. N, the particle

number had to be further corrected for maturation of mCherry, which was calculated as 50 %. Furthermore corrections for 8 % crosstalk of the meGFP into the mCherry channel had to be included. The obtained values for N where then divided by the observation volume to obtain the concentration of the fluorescent fusion proteins and their complexes. The volume was obtained by using the structural parameter sp approximating a cylindrical shape.

$$V = 2\pi\omega_{xy}^3 \cdot sp \tag{6.16}$$

6.2.4.7 Cell^R

All experiments monitoring the morphology of cells or localization of proteins were performed by a Cell^R system from Olympus (Olympus IX81) using a MT20 fluorescence lamp (Xe-lamp, Olympus). For imaging yeast cells an UPlanSApo 60x water objective with numerical aperture (NA) of 1.2 was used. Imaging of fluorescent fusion proteins was performed with the following filter settings:

Fluorophor	*Excitation filter*	*Emission Filter*
meyGFP	BP460-480HQ (470 GFP)	BA495-540HQ (GFP)
mCherry	BP545-580 (mKate2)	BA610IF (mKate2)
mCitrine	BP490-500HQ (500 YFP)	BA515-560HQ (YFP)

Dose-response and Cells to be images were grown over night in SD complete medium. Next day, yeast cells were diluted and grown in log phase (approx. 0.1-0.2*10^7 cells*ml^{-1}, OD_{600}:0.1-0.2) for low cell density preventing the formation of colonies.

6.2.4.8 Mating assay

The mating assay was done in a liquid culture and mating was observed quantitatively for 7 h at 30°C taking an image every 5 min using the time-lapse sequences function of the Olympus Cell^R system. For this purpose a LUCPlanFL N 40x air objective was used to monitor mating at several positions by defining a position list and using the motorized stage.
Cells were imaged in Labtek 8-well coverslides coated with ConcanavalinA. Coating was performed by incubation of the chambers with a solution of 2% ConcanavalinA in 1M NaCl for 30 min at RT followed by three wash steps with H_2O. The strain of interest and the mating tester strain 58 were separately cultured to an OD of 0.025, mixed and incubated for 30 min at 30°C to allow settling on ConcanavalinA coated cover slides.

6.2.5 Fluorescence activated cell sorting (FACS)

The expression levels of the reporter gene Fus1-meGFP were quantified using the FACS LSR II system. Yeast strains expressing this reporter were grown overnight

and diluted to an OD_{600} of 0.1. 1 mL cultures were stimulated with α-factor to a final concentration of 1 µM. The meGFP intensity was measured in unstimulated cells, and every 15 min after stimulation for a period of one cell cycle of approx. 90 min. For each time point 20.000 to 30.000 cells were sorted.

6.2.6 Data analysis, statistics and modelling

6.2.6.1 Morphological analysis using CellProfiler

For morphological analysis the cell image analysis software CellProfiler (Broad Institute) was used. Cells were segmented by nuclear Fus3-yemCitrine fluorescence and further analysed in terms of compactness, eccentricity and major axis length using the module MeasureObjectSizeShape. Compactness is the variance of the radial distance of the object's pixels from the centroid divides by the area. The eccentricity is the ratio of the distance between the foci of the ellipse and its major axis length. The value can be between 0 and 1, which are degenerated cases. An ellipse whose eccentricity is 0 is a circle, while an ellipse whose eccentricity is 1 is a line segment.

6.2.6.2 Western blot data analysis using ImageJ

Western blots were analysed in terms of band intensity using the image processing software ImageJ. Initially the image was corrected for the background intensity. This is important for precise comparison of the relative intensity of different bands. Therefor the mean intensity value of the background was measured by a rectangular selection of background with lowest signal and substracted from the whole image. In the next step the integrated intensity of a band is measured using the rectangular selection. This value was utilized for further calculations.

6.2.6.3 Linear regression analysis

The principal objective of applying the linear regression analysis here is to estimate the correct abundances of all possible species of the pheromone MAPK module, consisting of the four proteins Ste5, Ste11, Ste7 and Fus3. Mathematically, this problem can be represented as:

$$\mathbf{b} = \mathbf{a} \cdot X + \forall,\ a_i \geq 0 \ \forall i \tag{6.17}$$

where $a_i \in \mathbb{R}^+$ is a vector of the unknown variables, $b_j \in \mathbb{R}^+$ is the vector of known variables, X is the design matrix and $\forall_j \sim \mathcal{N}(0,\sigma_j^2)$ is an unknown error term. Given the model assumptions, $b_j = \sum_i x_{ij} \cdot a_i + \forall$, with $x_{ij} \in \{0,1\}$, and the purpose is to find **a,** which best explains **b**. This can be accomplished by

$$\underset{\mathbf{a}}{\operatorname{argmin}} \|X \cdot \mathbf{a} - \mathbf{b}\|^2 \tag{6.18}$$

which outranked other norms (such as L^1) in simulation studies. The optimization of this underdetermined regression problem was performed with the help of the limited memory variation of the Broyden-Fletcher-Goldfarb-Shanno algorithm[295].
In this case, the vector **a** represents the unknown concentrations of all possible species: the monomers Ste11, Fus3, Ste5, Ste7, the dimers Ste11-Fus3, Ste11-Ste5, Ste11-Ste7, Fus3-Ste5, Fus3-Ste7, Ste5-Ste7, the trimers Ste11-Fus3-Ste5, Ste11-Fus3-Ste7, Ste11-Ste5-Ste7, Fus3-Ste5-Ste7, and the tetramer Ste11-Fus3-Ste5-Ste7. The dimension of **a** is therefore 15 and can be reduced to 13 by removal of the non-existing complexes Ste11-Ste7 and Ste11-Fus3-Ste7.

The vector **b** contains the FCS measurements, performed for all possible pairs of the proteins Ste11, Fus3, Ste5 and Ste7 i.e. Ste7 Fus3, Ste11 Fus3, Ste11 Ste7, Ste11 Ste5, Fus3 Ste5 and Ste5 Ste7. One repetition of the experiment provides three values: the total concentrations of both tagged proteins (TC) and their complex concentrations (CC). Thus, the space of the observations is 10 dimensional, 4 dimensions for the TCs and 6 for the CCs. The length of **b** therefore depends on the number of different experiments conducted for the not stimulated, the shortly stimulated, and the long stimulated case (Fig. 3.5).

X is the design matrix which, given the biological assumptions i.e. that the system consists only of four proteins and their compounds, helps to describe the resulting FCS value as a function of the concentrations of all possible species. For example, the first three rows of X correspond to the FCS experiments in which Ste7 and Fus3 were measured, providing the values TC Ste7, TC Fus3 and CC Ste7 Fus3. This leads to the following three equations:

$$\text{TC Ste7} = 0\,[\text{Ste5} + 0\,[\text{Fus3} + 0\,[\text{Ste11} + 1\,[\text{Ste7} + 1\,[\text{Ste7-Fus3} + 1\,[\text{Ste7-Ste11} + 0\,[\text{Ste11-Fus3} + 0\,[\text{Ste5-Ste11} + 0\,[\text{Ste5-Fus3} + 1\,[\text{Ste7-Ste5} + 1\,[\text{Ste5-Ste11-Ste7} + 1\,[\text{Ste5-Ste7-Fus3} + 0\,[\text{Ste5-Ste11-Fus3} + 1\,[\text{Ste11-Ste7-Fus3} + 1\,[\text{Ste5-Ste11-Ste7-Fus3} \tag{6.19}$$

$$\text{TC Fus3} = 0\,[\text{Ste5} + 1\,[\text{Fus3} + 0\,[\text{Ste11} + 0\,[\text{Ste7} + 1\,[\text{Ste7-Fus3} + 0\,[\text{Ste7-Ste11} + 1\,[\text{Ste11-Fus3} + 0\,[\text{Ste5-Ste11} + 1\,[\text{Ste5-Fus3} + 0\,[\text{Ste7-Ste5} + 0\,[\text{Ste5-Ste11-Ste7} + 1\,[\text{Ste5-Ste7-Fus3} + 1\,[\text{Ste5-Ste11-Fus3} + 1\,[\text{Ste11-Ste7-Fus3} + 1\,[\text{Ste5-Ste11-Ste7-Fus3} \tag{6.20}$$

$$\text{CC Ste7-Fus3} = 0\,[\text{Ste5} + 0\,[\text{Fus3} + 0\,[\text{Ste11} + 0\,[\text{Ste7} + 1\,[\text{Ste7-Fus3} + 0\,[\text{Ste7-Ste11} + 0\,[\text{Ste11-Fus3} + 0\,[\text{Ste5-Ste11} + 0\,[\text{Ste5-Fus3} + 0\,[\text{Ste7-Ste5} + 0\,[\text{Ste5-Ste11-Ste7} + 1\,[\text{Ste5-Ste7-Fus3} + 0\,[\text{Ste5-Ste11-Fus3} + 1\,[\text{Ste11-Ste7-Fus3} + 1\,[\text{Ste5-Ste11-Ste7-Fus3} \tag{6.21}$$

The number of columns of X is equal to the dimension of **a** (15 or 13). The number of rows of X corresponds to the length of **b** (Fig. 3.5)

Bootstrap

Embedding the estimation process in a bootstrapping framework allows drawing conclusions on the estimates themself and also on their variability and stability[296]. Thus, for each of the three conditions (long-, shortly- and unstimulated), 1000 bootstrap samples of size 501 have been created, with data originating from all six

experimental settings (Ste7 Fus3, Ste11 Fus3, Ste11 Ste7, Ste11 Ste5, Fus3 Ste5, Ste5 Ste7). These samples were then tested using the previously described method, delivering an estimation of the distribution of the parameter vector **a.**
The complete statistical analysis was performed using the language and environment for statistical computing R (R Core Team (2012)), in particular the packages `stats` and `boot`.

6.2.6.4 Computational modelling

To explain how an ultrasensitive response can arise when phosphorylation regulates substrate sequestration, we constructed mathematical model based on the following experimentally validated assumptions:

i. Phosphorylation or dephosphorylation (with rate constants k_i and d_i respectively) of Ste11 by Fus3 takes place only when Ste11 is free in the cytosol.

ii. Each of the Ste11 phosphoforms can be sequestered on Ste5 with a unique rate of association/dissociation, proportional to the first-order rate constants k_i^a and k_i^d. The experimental evidence suggests that the affinity of binding is decreased upon Ste11 phosphorylation (Fig. 3.29).

This leads to the following system of differential equations (6.22):

$$\frac{d[Ste11]}{dt} = -k_0[Fus3][Ste11] + d_0[pSte11] - k_0^a[Ste5][Ste11] + k_0^d[Ste11 \cdot Ste5]$$
$$\frac{d[pSte11]}{dt} = k_0[Fus3][Ste11] - d_0[pSte11] - k_1^a[Ste5][pSte11] + k_1^d[pSte11 \cdot Ste5]$$
$$\frac{d[Ste11 \cdot Ste5]}{dt} = a_1[\alpha] + k_0^a[Ste5][Ste11] - k_0^d[Ste11 \cdot Ste5]$$
$$\frac{d[pSte11 \cdot Ste5]}{dt} = a_1[\alpha] + k_1^a[Ste5][pSte11] - k_1^d[pSte11 \cdot Ste5]$$
$$\frac{d[Ste5]}{dt} = k_0^d[Ste11 \cdot Ste5] - k_0^a[Ste5][Ste11] + k_1^d[pSte11 \cdot Ste5] - k_1^a[Ste5][pSte11]$$

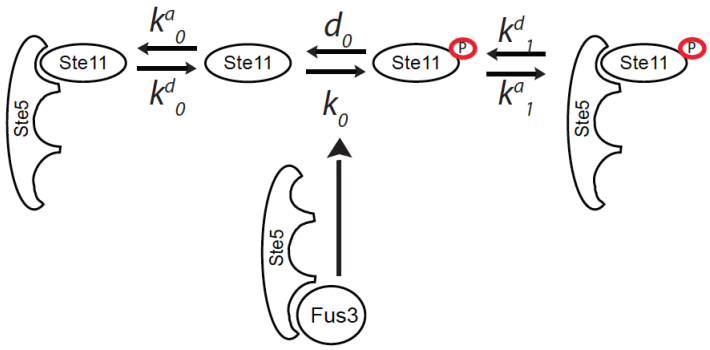

Fig. 6.8: Detailed representation of binding of unphosphorylated/phosphorylated Ste11 to Ste5 in ODE model.

The selective scaffold activation is proportional to the pheromone concentration $[\alpha]$. We assume that the affinity of binding of Ste11 on Ste5 depends on its phosphorylation status ($k_0^a \neq k_1^a$). Moreover, the sequestered Ste11 forms (as a fraction of the total Ste11 in the system, y) are the relevant forms that then activate the sequestered Ste7 (Ste7^s), which in turn activates Fus3 and thereby the mating pathway output. This is represented with the following minimal model: active Ste7 form is proportional to the sequestered Ste11 forms, whereas the active Fus3 form is proportional to the active Ste7. This captures the basic dynamical features of the downstream signalling without explicitly expressions about the Ste7 sequestration event, as well the cytosolic Ste7 form. We assume that the contribution of the cytosolic Ste7 form for Fus3 activation is negligent.

$$y = \frac{const \cdot [Ste11 \cdot Ste5] + [pSte11 \cdot Ste5]}{[Ste11] + [pSte11] + [Ste11 \cdot Ste5] + [pSte11 \cdot Ste5]} \tag{6.23}$$

$$\frac{d[Ste7^s]}{dt} = k_{3a} y - k_{3d}[Ste7^s]$$

$$\frac{d[Fus3]}{dt} = k_{4a}[Ste7^s] - k_{4d}[Fus3]$$

k_{3a}/k_{4a} and k_{3d}/k_{4d} are rates of activation and degradation of Ste7 and Fus3 respectively.
The negative feedback from Fus3 to Ste11, which changes its binding affinity to Ste5 is sufficient to create a switch-like dose-response to pheromone (Fig. 3.30). Removing the possibility to regulate Ste11 activity in the cytosol results only in sequestration of the unphosphorylated form of Ste11, which produces a hyperbolic Ste11 response to pheromone (Fig. 3.30). This shows that an ultrasensitive response can arise when phosphorylation regulates substrate sequestration, but substrate sequestration determines substrate activity.

List of parameters: $k_0 = k_1 = 0.8, d_0 = d_1 = 0.2\,, k_0^a = 18, k_0^d = 0.2, k_{3a} = k_{4a} = 0.8, k_{3d} = k_{4d} = 0.2, a_1 = 0.05$. The switch-like Fus3 response is robust to changes in the Ste11 affinity binding rate to Ste5 (k_i^a). For the set of parameters used here, the ultrasensitive response is preserved for $k_0^a \in [6,23]$.
The numerical simulations of this mathematical model were performed using the programming language C.

The binding affinities of unphosphorylated and phosphorylated Ste11 to Ste5 were calculated from LRA obtained concentrations (Fig. 3.19) and from the differences in Ste5 binding of unphosphorylated and phosphorylated Ste11 from the copurification experiments (Fig. 3.29): (6.23)

Ste5 (20.97 nM)
Ste11 (17.877 nM)
Ste5-Ste11 (7.037 nM)

Ste11(S243A)-Ste5/Ste11-Ste5 = 1.536
Ste11(S243E)-Ste5/Ste11-Ste5 = 0.41

$$K_d(Ste11 - Ste5) = \frac{[Ste5][Ste11]}{[Ste5 - Ste11]} = 53.28\ nM$$

$$K_d(Ste11(S243A) - Ste5) = \frac{17.13\ nM \cdot 14.033\ nM}{10.808\ nM} = 22.45\ nM \tag{6.24}$$

$$K_d(Ste11(S243E) - Ste5) = \frac{25.125\ nM \cdot 22.03\ nM}{2.885\ nM} = 191.8\ nM$$

7 References

1. Pryciak, P. M. & Huntress, F. A. Membrane recruitment of the kinase cascade scaffold protein Ste5 by the Gβγ complex underlies activation of the yeast pheromone response pathway. *Genes Dev.* **12,** 2684–2697 (1998).

2. Choi, K. Y., Satterberg, B., Lyons, D. M., Elion, E. A. Ste5 tethers multiple protein kinases in the MAP kinase cascade required for mating in S. cerevisiae. *Cell* **78,** 499–512 (1994).

3. Chen, R. E. & Thorner, J. Function and regulation in MAPK signaling pathways: lessons learned from the yeast Saccharomyces cerevisiae. *Biochim. Biophys. Acta* **1773,** 1311–1340 (2007).

4. Bhattacharyya, R. P. *et al.* The Ste5 scaffold allosterically modulates signaling output of the yeast mating pathway. *Science* **311,** 822–826 (2006).

5. Yu, R. C. *et al.* Negative feedback that improves information transmission in yeast signalling. *Nature* **456,** 755–61 (2008).

6. Malleshaiah, M. K., Shahrezaei, V., Swain, P. S. & Michnick, S. W. The scaffold protein Ste5 directly controls a switch-like mating decision in yeast. **465,** 101–105 (2010).

7. Marshall, C. J. Specificity of receptor tyrosine kinase signaling: transient versus sustained extracellular signal-regulated kinase activation. *Cell* **80,** 179–185 (1995).

8. Nagashima, T. *et al.* Quantitative transcriptional control of ErbB receptor signaling undergoes graded to biphasic response for cell differentiation. *J. Biol. Chem.* **282,** 4045–4056 (2007).

9. Neve, R. M., Holbro, T. & Hynes, N. E. Distinct roles for phosphoinositide 3-kinase, mitogen-activated protein kinase and p38 MAPK in mediating cell cycle progression of breast cancer cells. *Oncogene* **21,** 4567–4576 (2002).

10. Kholodenko, B. N., Hancock, J. F. & Kolch, W. Signalling ballet in space and time. *Nat. Rev. Mol. Cell Biol.* **11,** 414–426 (2010).

11. Kim, E. K. & Choi, E.-J. Pathological roles of MAPK signaling pathways in human diseases. *Biochim. Biophys. Acta* **1802,** 396–405 (2010).

12. Crews, C. M. & Erikson, R. L. Extracettutar Signals and Reversible Protein Phosphorytation: What to Mek of It All. *Cell* **74,** 215–217 (1993).

13. Seger, R. & Krebs, E. C., The MAPK signaling cascade. *FASEB J.* ***9,*** 726-735 (1995).

14. Widmann, C., Gibson, S., Jarpe, M. B. & Johnson, G. L. Mitogen-activated protein kinase: conservation of a three-kinase module from yeast to human. *Physiol. Rev.* **79,** 143–180 (1999).

15. Kyriakis, J. M. *et al.* Raf-1 actiaves MAP kinase-kinase. *Nature* ***358,*** 417-421 (1992).

16. Poulikakos, P. I., Zhang, C., Bollag, G., Shokat, K. M. & Rosen, N. RAF inhibitors transactivate RAF dimers and ERK signalling in cells with wild-type BRAF. *Nature* **464,** 427–430 (2010).

17. Hu, J. *et al.* Allosteric activation of functionally asymmetric RAF kinase dimers. *Cell* **154,** 1036–1046 (2013).

18. Gomez N. & Cohen P. Dissection of the protein kinase cascade by which nerve growth factor activates MAP kinases. *Nature* **353,** 170-173 (1991).

19. Seger, R. *et al.* Purification and characterization of mitogen-activated protein kinase activator(s) from epidermal growth factor-stimulated A431 cells. *J. Biol. Chem.* **267,** 14373–14381 (1992).

20. Anderson, N. G., Maller, J. L., Tonks, N. K., Sturgill, T. W., Requirement for integration of signals from two distinct phosphorylation pathways for activation of MAP kinase. *Nature* **343,** 651-653 (1990).

21. Dalby, K. N., Morrice, N., Caudwell, F. B., Avruch, J. & Cohen, P. Identification of regulatory phosphorylation sites in mitogen-activated protein kinase (MAPK)-activated protein kinase-1a/p90rsk That Are Inducible by MAPK. *J. Biol. Chem.* **273,** 1496–1505 (1998).

22. Chang, L. & Karin, M. Mammalian MAP kinase signalling cascades. *Nature* **410,** 37–40 (2001).

23. Hunter, T. Signaling-2000 and beyond. *Cell* **100,** 113–127 (2000).

24. Schlessinger, J. Cell signaling by receptor tyrosine kinases. *Cell* **103,** 211–225 (2000).

25. Bardwell, L. A walk-through of the yeast mating pheromone response pathway. *Peptides* **25,** 1465–1476 (2004).

26. Carol, A. L.-C. *et al.* Divergence in the MAP kinase regulatory network defined by MEK kinase and Raf. *Science* **260,** 315-319 (1993).

27. Waskiewicz, A. J. & Cooper, J. A. Mitogen and stress response pathways: MAP kinase cascades and phosphatase regulation in mammals and yeast. *Curr. Opin. Cell Biol.* **7,** 798–805 (1995).

28. Rhodes, N., Connell, L. & Errede, B. STE11 is a protein kinase required for cell-type-specific transcription and signal transduction in yeast. *Genes Dev.* **4,** 1862–1874 (1990).

29. Teague, M. A, Chaleff, D. T. & Errede, B. Nucleotide sequence of the yeast regulatory gene STE7 predicts a protein homologous to protein kinases. *Proc. Natl. Acad. Sci. U. S. A.* **83,** 7371–7375 (1986).

30. Courchesne, W. E., Kunisawa, R. & Thorner, J. A putative protein kinase overcomes pheromone-induced arrest of cell cycling in *S. cerevisiae*. *Cell* **58,** 1107–1119 (1989).

31. Elion, E. A, Grisafi, P. L. & Fink, G. R. FUS3 encodes a cdc2+/CDC28-related kinase required for the transition from mitosis into conjugation. *Cell* **60,** 649–664 (1990).

32. Qi, M. & Elion, E. A. MAP kinase pathways. *J. Cell Sci.* **118,** 3569–3572 (2005).

33. Sprague, G. F. Jr. Signal transduction in yeast mating: receptors, transcription factors, and the kinase connection. *Trends Genet.* **7,** 393-398 (1991).

34. Roberts, C. J. Signaling and circuitry of multiple MAPK pathways revealed by a matrix of global gene expression profiles. *Science* **287,** 873–880 (2000).

35. Wilkinson, L. E. & Pringle, J. R. Transient G1 arrest of *S. cerevisiae* cells of mating type alpha by a factor produced by cells of mating type a. *Exp. Cell Res.* **89,** 175–187 (1974).

36. Duntze, W., Manneys, T. R., Chemie, P. & Freiburg, U., Reversible arrest of haploid yeast cells at the initiation of DNA synthesis by a diffusible sex factor. *Exp. Cell. Res.* **76,** 99-110 (1973).

37. Madden, K. & Snyder, M. Cell polarity and morphogenesis in budding yeast. *Annu. Rev. Microbiol.* **52,** 687–744 (1998).

38. Dohlman, H. G. & Thorner, J. W. Regulation of G protein – Initiated signal transduction in yeast: paradigms and principles. *Annu. Rev. Biochem.* **70,** 703-754 (2001).

39. Stotzler, D., Kiltz, H.-H. & Duntze, W. Primary structure of alpha-Factor peptides from *Saccharomyces cerevisiae*. *Eur. J. Biochem.* **69,** 397–400 (1976).

40. Betz, R., Duntze, W. Purification and partial characterization of a-Factor, a mating hormone produced by mating-type-a cells from *Saccharomyces cerevisiae*. *Eur. J. Biochem.* **475,** 469–475 (1979).

41. Naider, F. & Becker, J. M. The alpha-factor mating pheromone of *Saccharomyces cerevisiae*: a model for studying the interaction of peptide hormones and G protein-coupled receptors. *Peptides* **25,** 1441–1463 (2004).

42. Hartwell, L. H. Mutants of *Saccharomyces cerevisiae* unresponsive to cell division control by polypeptide mating hormone. *J. Cell Biol.* **85,** 811–822 (1980).

43. Mackay, V. & Manney, T. R. Mutations affecting sexual conjugation and related processes in *Saccharomyces cerevisiae.* II Genetic analysis of nonmating mutants. *Genetics* **76,** 273-288 (1974).

44. Hagen, D. C., McCaffrey, G. & Sprague, G. F. Evidence the yeast STE3 gene encodes a receptor for the peptide pheromone a factor: gene sequence and implications for the structure of the presumed receptor. *Proc. Natl. Acad. Sci. U. S. A.* **83,** 1418–1422 (1986).

45. Burkholder, A. C. & Hartwell, L. H., The yeast a-factor receptor : structural properties deduced from the sequence of the STE2 gene. *Nucleic Acids Res.* **13,** 8463–8475 (1985).

46. Blumers, K. J., Johanna, E., Thorner, J. The STE2 Gene Product Is the ligand-binding component of the a-Factor receptor of *Saccharomyces cerevisiae*. *J. Biol. Chem.* **263,** 10836–10842 (1988).

47. Blumer, K. J. & Thorner, J., Receptor G protein signaling in yeast. *Annu. Rev. Pysiol.* **53,** 37–57 (1991).

48. Blumer, K. J. & Thorner, J. β and γ subunits of a yeast guanine nucleotide-binding protein are not essential for membrane association of the alpha subunit but are required for receptor coupling. *Proc. Natl. Acad. Sci. U.S.A.* **87,** 4363–4367 (1990).

49. Metodiev, M. V, Matheos, D., Rose, M. D. & Stone, D. E. Regulation of MAPK function by direct interaction with the mating-specific G α in yeast. *Science* **296,** 1483–1486 (2002).

50. Zheng, Y., Cerione, R. & Bender, A. Control of the yeast bud-site assembly GTPase Cdc42. *J. Biol. Chem.* **269,** 2369–2372 (1994).

51. Butty, A. C., Pryciak, P. M., Huang, L. S., Herskowitz, I. & Peter, M. The role of Far1p in linking the heterotrimeric G protein to polarity establishment proteins during yeast mating. *Science* **282,** 1511–1516 (1998).

52. Nern, A. & Arkowitz, R. A. A Cdc24p-Far1p-Gβγ protein complex required for yeast orientation during mating. *J. Cell Biol.* **144,** 1187–1202 (1999).

53. Peter, M. & Herskowitz, I. Direct inhibition of the yeast cyclin-dependent kinase Cdc28-Cln by Far1. *Science* **265,** 1228–1231 (1994).

54. Leberer, E., Dignard, D., Harcus, D., Thomas, D. Y. & Whiteway, M. The protein kinase homologue Ste20p is required to link the yeast pheromone response G-protein beta gamma subunits to downstream signalling components. *EMBO J.* **11,** 4815–4824 (1992).

55. Peter, M., Neiman, A. M., Park, H. O., van Lohuizen, M. & Herskowitz, I. Functional analysis of the interaction between the small GTP binding protein Cdc42 and the Ste20 protein kinase in yeast. *EMBO J.* **15,** 7046–7059 (1996).

56. Morreale, A. *et al.* Structure of Cdc42 bound to the GTPase binding domain of PAK. *Nat. Struct. Bio.* **7,** 384-388 (2000).

57. Winters, M. J., Lamson, R. E., Nakanishi, H., Neiman, A. M. & Pryciak, P. M. A membrane binding domain in the ste5 scaffold synergizes with gβγ binding to control localization and signaling in pheromone response. *Mol. Cell* **20,** 21–32 (2005).

58. Ohya, Y., Qadota, H., Anraku, Y., Pringle, J. R. & Botstein, D. Suppression of yeast geranylgeranyl transferase I Defect by alternative prenylation of two target GTPases, Rho1p and Cdc42p. **4,** 1017–1025 (1993).

59. Wu, C., Leberer, E., Thomas, D. Y. & Whiteway, M. Functional characterization of the interaction of Ste50p with Ste11p MAPKKK in *Saccharomyces cerevisiae. Mol. Biol. Cell* **10,** 2425–2440 (1999).

60. Truckses, D. M., Bloomekatz, J. E. & Thorner, J. The RA Domain of Ste50 adaptor protein Is required for delivery of Ste11 to the plasma membrane in the filamentous growth signaling pathway of the yeast *Saccharomyces cerevisiae. Mol. Cell. Biol.* **26,** 912-928 (2006)

61. Yerko, V. *et al.* Structurally unique interaction of RBD-like and PH domains is crucial for yeast pheromone signaling. *Mol. Biol. Cell* **24,** 409–420 (2013).

62. Garrenton, L. S., Young, S. L. & Thorner, J. Function of the MAPK scaffold protein, Ste5, requires a cryptic PH domain. *Genes Dev.* **20,** 1946–1958 (2006).

63. Whiteway, M. S. *et al.* Association of the yeast pheromone response G protein beta gamma subunits with the MAP kinase scaffold Ste5p. *Science* **269,** 1572–1575 (1995).

64. Yablonski, D., Marbach, I. & Levitzki, A. Dimerization of Ste5, a mitogen-activated protein kinase cascade scaffold protein, is required for signal transduction. *Proc. Natl. Acad. Sci. U.S.A.* **93,** 13864–13869 (1996).

65. Inouye, C. Ste5 RING-H2 Domain: Role in Ste4-Promoted oligomerization for Yeast pheromone signaling. *Science* **278,** 103–106 (1997).

66. Wang, Y. & Elion, E. A. Nuclear export and plasma membrane recruitment of the Ste5 scaffold are coordinated with oligomerization and association with signal transduction components. *Mol. Biol. Cell* **14,** 2543–2558 (2003).

67. Zalatan, J. G., Coyle, S. M., Rajan, S., Sidhu, S. S. & Lim, W. A. Conformational control of the Ste5 scaffold protein insulates against MAP kinase misactivation. *Science* **337,** 1218–1222 (2012).

68. Marcus, S., Polverino, A., Barr, M. & Wigler, M. Complexes between STE5 and components of the pheromone-responsive mitogen-activated protein kinase module. *Proc. Natl. Acad. Sci. U.S.A.* **91,** 7762–7766 (1994).

69. Printen, J. A. & Sprague, G. F. Jr. Protein-protein interactions in the yeast pheromone response pathway: Ste5p interacts with all members of the MAP kinase cascade. *Genetics* **138,** 609-616 (1994).

70. Lamson, R. E., Takahashi, S., Winters, M. J. & Pryciak, P. M. Dual role for membrane localization in yeast MAP kinase cascade activation and its contribution to signaling fidelity. *Curr. Biol.* **16,** 618–623 (2006).

71. Drogen, F. *et al.* Phosphorylation of the MEKK Ste11p by the PAK-like kinase Ste20p is required for MAP kinase signaling in vivo. *Curr. Biol.* **10,** 630–639 (2000).

72. Gartner, A, Nasmyth, K. & Ammerer, G. Signal transduction in *Saccharomyces cerevisiae* requires tyrosine and threonine phosphorylation of FUS3 and KSS1. *Genes Dev.* **6,** 1280–1292 (1992).

73. Errede, B., Gartner, A., Zhou, Z., Nasmyth, K. & Ammerer, G. MAPK kinase-related Fus3 from *S. cerevisiae* is activated by Ste7 *in vitro*. *Nature* **362,** 261-264 (1993).

74. Ma, D., Cook, J. G. & Thorner, J. Phosphorylation and localization of Kss1, a MAP kinase of the *Saccharomyces cerevisiae* pheromone response pathway. *Mol. Biol. Cell* **6,** 889–909 (1995).

75. Maeder, C. I. *et al.* Spatial regulation of Fus3 MAP kinase activity through a reaction-diffusion mechanism in yeast pheromone signalling. *Nat. Cell Biol.* **9,** 1319–1326 (2007).

76. Slaughter, B. D., Schwartz, J. W. & Li, R. Mapping dynamic protein interactions in MAP kinase signaling using live-cell fluorescence fluctuation spectroscopy and imaging. *Proc. Natl. Acad. Sci. U.S.A.* **104,** 20320–20325 (2007).

77. Bardwell, L. A conserved motif at the amino termini of MEKs might mediate high-affinity interaction with the cognate MAPKs. (1996). *Trends Biochem. Sci.* **21,** 373-374 (1996)

78. Bardwell, A. J., Flatauer, L. J., Matsukuma, K., Thorner, J. & Bardwell, L. A conserved docking site in MEKs mediates high-affinity binding to MAP kinases and cooperates with a scaffold protein to enhance signal transmission. *J. Biol. Chem.* **276,** 10374–10386 (2001).

79. Blackwell, E. *et al.* Effect of the pheromone-Responsive G_α and Phosphatase Proteins of Saccharomyces cerevisiae on the subcellular localization of the Fus3 mitogen-activated protein kinase. **23,** 1135–1150 (2003).

80. Song, D., Dolan, J. W., Yuan, Y. L. & Fields, S. Pheromone-dependent phosphorylation of the yeast STE12 protein correlates with transcriptional activation. *Genes Dev.* **5,** 741–750 (1991).

81. Elion, E. A., Satterberg, B. & Kranz, J. E. FUS3 phosphorylates multiple components of the mating signal transduction cascade: evidence for STE12 and FAR1. *Mol. Biol. Cell* **4,** 495–510 (1993).

82. Cook, J. G., Bardwell, L., Kron, S. J. & Thorner, J. Two novel targets of the MAP kinase Kss1 are negative regulators of invasive growth in the yeast Saccharomyces cerevisiae. *Genes Dev.* **10,** 2831–2848 (1996).

83. Tedford, K., Kim, S., Sa, D., Stevens, K. & Tyers, M. Regulation of the mating pheromone and invasive growth responses in yeast by two MAP kinase substrates. *Curr. Biol.* **7,** 228–238 (1997).

84. Dolan, J. W., Kirkman, C. & Fields, S. The yeast STE12 protein binds to the DNA sequence mediating pheromone induction. *Proc. Natl. Acad. Sci. U.S.A.* **86,** 5703–5707 (1989).

85. Company, M., Adler, C. & Errede, B. Identification of a Ty1 regulatory sequence responsive to Ste7 and Ste12. *Mol. Cell. Biol.* **8,** 2545-2554 (1988).

86. Harrison, R. & Delisi, C. Condition specific transcription factor binding site characterization in *Saccharomyces cerevisiae. Bioinformatics* **18,** 1289–1296 (2002).

87. Yuan, Y. L. & Fields, S. Properties of the DNA-binding domain of the *Saccharomyces cerevisiae* STE12 Protein. *Mol. Cell. Bio.* **11,** 5910-5918 (1991).

88. Trueheart, J., Boeke, J. D. & Fink, G. R. Two genes required for cell fusion during yeast conjugation: evidence for a pheromone-induced surface protein. *Mol. Cell. Biol.* **7,** 2316–2328 (1987).

89. White, J. M. & Rose, M. D. Yeast mating: getting close to membrane merger. *Curr. Biol.* **11,** 16–20 (2001).

90. Bardwell, L. *et al.* Repression of yeast Ste12 transcription factor by direct binding of unphosphorylated Kss1 MAPK and its regulation by the Ste7 MEK. *Genes Dev.* **12,** 2887–2898 (1998).

91. Chang, F. & Peter, M. Yeasts make their mark. *Nat. Cell Bio.* **5,** 294-299 (2003).

92. McCaffrey, G., Clay, F. J., Kelsay, K. & Sprague, G. F. Identification and regulation of a gene required for cell fusion during mating of the yeast *Saccharomyces cerevisiae. Mol. Cell. Biol.* **7,** 2680–2690 (1987).

93. Merlini, L., Dudin, O. & Martin, S. G. Mate and fuse : how yeast cells do it. *Open Biol.* **3,** 130008 (2013).

94. Freifelder, D. Bud position in saccharomyces cerevisiae. *J. Bacteriol.* **567,** 567–568 (1960).

95. Chant, J. & Herskowitz, I. Genetic control of bud site selection in yeast by a set of gene products that constitute a morphogenetic pathway. *Cell* **65,** 1203–1212 (1991).

96. Gimeno, C. J., Ljungdahl, P. O., Styles, C. A. & Fink, G. R. Unipolar cell divisions in the yeast *S. cerevisiae* lead to filamentous growth: regulation by starvation and RAS. *Cell* **68,** 1077–1090 (1992).

97. Brown, C. M., & Hough, J. S. Elongation of yeast cells in continous culture. *Nature* **206,** 676-678 (1965).

98. Shepard, M. G., Morphogenetic Transformation of Fungi. *Curr. Top. Med. Mycol.* **2,** 278-304 (1988).

99. Cullen, P. J. & Sprague, G. F. The regulation of filamentous growth in yeast. *Genetics* **190,** 23–49 (2012).

100. Roberts, R. L. & Fink, G. R. Elements of a single MAP kinase cascade in Saccharomyces cerevisiae mediate two developmental programs in the same cell type: mating and invasive growth. *Genes Dev.* **8,** 2974–2985 (1994).

101. Lorenz, M. C. & Heitman, J. The MEP2 ammonium permease regulates pseudohyphal differentiation in *Saccharomyces cerevisiae*. *EMBO J.* **17,** 1236–1247 (1998).

102. Lorenz, M. C. *et al.* The G protein-coupled receptor gpr1 is a nutrient sensor that regulates pseudohyphal differentiation in *Saccharomyces cerevisiae*. *Genetics* **154,** 609–622 (2000).

103. Cullen, P. J. *et al.* A signaling mucin at the head of the Cdc42- and MAPK-dependent filamentous growth pathway in yeast. *Genes Dev.* **18,** 1695–1708 (2004).

104. Lemaire, K., Van de Velde, S., Van Dijck, P. & Thevelein, J. M. Glucose and sucrose act as agonist and mannose as antagonist ligands of the G protein-coupled receptor Gpr1 in the yeast *Saccharomyces cerevisiae*. *Mol. Cell* **16,** 293–299 (2004).

105. Vadaie, N. *et al.* Cleavage of the signaling mucin Msb2 by the aspartyl protease Yps1 is required for MAPK activation in yeast. *J. Cell Biol.* **181,** 1073–1081 (2008).

106. Mösch, H. U., Roberts, R. L. & Fink, G. R. Ras2 signals via the Cdc42/Ste20/mitogen-activated protein kinase module to induce filamentous growth in *Saccharomyces cerevisiae*. *Proc. Natl. Acad. Sci. U.S.A.* **93,** 5352–5356 (1996).

107. Toda, T. *et al.* Cloning and characterization of BCY1, a locus encoding a regulatory subunit of the cyclic AMP-dependent protein kinase in *Saccharomyces cerevisiae*. *Mol. Cell. Biol.* **7,** 1371–1377 (1987).

108. Toda, T. *et al.* In yeast, RAS proteins are controlling elements of adenylate cyclase. *Cell* **40,** 27–36 (1985).

109. Roberts, R. L., Mösch, H. U. & Fink, G. R. 14-3-3 proteins are essential for RAS/MAPK cascade signaling during pseudohyphal development in *S. cerevisiae*. *Cell* **89,** 1055–1065 (1997).

110. Saito, H. Regulation of cross-talk in yeast MAPK signaling pathways. *Curr. Opin. Microbiol.* **13,** 677–683 (2010).

111. Flatauer, L. J., Zadeh, S. F. & Bardwell, L. Mitogen-Activated protein kinases with distinct requirements for Ste5 scaffolding influence signaling specificity in *Saccharomyces cerevisiae*. *Mol. Cell. Biol.* **25,** 1793–1803 (2005).

112. Maleri, S. *et al.* Persistent activation by constitutive Ste7 promotes Kss1-mediated invasive growth but fails to support Fus3-dependent mating in yeast. *Moll. Cell. Biol.* **24,** 9221–9238 (2004).

113. Yamamoto, K., Tatebayashi, K., Tanaka, K. & Saito, H. Dynamic control of yeast MAP kinase network by induced association and dissociation between the Ste50 scaffold and the Opy2 membrane anchor. *Mol. Cell* **40,** 87–98 (2010).

114. Wu, C., Jansen, G., Zhang, J., Thomas, D. Y. & Whiteway, M. Adaptor protein Ste50p links the Ste11p MEKK to the HOG pathway through plasma membrane association. *Genes Dev.* **20,** 734–746 (2006).

115. Gavrias V. *et al.* Saccharomyces cerevisiae 7EC1 is required for pseudohyphal growth. *Mol. Microbiol.* **19,** 1255–1263 (1996).

116. Madhani, H. D. Combinatorial Control Required for the Specificity of Yeast MAPK Signaling. *Science* **275,** 1314–1317 (1997).

117. Chou, S., Lane, S. & Liu, H. Regulation of mating and filamentation genes by two distinct Ste12 complexes in *Saccharomyces cerevisiae*. *Mol. Cell. Biol.* **26,** 4794–4805 (2006).

118. Liu, H., Styles, C. A. & Fink, G. R. Elements of the yeast pheromone response pathway required for filamentous growth of diploids. *Science* **262,** 1741–1744 (1993).

119. Leberer, E. *et al.* Functional characterization of the Cdc42p binding domain of yeast Ste20p protein kinase. *EMBO J.* **16,** 83–97 (1997).

120. Cook, J. G., Bardwell, L. & Thorner, J. Inhibitory and activating functions for MAPK Kss1 in the *S. cerevisiae* filamentous-. **390,** 98–101 (1997).

121. Farley, F. W., Satterberg, B., Goldsmith, E. J. & Elion, E. A. Relative dependence of different outputs of the *Saccharomyces cerevisiae* pheromone response pathway on the MAP kinase Fus3p. (1999).

122. Reményi, A., Good, M. C. & Lim, W. A. Docking interactions in protein kinase and phosphatase networks. *Curr. Opin. Struct. Biol.* **16,** 676–685 (2006).

123. Good, M., Tang, G., Singleton, J., Reményi, A. & Lim, W. A. The Ste5 scaffold directs mating signaling by catalytically unlocking the Fus3 MAP kinase for activation. *Cell* **136,** 1085–1097 (2009).

124. Burack, W. R. & Shaw, A. S. Signal transduction: hanging on a scaffold. *Curr. Opin. Cell Biol.* **12,** 211–216 (2000).

125. Schwartz, M. A. & Madhani, H. D. Control of MAPK signaling specificity by a conserved residue in the MEK-binding domain of the yeast scaffold protein Ste5. *Curr. Genet.* **49,** 351–363 (2006).

126. Patterson, J. C., Klimenko, E. S. & Thorner, J. Single-Cell analysis reveals that insulation maintains signaling specificity between two yeast MAPK pathways with common components. *Sci. Signal.* **3,** 1-11 (2010).

127. Peter, M., Gartner, A, Horecka, J., Ammerer, G. & Herskowitz, I. FAR1 links the signal transduction pathway to the cell cycle machinery in yeast. *Cell* **73,** 747–760 (1993).

128. Bao, M. Z., Schwartz, M. A, Cantin, G. T., Yates, J. R. & Madhani, H. D. Pheromone-dependent destruction of the Tec1 transcription factor is required for MAP kinase signaling specificity in yeast. *Cell* **119,** 991–1000 (2004).

129. Sabbagh, W. Jr., Flatauer, L. J., Bardwell, A. J., Bardwell, L. Specificity of MAP kinase signaling in yeast differentiation Involves transient versus sustained MAPK activation. *Mol. Cell.* **8,** 683–691 (2011).

130. Hao, N. *et al.* Combined computational and experimental analysis reveals mitogen-activated protein kinase-mediated feedback phosphorylation as a mechanism for signaling specificity. *Mol. Biol. Cell* **23,** 3899–3910 (2012).

131. Santos, S. D. M., Verveer, P. J. & Bastiaens, P. I. H. Growth factor-induced MAPK network topology shapes Erk response determining PC-12 cell fate. *Nat. Cell Biol.* **9,** 324–330 (2007).

132. Jackson, C. L. & Hartwell, L. H. Courtship in S. cerevisiae: both cell types choose mating partners by responding to the strongest pheromone signal. *Cell* **63,** 1039–1051 (1990).

133. Segall, J. E. Polarization of yeast cells in spatial gradients of alpha mating factor. *Proc. Natl. Acad. Sci. U.S.A.* **90,** 8332–8336 (1993).

134. Dohlman, H. G. *et al.* Sst2, a negative regulator of pheromone signaling in the yeast Saccharomyces cerevisiae : expression, localization, and genetic interaction and physical association with Gpa1 (the G-protein alpha subunit). *Mol. Cell. Biol.* **16,** 5194-5209 (1996).

135. Chan, R. K. & Otte, C. A. Isolation and genetic analysis of *Saccharomyces cerevisiae* mutants supersensitive to G1 arrest by a factor and alpha factor pheromones. *Mol. Cell. Biol.* **2,** 11-20 (1982).

136. Freeman, M. Feedback control of intracellular signalling in development. *Nature* **408,** 313–319 (2000).

137. Cori, G. T., Green, A. A. CRYSTALLINE MUSCLE PHOSPHORYLASE : II. PROSTHETIC GROUP. *J. Biol. Chem.* **151,** 31-38 (1943).

138. Krebs, E. G. & Fischer, E. H. The phosphorylase b to a converting enzyme of rabbit skeletal muscle. *Biochim. Biophys. Acta* **1000,** 302–309 (1956).

139. Goldbeter, A., Koshland, D. E. Jr. An amplified sensitivity arising from covalent modification in biological systems. *Proc. Natl. Acad. Sci. U.S.A.* **78,** 6840–6844 (1981).

140. Kholodenko, B. N. Cell-signalling dynamics in time and space. *Nat. Rev. Mol. Cell Biol.* **7,** 165–176 (2006).

141. Ferrell, J. E. Tripping the switch fantastic : how a protein kinase cascade can convert graded inputs into switch-like outputs. *Trends Biochem. Sci.* **4,** 460–466 (1996).

142. Koshland, D. E., Goldbeter, A. & Stock, J. B. Amplification and adaptation in regulatory and sensory systems. *Science* **217,** 220–225 (1982).

143. Yee, R. & Liebman, P. A. Light-activated phosphodiesterase of the rod outer segment . Kinetics and parameters of activation and deactivation. *J. Biol. Chem.* **253,** 8902-8909 (1978).

144. Hill, A. V. The possible effects of the aggregation of the molecules of haemoglobin on its dissociation curves. J. Phys. (1910).

145. Ferrell, J. E. & Ha, S. H. Ultrasensitivity part I: Michaelian responses and zero-order ultrasensitivity. *Trends Biochem. Sci.* **39,** 496–503 (2014).

146. Huang, C. Y. & Ferrell, J. E. Ultrasensitivity in the mitogen-activated protein kinase cascade. *Proc. Natl. Acad. Sci. U.S.A.* **93,** 10078–10083 (1996).

147. Bohr, C., Hasselbach, K. &Krogh, H. Ueber einen in biologischer Beziehung wichtigen Einfluss, den die Kohlensaurespannung des Blutes auf dessen Sauerstoffbindung uebt. *Acta Phys.* **16,** 402-412 (1904).

148. Ferrel, J. E. Jr. How responses get more switch-like as you move down a protein kinase cascade. *Trends Biochem. Sci.* **22,** *p289* (1997).

149. Brown, G. C., Hoek, J. B. & Kholodenko, B. N. Why do protein kinase cascades have more than one level. *Trends Biochem. Sci.* **22,** *p288* (1997).

150. Stadtman, E. R. & Chock, P. B. Superiority of interconvertible enzyme cascades in metabolic regulation: analysis of monocyclic systems. *Proc. Natl. Acad. Sci. U.S.A.* **74,** 2761–2765 (1977).

151. Sauro, H. M. & Kholodenko, B. N. Quantitative analysis of signaling networks. *Prog. Biophys. Mol. Biol.* **86,** 5–43 (2004).

152. Black, H. S. Stabilized feedback amplifiers. The Bell System Technical Journal (1934).

153. Umbarger, H. E., Evidence for a negative-feedback mechanism in the biosynthesis of isoleucine. *Science* **123,** p848 (1954).

154. Stelling, J., Sauer, U., Szallasi, Z., Doyle, F. J. & Doyle, J. Robustness of cellular functions. *Cell* **118,** 675–685 (2004).

155. Becskei, A., Serrano, L. Engineering stability in gene networks by autoregulation. *Nature* **405,** 590-593 (2000).

156. Oren, M. Regulation of the p53 tumor suppressor protein. *J. Biol. Chem.* **274,** 36031–36034 (1999).

157. Shin, S.-Y. *et al.* Positive- and negative-feedback regulations coordinate the dynamic behavior of the Ras-Raf-MEK-ERK signal transduction pathway. *J. Cell Sci.* **122,** 425–435 (2009).

158. Kholodenko, B. N. Negative feedback and ultrasensitivity can bring about oscillations in the mitogen-activated protein kinase cascades. *Eur. J. Biochem.* **267,** 1583–1588 (2000).

159. Nakayama, K., Satoh, T., Igari, A., Kageyama, R. & Nishida, E. FGF induces oscillations of Hes1 expression and Ras/ERK activation. *Curr. Biol.* **18,** R332–334 (2008).

160. Shankaran, H. *et al.* Rapid and sustained nuclear-cytoplasmic ERK oscillations induced by epidermal growth factor. *Mol. Syst. Biol.* **5,** p332 (2009).

161. Tiana, G., Krishna, S., Pigolotti, S., Jensen, M. H. & Sneppen, K. Oscillations and temporal signalling in cells. *Phys. Biol.* **4,** R1–17 (2007).

162. Monod, J. & Jacob, F. Cold Spring Harbor Symp. Quant. Biol. **26,** p389. (1961).

163. Lisman, J. E. A mechanism for memory storage insensitive to molecular turnover: A bistable autophosphorylating kinase. *Proc. Natl. Acad. Sci. U.S.A.* **82,** 3055–3057 (1985).

164. Reynolds, A. R., Tischer, C., Verveer, P. J., Rocks, O. & Bastiaens, P. I. H. EGFR activation coupled to inhibition of tyrosine phosphatases causes lateral signal propagation. *Nat. Cell Biol.* **5,** 447–453 (2003).

165. Ferrell, J. E. The Biochemical basis of an all-or-none cell fate switch in Xenopus Oocytes. *Science* **280,** 895–898 (1998).

166. Ferrell, J. E. Self-perpetuating states in signal transduction: positive feedback, double-negative feedback and bistability. *Curr. Opin. Cell Biol.* **14,** 140–148 (2002).

167. Ferrell, J. E. & Bhatt, R. R. Mechanistic studies of the dual phosphorylation of mitogen-activated protein kinase. *J. Biol. Chem.* **272,** 19008–19016 (1997).

168. Burack, W. R. & Sturgill, T. W. The Activating dual phosphorylation of MAPK by MEK Is nonprocessive. Biochem. **36,** 5929-5933 (1997).

169. Gotoh, Y., Masuyama, N., Dell, K., Shirakabe, K. & Nishida, E. Initiation of Xenopus Oocyte maturation by activation of the mitogen-activated protein kinase cascade. *J. Biol. Chem.* **270,** 25898–25904 (1995).

170. Matten, W. T., Copeland, T. D., Ahn, N. G. & Woude, G. F. Vande. Positive feedback between MAP Kinase and Mos during Xenopus Oocyte maturation. *Dev. Biol.* **492,** 485–492 (1996).

171. Edelsten, B. B. Biochemical Model with Multiple Steady States and Hysteresis. *J. Theor. Biol.* **29,** 57–62 (1970).

172. Gardner, T. S., Cantor, C. R. & Collins, J. J. Construction of a genetic toggle switch in Escherichia coli. *Nature* **403,** 339–342 (2000).

173. Lemmon, M. A & Schlessinger, J. Cell signaling by receptor tyrosine kinases. *Cell* **141,** 1117–1134 (2010).

174. Avraham, R. & Yarden, Y. Feedback regulation of EGFR signalling: decision making by early and delayed loops. *Nat. Rev. Mol. Cell Biol.* **12,** 104–117 (2011).

175. Clayton, A. H. a *et al.* Ligand-induced dimer-tetramer transition during the activation of the cell surface epidermal growth factor receptor-A multidimensional microscopy analysis. *J. Biol. Chem.* **280,** 30392-30399 (2005).

176. Grecco, H. E., Schmick, M. & Bastiaens, P. I. H. Signaling from the living plasma membrane. *Cell* **144,** 897–909 (2011).

177. Grasierger, B., Mintont, A. P., Delisit, C. & Metzger, H. Interaction between proteins localized in membranes. *Proc. Natl. Acad. Sci. U.S.A.* **83,** 6258–6262 (1986).

178. Kholodenko, B. N., Hoek, J. B. & Westerhoff, H. V. Why cytoplasmic signalling proteins should be recruited to cell membranes. *Trends Cell Biol.* **10,** 173–178 (2000).

179. Schmick, M. & Bastiaens, P. I. H. The interdependence of membrane shape and cellular signal processing. *Cell* **156,** 1132–1138 (2014).

180. Adam, G. & Delbrück, M. Reduction of dimensionality in biological diffusion processes. *Struct. Chem. Mol. Biol.* **10,** 198–215 (1968).

181. Nan, X. *et al.* Single-molecule superresolution imaging allows quantitative analysis of RAF multimer formation and signaling. *Proc. Natl. Acad. Sci. U.S.A.* **110,** 18519–18524 (2013).

182. Harding, A., Tian, T., Westbury, E., Frische, E. & Hancock, J. F. Subcellular localization determines MAP kinase signal output. *Curr. Biol.* **15,** 869–873 (2005).

183. Castro, D. *et al.* Phospholipase Cγ activates Ras on the Golgi apparatus by means of RasGRP1. *Nature* **424,** 694-698 (2003).

184. Andersen, S. S. Spindle assembly and the art of regulating microtubule dynamics by MAPs and Stathmin/Op18. *Trends Cell Biol.* **10,** 261–267 (2000).

185. Niethammer, P., Bastiaens, P. & Karsenti, E. Stathmin-tubulin interaction gradients in motile and mitotic cells. *Science* **303,** 1862–1866 (2004).

186. Kalab, P., Weis, K. & Heald, R. Visualization of a Ran-GTP gradient in interphase and mitotic Xenopus egg extracts. *Science* **295,** 2452–2456 (2002).

187. Muñoz-García, J. & Kholodenko, B. N. Signalling over a distance: gradient patterns and phosphorylation waves within single cells. *Biochem. Soc. Trans.* **38,** 1235–1241 (2010).

188. Brown, G. C. & Kholodenko, B. N. Spatial gradients of cellular phosphoproteins. *FEBS Lett.* **457,** 452–454 (1999).

189. Muñoz-García, J., Neufeld, Z. & Kholodenko, B. N. Positional information generated by spatially distributed signaling cascades. *PLoS Comput. Biol.* **5,** e1000330 (2009).

190. Neves, S. R. *et al.* Cell shape and negative links in regulatory motifs together control spatial information flow in signaling networks. *Cell* **133,** 666–680 (2008).

191. Page, M. I. & Jencks, W. P. Entropic contributions to rate accelerations in enzymic and intramolecular reactions and the chelate effect. *Proc. Natl. Acad. Sci. U.S.A.* **68,** 1678–1683 (1971).

192. Good, M. C., Zalatan, J. G. & Lim, W. A. Scaffold proteins: hubs for controlling the flow of cellular information. *Science* **332,** 680–686 (2011).

193. Levchenko, A., Bruck, J. & Sternberg, P. W. Scaffold proteins may biphasically affect the levels of mitogen-activated protein kinase signaling and reduce its threshold properties. *Proc. Natl. Acad. Sci.* **97,** 5818–5823 (2000).

194. Cacace, A. M. *et al.* Identification of constitutive and Ras-inducible phosphorylation sites of KSR: Implications for 14-3-3 binding, mitogen-activated protein kinase binding , and KSR overexpression. *Mol. Cell. Biol.* **19,** 229-240 (1999).

195. Ferrell, J. E. What Do Scaffold Proteins Really Do? *Sci. Signal.* **52,** pe1–pe3 (2000).

196. Rajakulendran, T., Sahmi, M., Lefrançois, M., Sicheri, F. & Therrien, M. A dimerization-dependent mechanism drives RAF catalytic activation. *Nature* **461,** 542–545 (2009).

197. DeWire, S. M., Ahn, S., Lefkowitz, R. J. & Shenoy, S. K. β-Arrestins and cell signaling. *Annu. Rev. Physiol.* **69,** 483–510 (2007).

198. Zhang, W., Sloan-lancaster, J., Kitchen, J., Trible, R. P. & Samelson, L. E. LAT : The ZAP-70 tyrosine kinase substrate that links T Cell receptor to cellular activation. *Cell* **92,** 83–92 (1998).

199. Lin, J. & Weiss, A. Identification of the minimal tyrosine residues required for linker for activation of T cell function. *J. Biol. Chem.* **276,** 29588–29595 (2001).

200. McKay, M. M., Ritt, D. A & Morrison, D. K. Signaling dynamics of the KSR1 scaffold complex. *Proc. Natl. Acad. Sci. U.S.A.* **106,** 11022–11027 (2009).

201. Zamir, E. & Bastiaens, P. I. H. Reverse engineering intracellular biochemical networks. *Nat. Chem. Biol.* **4,** 643–647 (2008).

202. Kitano, H. Systems biology: a brief overview. *Science* **295,** 1662–1664 (2002).

203. Pigolotti, S., Krishna, S. & Jensen, M. H. Oscillation patterns in negative feedback loops. *Proc. Natl. Acad. Sci.* **104,** 6533-6537 (2007).

204. Olsen, J. V *et al.* Global, in vivo, and site-specific phosphorylation dynamics in signaling networks. *Cell* **127,** 635–648 (2006).

205. Hartwell, L. H., Hopfield, J. J., Leibler, S. & Murray, A. W. From molecular to modular cell biology. *Nature* **402,** 47–52 (1999).

206. Alon, U. Biological networks: the tinkerer as an engineer. *Science* **301,** 1866–1867 (2003).

207. Csete, M. E. & Doyle, J. C. Reverse engineering of biological complexity. *Science* **295,** 1664–1669 (2002).

208. Verveer, P. J. Quantitative Imaging of lateral ErbB1 receptor signal propagation in the plasma membrane. *Science* **290,** 1567–1570 (2000).

209. Jarzombek *et al.* A negative feedback loop in the yeast mating MAPK module determines where and how to become a shmoo. *in preparation*

210. Schultz, C. Molecular tools for cell and systems biology. *HFSP J.* **1,** 230–248 (2007).

211. Tsien, R. Y. New calcium indicators and buffers with high selectivity against magnesium and protons: Design, synthesis, and properties of prototype structures. *Biochem.* **19,** 2396–2404 (1980).

212. Tsien, R. Y., Pozzan, T. & Rink, T. J. Calcium homeostasis in intact lymphocytes : Cytoplasmic free calcium monitored with a new, Intracellularly trapped fluorescent indicator. *J. Cell Biol.* **94,** 325–334 (1982).

213. Adams, S. R. *et al.* Fluorescence ratio imaging of cyclic AMP in single cells. *Nature* **349,** 694-697 (1991).

214. Zhang, J., Campbell, R. E., Ting, A. Y. & Tsien, R. Y. Creating new fluorescent probes for cell biology. *Nat. Rev. Mol. Cell Biol.* **3,** 906–918 (2002).

215. Dehmelt, L. & Bastiaens, P. I. H. Spatial organization of intracellular communication: insights from imaging. *Nat. Rev. Mol. Cell Biol.* **11,** 440–452 (2010).

216. Chudakov, D. M., Matz, M. V, Lukyanov, S. & Lukyanov, K. A. Fluorescent proteins and their applications in imaging living tells and tissues. *Physiol. Rev.* **90,** 1103–1163 (2010).

217. Wouters, F. S., Verveer, P. J. & Bastiaens, P. I. H. Imaging biochemistry inside cells Imaging fluorescence patterns. **11,** 203–211 (2001).

218. Verveer, P. J., Squire, A. & Bastiaens, P. I. H. Global Analysis of fluorescence lifetime Imaging microscopy data. **78,** 2127–2137 (2000).

219. Physics, E. Dynamics of fluorescence fluctuations in green fluorescent. **95,** 13573–13578 (1998).

220. Haustein, E. & Schwille, P. Fluorescence correlation spectroscopy: novel variations of an established technique. *Annu. Rev. Biophys. Biomol. Struct.* **36,** 151–169 (2007).

221. Kohl, T., Heinze, K. G., Kuhlemann, R., Koltermann, A. & Schwille, P. A protease assay for two-photon crosscorrelation and FRET analysis based solely on fluorescent proteins. *Proc. Natl. Acad. Sci. U.S.A.* **99,** 12161–12166 (2002).

222. Baudendistel, N., Müller, G., Waldeck, W., Angel, P. & Langowski, J. Two-hybrid fluorescence cross-correlation spectroscopy detects protein-protein interactions in vivo. *Chemphyschem* **6,** 984–990 (2005).

223. Kim, S. a, Heinze, K. G., Bacia, K., Waxham, M. N. & Schwille, P. Two-photon cross-correlation analysis of intracellular reactions with variable stoichiometry. *Biophys. J.* **88,** 4319–4336 (2005).

224. Krichevsky, O & Bonnet, G. Fluorescence correlation spectroscopy : the technique and its applications. *Rep. Prog. Phys.* **65,** 251–297 (2002).

225. Adkins, E. M. *et al.* Membrane mobility and microdomain association of the dopamine transporter studied with fluorescence correlation spectroscopy and fluorescence recovery after photobleaching. *Biochemistry* **46,** 10484–10497 (2007).

226. Jaqaman, K. & Danuser, G. Linking data to models: data regression. *Nat. Rev. Mol. Cell Biol.* **7,** 813–819 (2006).

227. Janes, K. A & Yaffe, M. B. Data-driven modelling of signal-transduction networks. *Nat. Rev. Mol. Cell Biol.* **7,** 820–828 (2006).

228. Chu, S. The Transcriptional Program of Sporulation in Budding Yeast. *Science* **282,** 699–705 (1998).

229. Claverie, J. Computational methods for the identification of differential and coordinated gene expression. *Hum. Mol. Gen.* **8,** 1821–1832 (2000).

230. Kholodenko, B. N. Untangling the signalling wires. *Nat. Cell Biol.* **9,** 247–249 (2007).

231. De la Fuente, A., Brazhnik, P. & Mendes, P. Linking the genes: inferring quantitative gene networks from microarray data. *Trends Genet.* **18,** 395–398 (2002).

232. Kholodenko, B. N. *et al.* Untangling the wires: a strategy to trace functional interactions in signaling and gene networks. *Proc. Natl. Acad. Sci. U.S.A.* **99,** 12841–12846 (2002).

233. Lucchesi, J. C. Synthetic lethality and semi-lethality among functionally related mutants of *Drosophila melanogaster*. *Genetics* **59, 37-44** (1967).

234. Bendert, A. & Pringle, J. R. Use of a screen for synthetic lethal and multicopy suppressee sutants to identify two new genes involved in norphogenesis in *Saccharomyces cerevisiae*. *Mol. Cell. Biol.* **11,** 1295–1305 (1991).

235. Tong, A. H. *et al.* Systematic genetic analysis with ordered arrays of yeast deletion mutants. *Science* **294,** 2364–2368 (2001).

236. Botstein, D. & Fink, G. R. Yeast: an experimental organism for modern biology. *Science* **240,** 1439–43 (1988).

237. Goffeau, A. *et al.* Life with 6000 Genes. *Science* **274,** 546-567 (1995).

238. Foury, F. Human genetic diseases : a cross-talk between man and yeast. *Gene* **195,** 1–10 (1997).

239. Marton, M. J. *et al.* Drug target validation and identification of secondary drug target effects using DNA microarrays. *Nature* **4,** 1293–1301 (1998).

240. Hinnen, A., Hicks, J. B. & Fink, G. R. Transformation of yeast. *Proc. Natl. Acad. Sci.* **75,** 1929–1933 (1978).

241. Knop, M. *et al.* Epitope tagging of yeast genes using a PCR-based strategy: more tags and improved practical routines. *Yeast* **15,** 963–972 (1999).

242. Janke, C. *et al.* A versatile toolbox for PCR-based tagging of yeast genes: new fluorescent proteins, more markers and promoter substitution cassettes. *Yeast* **21,** 947–962 (2004).

243. Huh, W.-K. *et al.* Global analysis of protein localization in budding yeast. *Nature* **425,** 686–691 (2003).

244. Uetz, P. *et al.* A comprehensive analysis of protein-protein interactions in *Saccharomyces cerevisiae*. *Nature* **403,** 623-627 (2000).

245. Mustacchi, R., Hohmann, S. & Nielsen, J. Yeast systems biology to unravel the network of life. *Yeast* **23,** 227–238 (2006).

246. Boone, C. Yeast systems biology: our best shot at modeling a cell. *Genetics* **198,** 435–437 (2014).

247. Hao, N. *et al.* Regulation of cell signaling dynamics by the protein kinase-scaffold Ste5. *Mol. Cell* **30,** 649–656 (2008).

248. Moore, T. I., Chou, C.-S., Nie, Q., Jeon, N. L. & Yi, T.-M. Robust spatial sensing of mating pheromone gradients by yeast cells. *PLoS One* **3,** e3865 (2008).

249. Erdman, S. & Snyder, M. A filamentous growth response mediated by the yeast mating pathway. *Genetics* **159,** 919–928 (2001).

250. Hao, N., Zeng, Y., Elston, T. C. & Dohlman, H. G. Control of MAPK specificity by feedback phosphorylation of shared adaptor protein Ste50. *J. Biol. Chem.* **283,** 33798–33802 (2008).

251. Colman-Lerner, A. *et al.* Regulated cell-to-cell variation in a cell-fate decision system. *Nature* **437,** 699–706 (2005).

252. Doi, K. *et al.* MSG5, a novel protein phosphatase promotes adaptation to pheromone response in *S. cerevisiae*. *EMBO J.* **13,** 61–70 (1994).

253. Bishop, a C. *et al.* A chemical switch for inhibitor-sensitive alleles of any protein kinase. *Nature* **407,** 395–401 (2000).

254. Marín, M. J. *et al.* Different modulation of the outputs of yeast MAPK-mediated pathways by distinct stimuli and isoforms of the dual-specificity phosphatase Msg5. *Mol. Genet. Genomics* **281,** 345–359 (2009).

255. Andersson, J., Simpson, D. M., Qi, M., Wang, Y. & Elion, E. a. Differential input by Ste5 scaffold and Msg5 phosphatase route a MAPK cascade to multiple outcomes. *EMBO J.* **23,** 2564–2576 (2004).

256. Stotz, A. & Linder, P. The ADE2 gene from *Saccharomyces cerevisiae*: sequence and new vectors. *Gene* **95,** 91-98 (1990).

257. Bush, A. & Colman-Lerner, A. Quantitative measurement of protein relocalization in live cells. *Biophys. J.* **104,** 727–736 (2013).

258. Pelkmans, L. Cell Biology. Using cell-to-cell variability-a new era in molecular biology. *Science* **336,** 425–426 (2012).

259. Bardwell, A. J., Flatauer, L. J., Matsukuma, K., Thorner, J. & Bardwell, L. A conserved docking site in MEKs mediates high-affinity binding to MAP kinases and cooperates with a scaffold protein to enhance signal transmission. *J. Biol. Chem.* **276,** 10374–10386 (2001).

260. Reményi, A., Good, M. C., Bhattacharyya, R. P. & Lim, W. A. The role of docking interactions in mediating signaling input, output, and discrimination in the yeast MAPK network. *Mol. Cell* **20,** 951–962 (2005).

261. Wu, R. *et al.* Correct interpretation of comprehensive phosphorylation dynamics requires normalization by protein expression changes. *Mol. Cell. Proteomics* **10,** M111.009654 (2011).

262. Stevenson, B. J., Rhodes, N., Errede, B. & Sprague, G. F. Constitutive mutants of the protein kinase STE11 activate the yeast pheromone response pathway in the absence of the G protein. *Genes Dev.* **6,** 1293–1304 (1992).

263. Takahashi, S. & Pryciak, P. M. Membrane localization of scaffold proteins promotes graded signaling in the yeast MAP kinase cascade. *Curr. Biol.* **18,** 1184–1191 (2008).

264. Bagnat, M. & Simons, K. Cell surface polarization during yeast mating. *Proc. Natl. Acad. Sci.* **99,** 27–32 (2002).

265. Strickfaden, S. C. *et al.* A mechanism for cell-cycle regulation of MAP kinase signaling in a yeast differentiation pathway. *Cell* **128,** 519–531 (2007).

266. Hanks, S. K., Quinn, A. M. & Hunter, T. The kinase family : Conserved protein phylogeny features and deduced phylogeny of the catalytic domains. *Science* **241,** 42–52 (2013).

267. Hanrs, S. K. & Hunter, T. The eukaryotic protein kinase superfamily : (catalytic) domam structure and classification. *FASEB J.* **9,** 576-596 (1995).

268. Kornev, A. P., Haste, N. M., Taylor, S. S. & Eyck, L. F. Ten. Surface comparison of active and inactive protein kinases identifies a conserved activation mechanism. *Proc. Natl. Acad. Sci. U.S.A.* **103,** 17783–17788 (2006).

269. Errede, B. & Ge, Q.-Y. Feedback regulation of map kinase signal pathways. *Phil. Trans. R. Soc. Lond. B* **351,** 143-149 (1996).

270. Limpert, E., Stahel, W. A. & Abbt, M. Log-normal distributions across the sciences: Keys and Clues. *Bioscience* **51,** 341 (2001).

271. Kinoshita, E., Takahashi, M., Takeda, H., Shiro, M. & Koike, T. Recognition of phosphate monoester dianion by an alkoxide-bridged dinuclear zinc(II) complex. *Dalton Trans.* 1189–1193 (2004).

272. Matheos, D., Metodiev, M., Muller, E., Stone, D. & Rose, M. D. Pheromone-induced polarization is dependent on the Fus3p MAPK acting through the formin Bni1p. *J. Cell Biol.* **165,** 99–109 (2004).

273. Hilioti, Z. *et al.* Oscillatory phosphorylation of yeast Fus3 MAP kinase controls periodic gene expression and morphogenesis. *Curr. Biol.* **18,** 1700–1706 (2008).

274. Bidlingmaier, S. & Snyder, M. Regulation of polarized growth initiation and termination cycles by the polarisome and Cdc42 regulators. *J. Cell Biol.* **164,** 207–218 (2004).

275. Garrenton, L. S. *et al.* Nucleus-specific and cell cycle-regulated degradation of mitogen-activated protein kinase scaffold protein Ste5 contributes to the control of signaling competence. *Mol. Cell. Biol.* **29,** 582–601 (2009).

276. Rosenfeld, N., Young, J. W., Alon, U., Swain, P. S. & Elowitz, M. B. Gene Regulation at the Single-Cell Level. *Science* **307,** 1962-1965 (2005).

277. Pedraza, J.M. & van Oudenaarden, A. Noise propagation in gene networks. *Science* **307,** 1965–1970 (2005).

278. Pitoniak, A. *et al.* Cdc42p-Interacting protein Bem4p regulates the filamentous growth MAP kinase pathway. *Mol. Cell. Biol.* **35,** 417–436 (2014).

279. Lochhead, P. A. Protein kinase activation loop autophosphorylation in cis: overcoming a Catch-22 situation. *Sci. Signal.* **2,** pe4 (2009).

280. Barkai, N. & Shilo, B.-Z. Variability and robustness in biomolecular systems. *Mol. Cell* **28,** 755–760 (2007).

281. Dar, A. C. & Shokat, K. M. The evolution of protein kinase inhibitors from antagonists to agonists of cellular signaling. *Annu. Rev. Biochem.* **80,** 769–795 (2011).

282. Ferrell, J. E. & Ha, S. H. Ultrasensitivity part III: cascades, bistable switches, and oscillators. *Trends Biochem. Sci.* **39,** 612–618 (2014).

283. Ferrell, J. E. & Ha, S. H. Ultrasensitivity part II: multisite phosphorylation, stoichiometric inhibitors, and positive feedback. *Trends Biochem. Sci.* **39,** 556-569 (2014).

284. McGrath, D. A. *et al.* Cks confers specificity to phosphorylation-dependent CDK signaling pathways. *Nat. Struct. Mol. Biol.* **20,** 1407–1414 (2013).

285. Qi, M. & Elion, E. A. Formin-induced actin cables are required for polarized recruitment of the Ste5 scaffold and high level activation of MAPK Fus3. *J. Cell Sci.* **120,** 712–712 (2007).

286. Maddox, P. *et al.* Microtubule dynamics from mating through the first zygotic division in the budding yeast *Saccharomyces cerevisiae. J. Cell Biol.* **144,** 977–988 (1999).

287. Hwang, E., Kusch, J., Barral, Y. & Huffaker, T. C. Spindle orientation in *Saccharomyces cerevisiae* depends on the transport of microtubule ends along polarized actin cables. *J. Cell Biol.* **161,** 483–488 (2003).

288. Evangelista, M. *et al.* Bni1p, a yeast formin linking Cdc42p and the actin cytoskeleton during polarized morphogenesis. *Science* **276,** 118-122 (1997).

289. Sheu, Y., Santos, B., Fortin, N., Costigan, C. & Snyder, M. Spa2p Interacts with cell polarity proteins and signaling components involved in yeast cell morphogenesis. *Mol. Cell. Biol.* **18,** 4053–4069 (1998).

290. Madden, K. & Snyder, M. Specification of sites for polarized growth in *Saccharomyces cerevisiae* and the influence of external factors on site selection. *Mol. Biol. Cell.* **3,** 1025–1035 (1992).

291. Zhao, Y. & Zhang, Z. Y. The mechanism of dephosphorylation of extracellular signal-regulated kinase 2 by mitogen-activated protein kinase phosphatase 3. *J. Biol. Chem.* **276,** 32382–32391 (2001).

292. Markevich, N. I., Tsyganov, M. A., Hoek, J. B. & Kholodenko, B. N. Long-range signaling by phosphoprotein waves arising from bistability in protein kinase cascades. *Mol. Syst. Biol.* **2,** 61 (2006).

293. Sun, J. *et al.* Enhancement of tunability of MAPK cascade due to coexistence of processive and distributive phosphorylation mechanisms. *Biophys. J.* **106,** 1215–1226 (2014).

294. Fitzpatrick, J. A. J. & Lillemeier, B. F. Fluorescence correlation spectroscopy: linking molecular dynamics to biological function in vitro and in situ. *Curr. Opin. Struct. Biol.* **21,** 650–660 (2011).

295. R.H. Byrd, P. Lu, J. Nocedal, and C. Zhu, A limited memory algorithm for bound constrained optimization. *SIAM Journal on Sci. Comp.* **16**, 1190-1208 (1995).

296. B. Efron & R. J. Tibshirani, *An Introduction to the Bootstrap.* Published by Chapmann & Hall, New York. (1993).

8 Supplementary Material

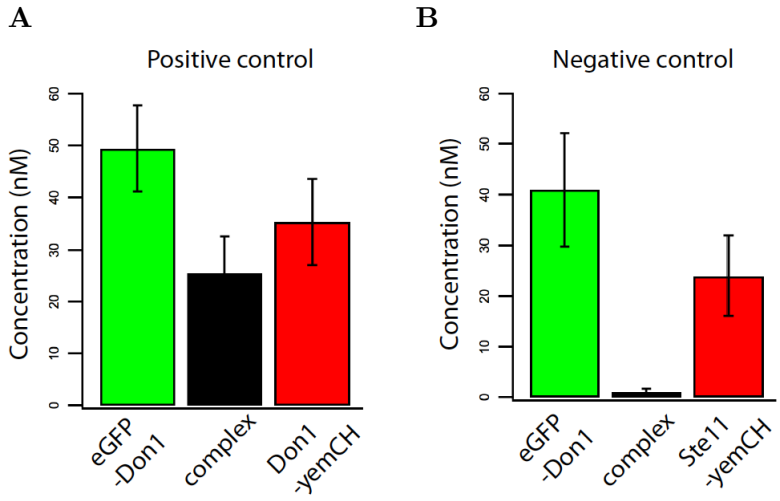

Fig. 8.1: Validation of the FCS measurements using controls. (A) Positive control using meGFP and 3ymeCherry fused to both ends of Don-1. **(B)** Negative control using cells that express meGFP-Don1 and Ste11-ymeCherry. The mean±s.e. from eight independent data sets is shown.

A
Unstimulated cells

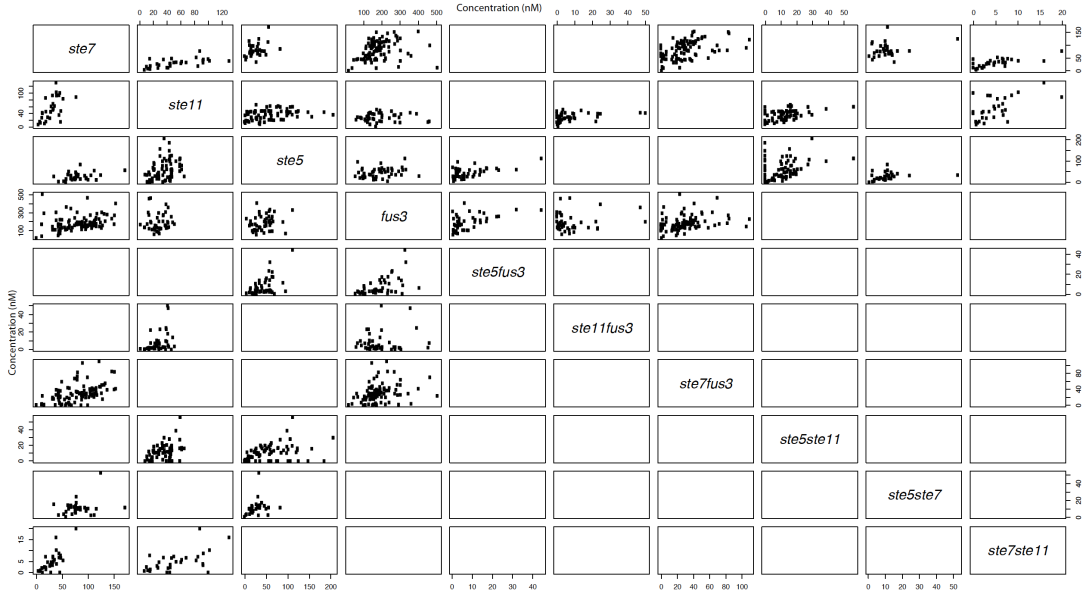

B
Short stimulation (2 – 7 min)

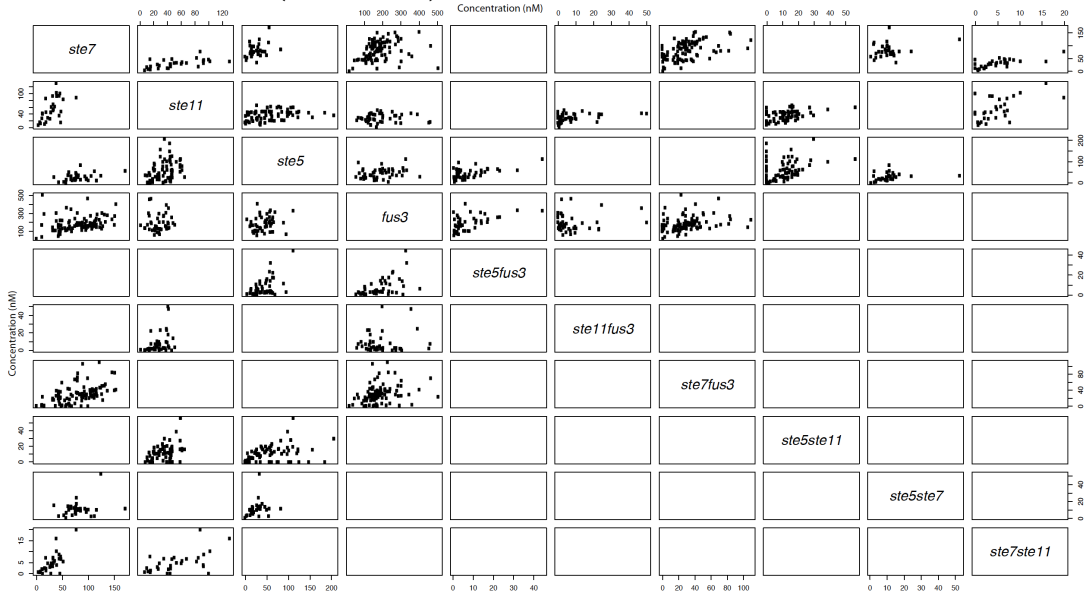

C
Long stimulation (40 – 60 min)

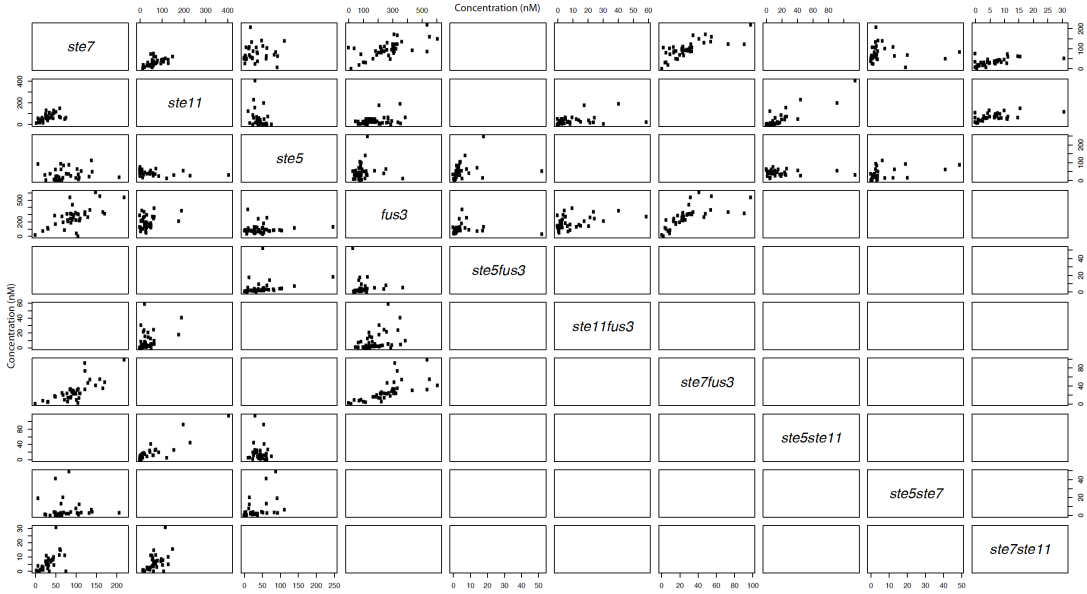

Fig. 8.2: Correlation analysis of the total concentrations of the MAPK module components Ste5, Ste11, Ste7 and Fus3 at different conditions. (A) TC and CC values from measurements in unstimulated vegetative cells. **(B)** TC and CC values from shortly stimulated cells. **(C)** TC and CC values from long stimulated cells.

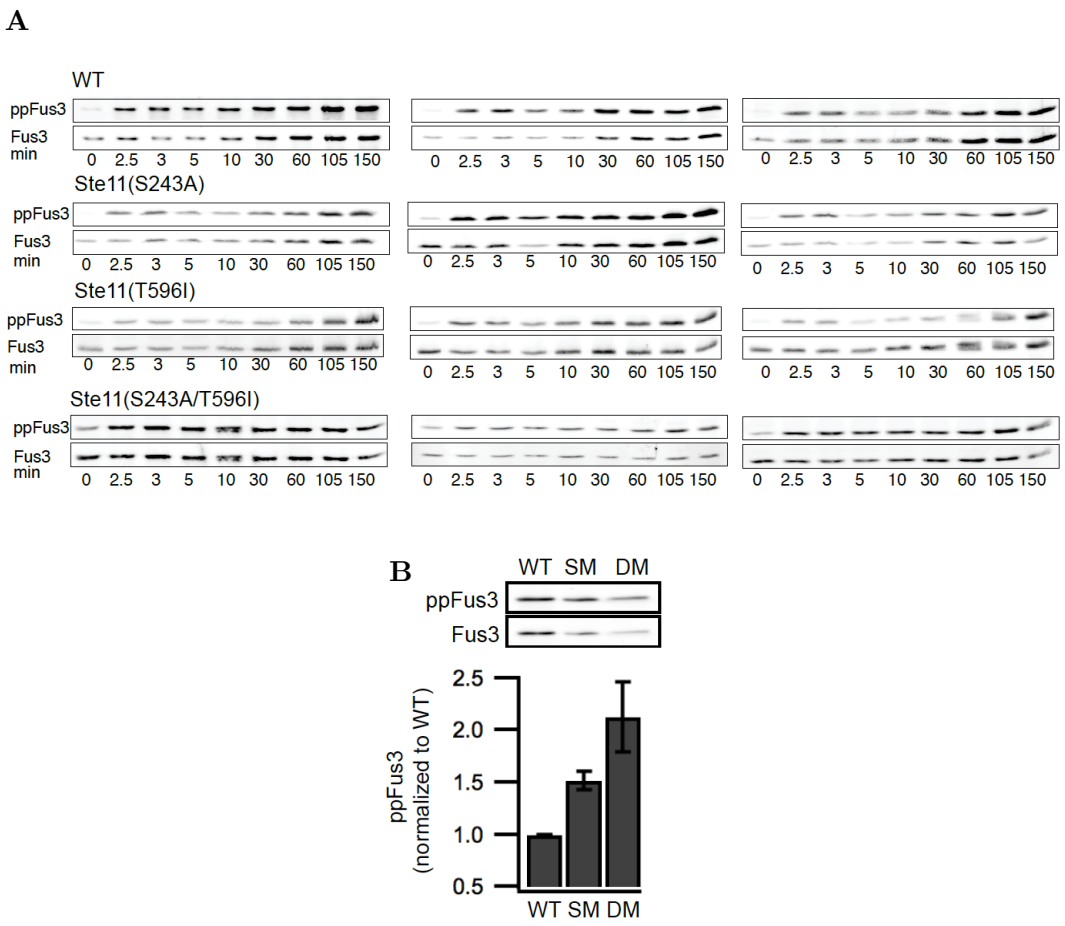

Fig. 8.3: Fus3 phosphorylation in Ste11 mutants as function of time. (A) Western blots showing ppFus3 and total Fus3 as function of time in WT, Ste11(S243A), Ste11(T596I) and Ste11(S243A/T596I) strains. Cells were stimulated with 100 nM α-factor. Quantification in Fig. 3.16 **(B)** Exemplary western blot showing ppFus3 (ppFus3/Fus3) in WT, Ste11(S243E) and Ste11(T596E) cells at 150 min post stimulation with 100 nM α-factor. Data was normalized to ppFus3 in WT cells. The mean±s.e. from three independent western blots is shown.

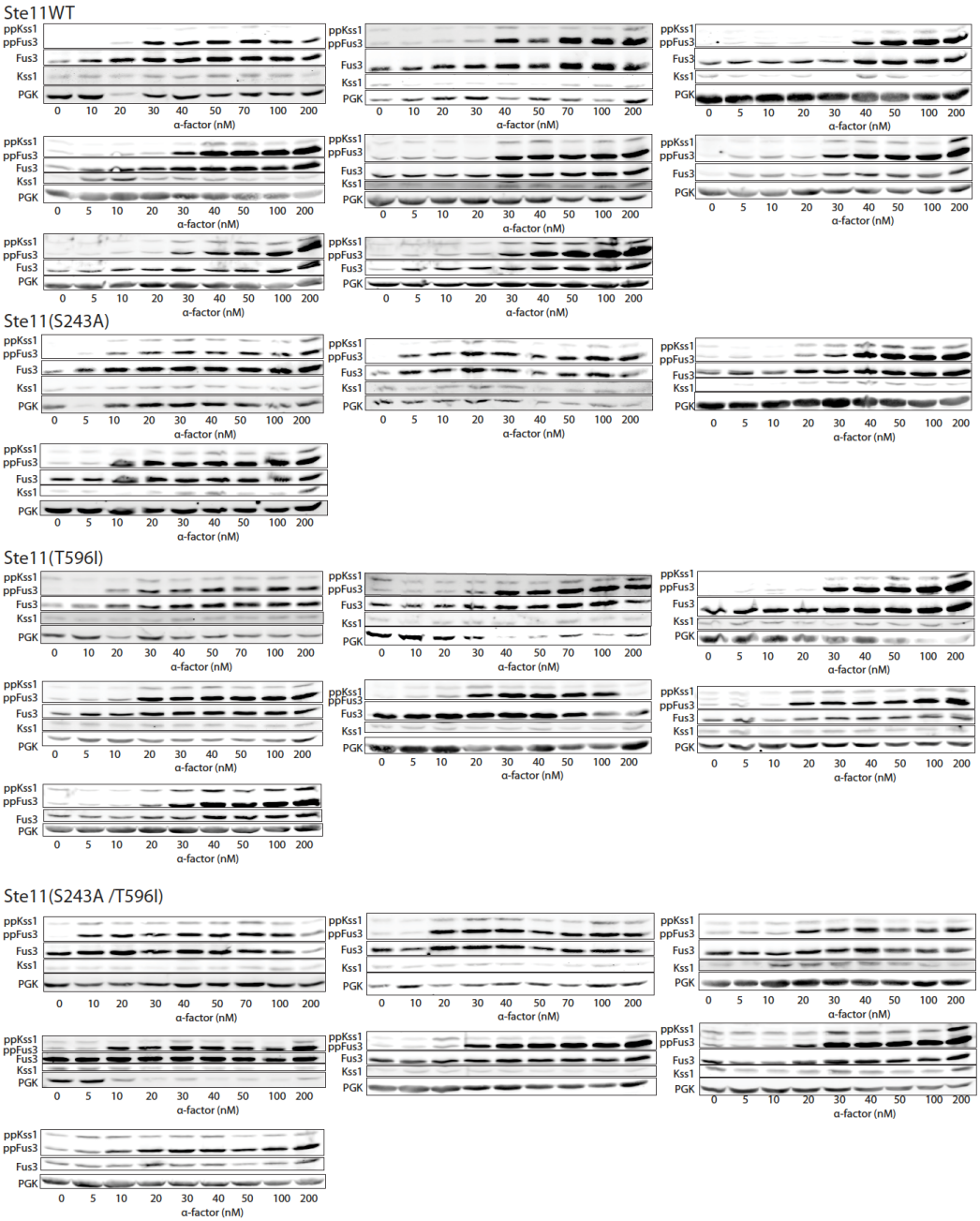

Fig. 8.4: ppFus3 pheromone dose-response. Western blots of the pheromone dose-response of ppFus3 and ppKss1 in WT, Ste11(S243A), Ste11(T596I) and Ste11(S243A/T596I) cells at 270 min post-stimulation. Yeast Phosphoglycerate Kinase was used as loading control. Quantification in Fig. 3.18.

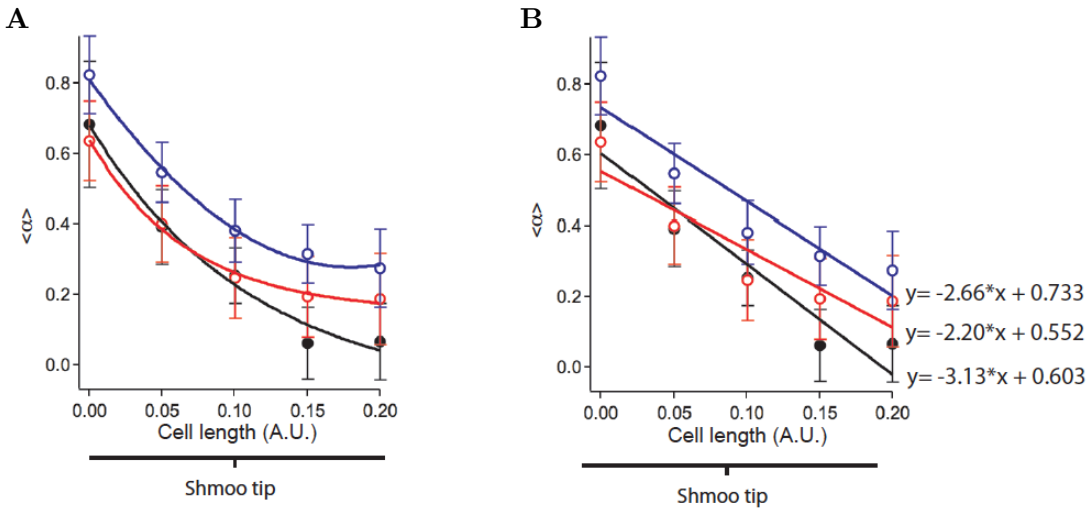

Fig. 8.5: ppFus3 gradient in the shmoo tip, the area between the tip of the mating projection and the nucleus. (A) Exponential fits of ppFus3 gradient in WT (black), Ste11(S243A) (red) and Ste11(S243A/T596I) (blue) cells. (B) Linear fits of ppFus3 gradient in WT (black), Ste11(S243A) (red) and Ste11(S243A/T596I) (blue) cells with corresponding equations. Data represented in Fig. 3.31.

Tab. 8.1: Two sided Student's *t*-test to assess significance of the differences in the concentrations of the TC and CC values measured by FCS at the different conditions. P indicates *p*-value. Concentrations are significantly different when P<0.05. Highlighted values (bold, italic) show high significance. (US = unstimulated, SS = short stimulation, LS = long simulation)

	TC Ste5			TC Ste11			TC Ste7		
	US vs SS	US vs LS	SS vs LS	US vs SS	US vs LS	SS vs LS	US vs SS	US vs LS	SS vs LS
t	0.8656	1.0879	-0.1705	-1.2667	-2.4847	1.4957	0.1562	0.4537	-198
df	261.384	250.124	236.999	181.1	134.815	189.611	180.264	195.921	220.787
p	0.3875	0.2777	0.8648	0.2069	***0.01419***	0.1364	0.876	0.6506	0.8432

	TC Fus3		
	US vs SS	US vs LS	SS vs LS
t	2.1077	0.5748	1.1346
df	264.204	221.29	257.714
p	***0.036***	0.566	0.2576

	CC Ste5 Ste11			CC Ste5 Ste7			CC Ste5 Fus3		
	US vs SS	US vs LS	SS vs LS	US vs SS	US vs LS	SS vs LS	US vs SS	US vs LS	SS vs LS
t	-1.4835	-1.498	0.7977	0.2483	2.2719	-1.3368	3.2294	1.6516	1.0923
df	74.614	36.1	41.718	51.215	55.176	68.212	62.844	91.93	58.155
p	0.1422	0.1428	0.4296	0.8049	***0.02701***	0.1857	***0.001973***	0.102	0.2792

	CC Ste11 Ste7			CC Ste7 Fus3			CC Ste11 Fus3		
	US vs SS	US vs LS	SS vs LS	US vs SS	US vs LS	SS vs LS	US vs SS	US vs LS	SS vs LS
t	-1.7679	-0.9407	-0.8038	1.5227	0.2835	0.8833	1.6937	-0.1728	1.8906
df	61.926	62.101	68.695	122.07	73.302	67.604	72.476	90.951	76.394
p	0.08201	0.3505	0.4243	0.1304	0.7776	0.3802	0.09461	0.8632	0.06247

Tab. 8.2: Comparison of concentration distributions of protein-species at different conditions from the unconstrained LRA (Fig. 3.6). Overlap values represent the size of overlapping area of two distributions. The lower the overlap the bigger the difference in the concentration distributions. Overlap of 1 indicated no differences. Relative difference (Rel. diff.) represents the distance of the canters (mean) of two distributions. Data was analysed by Jakob Wieczorek, TU Dortmund, Faculty of Statistics.

	US & SS		US & LS		SS & LS	
Protein species	overlap	rel. diff.	overlap	rel. diff.	overlap	rel. diff.
Ste11	0.66	0.13	0.39	0.27	0.67	0.16
Fus3	0.45	0.07	0.71	0.03	0.71	0.05
Ste5	0.65	0.11	0.51	0.23	0.81	0.13
Ste7	0.74	0.04	0.76	0.06	0.92	0.01
Ste11- Fus3	0.26	0.42	0.85	0.08	0.19	0.47
Ste5-Ste11	0.29	0.20	0.16	0.36	0.46	0.20
Ste11- Ste7	0.16	0.39	0.39	0.28	0.60	0.16
Ste5-Fus3	0.03	0.57	0.30	0.37	0.43	0.32
Ste7-Fus3	0.38	0.14	0.79	0.02	0.52	0.13
Ste5- Ste7	0.66	0.03	0.14	0.42	0.33	0.40
Ste5-Ste11-Fus3	0.80	0.38	0.69	0.57	0.88	0.31
Ste11-Ste7-Fus3	0.73	0.82	0.73	0.84	0.96	0.11
Ste5-Ste11-Ste7	0.91	0.39	0.86	0.73	0.95	0.56
Ste5-Ste7-Fus3	0.69	0.77	0.71	0.78	0.94	0.04
Ste5-Ste11-Ste7-Fus3	0.97	0.84	0.97	0.53	0.99	0.65

Tab. 8.3: Comparison of concentration distributions of protein-species at different concentrations from the constrained LRA (Fig. 3.9). Overlap values represent the size of overlapping area of two distributions. The lower the overlap the bigger the difference in the concentration distributions. Overlap of 1 indicated no differences. Relative difference (Rel. diff.) represents the distance of the canters (mean) of two distributions. Data was analysed by Jakob Wieczorek, TU Dortmund, Faculty of Statistics.

	US & SS		US & LS		SS & LS	
Protein species	overlap	rel. diff.	overlap	rel. diff.	overlap	rel. diff.
Ste11	0.40	0.21	0.30	0.26	0.81	0.06
Fus3	0.48	0.07	0.73	0.03	0.72	0.04
Ste5	0.80	0.03	0.65	0.14	0.70	0.17
Ste7	0.55	0.12	0.63	0.09	0.89	0.04
Ste11- Fus3	0.24	0.43	0.87	0.07	0.17	0.47
Ste5-Ste11	0.79	0.08	0.26	0.45	0.38	0.41
Ste11- Ste7	-	-	-	-	-	-
Ste5-Fus3	0.02	0.59	0.28	0.38	0.41	0.33
Ste7-Fus3	0.29	0.16	0.75	0.03	0.50	0.14
Ste5- Ste7	0.39	0.48	0.07	0.86	0.53	0.74
Ste5-Ste11-Fus3	0.71	0.57	0.56	0.49	0.85	0.15
Ste11-Ste7-Fus3	-	-	-	-	-	-
Ste5-Ste11-Ste7	0.20	0.34	0.58	0.17	0.46	0.21
Ste5-Ste7-Fus3	0.84	0.55	0.87	0.55	0.96	0.01
Ste5-Ste11-Ste7-Fus3	0.82	0.16	0.77	0.36	0.92	0.24

Tab. 8.4: Modified yeast strains used in this work.

Strain	Genotype	Source
ESM356-1	MATa ura3-53 leu2Δ1 his3Δ200 trp1Δ63 (parental strain for all strain construction)	Maeder *et al.*
YCM58	sst1Δ::hphNT1	Maeder *et al.*
YCM434-1	STE5::3m-eGFP::kanMX, FUS3::3mCherry::hphNT1, Δsst1::natNT2	Maeder *et al.*
YCM435-2	STE7::3m-eGFP::kanMX, FUS3::3mCherry::hphNT1, Δsst1::natNT2	Maeder *et al.*
YCM436-1	STE11::3m-eGFP::kanMX, FUS3::3mCherry::hphNT1, Δsst1::natNT2	Maeder *et al.*
YCM439-1	STE7::3m-eGFP::kanMX, STE5::3mCherry::hphNT1, Δsst1::natNT2	Maeder *et al.*
YCM446-3	STE11::3m-eGFP::kanMX, STE5::3mCherry::hphNT1, Δsst1::natNT2	Maeder *et al.*
YCM458-1	STE7::3m-eGFP::kanMX, STE11::3mCherry::hphNT1, Δsst1::TRP1	Maeder *et al.*
YCM449-1	nat::Pcyc::eGFP-DON1::3mCherry::KanMX6	Maeder *et al.*
YCM452-1	STE11::3mCherry::hphNT1, ESM356-1, nat::Pcyc-eGFP-DON1, STE11::3mCherry::hphNT1	Maeder *et al.*
YCM515-2	STE7::3m-eGFP::kanMX, STE11::3mCherry::hphNT1, Δsst1::;natNT2,Δ Kss1::TRP1	Maeder *et al.*
sCH46	YCM58, ΔKss1::natNT2, Fus1::3m-eGFP::kanMX	this study
sCH47	YCM58, Fus1::3m-eGFP::kanMX	this study
sJJ38	YCM458-1 (STE7::3m-eGFP::kanMX, STE11::3mCherry::hphNT1, Δ sst1::natNT2), ΔSte5::HIS3	this study
sJJ39	YCM436-1 (STE11::3m-eGFP::kanMX, FUS3::3mCherry::hphNT1, Δsst1::natNT2,) ΔSte5::HIS3	this study
sJJ40	YCM435-2 (STE7::3m-eGFP::kanMX, FUS3::3mCherry::hphNT1, Δsst1::natNT2), ΔSte5::HIS3	this study
sJJ46	sCH46, Ste11::S243A::HIS3	this study
sJJ47	sCH46, Ste11::S485A::HIS3	this study
sJJ48	sCH46, Ste11::T596I::HIS3	this study
sJJ49	sCH46, Ste11::S616A::HIS3	this study
sJJ53	YCM515-2, ΔFus3::HIS3	this study
sJJ65	YCM436-1, Fus3::T180A,Y182F::HIS3, Fus3TYAF::3mCherry:hphNT1	this study
sJJ79	sCH46, Ste11::S243E::HIS3	this study
sJJ80	sCH46, Ste11::S485E::HIS3	this study
sJJ81	sCH46, Ste11::T596E::HIS3	this study
sJJ82	sCH46, Ste11::S616E::HIS3	this study
sJJ84	sJJ65, ΔSte5::HIS3	this study
sJJ108	sJJ46, Ste11:T596E::TRP1	this study
sJJ109	sJJ79, Ste11::T596I::TRP1	this study
sJJ112	sCH47, Ste11::S243A::TRP1	this study
sJJ113	sCH47, Ste11::T596I::klURA3	this study
sJJ115	YCM58,Fus3::mCitrine::HIS3	this study
sJJ116	YCM58, Fus3::mCitrine::HIS3, Ste11::S243A::TRP1	this study
sJJ117	YCM58, Fus3::mCitrine::HIS3, Ste11::S243A::TRP1, Ste11::T596I::klURA3	this study
sJJ118	115,Δ Kss1::TRP1	this study
sJJ119	116, ΔKss1::klURA3	this study
sJJ120	117, ΔKss1::TRP1	this study
sJJ121	sJJ46, Ste11::T596I::TRP1	this study
sJJ122	121, ΔFus3::kanMX	this study
sJJ123	121, ΔSte5::TRP1	this study
sJJ124	YCM58, Ste7::3mCherry::kanMX	this study
sJJ128	YCM515-2, Ste11(T596I)::URA3	this study
sJJ130	YCM446-3, Ste11::S243A::TRP1, Ste11::3m-eGFP::hphNT1	this study

sJJ131	YCM446-3, Ste11::S243E::TRP1, Ste11::3m-eGFP::hphNT1	this study
sJJ132	YCM446-3, Ste11::T596I::TRP1, Ste11::3m-eGFP::hphNT1	this study
sJJ133	YCM446-3, Ste11::T596E::TRP1, Ste11::3m-eGFP::hphNT1	this study
sJJ136	sJJ112, Ste11::T596I::HIS3	this study
sJJ137	YCM446-3, Ste11::S243A::TRP, Ste11::T596I::HIS3	this study
sJJ138	YCM434-1, Ste11::6HA::HIS3	this study
sJJ139	YCM434-1, Ste11::S243A::TRP1	this study
sJJ140	YCM434-1, Ste11::T596I::TRP1	this study
sJJ141	YCM434-1, Ste11::S243E::TRP1	this study
Mating tester 58	MATα, his1, LYS2, ARG4, HIS3, HIS4, TRP1, LEU2, URA3,	Gerben Vader

9 Curriculum vitae

Persönliche Daten

Johann Blasius Jarzombek
Chemnitzer Str.123
44139 Dortmund

Mobil: 01637390801
E-Mail: Johann.Jarzombek@tu-dortmund.de

Geboren am 18.05.1984, Tarnowitz (Polen)
Ledig, 1 Kind (geboren am 02.12.2012)

Akademische Karriere

08/2010 - dato	Max-Planck-Institut für molekulare Physiologie Dortmund Promotion bei Prof. Dr. Philippe Bastiaens, Abteilung 2. *Thema:* "MAPK related phenotypic decisions in yeast" *Methoden:* Konfokale Fluoreszenzmikroskopie, Fluoreszenz-Korrelationsspektroskopie, Durchflusszytometrie, Proteinbiochemie (*Western Blot*, Immunopräzipitation), gentechnische Modifikationen (PCR, Klonierung). Vorraussichtlicher Abschluss der Promotion: 05/2015

Konferenzen

23/05/2014 - 27/05/2014	EMBO conference: Cellular signalling and cancer therapy. Cavtat, Kroatien. Posterpräsentation: "A negative feedback from Fus3 to Ste11 in yeast determines when and how to become a shmoo".
07/02/2014	7. Tag der Chemie, Technische Universität Dortmund. Posterpräsentation: "A negative feedback loop between Fus3 and Ste11 ensures precise formation of the mating projection" (Preis für beste Posterpräsentation).
22/10/2013	"Bio.dortmund marketplace", ISAS Dortmund. Posterpräsentation: "A negative feedback loop between Fus3 and Ste11 ensures precise formation of the mating projection".

28/08/2012 - 01/09/2012	International Conference on Systems Biology, Heidelberg – Mannheim.

Publikationen

In Vorbereitung	"A negative feedback from Fus3 to Ste11 in yeast determines when and how to become a shmoo". (Johann B. Jarzombek, Christina-Maria Hecker, Jakob Wieczorek, Lisa S. Karajannis, Aneta Koseska, Katja Ickstadt, Philippe I. H. Bastiaens - wird eingereicht bei *Nature Cell Biology*).

Hochschulausbildung

10/2008 - 06/2010	Technische Universität Dortmund Master Studiengang Chemische Biologie Masterarbeit: "Inhibition of pheromone-induced MAP kinases in yeast using gatekeeper mutations". Abschluss: Master of Science (1.6)
10/2004 - 06/2008	Technische Universität Dortmund Bachelor Studiengang Chemische Biologie Bachelorarbeit: "Design of oxidative stable zinc finger domains for extracellular detection of DNA". Abschluss: Bachelor of Science (2.9)

Zivildienst

10/2003 - 08/2004	Caritasverband für die Stadt Bottrop e.V. (Seniorenberatung)

Schulausbildung

08/1994 - 06/2003	Josef-Albers-Gymnasium Bottrop Allgemeine Hochschulreife (3.0)

Dortmund, den 26.03.2014

Johann Jarzombek

10 Acknowledgements

First of all I would like to thank Prof. Dr. Philippe I. H. Bastiaens for his guidance during the last years and for the continuous development of my interesting thesis. Thanks for the exiting insights into your ways of scientific thinking and practice.
Furthermore, I am very thankful to Prof. Dr. Andrea Musacchio for taking over the job as second reviewer.
I am deeply thankful to Dr. Christina Maria Hecker for her scientific support but even more for here valuable advises beyond science.
I would also like to thank the members of the slowly disappearing yeast group, Dr. Ali Kinkhabwala, Maja Barbara Sinn and especially Lisa Sophia Karajannis for motivating, fruitful discussions. At this point I would like to appoint Aneta Koseska as an honorary member of the yeast group, to thank for all her tireless efforts and support, and to excuse for the "bumpy" start.
A big thank you goes to Wayne Stallaert and Antonio Konitsiotis for correcting my thesis.
Special thanks go to Kirsten Michel, for her technical support and her beautiful immune-precipitations and for maintaining the laboratory.
During the last years I had the great privilege to meet a lot of interesting people and to win new friends that I would like to thank here: Björn Papke, Martin Bierbaum, Rahul Ravindran, Eulashni Chunthapursat, Thies Klüßendorf, Hernan Grecco, Jian Hou, Ola Sabet, Sven Fengler, Nashiket Vartak, Marton Gelleri, Rabea Stockert, Jana Mallah, Martin Baumdick, Yannick Brüggemann, Georgia Xouri, Angel Stanoev, Jens Christmann, Amit Mhamane, Jan Hübinger, Tanja Forck, Rahuman Sheriff, Klaus Schürmann, Malte Schmick, Astrid Krämer, Sven Müller, Dina Truxius, Katrin Prost. Sorry if I should have forgotten anyone.
Finally I would like to thank my family, friends and especially my future wife Laura and my beautiful son Jonathan.